Universidade do Minho
Escola de Engenharia

Isis Elizabeth Rodríguez Pérez

Experimental characterization and retrofitting of masonry barrel vaults from Yucatan churches, Mexico.

January 2023

Experimental characterization and retrofitting of masonry barrel vaults from Yucatan churches, Mexico.

Isis Elizabeth Rodríguez Pérez

UMinho | 2023

Universidade do Minho
Escola de Engenharia

Isis Elizabeth Rodríguez Pérez

Experimental characterization and retrofitting of masonry barrel vaults from Yucatan churches, Mexico

Doctoral Thesis

Doctoral Program in Civil Engineering

Work performed under the supervision of
Professor Doutor Paulo José Brandão Barbosa Lourenço
Professora Doutor Graça de Fátima Moreira de Vasconcelos

January 2023

DIREITOS DE AUTOR E CONDIÇÕES DE UTILIZAÇÃO DO TRABALHO POR TERCEIROS

Este é um trabalho académico que pode ser utilizado por terceiros desde que respeitadas as regras e boas práticas internacionalmente aceites, no que concerne aos direitos de autor e direitos conexos.
Assim, o presente trabalho pode ser utilizado nos termos previstos na licença abaixo indicada.
Caso o utilizador necessite de permissão para poder fazer um uso do trabalho em condições não previstas no licenciamento indicado, deverá contactar o autor, através do RepositóriUM da Universidade do Minho.
Licença concedida aos utilizadores deste trabalho



Atribuição
CC BY
https://creativecommons.org/licenses/by/4.0/

ACKNOWLEDGEMENTS

After a period of almost six years invested in the research, I am pleased to present this project to the scientific community. However, this Doctoral Thesis involves much more than the work reflected in this final document, since it represents a whole set of knowledge and experiences acquired. Furthermore, behind personal achievements, besides a considerable self-effort, a large number of contributions, support, suggestions, comments, or criticisms coming from many people usually are hidden. Their importance is so valuable that, without them, it would certainly have been very difficult to get any noteworthy result. So that, it is a pleasure to express my deepest gratitude to all people who made this research work possible, to wit:

A special mention goes to my supervisor Professor Paulo Loureço, It is undeniable his total support from the first moment I contact him in order to study for the PhD, when I arrived in Portugal and throughout my doctoral training. It is through Prof. Paulo Lourenco that I met the wonderful task force that has accompanied me during this time, my direct advisor Prof. Graça Vasconcelos, laboratory technicians António Matos, Carlos Manuel Jesus, and Marco Jorge, and Postdoctoral Javier Ortega. It is undeniable their total support, training and technical suggestions.

My heartfelt acknowledge to my direct advisor, Prof. Graça Vasconcelos. I would like to highlight their excellent professionalism and the highest human qualities. Thanks for your ethics, advice, guidance, patience, support, and great ability to listen in those not-so-good moments. Both Professor Paulo Loureço and Prof. Graça Vasconcelos, thank you for trusting in me and for the opportunity to be part of this research group. I feel like a lucky person because I met them and had the opportunity to learn from both.

I would also like to recognize that this work was supported and financed in their different stages by (1) the Teacher Professional Development Program, PRODEP (Spanish acronym) from Mexico, (2) FCT / MCTES through national funds (PIDDAC) under the R&D Unit, Institute for Sustainability and Innovation in Structural Engineering (ISISE), under reference UIDB /04029/2020, (3) LANNBIO Cinvestav Mérida, under support from projects FOMIX-Yucatán 2008-108160 CONACYT LAB-2009-01-123913, 188345, 204822, 292692, 294643 and technical help is acknowledged to MSc. D. Aguilar and Ing. Daniel Poot" and (4) the *Fassa Bortolo* company.

I would like to express my total thanks to *Fassa Bortolo* company based in Italy for providing all the materials, equipment, and tools for the strengthening of the experimental model as well as the specialized technical team for the execution of the strengthening works.

Thanks to the Department of Civil Engineering (DEC) of the University of Minho for providing the facilities and resources of the LEST laboratories for developing this research work. As well as the Laboratories of Construction and Mechanics of Materials from the School of Engineering of the Autonomous University of Yucatan and the technical help is acknowledged to Ing. F. Duarte, Ing. A. Martinez, Ing. R. Valencia, Ing. J. Cab and M.I. M. Chi. The author wishes to express their gratitude to the National Institute of Anthropology and History of Mexico, INAH (Spanish acronym), Dimension of Ecclesiastical of Properties and Sacred Art, DIBEAS (Spanish acronym) from the Archdiocese of Yucatan for the total support received by their Technical Director and friend, Arch. Ignacio Antonio Bojórquez Carvajal. Finally, but not less important to the Autonomous University of Yucatan and the School of Architecture for all their support, whit a special mention to Lic. Luz Ceballos, thank you so much to take care of my back and help me with all administrative processes.

I want to express my total gratitude to all friends that I made during this long experience Rafa, Xinyu, Meera, Antonio, Alberto, Nicoletta and so ones; some of them practically my new family in Portugal, Norma, Edu, Daniela, Esteban, Leslie, Elesban, Oscar, Rafa and Isabel; all you contributed very nice things to our lives and I feel very lucky to have coincided with you.

I want to say special thanks to all my family for your motivation and support. Last but not least, I want to express my sincere thanks to Daniel, for agreeing to go on this adventure with me even with all the statistics stacked against us and I lovingly thank my sons for being good kids no matter how challenging their new life was and especially thanks to all three for staying in this rollercoaster period that was our lives, I will always be indebted with you. Thank you for believing in me, and for your special care and attention to me, especially in the most difficult moments. You are the ones who helped me to endure all my frustrations and obstacles. Thank you for your unconditional trust, timely encouragement, and endless patience. I dedicate this achievement to you.

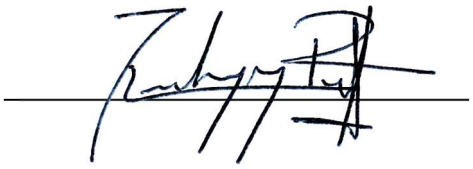
STATEMENT OF INTEGRITY

I hereby declare having conducted this academic work with integrity. I confirm that I have not used plagiarism or any form of undue use of information or falsification of results along the process leading to its elaboration.

I further declare that I have fully acknowledged the Code of Ethical Conduct of the University of Minho.
University of Minho, January 2023

Full name: Isis Elizabeth Rodríguez Pérez

Signature



RESUMO

No México existe um enorme conjunto de construções religiosas, principalmente igrejas, que foram construídas paralelamente à evolução da história do país dos séculos XVI a XVIII. Estas apresentam valor histórico, que merece ser preservado por meio de uma conservação efetiva. A maioria das igrejas apresenta hoje em dia deterioração e danos, que resultaram no colapso de algumas dessas igrejas.

Esta investigação foca-se na caracterização de materiais e na análise estrutural de componentes de igrejas do estado de Yucatán, localizadas no sul do México e construídas entre os séculos XVI e XVIII. O foco é a análise experimental do comportamento estrutural de abóbadas de berço em igrejas de vão único e formato retangular. A investigação visa preencher lacuna relacionada com a ausência de dados sobre a: (i) caracterização mecânica de materiais de alvenaria e alvenaria de pedra das igrejas de Yucatán; (ii) análise estrutural de abóbadas de berço típicas de alvenaria em relação a assentamentos verticais diferenciais; (iii) possível melhoria do desempenho estrutural de abóbadas de alvenaria submetidas a assentamentos verticais diferenciais após o reforço. Neste contexto, foram definidos quatro objetivos específicos: (1) caracterização morfológica das igrejas de Yucatán: (2) caracterização geométrica das igrejas; (3) caracterização mecânica de materiais; (4) avaliação estrutural do comportamento de abóbadas semicirculares sob assentamentos verticais antes e depois do reforço.

O plano de trabalhos foi composto principalmente por quatro tarefas para responder diretamente aos objetivos da investigação: (i) Tarefa 1 relacionada com a caracterização morfológica e construtiva das igrejas de Yucatan (objetivos de investigação 1), (ii) Tarefa 2 focada na caracterização geométrica de igrejas de Yucatán; (objetivo de pesquisa 2) (iii) a Tarefa 3 relacionada com a caracterização mecânica e física dos materiais provenientes de igrejas de Yucatan (objetivo de investigação 3); (iv) Tarefa 4 destinada à avaliação estrutural experimental de abóbadas de berço semicirculares submetidas a assentamentos diferenciais e do desempenho do sistema de reforço proposto (objetivo de investigação 4).

Como principais resultados, salienta-se a: (1) obtenção das propriedades mecânicas e físicas dos materiais das igrejas de Yucatan; (2) obtenção do comportamento estrutural de abóbadas de berço sob assentamentos verticais; (3) avaliação do desempenho de uma técnica de reforço baseada malhas de fibra de vidro embebida em argamassa de reboco (GFRM).

Palavras-chave: abóbadas de alvenaria de pedra, argamassa reforçada com fibra de vidro, assentamentos verticais diferenciais, correlações geométricas, ensaios não destrutivos (NDT), igrejas de Yucatán, calcário, mecanismos de colapso, modos de falha, tratados históricos de construção.

ABSTRACT

In Mexico, there is a huge set of religious constructions, especially churches, which were built in parallel with the country's history evolution from sixteenth to eighteenth centuries. They are considered to have historical value, which deserves to be preserved through effective conservation. Most Mexican churches nowadays evidence decay and damage, which resulted in the collapse of some churches.

This research focuses on materials characterization and structural analysis of structural members of churches from Yucatan state, located in southern Mexico and built from the sixteenth to eighteenth centuries. The focus is the experimental structural analysis of barrel vaults from single span and rectangular shape. The research aims at overcoming a research gap related to the absence of information on: (i) the mechanical characterization of masonry materials and stone masonry from the Yucatan churches; (ii) structural analysis of masonry typical barrel vaults against differential vertical settlements; (iii) possible enhancement of the structural performance of masonry vaults against differential vertical settlements after strengthening. In this context, four main specific objectives have been defined, namely: (1) morphological characterization of Yucatan churches: (2) Geometrical Characterization of Yucatan churches; (3) Mechanical characterization of stone materials; (4) structural assessment of the behaviour of semi-circular vaults under vertical settlements before and after retrofitting.

The research plan was composed mainly by four technical tasks to directly answer the research objectives: (i) Task 1 dealing with morphological and constructive characterization of Yucatan churches (research objectives 1), (ii) Task 2 focused on the geometrical characterization of Yucatan churches; (research objective 2) (iii) Task 3 is mainly related with the mechanical and physical characterization of raw materials from Yucatan churches (research objective 3); (iv) Task 4 aimed at carrying out the experimental structural assessment of semi-circular masonry barrel vaults under vertical settlements and the evaluation of the effectiveness of the proposed retrofitting system (research objective 4).

As the main outcomes, it is possible to mention: (1) obtainment of the mechanical and physical properties of materials from Yucatan churches; (2) obtainment of the overall structural behaviour of barrel vaults under vertical settlements; (3) assessment of the performance of a retrofitting technique based on glass fibre mesh with mortar (GFRM).

Keywords: collapse mechanisms, differential vertical settlements, failure modes, geometrical correlations, glass fibre–reinforced mortar, historical construction treatises, non-destructive testing (NDT), rubble stone masonry, stone masonry vaults, Yucatan churches, limestone.

Table of contents

Chapter 1. ... 1
1.1. Introduction, background, and motivation ... 2
1.2. Research objectives ... 4
1.3. Research methodology ... 5
1.4. Outline and organization of the thesis ... 7
Chapter 2. ... 10
2.1. Introduction ... 11
2.2. Architectural and morphological characteristics ... 13
2.2.1. Architectonic overview on Yucatan churches ... 13
2.3. Systematic survey on selected Yucatan churches ... 16
2.3.1. Wall's morphology ... 19
2.3.2. Vault's morphology ... 21
2.3.3. Vault-wall connections ... 23
2.4. Characterization of common damages ... 24
2.4.1. Structural damage ... 25
2.4.2. Material ageing and environmental effects ... 33
2.5. Concluding remarks ... 37
Chapter 3. ... 39
3.1 Introduction ... 40
3.2 Yucatan churches database – geometrical information ... 40
3.3 Statistical analysis of main geometric parameters ... 42
3.4 Derivation of empirical relations from statistical analysis ... 45
3.4.1 Comparison with data of other Mexican churches ... 47
3.5 Analysis of the backfill at the extrados of the masonry barrel vaults ... 50
3.6 Empirical rules from European historical construction treatises ... 55
3.6.1 Review of European historical construction treatises ... 55
3.6.2 Analysis of the Yucatan churches parameters to the light of the treatises ... 64
3.7 Concluding Remarks ... 67
Chapter 4. ... 69
4.1. Introduction ... 70
4.2. Survey of limestone and mortars from historical churches ... 71
4.3. Experimental campaign ... 75
4.3.1. Petrographic and mineralogy characterization ... 75
4.3.2. Physical and mechanical characterization ... 76
4.4. Microscopic and mineralogical analysis ... 79

4.4.1. Petrography 79
4.4.2. Mineralogic analysis 84
4.4.3. Scanning electronic microscopic analysis 88
4.5. Physical properties 91
4.5.1. Apparent density, open porosity and water absorption by immersion 91
4.5.2. Water absorption by capillarity 95
4.6. Compressive behaviour and key mechanical properties 99
4.6.1. Static Elastic modulus 99
4.6.2. Stress-strain diagrams and compressive strength 101
4.6.3. Crack patterns 105
4.7. Concluding Remarks 107
Chapter 5 109
5.1 Introduction 110
5.2 Non-destructive testing (NDT) 111
5.3 Physical and mechanical properties 112
5.4 Results from NDT 114
5.4.1 Rebound hardness number (N) 114
5.4.2 Ultrasonic pulse velocity (UPV) 115
5.5 Prediction of physical and mechanical properties from NDT 118
5.6 Relations between physical and mechanical properties 126
5.7 Concluding Remarks 130
Chapter 6 132
6.1 Introduction 133
6.2 Behaviour and collapse mechanisms of masonry vaults 134
6.3 Brief review on past experimental research 137
6.3.1 Scale and geometry for experimental models 137
6.3.2 Load conditions 139
6.3.3 Support conditions 141
6.4 Characterization of stone masonry 142
6.4.1 Geometric and morphological characteristics of wallets 142
6.4.2 Construction of the experimental wallets 144
6.4.1 Experimental setup and loading protocol 145
6.4.2 Uniaxial compression behaviour of the masonry 146
6.5 Experimental model of the barrel vault 148
6.5.1 Geometry 148
6.5.2 Selection of materials for masonry walls and vaults 151

6.6 Construction of the experimental model 153
6.7 Prediction of the experimental behaviour of the vault 154
6.8 Experimental setup and loading protocol 158
6.8.1 Instrumentation of the experimental model 161
6.8.2 Photographic record design 162
6.9 Stone masonry vault analysis and discussion of experimental results 163
6.9.1 Validation of the experimental model 163
6.9.1 Deformation analysis 166
6.9.1 Analysis of crack pattern and definition of collapse mechanism 170
6.10 Concluding Remarks 176
Chapter 7 178
7.1 Introduction 179
7.2 Strengthening techniques 179
7.3 Strengthened vault process 180
7.3.1 Materials, tools and equipment's 181
7.3.1 Description of strengthened process 184
7.4 Experimental setup and loading protocol 189
7.4.1 Instrumentation of the experimental model 189
7.4.2 Photographic record design 190
7.5 Analysis of experimental results 190
7.5.1 Validation of the experimental test 191
7.5.2 Analysis of the structural behaviour 193
7.6 Assessment of the retrofitting effectiveness 201
7.7 Concluding Remarks 206
Chapter 8. 208
8.1. Introduction 209
8.2. Summary of conclusions 210
8.2.1. Characterization of Yucatán churches (research objective from 1 to 3) 210
8.2.2. Geometrical Characterization (research objective 2). 211
8.2.3. Material characterization (research objective 3). 213
8.2.4. Structural assessment stone masonry vaults under vertical differential settlement (research objective 4). 214
8.2.5. Thesis outcomes 216
8.3. Future research 217
REFERENCES. 208
Annex 2.1 233

Annex 2.2 238
Annex 3.1 242
Annex 3.2 251
Annex 6.1 254
Annex 7.1 257

List of figures

Figure 1-1. Research design diagram 7
Figure 1-2. Scheme of the organization of the thesis 9
Figure 2-1. Examples of; (a) evolutionary process by stages (Kalisch, 2005), (b) open chapel from Dzibilchaltún and (b) full church after the completion, Tixkuncheil, Baca, Yucatan. Photographs by (Montaño, 2020; Tixkuncheil, 2020) 12
Figure 2-2. Architectonic style of the churches; (a) Franciscan architectonical style, (b) Belfry, (c) Bell towers and ornamentation added in the Motul church after 1754 (Kalisch, 2005), (c) example of churches built by secular clergy - Tecoh church from late seventeenth century (Tamayo, 2004). Photographs by (a) (Mendez, 2017), (b)(Cardos, 2008), (c)(Moreno, 2020) and (d) (Padilla, 2018) 14
Figure 2-3. Cathedral of San Idelfonso in Mérida, Yucatán. Photographs by (Méridaelite, 2020) 14
Figure 2-4. (a) Neoclassical architectural style. Lourdes Church from 1889 (Sulu and Navarrete 2014); (b) Neogothic architectural style. Our Lady of Carmen from 1908 (Niglio, 2016); (c) Architectural style Mannerist-Baroque like .Cantón Palace, which was built from 1904 to 1911 from (INAH, 2020b). Photograph from (a) (MTMM, 2013), (b) (Panoramio, 2018) and (c) (López, 2020) 15
Figure 2-5. Natural stone masonry of Yucatan churches. Chancenote Church 17
Figure 2-6. Architectonic plan of passageways, interior view and its connections with interior and exterior spaces of the church. Adapted from Vega et al. (1945) 17
Figure 2-7 Types of vaults; (a) ribbed vaults in presbyteries of Izamal, (b) stone masonry vaults; (b) mix-system vaults. Stone masonry with wooden logs 18
Figure 2-8. Typology of architectonical plan 19
Figure 2-9. Some typical sections of the walls from (a) centre of Mexico (Chávez et al., 2012), (b) Yucatan churches (south of Mexico), (c) Italy (Rovero et al., 2016) and (d) Italy (Binda et al., 1994) 21
Figure 2-10. Cross section of masonry vaults; (a) flat stones working as voussoirs. Uayma, church; (b) detail of cross section of the vault, (c) backfill at the extrados. Uayma church (d) partial coss section of the barrel vaults and plan view focusing in the detail of the minimum interlocking of stones 22
Figure 2-11. Bond of stone masonry vaults; (a) longitudinal mortar joints and misaligned transversal mortar joints and (b) running masonry bond 23
Figure 2-12. Backfilling in the extrados and wall vault connection. Proposal based on visual inspection 23
Figure 2-13. Some schemes provided for vault-wall connection; (a) vault - wall connection according to Tamayo (2004); (b) vault - wall connection according to Ruppert and Denison (1943) and Satterthwaite, (1944); (c) wall-vault connection according to Kalisch (2005) 24
Figure 2-14. Cracking patterns: (a) detached connection between the façade and longitudinal walls, (b) cracks in weak sections of façade walls and (c) cracks in weak sections of longitudinal wall 26
Figure 2-15. (a) Spiral stairs of Yucatan churches, (b) inside view of diagonal cracking near the corner connection and (c) external view of diagonal cracking near the corner connection 26
Figure 2-16. Cracking pattern in longitudinal wall – mostly horizontal cracking 26
Figure 2-17. Longitudinal cracks. (a) exterior view of Mama church, (b) exterior view of Xcan church 27
Figure 2-18. Cracks inside passageway. (a) joint vault-wall inside the passageway, (b) crack located throughout the keystone, (c) keystone crack close to the end of the passageway, (d)

cracking in vault and wall close to the façade and thickness-crack in vault (Tixmehuac, Yucatan) 28
Figure 2-19 Crack patterns at the vaults: (a) longitudinal cracks in the keystone of the vaults, (b) longitudinal crack on collapsed vault, (c) cracking Y shaped pattern and (d) cracking pattern in Y shaped in collapsed church 28
Figure 2-20. cracking pattern at extrados near to façade wall section 29
Figure 2-21. Influence of edge effects resulting from the interaction of the cannon vaults with frontal walls (Adapted by (Rodriguez, 2006) 29
Figure 2-22. Cracking pattern in the rooftop and associated collapse 29
Figure 2-23. Barrel vault with shorter high and cracking pattern form both (a) Mama and (b) Tixmehuac churches 30
Figure 2-24. (a) Collapse of both main and choir vaults in Uayma church and (b) closeup view of the collapse reduced vault in the choir 30
Figure 2-25. Cracks in the joint buttresses-wall for three different churches (a) Xcan, (b) Tixmehuac and (c) Mama 31
Figure 2-26. Vault deformations in the Xcan church 31
Figure 2-27. Longitudinal section at keystone of Tixmehuac church 32
Figure 2-28. The span of the vault at centre is bigger than extremes. Xcan church 32
Figure 2-29. Deformations of cross section in the vault near the main façade (line1), in the centre (line2) and near the back-façade (line 3) 32
Figure 2-30. Tilts in walls (a) superposition of the cross sections at the main façade (line1), in the centre (line2) and near the back-façade (line 3) and (b) an example of the tilt dimensions measured in each cross section. 33
Figure 2-31. Out of the plane displacement (a) a clear tilt between wall towers and centre part of the wall, (b) the typical cracking pattern in the main façade of partial collapsed churches and (c) the typical cracking pattern in the main façade after retrofitted works 33
Figure 2-32. Examples of detachment decay patterns. (a) blistering and (b) disintegration 34
Figure 2-33. Examples of detachment decay patterns. (a) fragmentation and (b) disintegration 34
Figure 2-34. Material loss, (a) matrix loss in stone units and (b) mortar loss on masonry stone walls 34
Figure 2-35. Material loss. (a) missing parts due to lightning strike and (b) perforations on masonry stone wall due to anthropogenic factors 35
Figure 2-36. Examples of crusts, (a) black crust under the cornices of facades and (b) salt crust on decorative elements 35
Figure 2-37.Chromatic alterations (a) colouration inside the churches and (b) bleaching facades 35
Figure 2-38. Chromatic alterations (a) moist areas clearly identified on vaults and (b) staining in lateral façade 36
Figure 2-39. Superficial alterations and deposits (a) due to anthropogenic factors, graffiti and (b) soiling due to lack of maintenance 36
Figure 2-40. Examples of biological colonization. (a) Algae-and (b) Lichens 36
Figure 2-41. Examples of biological colonization. (a) moss, (b) Plants and trees, and (c) tree roots inside masonry after collapse 37
Figure 2-42. a) Alamo tree from (Herbario CICY, 2020), b) Alamo on masonry construction and c) masonry after burning roots Concluding Remarks 37
Figure 3-1. Key geometric variables of the cross section of one span churches 41
Figure 3-2. Statistical analysis; (a) single regression between the span (L) and height of wall (Hw) - Phase 2; (b) histogram defined for the height of walls (Hw) and adjustment of normal distribution. See 72Annex 3.1 43
Figure 3-3. Geometrical proposal for semi-circular barrel vaults (image in proportion with dimensions) 45

Figure 3-4. (a) Churches with significant statistical correlation between height of the walls and span; (b) histogram for the height wall/span ratio. See Annex 3.2 45
Figure 3-5. Statistical information for the ratio between the span (L) and the key geometric parameters; (a) ranges of frequencies selected for geometric parameters to span ratio; (b) proposed parameters to span ratios 46
Figure 3-6. Comparison of the variation with the span (L) of key geometric parameters of churches with barrel-vaults and single span; (a) Hv vs L, (b) tv vs L, (c) Hw vs L, (d) tw vs L, (e) H vs L and (f) rock seismic acceleration map, adapted from PRODISIS (2017) 49
Figure 3-7. Statistical analysis: (a) backfill height and span ratio (Ew/L) and (b) backfill height to height of the vault ratio (Ew/Hv) 51
Figure 3-8. Definition of the backfill height regarding to the; (a) span (L) and (b) height of vault (Hv) 51
Figure 3-9. Percentage of backfill height found for different churches regarding to the; (a) span (L) and (b) height of the vault (Hv) 52
Figure 3-10. Identification of centre angle for barrel vaults 53
Figure 3-11. Relation between backfill height to span ratio (Ew/L) with: (a) central angles, (b) aperture angle 54
Figure 3-12. (a) La Hire theory: definition of thrust and sliding-wedge concept, (b) mechanism of the collapse and (c) transmission of loads. Adapted from (La Hire, 1712; Huerta and Hemando, 1998) 62
Figure 3-13. (a) First application of simplified La Hire theory by Belidor and (b) application examples on full buildings (Belidor, 1725) 63
Figure 3-14. Empirical rules from European historical construction treatises 64
Figure 3-15. Geometric profiles of single span churches with barrel vaults; (a) derived empirical rules for Yucatan churches; (b) geometry rules from European historical construction treatises 65
Figure 3-16. Comparison between the Yucatan churches and the historical rules; (a) Thickness of the vault, (b) Thickness of the wall, (c) Height of the wall and (d) Height infill at extrados of vaults 66
Figure 3-17. Comparative analysis of geometric parameters from churches of Mexico and proposals provided in historic treatises 67
Figure 4-1. Examples of partially collapsed churches: (a) San Jose Church from seventeenth century, Petulillo, Peto, (b) San Francisco church from eighteenth century, Kikil, Timizin 72
Figure 4-2. Spatial distribution of selected churches as case studies and general lithology of Yucatan state (adapted from (García and Graniel, 2010)) 72
Figure 4-3. Cylindrical specimen: (a) extraction direction, (b) orientation of the bedding planes (β) 74
Figure 4-4. Limestone samples: (a) stone block, (b) view of some prepared core samples (c) defined bedding planes, (d) random or absence of clear bedding planes 74
Figure 4-5. Devices used for the mechanical characterization; (a) under cyclic tests, (b) under monotonic tests 77
Figure 4-6. Macroscopic image of the 16 studied lithotypes 81
Figure 4-7. Micrographs of the studied lithotypes: a) P1SIS; b) P2SIS; c) P3PE; d) P4PE; e) P6ICH; f) P7ICH; g) P8KIK; h) P9KIK (cross polarized light) 82
Figure 4-8. Micrographs of the studied lithotypes: a) P10KIK; b) P11KIK; c) P12CHA; d) P13CHA; e) P14TIX; f) P15TIX; g) P16TIX; h) P17TIX (cross polarized light) 83
Figure 4-9. Examples of typical diffractogram from natural mortar samples. (a) render mortars, (b) joint mortars. C=Calcite, A=Ankerite, H=Hydrotalcite, G=Gypsum, K=Kaolinite, Ar=Aragonite, Q=Quartz, Cl=Clinochlore, V=Vaterite 84
Figure 4-10. (a) Typical diffractograms of natural samples and (b) diffractograms of mineral phases after decarbonation. C=Calcite, A=Ankerite, CM= Calcite Magnesia 87
Figure 4-11. EDS analysis from sample P8KIK; (a) clear zone, (b) dark zone 88

Figure 4-12.Scanning electron microscopy photomicrographs; (a) compact samples, (b) porous samples..... 89
Figure 4-13. Scanning electron microscopy photomicrographs; voids 90
Figure 4-14. Scanning electron microscopy photomicrographs; Microcracks..... 90
Figure 4-15. Scanning electron microscopy photomicrographs; Fossil microorganisms..... 91
Figure 4-16. Scanning electron microscopy photomicrographs; (a) hexagonal structures and (b) thin and elongated crystals 91
Figure 4-17. Power regression model analysis; (a) porosity vs density and (b) density vs water absorption 92
Figure 4-18. Box plot for each stone type; (a) apparent density, (b) open porosity and (c) water absorption by immersion..... 93
Figure 4-19. Grouping the limestones according to values of; (a) apparent density; (b) open porosity and (c) water absorption by immersion..... 94
Figure 4-20. Capillary water absorption kinetics for the different limestone groups; (a) group 1, (b) group 2, (c) group 3..... 97
Figure 4-21. Capillary water absorption coefficient (Cw) [kg/(m².s1/2)] by groups and bedding planes 98
Figure 4-22. Box diagram of Static Elastic modulus (E) by limestone group and by bedding planes..... 100
Figure 4-23. Box diagram of uniaxial compressive strength (fc) for the limestone groups considered and according to bedding planes..... 102
Figure 4-24. Stress-strain behaviour of limestones; (a) group 1; (b) group 2; (c) group 3..... 103
Figure 4-25. Stress-strain behaviour of limestones; (a) general behaviour of limestone, (b) four distinct stages of the curves strain-stress for each group..... 103
Figure 4-26. Failure modes under uniaxial compression observed in this study..... 105
Figure 4-27. Percentage of specimens (a) by failure mode and (b) by groups 106
Figure 4-28. Percentage of specimens by mode of failed regarding to (a) fc and (b) η 106
Figure 5-1. Details of NDT: a) Schmidt hammer, b) stone surface treated, c) perpendicular readings at surface 112
Figure 5-2. Ultrasonic test conducted using the Pundit Lab PROCEQ equipment..... 112
Figure 5-3. (a) Physical properties namely: apparent density (ρ), open porosity (η), water absorption by immersion at atmospheric pressure (Ab) and (b) mechanical properties namely. compression strength (fc) and static elastic modulus (E)..... 113
Figure 5-4. Rebound hardness number (N) by groups..... 114
Figure 5-5. Ultrasonic pulse velocity (UPV). (a) dry samples and (b) saturate samples 117
Figure 5-6. Relationship of Rebound hardness number (N) with physical and mechanical properties and equations of empirical correlations 119
Figure 5-7. The relationship between Schmidt hammer hardness and fc for limestones and sedimentary stones from different researchers 121
Figure 5-8. Relationship between ultrasonic pulse velocity (UPV) and physical and mechanical properties..... 122
Figure 5-9. Comparison of the regression equation of the current study with those equations from the literature review: (a) fc vs UPV of limestones, (b) E vs UPV..... 124
Figure 5-10. Comparison of the regression equations of the current study with those equations from the literature review: (a) ρ vs UPV, (b) η vs UPV 125
Figure 5-11. Correlations between physical properties; (a) Cw vs Ab; (b) Cw vs □□(c) Cw vs □□(d) □vs□ 127
Figure 5-12. Correlation between compressive strength and modulus of elasticity 128

Figure 5-13. Statistical correlation between modulus of elasticity (E) and physical properties; (a) E vs. open porosity; (b) E vs. density; (c) E vs water absorption by immersion; (d) E vs capillary coefficient 129
Figure 5-14. Statistical correlation between compressive strength (fc) and physical properties; (a) fc vs. open porosity; (b) fc vs. density; (c) fc vs water absorption by immersion; (d) fc vs capillary coefficient 130

Figure 6-1. Main collapse mechanisms of masonry arch due to supports settlement according to Zampieri (2018) 135
Figure 6-2. (a) parts of the vault and (b) De Guglielmo model and hinges on arches (De Guglielmo et al., 2015) 136
Figure 6-3. Main theoretical collapse mechanisms of masonry buttressed arches considering three types of support settlement (horizontal, vertical and inclined) (Zampieri et al., 2019b) 136
Figure 6-4. Full experimental models; (a) model proposed by (Marini, Giardina, Riva, and Giuriani, 2008); (b) model proposed by Baratta et al. (2008) 137
Figure 6-5. Monumental buildings models at reduced scale. (a) Typical colonial temple of central Mexico from 17th and 18th (M Chávez and Meli, 2008). (b) Mustafa Pasha Mosque from 15th century (Krstevska et al., 2008) 138
Figure 6-6. Vertical load application system: (a) side view of the loading apparatus, (b) load distribution at the wall to edge, (c) cup-springs at the base reducing the vertical bar stiffness (Marini et al., 2008) 140
Figure 6-7. Load application system (Marini et al., 2008) 140
Figure 6-8. Vertical displacement to reproduce the differential settlements: (a) displacement applied on full scale model using hydraulic jacks (Castellano et al., 2021b), (b) displacement applied on small scale model using hydraulic jacks (Ferrero et al., 2022)and (c) displacement applied using mechanical jacks(Torres et al., 2019) 140
Figure 6-9. Boundary conditions: (a) support conditions to allow rotations at the base (Giuriani et al., 2009) and (b) C-beam steel to avoid horizontal displacements (Golebiewski et al., 2017) 141
Figure 6-10. Boundary conditions: (a) experimental arch between two reaction walls (Paolo Girardello et al., 2013) and (b) metallic profiles and tied with four rods (Garmendia et al., 2015b) 142
Figure 6-11. (a) support with vertical rebars (Marini et al., 2008); (b) prestressing clamps and anchoring bars (Marini et al., 2017) 142
Figure 6-12. Masonry wallets with a rectangular base proposed to represent (a) walls and (b) vaults 143
Figure 6-13. Construction of the walls' and vaults' wallets (a) and (c) falsework, while (b) and (d) wallets 144
Figure 6-14. Setup arrangement (a) load frame, (b) wall's wallets setup and (c) vault's wallets setup 145
Figure 6-15. Wall samples behaviour. (a) Development of the experiment, force-displacement diagram and (b) stress-strain diagrams 146
Figure 6-16. Vault samples behaviour. (a) Development of the experiment, force-displacement diagram and (b) stress-strain diagrams 147
Figure 6-17.Representative cross section. (a) reduced scale model at 30%, (b) experimental cross section, rooftop view and cut section A 148
Figure 6-18. Morphological characteristics of walls and vault masonry bonds, rooftop and elevation 149
Figure 6-19. Morphological characteristics of walls and vault masonry bonds, cross section of wall and vault, stones shape and stone dimension 150
Figure 6-20. (a) Lithology of Portugal, (b) calcium carbonates area and (c) limestones area and location of quarry selected for the delivery of stone for the experimental model. (Direção-Geral do Território, 2022) 151

Figure 6-21. Construction of the experimental model. (a) curved steel formwork, (b) construction of the walls, (c) vault construction and (d) placement of the key stone of the vault..... 153
Figure 6-22. Final view of the experimental model. (a) wall extension on the extrados and (b) full experimental model 154
Figure 6-23. Numerical crack prediction 156
Figure 6-24. Induced displacement and vertical reaction from displaced support..... 157
Figure 6-25. Crack widths Ecw1. a) Vault-Wall connection closes the displaced support, (b) Vault-Wall connection closes the fixed support and (c) keystone position 157
Figure 6-26. Load conditions of experimental model submitted to self-weight and differential settlement 158
Figure 6-27. Vertical displacement rigid device 159
Figure 6-28. Support rotation constraint 160
Figure 6-29. Acquisition data setup (a) LVDT device, (b) actuators and (c) LVDT displacement range (in mm) 160
Figure 6-30. LVDT location 162
Figure 6-31. Auxiliary frame to support the vaults LVDTs..... 162
Figure 6-32. Photographic device positions..... 163
Figure 6-33. Definition of displacement signs for use in graphs 164
Figure 6-34. Validation of the experimental system. (a) analysis of vertical displacement applied at the uniform way by comparing the force and the internal transducer displacement from the actuators, (b) evolution of the displacement at the top of the left wall 165
Figure 6-35. Evolution of displacement with time (a) displacement measured at the steel base and (b) rotations of the steel base..... 165
Figure 6-36. (a) Analysis of model deformations in the plane and displacement at key points at an induced vertical displacement (b) Moment A with 0.24mm, (c) Moment B with 0.95mm, (d) Moment C with 1.58mm, and (e) Moment D with 2.34mm..... 166
Figure 6-37. In-plane deformations at different stages (a) Moment E with 3.0mm. (b) Moment F with 3.89mm, and (c) Moment H with 25.99mm..... 167
Figure 6-38. Vertical vault deformations regarding to the induced vertical displacement, which shown different displacement ranges: (a) LVDT V1, V2 and V3 in mm, while (b) LVDT V4 and V5 in microns 168
Figure 6-39. Evaluation of the behaviour of the supporting walls. (a) diagonal displacement in the walls and (b) relative horizontal displacement between supporting walls..... 169
Figure 6-40. Displacement at key points at an induced vertical displacement of 0.24mm. (a) LVDTs records and (b) proposal of global movement of the experimental model..... 170
Figure 6-41. Moment B at 0.95mm of induced displacement. (a) LVDTs displacement records and (b) proposal of global movement of the experimental model..... 171
Figure 6-42. Moment C with 1.58mm of induced displacement. (a) LVDTs records and (b) behaviour description..... 171
Figure 6-43. Moment D with 2.34mm of induced displacement. (a) LVDTs records and (b) behaviour description..... 172
Figure 6-44. First crack in the vault at extrados located at the wall-vault connection..... 172
Figure 6-45. Moment E with 3mm of induced displacement. (a) LVDTs records and (b) behaviour description..... 173
Figure 6-46. (a) Second crack at the intrados of the vault-wall connexion and (b) crack of belonging to hinge D..... 173
Figure 6-47. (a) Displacements of key points when induced displacement of 3.89mm; (b) Proposal of rigid blocks movement 174

Figure 6-48. (a) Displacements of key points when induced displacement of 4.86mm; (b) Proposal of rigid blocks movement 174
Figure 6-49. (a) Displacements of key points when induced displacement of 25.99mm; (b) Proposal of rigid blocks movement 175
Figure 6-50. Behaviour of the experimental model. (a) From 150 to 529 seconds and (b) from 645 to 3508 seconds 175
Figure 6-51. a) Proposal for the final collapse mechanism at the end of this experiment and (b) Mechanism VII and VIII from (Zampieri et al., 2019b) 176
Figure 7-1. Strengthening system; (a) Mesh of fibber glass and (b) hydraulic lime mortar 181
Figure 7-2. Strengthening system; (a) Connector elements and (b) chemical anchorage 181
Figure 7-3. Tools and equipment's 183
Figure 7-4. Removal of existing plaster (a) at intrados, (b) at extrados and (c) rough and clean surface 184
Figure 7-5. Preparation of materials (a) mesh, (b) L-shape connectors and (c) protector hose 184
Figure 7-6. Anchorage position. In plant view, elevation view and intrados view 185
Figure 7-7. Anchorage of the mesh to the structure; (a) double L connector and (b) single L connector 186
Figure 7-8. Preparation of the anchorages; (a) drill on vault, (b) drill on walls (c) clean with air and (d) protective hose placement 186
Figure 7-9. Prepared vault. (a) intrados left side, (b) elevation view and (c) intrados left view 187
Figure 7-10. Quality control of the mortar (a) mortar preparation, (b) mortar workability tests and (c) preparation of test specimens 187
Figure 7-11. (a) wetting of the structure and (b) protection of the space 188
Figure 7-12. Strengthening process (a) projection of mortar, (b) uniform distribution of mortar layer, (c) embedment of the mesh on fresh mortar, (d) insertion of the L-shape connectors and (e) second layer of mortar 188
Figure 7-13. Increased LVDT in instrumentation setup 189
Figure 7-14. Photographic device positions (a) elevation view and (b) plant view 190
Figure 7-15. Definition of displacement signs 190
Figure 7-16. Evolution of the experimental test (a) force regarding to induced displacement records by internal transducers of the actuator and (b) force regarding to settlement control point in the steel base 191
Figure 7-17. Evolution of the steel base´s displacements; (a) displacement comparison between internal transducer of the actuator and settlement control points and (b) Settlement control point behaviour though the experiment 192
Figure 7-18. (a) Evolution of displacement in the masonry vault and walls for increasing induced vertical displacement. (b) Vault displacement close up view and (c) wall displacement close up view 194
Figure 7-19. Deformation behavior of the model: (a) Moment A at 162s, (b) Moment B at 662s, (c) Moment C at 1725s, and (d) Moment D at 2097s 195
Figure 7-20. (a) Crack the at the base of the right wall; (b) scheme of the hinge at the base of the right wall 196
Figure 7-21. Displacement of the model at Moments from C to E. (a) R points plot and (b) V points plot 196
Figure 7-22. Development of hinge at the vault-wall connection; (a) cracking at the vault-wall connection, (b) scheme of hinge B 196
Figure 7-23. Deformation behaviour of the model: (a) Moment E at 2371s, (b) Moment F at 2685s, (c) Moment G at 3529s, (d) Moment H at 3901s, (e) Moment I at 5265s and (f) Moment J at 6512s 197

Figure 7-24.Displacement of the model at Moments from F to H. (a) R points plot and (b) V points plot.... 198
Figure 7-25. Moment F with 19.85mm of induced displacement. (a) LVDTs records and (b) behaviour description, (c) hinge C locations and damage.... 198
Figure 7-26. (a) Damage corresponding to hinge D, (b) relative location of hinges D and C locations and (c) hinge A location 199
Figure 7-27. Evolution of the vertical vault´s displacements.... 200
Figure 7-28. Displacement of the model at Moments from G to J. (a) R points plot and (b) V points plot.... 200
Figure 7-29. (a) Progress to the extrados of cracking related to hinge C' and (b) general view of the four hinges 200
Figure 7-30. Evolution of displacements of key points in walls (a) experimental model and (b) strengthening experimental model.... 202
Figure 7-31. Evolution of the spacing between stone masonry walls measured by W3a and W3b displacements: (a) BS model; (b) AS model.... 203
Figure 7-32. Evolution of displacements of key points in vaults (a) BS experimental model and (b) strengthening experimental model (AS model).... 203
Figure 7-33. Comparative behaviour between the BS model and AS model (a) Moment A of the BS model, (b) Moment A of the AS model, (c) Moment B of the BS model, (d) Moment B of the AS model, (e) Moment C of the BS model, (f) Moment C of the AS model, (g) Moment D of the BS model, (h) Moment D of the AS model 204
Figure 7-34. Comparative behaviour between the BS model and AS model (a) Moment E of the BS model, (b) Moment E of the AS model, (c) Moment F of the BS model, (d) Moment F of the AS model, (e) Moment G of the BS model, (f) Moment G of the AS model, (g) Moment H of the BS model, (h) Moment H of the AS model.... 205
Figure 7-35. Final hinge configuration of the AS model 206

List of tables

Table 1-1 Experimental characterization at the materials level 6
Table 2-1. Characteristics of the masonry bond of walls. Sample from Conkal church 20
Table 3-1. Coefficient of variation obtained for statistical correlations between different geometric key parameters 44
Table 3-2. Selected frequency range for each phase 44
Table 3-3. Significant statistical correlation between geometric variables and span 46
Table 3-4. Relationships between key geometric parameters and span for additional churches in Mexico. 48
Table 3-5 – Authors of historical manuscripts, manuals, and treatises from sixteenth to eighteenth centuries. 56
Table 3-6. Rules for the thickness of the walls 57
Table 3-7. Thickness of vault (tv) and the backfill at the extrados of vaults (Ew) 58
Table 3-8. Graphic Rules for piers and walls proposed by Rodrigo Gil de Hontañón 59
Table 3-9. Paladio's rules to determine the height of the vault (Hv) 59
Table 3-10. Graphic Rules for piers and walls proposed by different authors 61
Table 4-1. Identification code of stone blocks 73
Table 4-2. Identification code of mortars 73
Table 4-3. Core samples tested for each limestone block and the number of specimens according to the bedding planes 74
Table 4-4. Classification of strength anisotropy index 78
Table 4-5. Classification of index by modulus anisotropy 79
Table 4-6. Mineral phases identified in render mortar samples 85
Table 4-7. Mineral phases identified in joint mortar samples 86
Table 4-8. Mineral phases identified in the stone samples 88
Table 4-9. Limestone values of; (a) apparent density, ρ; (b) open porosity, η and (c) water absorption by immersion Ab 94
Table 4-10. Physical properties of limestones 95
Table 4-11. Average values of capillary water absorption coefficient (Cw) [kg /(m^2.s1/2)] and factor Fwc. 96
Table 4-12. Static modulus of elasticity (E) and index of modulus anisotropy (IaE) 99
Table 4-13. Modulus of elasticity of limestones 100
Table 4-14. Compressive experimental strength (fe), corrected compressive strength (fc) for parallel (//) and perpendicular ($\perp$) direction to the bedding planes and strength anisotropy index ($I\sigma c$) 101
Table 4-15. Results of compressive strength, density and open porosity by groups 104
Table 5-1. Average values of apparent density (ρ), open porosity (η), water absorption by immersion at atmospheric pressure (Ab), Rebound hardness number by Schmidt hammer (N), uniaxial compression strength (fc) and static elastic modulus (E) 113
Table 5-2.Average values of the rebound hardness number (N) and coefficient of variation (CV) 114
Table 5-3. Rebound hardness number (N) found for limestone 115
Table 5-4. Ultrasonic pulse velocity (UPV) 116
Table 5-5.Ultrasonic pulse velocity recorded in limestone worldwide 117
Table 5-6. Correlation between Schmidt hammer hardness with uniaxial compressive strength (fc), Elasticity modulus (E), density (ρ) and open porosity (η) 120
Table 5-7. Empirical statistical correlations between uniaxial compressive strength (fc) and ultrasonic pulse velocity (UPV) 123

Table 5-8. Empirical equations correlating modulus of elasticity (E) and ultrasonic pulse velocity (UPV) 124
Table 5-9. Empirical equations correlated dry density (ρ) and ultrasonic pulse velocity (UPV) 125
Table 5-10. Empirical equations correlated open porosity (η) and ultrasonic pulse velocity (UPV) 125
Table 6-1. Scaled stone sizes 143
Table 6-2. Vault and wall wallet dimensions 144
Table 6-3. Mechanical characteristics of masonry wall wallets 146
Table 6-4. Mechanical characteristics of masonry vault wallets 147
Table 6-5. Scaled stone sizes 150
Table 6-6. Most important mechanical and physical properties of limestone from Yucatan churches 152
Table 6-7. Compressive strength and tangent modulus in limestone 152
Table 6-8. Nomenclature code description 162
Table 7-1. Mesh Fassanet ARG plus 181
Table 7-2. Mortar Malta Structural NHL 77 182
Table 7-3. Fassa Glass Connector L 182
Table 7-4. Platform rotation during the test 193

Chapter 1.
Introduction

Abstract:
This Chapter presents the background, motivation, thesis objectives, research methodology, outline and organization of the thesis.

1.1. Introduction, background, and motivation

Mexican churches built between sixteenth and eighteenth centuries are considered an important stock of the built heritage. Different religious orders arrived by the sixteenth century to the country in order to carry out the spiritual conquest and evangelization of the different indigenous groups. In this context, Mendicant orders as Franciscans in 1523, Dominicans in 1526 and Augustinians after 1533, play the major role in the evangelization process (Gonzalez and Espinosa, 2015). This evangelization process was supported by the massive construction of masonry churches that are distributed in most of the Mexican territory. Recently, in 2018 and according to the Mexican law, these buildings have been considered historical monuments and a built heritage legacy that is essential to preserve (Camara de Diputados, 2018).

In 1545, the Franciscans started to construct religious buildings in Yucatan. Since this state is a Maya region, some existing construction strategies were used in order to get control over the natives. The churches were built over the most important local constructions. The monks had the support of a huge number of native inhabitants, and they took into consideration the importance of the Mayan traditions. The Yucatan churches are identified as massive structures based on loadbearing walls and vaults, built with stone masonry and lime mortar, generally supported by superficial foundations with the same construction system used for the walls and, in the best case scenario, by using slightly larger stones (Kalisch, 2005; Rodríguez Pérez et al., 2021; Tamayo, 2004b). They are also characterized generally by simple prismatic volumes, with plan three main configurations, namely (1) one nave with rectangular simple shape, (2) Latin cross or (3) three naves. They are mostly covered with vaults built with two main constructive systems, namely: (a) stone masonry vaults and (b) mix-system composed of stone masonry vaults with wooden logs. The vaults are usually supported by aligned longitudinal walls with large thickness or columns/pillars/pilasters. When lateral thrusts induced by vaults are high, external buttresses can be identified (García and Meli, 2007; Gogoy, 1984; INAH, 2020; Kubler, 2009; Rivera, 2003; Rodriguez, 2006; Tamayo, 2004b; Vega, Rubio, Garcia, Barrera, and Fernandez, 1945a, 1945b). It has been also realized that masonry Yucatan churches were mostly built progressively throughout long time, contributing for: (1) the absence or bad connection between the structural elements; (2) the use of different constructive technique and expertise used among structural elements; (3) differences in the structural behaviour.

Nowadays, these churches experience mechanical effects as cracking, deformations, tilts and settlements, which together with the material ageing and environmental effects, such as surface

alterations, disintegration and biological growth, has led to partial collapses at some churches, which need urgent rehabilitation works. The nature and origin of the damage remains unknown. Probable reasons for the damages are: 1) ageing of material, 2) differential settlements generated by lateral wall instability, 3) settlement of the foundations due to soil degradation or non-uniform soil stratigraphy, 4) support failure due to poor foundations or 5) stress concentrations. According to Nash (1961), the most probable reasons are related with the foundations problems, probably because during construction time, not much attention was paid to soil characteristics since the science of soil mechanics was developed after 1925. Therefore, it is considered that new knowledge about the structural behaviour of Yucatan religious buildings is relevant in the scope of the preservation of these buildings.

It is important to notice that a great number of worldwide investigations about masonry structures have been carried out. Indeed, masonry was identified as one of the most used structural systems in many worldwide historical buildings, especially in religious buildings, such as churches. Numerical and experimental campaigns have been carried out to gain knowledge about: 1) the assessment of mechanical behaviour of different structural components under different loading conditions 2) different types of retrofitting solutions and 3) the assessment of the efficiency of different strengthening /retrofitting interventions (D'Ayala et al., 2008; Lourenco, 2009; Mendes and Lourenço, 2009; Orduña and Lourenço, 2005; Roca et al., 2007).

However, limited studies are known on the structural analysis of ancient historical religious buildings in Mexico, particularly in case of rubble masonry composed of irregular masonry units linked with mortar. In particular, a search on detailed data about Yucatan churches revealed that there is not enough information about constructive processes, geometrical features, structural elements components and corresponding structural behaviours. Almost no experimental characterization exists on the raw masonry materials used in the constructions of that churches. Any information about the characterization of structural elements of the churches, namely masonry vaults, masonry walls or connections was found. Therefore, the research gap is relevant at different levels, namely at: (a) the material level, with lack of information on the mechanical behaviour of masonry material and masonry as a composite material; (b) the structural level mostly with the lack of insight on the behaviour of stone masonry vaults, representative of Yucatan churches, and interaction with masonry walls.

The research presented in this thesis focuses on churches built between the sixteenth and eighteenth centuries, located in Yucatan state and recognized as patrimonial heritage of Mexico. In fact, the

present research work intends to provide useful information and insight on: (i) the materials and mechanical properties of stone masonry representative of Yucatan churches; (ii) the structural analysis of typical stone masonry vaults under vertical settlements, assuming that this can result in the observed damage in the vaults; (iii) possible strengthening solutions aiming at improving the structural behaviour regarding to vertical settlements.

1.2. Research objectives

It is believed that differential settlements are the origin of several common structural damages on historical masonry constructions, and it is assumed that it can represent one of the possible causes of the damage observed in stone masonry vaults in Yucatan churches. However, throughout the literature review, it was observed that few studies have dealt with the problem of differential settlements and related damage. Since vertical settlements are much more difficult to simulate in laboratory tests than horizontal displacement, few research focused on this topic. Consequently, the effect of the settlement on the structural behaviour of masonry vaults and arches is not yet much explored.

Therefore, due to the scarce information on the mechanical behaviour of the masonry vault-wall system under settlements, the present work aims mostly at contributing to enlarge the experimental data concerning the mechanical behaviour and collapse mechanisms of stone masonry vaults typical from Yucatan churches under differential vertical settlements. The main specific objectives of this work are:

1) Morphological characterization of Yucatan churches. The aim is to define the most representative constructive system and obtain enough information about the main morphological characteristics of the structural elements and connections in order to reproduce them at the laboratory, as closely as possible to the real structures.

2) Geometrical characterization of Yucatan churches. Basic information about the geometry is relevant to assess the structural behaviour throughout experimental or numerical models.

3) Mechanical characterization of stone materials. The main goal is to identify the raw materials (stone and mortar), obtain the mechanical properties and study the stone masonry as a composite material.

4) Structural assessment of the behaviour of semi-circular vaults under vertical settlements and evaluation of the effectiveness of the application of a retrofitting system.

1.3. Research methodology

For the accomplishment of the research objectives, a research work plan was designed and planned. In this scope, four technical tasks were defined: (1) architectural survey and data collection; (2) geometrical characterization of Yucatan churches; (3) experimental material characterization and (4) structural assessment of stone masonry vaults. The development of the research work plan requires the use of different qualitative and quantitative research methods, namely; (i) preliminary literature survey and definition of research gaps; (ii) on site visual inspection and use of simple survey techniques; (iii) statistical data analysis; (iv) multi-scale experimental analysis. A scheme of the research methodology is illustrated in Figure 1-1.

The research will focus on religious constructions from the sixteenth to the eighteenth century from the southern Mexico (Yucatan region). Yucatan churches have different morphologic features of the structural elements (walls and vaults) and geometric characteristics identified by the span, total height, thickness and height for both walls and vaults, among others. Basic information about the geometry is relevant to assess the structural behaviour throughout experimental or numerical models, and thus typical profile of Yucatan churches must be defined as a representative geometrical model. The acquisition of morphologic and geometrical data (Task1) requires: (i) archive research, which include historical overview and architectonic styles, morphological and geometrical information available from public and private repositories, such as National Institute of Anthropology and History (INAH, acronym in Spanish), Dimension of Ecclesiastical properties and Sacred Art of the Archdiocese of Yucatan (DIBEAS, acronym in Spanish), Yucatan State Government Restoration Department, School of Architecture of the Autonomous University of Yucatan (FAUADY, acronym in Spanish) and Specialized engineering services of private businesses; (ii) in-situ visual inspection campaigns with photographic record of Yucatan churches, namely survey on partially collapsed churches. Besides the geometrical features, this phase is important for the characterization of the main structural elements such as walls, vaults, and walls-vaults connections. The geometrical characterization requires statistical analysis of the data collected on the churches inspected. The definition of the typical profile of Yucatan churches needs to be defined (Task 2), which will be made based on the churches database that should be built after archive and in-situ survey. The statistical analysis for the definition of the geometric characteristics of the church profile will require: (1) quantitative analyses of the data by (i) analysis of the presence of outliers; (ii) normality tests to evaluate whether the geometric data follows a normal distribution by both graphical and numerical methods. In this scope is also important to characterize

the normal distributions based on the measures of skewness and kurtosis and evaluate possible deviations from the Gauss distribution; (2) approximation to the most typical geometrical profile of Yucatan churches.

The materials characterization (Task 3) of the materials used on Yucatan churches intends to be carried out through multi-scale experimental testing campaign on different limestones involving; (1) material collection from partial collapse Yucatan churches; (2) physical and experimental mechanical characterization of limestones; (i) use of advanced experimental techniques to obtain information about petrographic and micro-structure of limestones, chemical and mineralogic composition; (ii) physical and mechanical characterization of small samples to obtain the main key physical and mechanical properties, see Table 1-1.

Table 1-1 Experimental characterization at the materials level

Macro-scale	Micro-scale
1. Physical properties: - open porosity, water absorption at atmospheric pressure and water absorption. - coefficient and capillarity porosity and capillary absorption coefficient.	1. Chemical identification through X-rays and EDS (Energy Dispersive Spectrometer) by SEM
2. Mechanical properties: compression strength, elastic modulus, uniaxial-strain diagrams and crack patterns.	2. Mineralogical identification by X-rays diffraction technique, for both natural and decarbonated samples
3. The relation between mechanical and physical properties of limestones is investigated through a set of statistical correlations based on the experimental data and using single regression analysis.	3. Analysis of micro-structures through scanning electron microscopy (SEM)

The fourth task will be composed of the experimental characterization of: (1) stone masonry as a composite material. It is intended to represent both stone and masonry vaults typical masonry bonds and obtain the key mechanical properties under uniaxial compression load; (2) experimental structural analyses of typical stone masonry vault under vertical settlements taking into consideration realistic walls-vault connection. It is intended to retrofit the stone masonry vault, test it again under the same loading condition to compare with the reference unstrengthen vault. The definition of the experimental models intended to be defined through morphological and geometrical features obtained in Task 1 and Task 2.

It is stressed that the research will focus on religious constructions from the sixteenth to the eighteenth century from the southern Mexico (Yucatan region), but it is considered that the knowledge gathered within this work can be applied in buildings around the world with similar characteristics. Therefore, one important output is the experimental data that will be available on the physical and mechanical properties stone masonry materials and vaults and possible guidelines for vaults retrofitting. The knowledge gathered on the mechanical behaviour and collapse mechanism of the plain and retrofitted

masonry walls-vault system under differential vertical settlements can be of great advantage in the decision process related to the strengthening possibilities of ancient masonry structures.

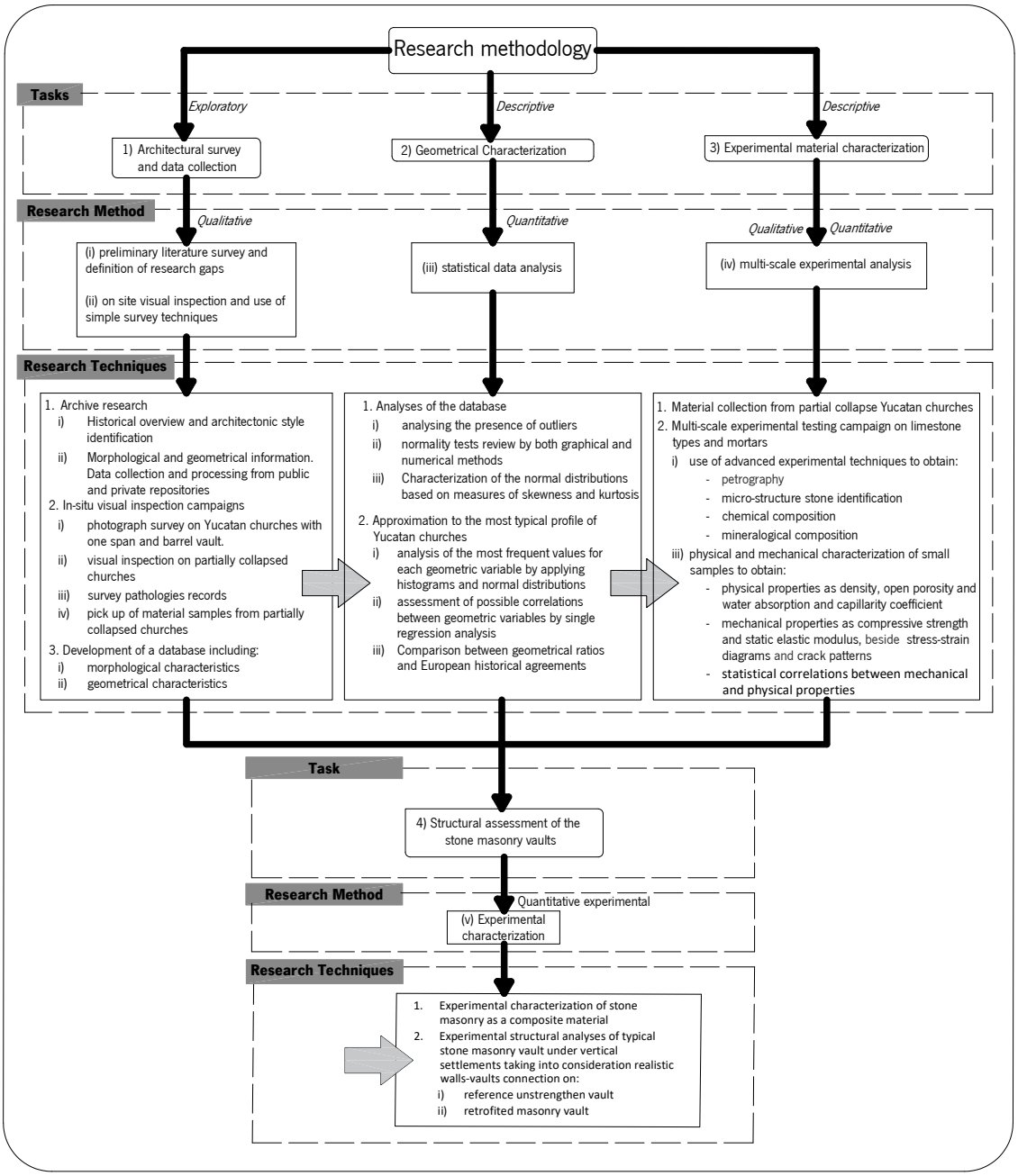


Figure 1-1. Research design diagram

1.4. Outline and organization of the thesis

The thesis is structured in eight chapters, see Figure 1-2. **Chapter 1** presents briefly the research motivation and objectives of this study, as well as the organization of the different chapters.

In **Chapter 2**, a detailed historical and architectonic review of representative Yucatan churches is provided. A description of architectural features and of the structural elements and connections is presented and discussed. In addition, an overview of the most common damage and decay patterns on materials and structural elements is also presented. This work is based on existing information from the literature and on the visual inspection carried out by the author in different churches of the Yucatan state, mostly from sixteenth to eighteenth centuries.

Chapter 3 deals with the definition of a database of 44 Yucatan churches with information obtained from archive research and in-situ inspection, which includes the geometric features of the churches´ cross-section. In this chapter, linear correlations are studied between the geometric parameters characterizing the typical cross section on one nave churches (e.g., span, total height, thickness and height for both walls and vaults, etc). Additional churches from different regions of Mexico intended to be also analysed and included for a systematic comparison. Besides the simple relations between basic geometric parameters as a function of the span of the churches with semi-circular canon vaults, further comparisons with empirical relations are provided in historical treatises from sixteenth to eighteenth centuries.

Chapter 4 aims at the characterization of limestones and mortars belonging to masonry churches from sixteenth to eighteenth centuries and located in Yucatan region in Mexico. In this chapter, details of the multi-scale experimental campaign are provided, and main results are presented and discussed. The advanced experimental characterization of local stones includes the petrographic and micro-structure of stone, chemical and mineralogical composition characterization. The physical and experimental mechanical characterization of stone is carried out on small stone samples to obtain the main key physical and mechanical properties.

Chapter 5 presents the effectiveness of two non-destructive tests performed (Schmidt hammer [N] and ultrasonic pulse velocity [UPV]) to predict physical and mechanical properties of the limestone from Yucatan churches. It aims also at understanding the influence of factors such as anisotropy and moisture content in the values of UPV. In this regard, a statistical study is carried out through statistic correlations between NDT indexes and physical and mechanical properties, as well as between physical and mechanical properties.

Chapter 6 details the activities and tasks needed to perform the experimental tests to characterize the structural behaviour of vaults under differential vertical settlements. In addition, the results of uniaxial compression tests carried out on a set of stone masonry wallets, representing walls and vaults

masonry bond, are presented and discussed. The main details of the experimental model composed of representative stone masonry walls, vault and walls-vault connection, intended to represent a scaled typical cross section profile of Yucatan churches are presented. The main results of the of the experimental test of the scaled cross-section model submitted to differential vertical settlement are presented and discussed. The analysis of results focuses in the displacement time evolution, rigid body movements, cracks patterns and definition of the main collapse mechanism.

Chapter 7 describes the retrofitting process the stone masonry vault tested in Chapter 6 and previously damaged. The technique to be used is a textile reinforced render mortar applied both at intra and extrados of the masonry vault. The analysis of the experimental results of the retrofitted experimental model submitted to vertical settlements includes the time- displacements evolution of the complete experimental model composed of the masonry walls and vault, relation with the development of cracks and consequent hinges experienced by the model, crack patterns and collapse mechanism. A comparative analysis between reference and retrofitted models is also provided.

Chapter 8 summarizes the main conclusions of the work and presents future research lines.

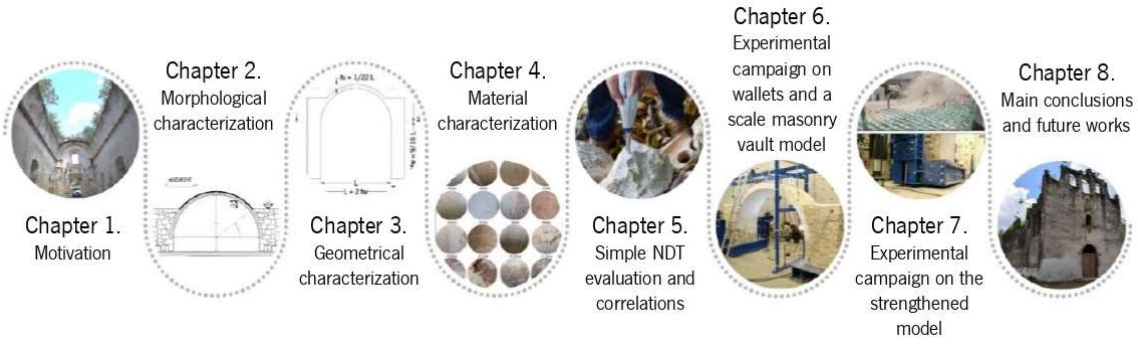


Figure 1-2. Scheme of the organization of the thesis

Chapter 2.
Architectonical, morphological, and pathological characterization

Abstract:
A detailed historical and architectonic overview of representative Yucatan churches is provided in this chapter. A description of architectural features, of the main characteristics of the structural elements and connections is presented and discussed. In addition, an overview of the most common damage and decay patterns on materials and structural elements is also presented. This work is based on existing information from the literature and on the visual inspection carried out in different churches of the Yucatan state, mostly from XVI to XVIII centuries.

2.1. Introduction

Yucatan churches consist of an important stock of the built heritage in Mexico. They are massive structures, where loadbearing stone masonry walls and vaults represent the main structural elements. Both stone masonry walls and vaults were built with limestone and lime mortar.

The first Spanish explorers arrived in America in 1492 developing a process of occupation. Some years later, Mendicant orders also arrived to carry out the spiritual conquest and evangelization of the different indigenous groups. The first to arrive were the Franciscans in 1523, the Dominicans arrived in 1526 and later the Augustinians arrived in 1533 (Gonzalez and Espinosa, 2015). The evangelization process was supported by the massive construction of churches everywhere they arrived. In 1545 the Franciscans started to construct the Yucatan religious buildings. In order to get control over the Mayan natives, churches were built over the most important Mayan constructions with the support of a huge number of inhabitants and taking into consideration the importance of the Mayan traditions. In places with higher population or higher importance to Mayan people, churches were built attached to convents. In small villages with lower population, religious temples as churches were the result of an evolutionary process involving different stages, see Figure 2-1: (1) construction of a first 'visiting chapel' or 'open chapel', which consisted in a presbytery without walls and ceilings; (2) completion of the first construction with adjacent volumes, in which walls and ceilings were added by using organic materials like wood and sheets; (3) replacement of organic materials by inorganic materials like limestone and lime (Landa, 1566). Masonry is amongst the most used structural systems in many worldwide historical buildings, especially in religious temples, such as churches. Since early stages of civilization, stone masonry became popular because of the easy availability or because of the associated social status.

According to the Mexican law, these stone masonry churches have been considered historical monuments in 2018, being thus considered as a built heritage legacy that is essential to preserve (Camara de Diputados, 2018). The requirement for conservation and repairing historical masonry constructions resulted in the development of different numerical and experimental tools aiming at describing the mechanical behaviour of materials and masonry structural elements, namely at the level of collapse mechanism under certain loading conditions, load capacities and strengthening possibilities (D'Ayala et al., 2008; Lourenco, 2009; Mendes and Lourenço, 2009; Orduña and Lourenço, 2005; Roca et al., 2007).



(a)





(a) (b)

Figure 2-1. Examples of; (a) evolutionary process by stages (Kalisch, 2005), (b) open chapel from Dzibilchaltún and (b) full church after the completion, Tixkuncheil, Baca, Yucatan. Photographs by (Montaño, 2020; Tixkuncheil, 2020)

Basic information about the geometry of buildings and structural elements and materials is required to design numerical and experimental models, namely features of the connections between structural elements and characteristics and mechanical properties of materials. With this respect, it should be mentioned that there is few or not consistent information regarding the mechanical properties of materials, and the configuration of the connections among the structural elements is not completely known and thus they are characterized by an important level of uncertainty. In Yucatan churches the knowledge of masonry bonds, cross sections of walls and vaults, of connections between walls and between walls and vaults, regarding to which also few information is available (Kalisch, 1997; Tamayo, 2004) is very scarce. In addition, only few works have been identified on the experimental characterization of masonry as composite material in Mexico old buildings (Chávez, Sánchez-Ramírez, and Meli, 2012; Fernández, Gómez, Varela, and Vargas, 2009; Tejeda and Silva, 2002).

Mexican churches present different plan typologies, namely: (1) one span, with or without lateral chapels; (2) three spans, also called basilica plan and (3) latin cross with single span (García and Meli, 2007; Gogoy, 1984; Kubler, 2009). Different types of vaults can be also observed, namely: (1) continuous barrel vaults with and without arches; (2) barrel vaults with lunettes, and (3) ribbed cross-vaulting (García and Meli, 2008). The churches with one span and barrels vaults are the most common typology (García and

Meli, 2008; Rivera, 2003). In particular, Yucatan churches present the three plan typologies mentioned before but with different vault typologies at the main nave, namely: (a) barrel vaults with and without arches, (b) groin vaults and (c) sail vaults with and without coffers. Some of the churches collapsed or exhibit pathologies such as: (1) important deformations of vaults; (2) longitudinal cracks at vaults intrados, showing a Y-shaped near the façade and presbytery walls; (3) longitudinal cracks at thirds of vaults extrados; (4) crack at the extrados of the vaults parallel to the cross section and very close to the façade wall; (5) detachment at the connexions between the façade and longitudinal walls through vertical or diagonal cracks; (6) cracks in the weak section of walls; (7) horizontal, vertical or diagonal cracks at the longitudinal walls; (8) detachment of buttresses and (9) cracks in the pilasters and arches of bell towers and belfry (Rodriguez, 2006). The assessment of reasons on the basis of such observed damage requires more research so that mitigation or repair measures can be provided. As these churches have different thickness for the walls and vaults and also for the height of the vaults, a research on a more detailed study of their geometry is required so that both accurate experimental and numerical models can be derived.

Therefore, to improve the knowledge about the common one nave (single span) Yucatan churches in Mexico, it was decided to carry out a detailed study on the historical Yucatan churches from sixteenth to eighteenth centuries. To achieve enough information about the architectonic, constructive and the most frequent damages of single span Yucatan churches, this chapter was structured in three stages: (1) preliminary studies, which include historical overview of the architectonic styles; (2) morphological characterization of main structural elements as walls, vaults and connections; (3) description of the main structural damages.

2.2. Architectural and morphological characteristics

2.2.1. Architectonic overview on Yucatan churches

The period called Viceroyalty of the New Spain developed since 1542, date of the foundation of the City of Merida, until the second third of the nineteenth century. This period was marked by different political phases such as the conquest, the colony war and independence. Since it was a long period, around 300 years, the architectural style in Yucatan suffered several transformations from simple prismatic volumes to diverse ornamentations in the buildings such as gargoyles of stone carved for evacuation of rainwater, arches, Tuscan columns and in some cases with Romanesque type capitals, balconies outgoing or flush with the wall with wooden bars. At the top of the walls pinnacles and battlements can also be seen. In

the corners, stone elements and mortar or stone cornices with simple mouldings are other characteristic elements (Ching, 2011; Navarrete, 1998).

The architectonic style on churches in the beginning of the second half of the sixteenth century was ruled by the Franciscan principles based on simplicity and poverty (Figure 2-2a). The bell towers were forbidden as an austerity message and instead of these the belfry was adopted (Figure 2-2b) (Martínez de Aguirre, 1995; Urióstegui et al., 2014). At this time, the use of vaults was only allowed in the presbytery of churches or in cathedrals, like San Idelfonso Cathedral in Mérida City which was built from 1562 to 1598 (Figure 2-3). It was the first cathedral built in North America, the oldest in Mexico and the second oldest in all Latin America, after Santo Domingo Cathedral in the Dominican Republic (Bravo, 2013; Bretos, 1992).



Figure 2-2. Architectonic style of the churches; (a) Franciscan architectonical style, (b) Belfry, (c) Bell towers and ornamentation added in the Motul church after 1754 (Kalisch, 2005), (c) example of churches built by secular clergy - Tecoh church from late seventeenth century (Tamayo, 2004). Photographs by (a) (Mendez, 2017), (b)(Cardos, 2008), (c)(Moreno, 2020) and (d) (Padilla, 2018)



Figure 2-3. Cathedral of San Idelfonso in Mérida, Yucatán. Photographs by (Méridaelite, 2020)

Over time, with the process of secularization and the law of suppression of religious orders, the existing churches suffered important transformations. This process took place gradually from 1581 to 1754, resulting also in the gradual transformation of the churches (Kalisch, 2005; Tamayo, 2004). In some churches, towers and ornamentations in their main façade were added (Figure 2-2c). The churches built by secular clergy followed other architectonic styles characterized by the bell towers with two or three height levels (Figure 2-2d) (Echánove, 1944; Ponce de Leon, 2000; Tamayo, 2004; Urióstegui et al., 2014)The architectonic trend called 'The Porfiriato' predominated in Mexico from 1877 to 1915. In this period, the President Porfirio Diaz established policies in the economic, political and in the socio-cultural sphere, leading to economic, social and political stability (Serrano, 2012). New stately mansions and churches inspired by French and Italian architectures were constructed. At the same time, several modifications were carried out in existing structures, namely ornamentations and finishing were attached to churches and regular houses. In some cases, they were so excessive to the point that the origin of the building's architecture is not recognized resulting in the architectonic style called eclecticism.



(a) (b) (c)

Figure 2-4. (a) Neoclassical architectural style. Lourdes Church from 1889 (Sulu and Navarrete 2014); (b) Neogothic architectural style. Our Lady of Carmen from 1908 (Niglio, 2016); (c) Architectural style Mannerist-Baroque like .Cantón Palace, which was built from 1904 to 1911 from (INAH, 2020b). Photograph from (a) (MTMM, 2013), (b) (Panoramio, 2018) and (c) (López, 2020)

The eclecticism style has four tendencies, namely neoclassical, French-fried, Mannerist-Baroque (observed only in palaces) and Neo-Gothic (Figure 2-4), which share common elements but have specific different characteristics. The common elements of these architectural trends are: (a) verticality in doors and windows; (b) frame away from the street and at a high level characterizing the social status of the owners; (c) access stairways; (d) lobbies of large dimensions and double height; (e) some houses with semi-basement; (f) ornamental profusion in carpentry and blacksmithing; (g) crests with vegetable or geometric representations, (i) shields (Ayuntamiento_de_Mérida, 2000; Ching, 2011; Navarrete, 1998; Rivero and Gutiérrez, 2013).

2.3. Systematic survey on selected Yucatan churches

In Mexico, the National Institute of Anthropology and History (INAH), is the highest federal representative that governs the properties declared as historical monuments. INAH developed a National Catalogue of National Monuments (INAH, 2020a), containing 117 churches considered as historical monuments from sixteenth to eighteenth centuries. In the catalogue, information about history, general architectonic plans or materials can be found but no detailed geometric information is available. Therefore, complex administrative procedures were followed to request the repositories with geometric information available in public and private institutions such as INAH, Commission of Ecclesiastical Properties and Sacred Art of the Archdiocese of Yucatan, Yucatan State Government Restoration Department, Faculty of Architecture of the Autonomous University of Yucatan and Specialized engineering services of private businesses. Combining the information gathered from the sources before mentioned with the information taken from literature (Tamayo, 2004; Vega et al. 1945a, 1945b), it was possible to define a database of 44 churches from sixteenth to eighteenth centuries (see Annex 2.1), which represent 38% of the existing churches in Yucatan state. The database was composed of three main sections, namely: (1) general information, which includes the location of the building, the identification number, name and construction century; (2) architectural features, including type of plan, material and typology by cross section of walls, typology and material of vaults and buttresses; (3) geometrical characteristics, namely all dimensions related to the main plan, walls and vaults such as span, lengths, heights and thickness. It should be underlined that additional visual inspection was performed on partially collapsed churches to better understand the morphology of the cross section of the main structural elements.

The statistical analysis of the walls belonging to the 44 churches under analysis shows that 100% of churches have very thick stone masonry walls with three leaves and some of them have passageways inside (Figure 2-5 and Figure 2-6). This configuration is similar to 'parapet-walkways' from medieval castles but inside the wall. Its literal translation from Spanish language is “road of round'' or ''road blind hen”. Passageways are modest galleries inside the walls that sometimes develop along the perimeter of the church (e.g. San Cristobal church in Merida city) and other times are located only in one section of the church, often in the longitudinal walls (e.g. Motul - first passageway built in Yucatan and Mama and Tixmehuac churches). There are particular cases where there exist two passageways in the same wall at distinct levels (e.g. Dzemul church). Its function aimed mainly the maintenance of the building (Tamayo 2004; Bretos 1987; Echánove 1944; Ramos 1989; Olmos 1994; Urióstegui et al. 2014).



Figure 2-5. Natural stone masonry of Yucatan churches. Chancenote Church

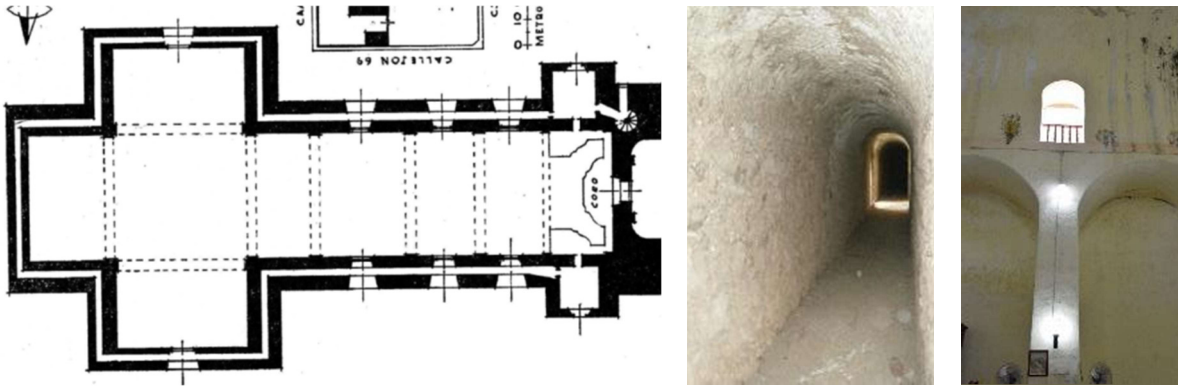


Figure 2-6. Architectonic plan of passageways, interior view and its connections with interior and exterior spaces of the church. Adapted from Vega et al. (1945)

Concerning to vaults, they are curved surface construction elements, usually built of stone masonry that works mainly in compression. The geometry of the vaults is generated by the translation of a generating arc in one or two directions or axes and, as a result, elements with simple or double curvature are obtained. They are usually supported on aligned longitudinal walls or columns/pillars/pilasters and have square or rectangular architectural plan. When lateral thrusts induced by vaults are high, they must be countered with different elements such as walls of large masses, buttresses or flying buttresses.

Its structural function is to cover large spans supporting its self-weight and the weight of other elements of normal use on the structure with adequate structural performance and without cracking. The vaults can be of different shape, composed of different materials and built with different construction methods. Regarding the shape, different typology of vaults can be found, namely barrel vaults with or without transversal arches, ribbed vaults, groin vaults and sail vaults with and without coffers. Regarding to materials, it could be built with stones, bricks or perishable materials such as wood. The constructive system is usually associated to the material, being the vault constructed with masonry using bricks or stones, or with a mix-system of wooden logs and masonry.

In this research the Yucatan churches were classified in four large groups according to the typologies of the vaults: (a) churches with vaults of Type 1, which are barrel vaults with and without arches; (b) churches with vaults of Type 2, built with wooden logs and infill masonry; (c) churches with vaults of Type 3, composed of groin and sail vaults with and without coffers; (d) vaults of Type 4, which were rebuilt or uncovered and were not considered in the present analysis. The Ribbed vaults were not mentioned because in Yucatan region, this typology was often used in the presbytery but not on the nave of churches. Examples of this type of vaults can be seen in the Churches of Mani, Dzidzantun, Valladolid, Izamal, Church of Nuns in Merida, among others, see Figure 2-7a. The statistical analysis of the 44 Yucatan churches in the database showed that 59% have barrel vaults (type 1), 14% of the churches have vaults of type 2 with wooden logs and infill masonry, 11% of the churches have groin or sail vaults (type 3) and about 16% of the churches have rebuilt or collapsed vaults (type 4). Concerning to the materials, limestone, lime and wooden logs were mostly used in Yucatan churches from sixteen to eighteen centuries. About the constructive systems of the vaults, two types of construction techniques have been identified, namely: (1) stone masonry vaults (Figure 2-7b), mostly found in constructions from the sixteenth century and later; (2) mix-system consisting of wooden logs filled with stone masonry and stiffened by masonry arches (Figure 2-7c), mostly seen in buildings of the seventeenth century or later.



(a) (b) (c)

Figure 2-7 Types of vaults; (a) ribbed vaults in presbyteries of Izamal, (b) stone masonry vaults; (b) mix-system vaults. Stone masonry with wooden logs

It is believed that the use of barrel vaults in Yucatan churches resulted from the original Spanish influence in the new Spain. However, different studies revealed that stone masonry barrel vaults were built from 390 to 250 BC in Mayan culture but with shorter spans (Carrasco, 2004; Eccott, 2003; Hohmann, 2005; Rodríguez Campera, 2008). This appears to indicate that the Mayan people gathered previous knowledge of this constructive system, which should have been recovered by the Spanish builders which adapted it to larger spans.

The selected Yucatan churches were also analysed regarding to the plan configuration through histogram diagrams (Figure 2-8). The results show that 77% of churches have a single span, 9 % of the churches have Latin cross plan configuration and 14% of the churches have three spans.

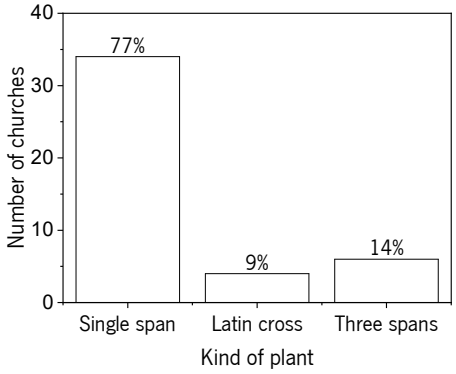


Figure 2-8. Typology of architectonical plan

2.3.1. Wall's morphology

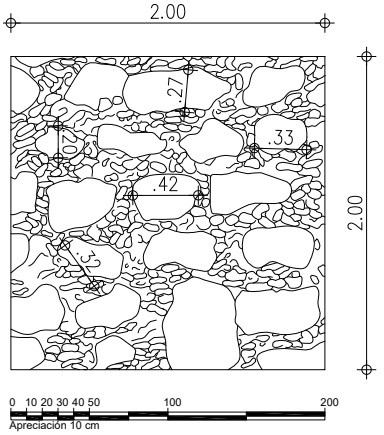
The analysis on the database with 44 churches showed that the walls of the selected Yucatan churches were mostly built with rubble masonry composed of irregular masonry units linked with mortar. In Yucatan state, the most abundant material is limestone and this justifies the reason by which the Yucatan churches were built always with limestone and lime mortar (Figure 2-5).

According to Kalisch (2005) and Tamayo (2004) Yucatan churches and monasteries from sixteenth to second third of the nineteenth century are characterized by ashlar masonry in façades and by ordinary masonry for the remaining walls. Both emphasize the use of local stone roughly carved and wide mortar joints due to the irregularity of the stones. Tamayo (2004) points out that: (1) the stone unit dimensions are not greater than 30 cm but larger size units can be used at the base of the walls; (2) the mortar joints are wedged with slim small stones horizontally placed. Both authors refer that horizontal joint are aligned. Regarding to vertical joints, Kalisch (2005) mentions that verticals joints are unaligned each two horizontal courses. This irregular masonry bond is observed in churches such as Sisal, Calotmul, Conkal, Ticum, Kini, Opichen, Popola, Tixmehuac, Chablekal, Ichmul and Ticuch.

Following the reduced information about the stone walls morphology, it was decided to carry out a survey on the masonry arrangement on selected churches. Taking into account the real scale of the masonry units, masonry bonds of the masonry walls were drawn. In each drawing, five dimensions of the stones were measured, and its average was calculated (d = average). From all average records, the general average of stone dimension (da) was calculated. It was seen that in the churches analysed, the masonry stones dimensions range from 0.20m to 0.60m, with an average (da) of 0.28m, see Table 2-1 and Annex

2.2. The stones were not worked or roughly worked, being placed as they were found in the quarries. Additionally, the stone that approach the rectangular shape have an approximate proportion of 1:2 (height:length) and the smallest dimension is not lesser than 0.20m. Regarding to alignment of mortar joints it is possible to recognize some type of horizontal alignment of the stones, but no vertical alignment was identified. It is possible to see that the stones are laid in very thick mortar joints.

Table 2-1. Characteristics of the masonry bond of walls. Sample from Conkal church

Zoom of photography	Masonry section	Dimension of stone
	 d = 0.31	 di = 0.30m

Regarding the cross section of masonry walls in Yucatan churches, no information was found in literature. Chavez et al. (2012) pointed out a proposal for the cross section of three stone masonry walls for buildings in centre of Mexico (Figure 2-9a). In case of Yucatan, based on the visual inspection carried out on partially collapsed churches, it was possible to observe that three-leaf walls predominate, which would be expected due to the high thickness. In secondary walls on the main buildings and belfry are mainly two-leaf walls. It was also observed that the outer-leaf do not show any other type of connection towards the inner part of the cross section apart from the mortar (Figure 2-9b). The internal leaf is a mixture mortar and smaller size stones raging in average from 5cm to 30cm. Both internal and external leaves are very well bonded with lime mortar. These observations are in concordance with Lourenço (1998) who states that when the walls are very thick, more than one leaf of masonry would be used, namely ashlar or roughly regular masonry at the outer-leaf and irregular stones or rubble masonry at the inner leaf. Additionally, studies developed by several authors on stone masonry walls, in Italy, Mexico and Portugal point out that the transversal section of the walls can have different configuration (Figure 2-9): (1) single leaf, either with ashlars or stones; (2) two leaves, either separated by a continuous mortar joint or with/without filling material; (3) three leaves made with two external leaves with ashlars or masonry and one internal leaf

made with different types of rubble filling (Binda et al. 1994; Borri et al. 2015; Chávez et al. 2012; Lourenço 1998; Mendes 2012; Rovero, et al. 2016).

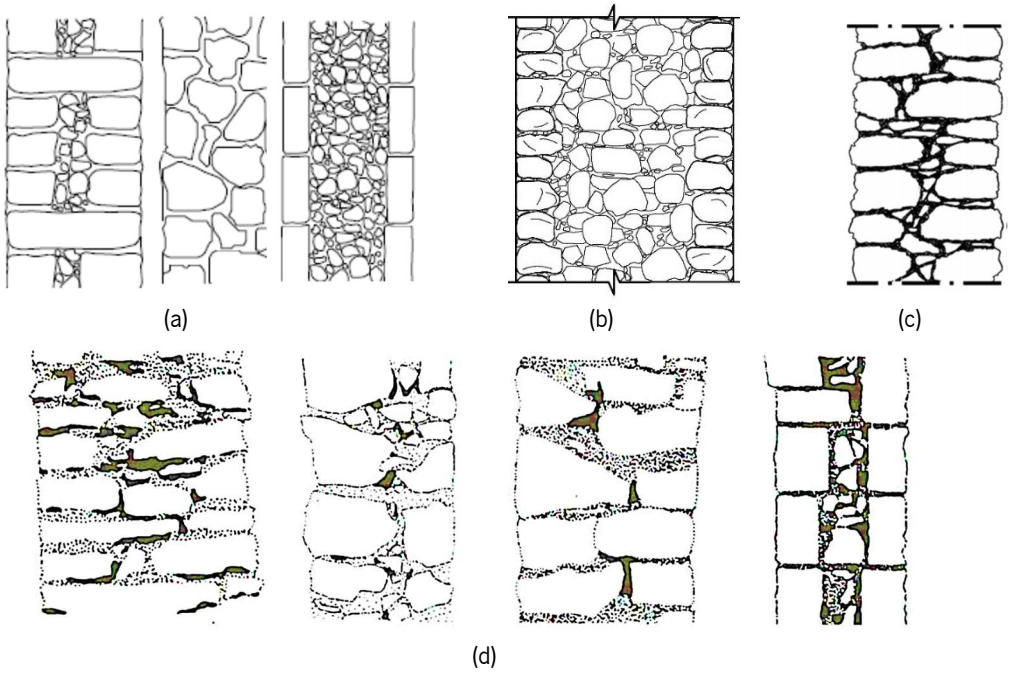


Figure 2-9. Some typical sections of the walls from (a) centre of Mexico (Chávez et al., 2012), (b) Yucatan churches (south of Mexico), (c) Italy (Rovero et al., 2016) and (d) Italy (Binda et al., 1994)

In relation to the wall connections, it was observed that stone ashlars were mostly used at the external corners (only external leaf) of the façade walls. Usually, the ashlars with greater dimension are placed at alternate courses to avoid continuous vertical joints and to achieve thus a good connection. Nevertheless, there are buildings where interlocking at the corners do not exist. In these cases, very deficient connections can be found due to the use of small vertical ashlars, working only as decorative. The connection between the walls should rely only on the use of abundant mortar to link all the mortar stone units. Indoor corners show no interlocking between the walls being seen often a vertical joint between the walls, revealing the absence of connections.

2.3.2. Vault's morphology

The availability of stone in local quarries influenced the preference for stone masonry systems. The stone vaults are characterized by the easiness of the execution system, by the possibility of covering larger spans and by the durability of the construction system. The visual inspections over the partially collapsed vaults mentioned before revealed that the cross section of the masonry vaults system is constituted mainly by three layers, namely: (a) a layer with flat stones working as voussoirs (Figure 2-10a and b); (b) a backfill layer with a thickness ranging from 5cm to 15cm composed of a mixture of small stones very well bonded with lime mortar (Figure 2-10b). This layer is regionally known as *bahpek*. According to Ramos and León

(2013), it can be classified as "Rigid or Cemented Filling"; (c) a thin layer of lime mortar applied as a finishing both at intrados and extrados (Figure 2-10b). At the extrados, the covering mortar was placed at certain slopes for water drainage.

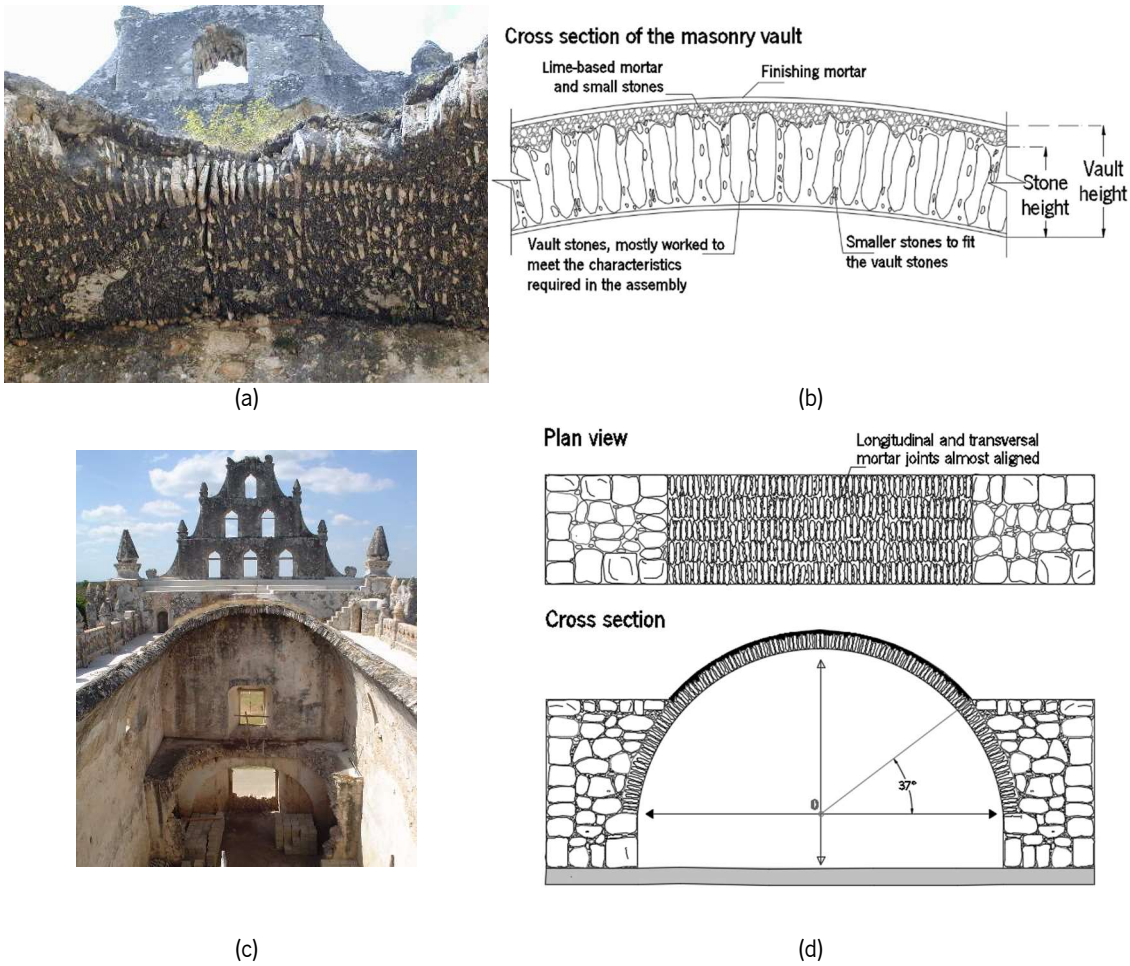


Figure 2-10. Cross section of masonry vaults; (a) flat stones working as voussoirs. Uayma, church; (b) detail of cross section of the vault, (c) backfill at the extrados. Uayma church (d) partial coss section of the barrel vaults and plan view focusing in the detail of the minimum interlocking of stones

According to Kalish (2005) and Tamayo (2004) the flat stones voussoirs have thickness (*t*) ranging from 0.10m to 0.15m, the height (*h*) varies from 0.30m to 0.40m and the depth (*d*) ranges from 0.40 m to 0.60 m. The stone masonry bond is characterized by longitudinal mortar joints and misaligned transversal mortar joints. The overlapping of the longitudinal stones is very small, being mostly attributed to the irregular size of the flat stones, which agrees with the visual inspection carried out in some collapsed Yucatan churches (Figure 2-10d).

This masonry bond is in agreement with the findings pointed out by other authors such as the ones observed in Pergamo and Efeso (Turkey) (Bachmann and Schwarting, 2013; Nohlen, 1999), Hidalgo and Morelos (Mexico), Amman (Jordan) (El-Khalili, 2014), Kazeroun, Kazerum and Firozabad (Iran) (Motlagh,

2010) and Merida (Spain). However, it should be underlined that running masonry bond is also commonly found in barrel vaults, namely in Yucatan, Mexico (Kalisch, 2005), Merida, Lerida and Guadalajara (Spain) (Ramos and León, 2013), and Pamukkale (Turkey), see Figure 2-11.



Pergamo, Turkey
(a)



Merida, España
(b)

Figure 2-11. Bond of stone masonry vaults; (a) longitudinal mortar joints and misaligned transversal mortar joints and (b) running masonry bond

2.3.3. Vault-wall connections

The wall-vault connections are mainly characterized by the embedment of the vaults starting stones into the masonry walls. In Yucatan churches, it is common that the free span of the vaults is reduced due to the extension of the wall's height over the extrados of the vault. This aspect will be analysed in detail in the present research (Figure 2-12).

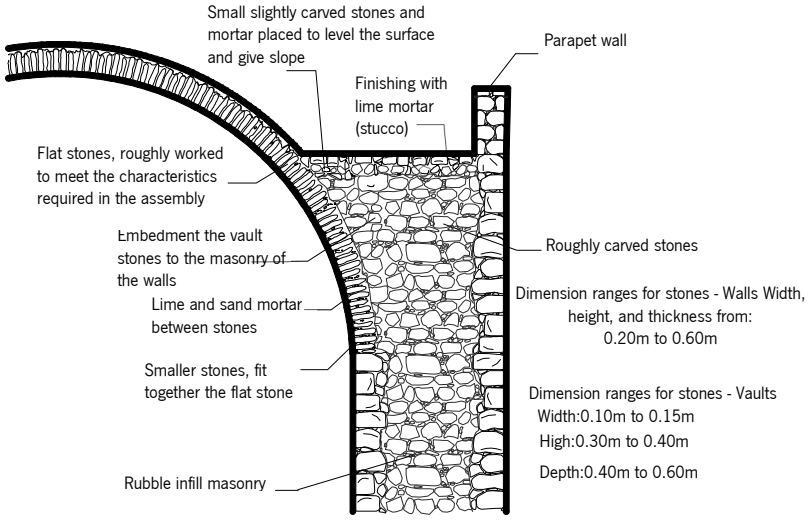


Figure 2-12. Backfilling in the extrados and wall vault connection. Proposal based on visual inspection

The apparent connection between the vault and the backfill material is only attributed to the irregular size of the roughly carved stones and cannot be considered as an intentional connection. Based on the visual

inspection of the partial collapsed churches, a scheme for the connection between barrel vaults and thick masonry walls is proposed in Figure 2-12. It should be mentioned that due to the difficulty in the visualization of this constructive detail, very few information on this issue is available in literature. Tamayo (2004) provided a detail on this connection for churches but with low thickness walls, see Figure 2-13a.

In case of churches with thick walls, two cross sections of the vault-walls connections were found in the literature and in certain extent are in agreement with the proposal provided herein. The first one is a representation of a barrel vault system used in archaeological Mayan site La Muñeca, in Calakmul (Eccott, 2003; Hohmann, 2005; Ruppert and Denison, 1943; Satterthwaite, 1944), see Figure 2-13b.

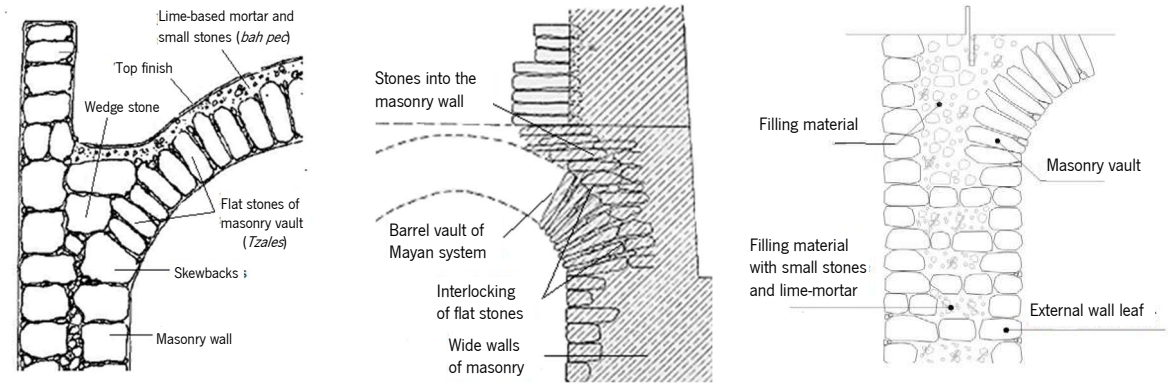


Figure 2-13. Some schemes provided for vault-wall connection; (a) vault - wall connection according to Tamayo (2004); (b) vault - wall connection according to Ruppert and Denison (1943) and Satterthwaite, (1944); (c) wall-vault connection according to Kalisch (2005)

However, in this case the interlocking between the flat stones used as voussoirs and the horizontal stones into the masonry wall appears to be slightly better. The second proposal for vault-wall connection was provided by Kalisch (2005) and is also close to the one proposed in this research (Figure 2-13c). In this scheme, connecting stone elements between internal and external leaves of the wall are identified, which could not be seen during the visual inspection carried out throughout the present research.

2.4. Characterization of common damages

Old masonry buildings may often present structural damage and non-structural decay. These can be the result of material ageing, environmental or mechanical effects. The material ageing and environmental effects on their constituents are related to the freeze-thaw, chemical reactions, bio-deterioration, biological growth among others. These effects can be classified as surface alterations, disintegration and biological growth. The mechanical effects appear when the fabric cannot resist increase of loads due to earthquakes

actions, extremely strong winds, foundation settlements, scour or modern loads on ancient structures. The mechanical effects can be identified mostly as cracks, deformations and tilts (or leaning).

Some of the churches collapsed or exhibit mechanical pathologies such as: (1) important deformations of vaults; (2) longitudinal cracks at vaults intrados, showing a Y-shaped near the façade and presbytery walls; (3) longitudinal cracks at thirds of vaults extrados; (4) crack at the extrados of the vaults parallel to the cross section and very close to the façade wall; (5) detachment at the connexions between the façade and longitudinal walls through vertical or diagonal cracks; (6) cracks in the weak section of walls; (7) horizontal, vertical or diagonal cracks at the longitudinal walls; (8) detachment of buttresses and (9) cracks in the pilasters and arches of bell towers and belfry (Rodriguez, 2006).

Structural damages were identified in Yucatan churches from visual inspection and recorded on a photography surveys. Both collapsed and no collapsed churches were reviewed in order to correlate the damage pattern between them. Also, material ageing and environmental effects were observed as surface alterations, disintegration and biological growth and are described herein. In this section, all pathology observed on visual inspection is described and identified with photographs. Note that in this review both structural and non-structural damages are described but not all pathologies were observed in the same church.

2.4.1. Structural damage

Cracks, deformations, and tilts were observed on both vaults and walls. In some cases, poorly performed interventions or lack of attention to mechanical damages caused the collapse of these churches.

It was also observed that the aging of materials, environmental effects and the lack of care and maintenance produce the mortar decay, which triggers progressive mechanical damages when the system with a deteriorated mortar is not capable of resisting the mechanical stresses demanded.

2.4.1.1. Cracking

Vertical cracks were observed in the façades resulting in the detachment of wall and at corner connection, see Figure 2-14a. Furthermore, above the door and window openings, considered as weak sections, cracks were observed on both façade walls and longitudinal walls (Figure 2-14b and c). Additionally, on longitudinal walls two different cracking patterns were observed, namely: (1) diagonal cracking closes the corner connection with the main façade and (2) horizontal cracks. Yucatan churches have spiral stairs (Figure 2-15a) placed inside of longitudinal walls next to the façade wall to get up at choir and rooftop.

The reduction in wall thickness, due to the staircase can be considered as a weak plane, and diagonal cracks suggest the out of plane displacement of the façade, see Figure 2-15b and c.



Tixhualactun (a) | Akil (b) | Kikil (c)

Figure 2-14. Cracking patterns: (a) detached connection between the façade and longitudinal walls, (b) cracks in weak sections of façade walls and (c) cracks in weak sections of longitudinal wall



Xcan (a) | Kikil (b) | Ticul (c)

Figure 2-15. (a) Spiral stairs of Yucatan churches, (b) inside view of diagonal cracking near the corner connection and (c) external view of diagonal cracking near the corner connection



Xcan (a) | Tixmehuac (b)

Figure 2-16. Cracking pattern in longitudinal wall – mostly horizontal cracking

In some churches, horizontal cracks were observed in longitudinal walls in both internal and external masonry leaf. Inside, the horizontal cracks are placed at approximately 1/3 of the wall height from the

ground and change to diagonal cracks with approximately 45° of slope near the door openings (Figure 2-16a). Theses cracks suggests an out-of-plan bending behaviour of the longitudinal wall.

Outside, the horizontal cracks have two different heights: (1) as shown in Figure 2-16b it is located at approximately 1/3 of the wall height from the ground and (2) as shown in Figure 2-17, the horizontal cracks can be located at approximately 2/3 of the wall height from the ground. In the exterior leaf the crack is aligned with the top of the opening (spyhole) of the passageways and can be the consequence of both poorly performed constructive stages or mechanical behaviour for weakness plane. These cracks suggest that the wall is not enough to offset the vault thrusts, which could be possible because in this place is located the passageways of the church (Figure 2-6) reducing the effective cross section of the wall. Inside of passageways frequently there are several damages and poor or no connecting elements, see Figure 2-18a.



Mama Xcan

Figure 2-17. Longitudinal cracks. (a) exterior view of Mama church, (b) exterior view of Xcan church

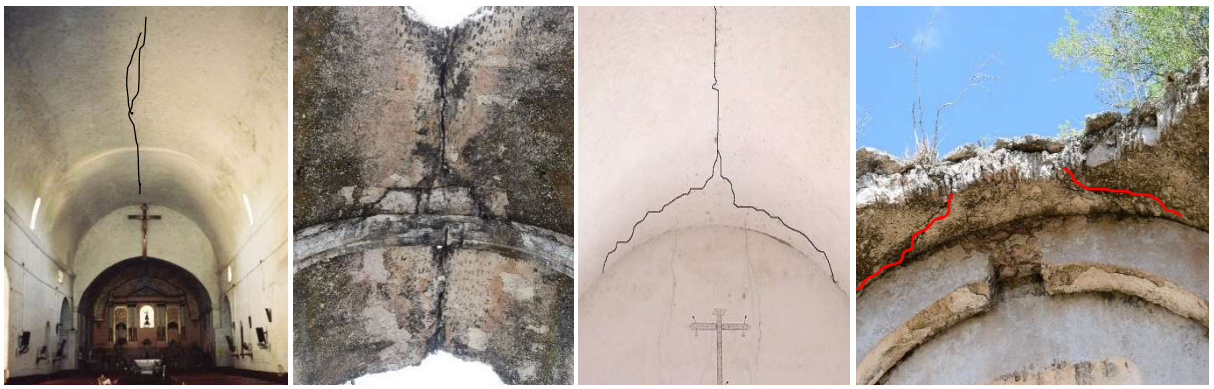
The damages observed on passageways were mostly cracks on walls and vaults, loss of units and of mortar (Figure 2-18). Due to this damage, holes in the masonry are observed. Sometimes, the crack in the keystone of the vault develops throughout the passageways and extends to the joint between vault and front wall (Figure 2-18b, c and d). Furthermore, important deviation of the keystone-crack at openings were observed (Figure 2-18b) until connect to the horizontal crack in the masonry exterior leaf (Figure 2-17). Since the thrust line on walls with passageways is not equal to solid walls, these cracks suggest that the longitudinal wall over the passageway is dividing into two parts because of the reduction of effective thickness of the wall and the redirection of the thrust lines. The cracks in Figure 2-18d showed thickness lower than 1cm. They were located close to the corner connection with the main façade, which means that they could be the internal damage described as diagonal cracks (Figure 2-15).



(a) (b) (c) (d)

Figure 2-18. Cracks inside passageway. (a) joint vault-wall inside the passageway, (b) crack located throughout the keystone, (c) keystone crack close to the end of the passageway, (d) cracking in vault and wall close to the façade and thickness-crack in vault (Tixmehuac, Yucatan)

Vaults are the most vulnerable structural element because its thicknesses, location and weight. Any very small displacement of wall or supports causes cracks in the vault. For this reason, both intrados and extrados were inspected in order to define the cracking pattern of this element. In the intrados of the vaults longitudinal cracks in the keystone were observed (Figure 2-19a and b). These cracks split in two near the ends of the vault, showing a Y configuration (Figure 2-19c and d).



Temax (a) Kikil (b) Mama (c) Kikil (d)

Figure 2-19 Crack patterns at the vaults: (a) longitudinal cracks in the keystone of the vaults, (b) longitudinal crack on collapsed vault, (c) cracking Y shaped pattern and (d) cracking pattern in Y shaped in collapsed church

The Y-shaped crack was observed in both 1) constant and 2) variable thickness vaults. Furthermore, the Y-shaped crack showed lower opening in vaults supported by walls of constant thickness, contrarily to the walls of variable thickness (with chapels). The same section at extrados shows visible transversal cracks close to the façade walls, which suggest the rotation of the facade wall towards the front, see Figure 2-20.

According to Rodríguez (2006) the Y-shaped crack is the consequence of edge-effect, which results from the interaction between the vaults and the masonry façade walls. This study was focused on vaults of constant thickness supported by walls with variable thickness (witch chapels). It was seen that the length

of the edge effect is important in a length ranging from 16% and 20% of total length of the vault for vaults with variable and constant thickness respectively (Figure 2-21).



Tixmehuac

Figure 2-20. cracking pattern at extrados near to façade wall section

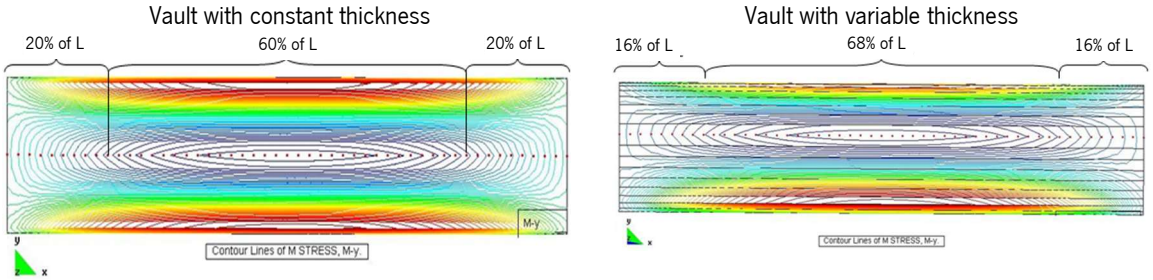


Figure 2-21. Influence of edge effects resulting from the interaction of the cannon vaults with frontal walls (Adapted by (Rodriguez, 2006)



Mama (a) Tixmehuac (b) Kikil (c) Tixhualactunc (d)

Figure 2-22. Cracking pattern in the rooftop and associated collapse

Additionally, at extrados the cracking pattern is characterized by tow cracks at thirds of the vault further mortar detachment and humidity (Figure 2-22a and b). When these damages are not repaired, the consequent collapse occurs, as supported by the cases of the Kikil and Tixhualactum churches. (Figure 2-22c and d). Furthermore, often that vaults in the rooftop shown a longitudinal crack close the walls, as illustrated in Figure 2-22b. Probably this crack is the same crack observed as damage in the passageways vault (Figure 2-18b and c). All observed before could be the first signs of mechanisms that conduce to the collapse, the centre part of the vault as shown Figure 2-22 c and d.

The choirs in the Yucatan churches were usually built with reduced-vault and using the same constructive typology as main vaults. They were used as mezzanine and thus the extrados of the vault was filled with rubble filling (Figure 2-23).



Mama Tixmehuac

Figure 2-23. Barrel vault with shorter high and cracking pattern form both (a) Mama and (b) Tixmehuac churches



Figure 2-24. (a) Collapse of both main and choir vaults in Uayma church and (b) closeup view of the collapse reduced vault in the choir

Nowadays, these vaults show cracks close to the supports, approximately at ¼ of the span (Figure 2-23). In churches where the choirs collapsed, these cracks described a semi-circular shape in plan-view (Figure 2-24).

The buttresses are not a very common constructive element in the Yucatan churches and the existing buttresses frequently were used as corrective element, so they were added after the church was finished. Therefore, they are connected in an adequate way to the longitudinal walls, which is confirmed by the cracks along the interface between the buttresses and walls (Figure 2-25).



Xcan Tixmehuac Mama

Figure 2-25. Cracks in the joint buttresses-wall for three different churches (a) Xcan, (b) Tixmehuac and (c) Mama

2.4.1.2. Deformation

The most visible deformations are located generally is in the vaults. The vault shows longitudinal and transversal deformations. In some cases, previous interventions have negatively affected the structural continuity, mechanical behaviour and the appearance of the vaults, see Figure 2-26.



Xcan Tixmehuac

Figure 2-26. Vault deformations in the Xcan church

Resulting from the deformation, these vaults have different height along the longitudinal direction, being higher at the extreme (for example close the main façade) than at the centre of the vault (Figure 2-27). On the other hand, the span of the vault at centre is bigger than extremes (Figure 2-28), since at plant level the same transversal dimensions along the church were observed. The increase of the span probably is due to the lack of out-of-plane restriction in the walls due to the absence of buttresses. Therefore, only both the façade and presbytery walls restrain the out-of-plane displacement of the longitudinal wall, leaving the centre unrestricted.

The three-dimensional survey of the church with a total station allow the determination of the cross and longitudinal section of the church at the point of interest, using computer-aided design software and without destructive tests (Figure 2-27 and Figure 2-29). The behaviour of the vault with and without out-of-plane restraints is generally analysed by comparing the cross sections of the centre with respect to the ends. It is also common that semi-circular cross section presents different deformations along the length of the vault. Figure 2-29 superimposed the geometry and shows the vault deformation near the main

façade (line 1), in the centre (line 2) and near the back-façade (line 3). From this, it is evident the important transversal deformation of the full vaults.

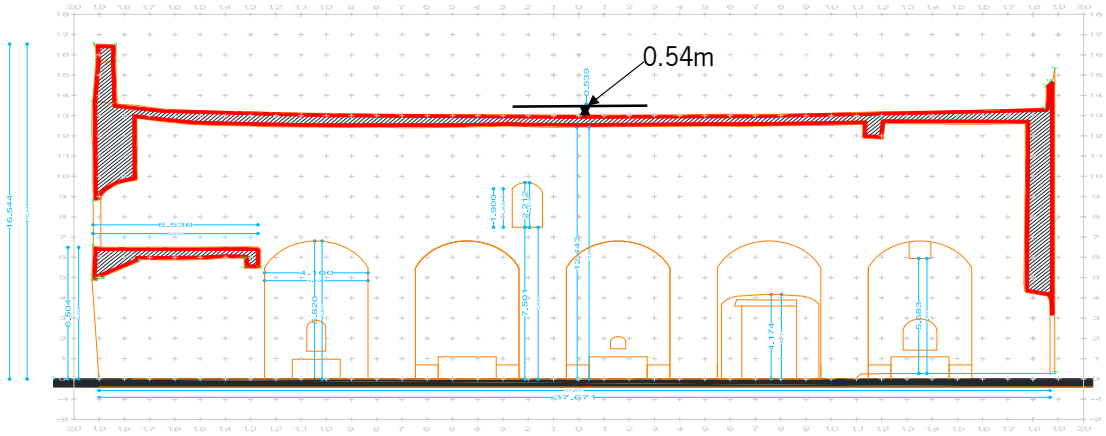


Figure 2-27. Longitudinal section at keystone of Tixmehuac church

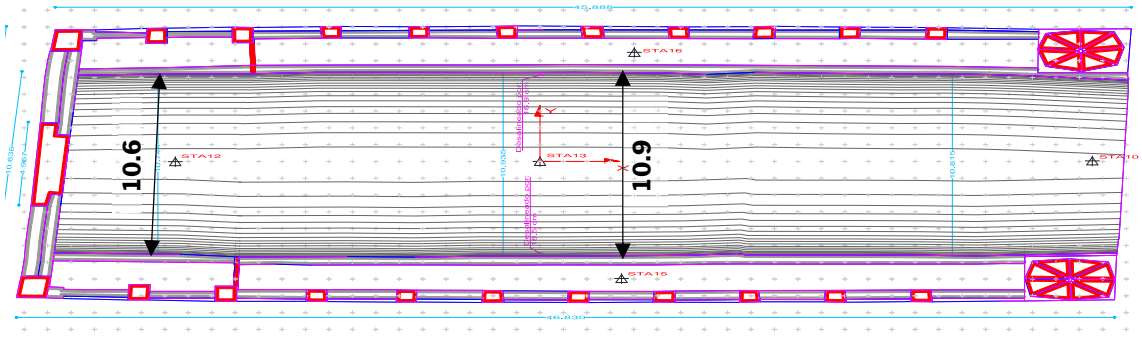
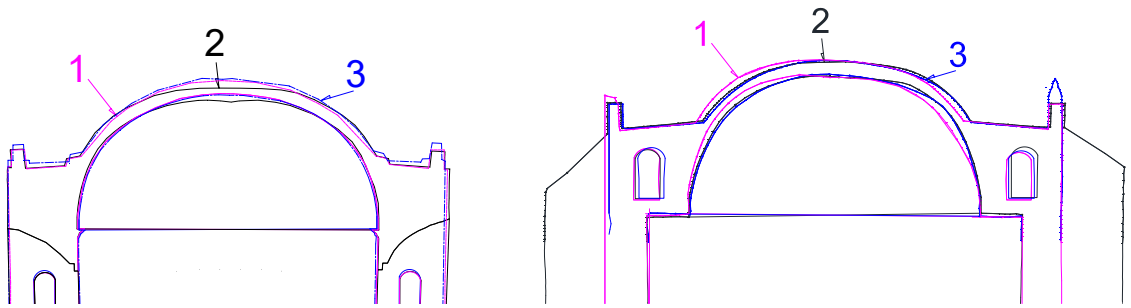


Figure 2-28. The span of the vault at centre is bigger than extremes. Xcan church

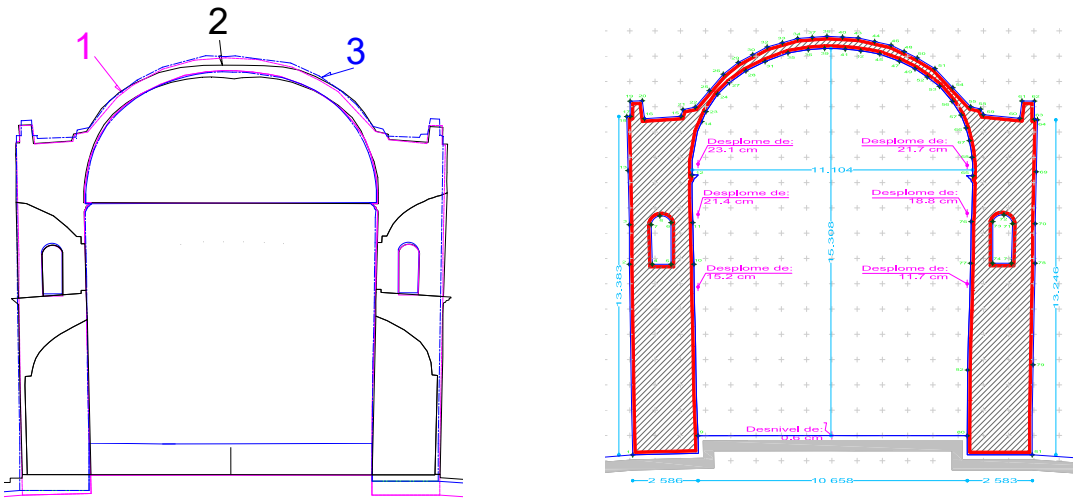


(a) Xcan (b) Tixmehuac

Figure 2-29. Deformations of cross section in the vault near the main façade (line1), in the centre (line2) and near the back-façade (line 3)

2.4.1.3. Tilts (or leaning)

The longitudinal walls show out of plane tilts as illustrated in Figure 2-30. The span between supports is shorter than the vault span, indicating that the walls are inclined. From a total station survey of 5 cross sections of the church, it was possible to see that the tilt sizes were from 0.12m to 0.30m being higher in sections far from the front or back façade walls.



(a) Xcan (b) Mama

Figure 2-30. Tilts in walls (a) superposition of the cross sections at the main façade (line1), in the centre (line2) and near the back-façade (line 3) and (b) an example of the tilt dimensions measured in each cross section.

In some churches, main façade shows out of the plane displacement (Figure 2-31a), which results in mostly vertical cracks and detachment of the main façade from the towers (Figure 2-31b,c).



(a) Tixhulactun (b) Kikil (c) Ixcan

Figure 2-31. Out of the plane displacement (a) a clear tilt between wall towers and centre part of the wall, (b) the typical cracking pattern in the main façade of partial collapsed churches and (c) the typical cracking pattern in the main façade after retrofitted works

2.4.2. Material ageing and environmental effects

The stone of churches shows typically surface alterations as detachment, material loss, chromatic changes, deposits and biological colonization.

Detachment decay patterns as blistering, disintegration, and fragmentation were observed in almost all observed churches (Figure 2-32and Figure 2-33). Blistering and disintegration are decay patterns that develop as a consequences of material ageing. Fragmentation is a decay patterns that can result also: (1) from human activities which hit hard on the stone: (2) because the stone blocks are subjected to overloads, which means, large weight supported by a small area.



(a) Ichmul



(b) Opichen

Figure 2-32. Examples of detachment decay patterns. (a) blistering and (b) disintegration



(a) Xcan



(b) Opichen

Figure 2-33. Examples of detachment decay patterns. (a) fragmentation and (b) disintegration

The material loss can be reported in different ways as: (1) erosion with loss of the matrix in the stone (Figure 2-34a), (2) erosion of mortar in the masonry joins (Figure 2-34b), (3) missing parts as consequence of environment events such as lightning or anthropogenic activities (Figure 2-35a) and (4) perforations as a consequence of drilling for research purposes, repairs, loss of cohesion of the mortar or anthropogenic activities, see Figure 2-35b.



(a) Opichen



(b) Sisbic

Figure 2-34. Material loss, (a) matrix loss in stone units and (b) mortar loss on masonry stone walls



(a) Chancenote



(b)-Xcan

Figure 2-35. Material loss. (a) missing parts due to lightning strike and (b) perforations on masonry stone wall due to anthropogenic factors

The chromatic alterations were observed in three different ways: (1) crust, (2) chromatic alterations and (3) superficial alterations and deposits. Both black crust and salt crust were observed (Figure 2-36). Regarding to Chromatic alterations, it is referred to colouration, bleaching, moist areas, and staining (Figure 2-37 and Figure 2-38). Deposits, graffiti, and soiling were also seen (Figure 2-39).



(a) Opichen



(b) Mérida, La Mejorada

Figure 2-36. Examples of crusts, (a) salt crust on decorative elements and (b) black crust under the cornices of facades



(a) Petulillo



(b) Tabi

Figure 2-37.Chromatic alterations (a) colouration inside the churches and (b) bleaching facades



(c) Chancenote



(d) Tetiz

Figure 2-38. Chromatic alterations (a) moist areas clearly identified on vaults and (b) staining in lateral façade



(a) Ichmul



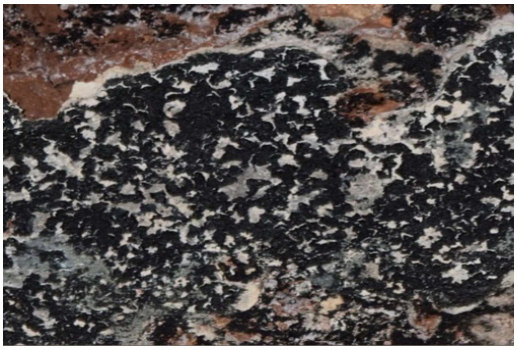
(b) Mama

Figure 2-39. Superficial alterations and deposits (a) due to anthropogenic factors, graffiti and (b) soiling due to lack of maintenance

In almost all churches biological colonization, such as algae, lichens, moss, and plants, was recorded (Figure 2-40 and Figure 2-41). The natural stone masonry of Yucatán churches is an irregular material with a high content of mortar capable of absorbing water and keeping humid. These are characteristics that provide an ideal environment for the colonization of organisms and plants adapted to living in rocks, capable of growing and develop in these kinds of environments.



(a) Kikil



(b) Chancenote

Figure 2-40. Examples of biological colonization. (a) Algae-and (b) Lichens

Churches that remained closed for a long time show important biological colonization (algae, lichens, moss, plants) due to lack of ventilation and sunlight, humidity concentration and lack of maintenance. The roots of biological colonization developing outside create access chains to rainwater, which wash the

fine material and cause the deterioration of the masonry in both vaults and walls. The excess moisture causes also loss of cohesion, erosion, blistering, detachment, and disintegration of the mortar.



(a) Tixhualactun (b) Petulillo (c) Sucopo

Figure 2-41. Examples of biological colonization. (a) moss, (b) Plants and trees, and (c) tree roots inside masonry after collapse

The most frequent and destructive tree found in Yucatan churches is the Ficus maxima Mill (Herbario CICY, 2020), local name *álamo*, see Figure 2-42. This type of vegetation is one of the most difficult to remove since the roots are very resistant to commercial fungicides. Due to this, local practices to remove the tree are very dangerous and put the building at greater risk. In common practice, the inhabitants pour kerosene and set it on fire, which further deteriorates the masonry. Therefore, the growth of plants in masonry is considered one of the most harmful pathologies because it develops slowly and can be very destructive over time.



Figure 2-42. a) Alamo tree from (Herbario CICY, 2020), b) Alamo on masonry construction and c) masonry after burning roots
Concluding Remarks

2.5. Concluding remarks

The main aim of this work was to study the morphological and general geometrical characteristics of representative Yucatan historical churches. The architectural review show that Yucatan churches are mostly of single span, have stone barrel vaults and thick stone masonry walls. Morphological studies reveal that the masonry walls are three leaves through the thickness and were constructed mostly

disorderly as only horizontal joints are roughly aligned and the round stone units were roughly cut. Regarding to the connections between transversal walls, it was seen that: (1) in walls built at the same time, the connection is assured by the monolithic behaviour of the composite material composed of round limestone with different dimensions linked by lime mortar; (2) in walls built at different times, the connection usually does not exist or it is poor by using stones units as connectors each 2 or 3 stones layers. The vaults have a configuration similar to the stone roman vaults, characterized by longitudinal mortar joints aligned and the transversal mortar joints not aligned with a minimum interlocking associated to the irregular size of flat stones.

The damages observed are the result of the lack of both maintenance and use of the churches. These two factors contribute to increase both the percentage of humidity inside and the biological colonization outside. The roots of biological colonization outside open the way to the rainwater, which wash the fine material and cause the deterioration of the masonry in both vaults and walls. While the excess moisture causes loss of cohesion, erosion, blistering, detachment, and disintegration of the mortar. This type of decay results in the decay of mortar and triggers the mechanical damage observed since the system with a decayed mortar is not capable of resisting the mechanical stresses demand. Among the mechanical damages, it is important to mention the cracking, deformation, and tilting. It is suggested that the most dangerous cracks are placed longitudinally in the vault, while the largest tilting and deformations are located in the middle of the vault length. These damage cracks, deformations and tilting need to be addressed promptly since they combined can induce structure collapse.

Chapter 3.
Geometrical characterization

Abstract:
A database of 44 Yucatan churches was built with the geometric features of the cross section and linear correlations were studied between the geometric parameters. Additional churches from different regions of Mexico were also considered for a systematic comparison. Besides, simple geometric relations between geometric key parameters as a function of the span of the churches with semi-circular canon vaults were derived and further compared with empirical relations provided in historical treatises from sixteen to eighteen centuries was carried.

3.1 Introduction

As mentioned in Chapter 2, aiming at characterizing the main geometric and morphologic features of Yucatan churches from sixteenth to eighteenth centuries, a database with 44 churches was defined. This database represents about 38% of the existing churches in Yucatan state. The database was composed of three main sections, namely: (1) general information, which includes the location of the building, the identification number, name and construction century; (2) architectural features, including type of plan, material and typology by cross section of walls, typology and material of vaults and buttresses; (3) geometrical characteristics, namely all dimensions related to the main plan, walls and vaults such as span, lengths, heights and thickness.

This chapter is focused mainly on the geometrical characterization based on the features of the 44 churches of the database. This aims at finding geometric relations between geometric key parameters of the structural elements and to derive empirical rules describing the representative profile of the typical cross section of the churches. In addition, given the inexistence of construction treatises in Mexico (N. García and Meli, 2007), a comparison was carried out between the derived geometrical rules for one nave Yucatan churches with barrels vaults with geometrical rules provided in European historical construction treatises.

It should be mentioned that geometric characteristics of buildings are of utmost importance if experimental and numerical analysis is required to assess its structural behaviour, which justify an increasing interest in inspection and representation of 3D geometrical models of existing buildings. For example, the knowledge of possible geometrical rules that were in the basis of construction of structural elements, such as vaults, is particularly useful in case of buildings characterized by this constructive element. According to Brencich and Morbiducci (2007) scarce studies are available on the geometric characteristics of historic structures that enables an enlarged and systematic analysis of this construction typology.

3.2 Yucatan churches database – geometrical information

From the previous reviews on Chapter 2 on a database whit 44 churches from Yucatan, which represent the 38% of churches on Yucatan region, different plan typologies were register as (1) one span, with or without lateral chapels; (2) three spans, also called basilica plan and (3) latin cross with single span; furthermore different types of vaults, namely: (1) continuous barrel vaults with and without arches; (2) barrel vaults with lunettes, and (3) ribbed cross-vaulting, from which it was clear the

predominance of single span churches with continuous barrel vault, both walls and vaults based on natural stone masonry. Aiming at obtaining a better idea about their geometry features for further structural and experimental assessment, it was decided to perform a statistical analysis of some geometric parameters characterizing the cross section of one nave churches. The dimensions characterizing the typical cross section of the one span Yucatan churches are the span (*L*), length (*d*), total height at intrados (*H*), height of the wall (*Hw*), height of the vaults (*Hv*), thickness of masonry walls (*tw*), thickness of vaults (*tv*) and the height of backfill at the extrados (*Ew*) (Figure 3-1).

An investigation of the possible correlations between some selected variables through statistical analysis will be carried out. For this, two approaches will be followed, namely: (a) statistical analysis of main geometric parameters (section 3.3) and (b) derivation of empirical relations (section 3.4). In addition, the geometrical ratios between backfill height with both span and height of the vault will be investigated. An analysis of the reduction of the vault span induced by the backfill and its ratio with the European historical construction treatises is also provided (sections 3.5 and 3.6).

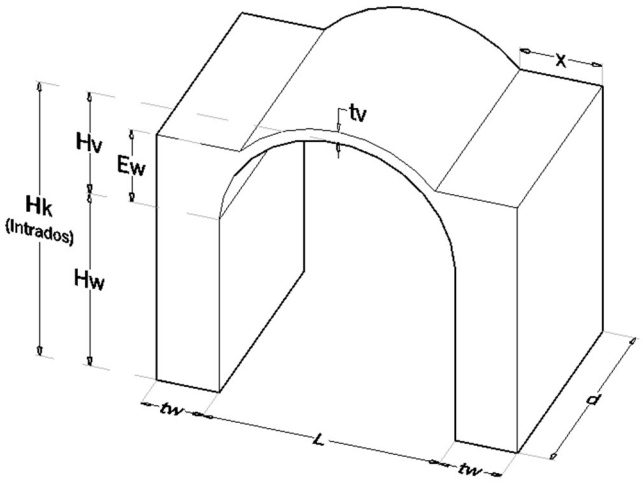


Figure 3-1. Key geometric variables of the cross section of one span churches

The statistical analysis on the database requires a previous quality of the data by analysing the presence of outliers. After this, simple regression analysis is carried out to investigate the statistical dependence between two parameters. In addition, the histogram of each parameter should be defined, and different distribution models were studied to understand which statistical distribution model better described the data. Normality tests needs to be performed to examine whether the data values follow a normal distribution by both graphical and numerical methods. For each distribution model, Goodness-of-Fit tests are going to be performed using the empirical distribution function (EDF). The

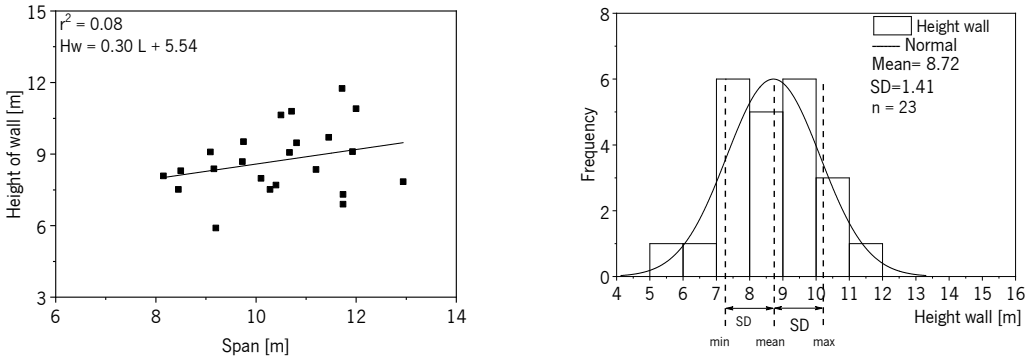
characterization of the normal distributions is then carried out based on the measures of skewness (s) and kurtosis (k) to evaluate possible deviations from the Gauss distribution.

This statistical analysis will be also extended to other Mexico churches from other regions, so that a comparison with the results obtained in Yucatan churches could be carried out. For this, wide literature review was performed on churches with one span and barrel vaults from Oaxaca (south), Michoacan (west) and Morelos (centre). From this information, it will be possible to define a database with other Mexican churches (Alejo et al., 2014; García et al. 2008; INAH, 2020b; Kubler, 2009).

3.3 Statistical analysis of main geometric parameters

In a first phase (Phase 1), it was decided to find general statistical correlations between the different geometric key parameters by considering all the churches in the database (44 churches), independently on the type of vault and the type of plan configuration, even if as already mentioned, 77% of the churches in the database were single span churches. In the second phase (Phase 2), it was decided to consider only churches with barrel vaults, regardless the shape, namely semi-circular, high vaults or reduced vaults (26 churches). Finally, the third phase of analysis (Phase 3) considers only semi-circular barrel vaults (15 churches with Hv=0.5L, ±10%).

From the data, for each phase and for each geometric variable previously mentioned characterizing one span churches (Figure 3-1), regression analysis was carried out aiming at assessing the possibility of a correlation between two variables. From the regression analysis, equations corresponding to the best-fit and coefficients of correlation (r^2) were derived. In this research it was assumed that a coefficient of correlation (r^2) greater than or equal to 0.6 would be acceptable, see Figure 3-2a and Table 3-1. In addition, the analysis of the most frequent values for each geometric variable was also carried out through histograms and normal distributions of the data were studied to assess its efficiency in the statistical description of the variable, see Figure 3-2b. From these, it was possible to define minimum, maximum, and average values of the main frequencies and evaluate the percentage of data lying in specific intervals by applying the 68–95–99.7 statistic rule. This procedure allowed to assess the percentage of data lying within a range centred in the average value with a length of two, four and six standard deviations (SD), representing 68.27%, 95.45% and 99.73% of the data, respectively. In this research, the assessment of normal distribution was based on the range corresponding to 68% of the data within the range ±SD, see Figure 3-2b.



(a) (b)

Figure 3-2. Statistical analysis; (a) single regression between the span (*L*) and height of wall (*Hw*) - Phase 2; (b) histogram defined for the height of walls (*Hw*) and adjustment of normal distribution. See 72Annex 3.1

Regarding to the single regression analysis between all key geometric parameters by considering all data (complete database) (Phase 1), it is observed that the coefficient of correlation is very low for all defined correlations, see Table 3-1and Annex 3.1. The unique exception is the relation between the total height of the churches (*H*) and the height of the walls (*Hw*), for which a coefficient of variation greater than 0.60 (r^2*=0.87*) was achieved. The equation for this linear fitting is *Hw=0.75 H-1.8*, which means that the height of the walls (*Hw*) is probably governed by the total height of the churches and not by the type of vault adopted. Additionally, the height of the walls (*Hw*) could be predicted approximately as 75% (±1.8m) of the total height of the church (*H*). When the churches with barrel vaults are considered (Phase 2), it is seen that three statistical correlations with a coefficient of correlation greater than 0.6 were found between geometrical variables, namely: (1) height of the vault (*Hv)* vs span (*L)* (r^2*=0.73*); (2) height of the vault (*Hv) vs* total height of the church *(H)* (r^2*=0.64*); (3) height of the walls (*Hw) vs* total height of the church *(H)* (r^2*=0.92*). This appears to indicate that the height of barrel vaults (*Hv*) can be obtained with a reasonable accuracy through the following expressions *Hv=0.39L+1.06* and *Hv=0.28H+1.18* and height of the walls (*Hw)* can be obtained through the expression *Hw=0.72H-1.18.*

As expected, by considering the data corresponding to the churches with semi-circular barrel vaults (Phase 3), the correlation between the height of the vaults and the span is very significant (*L* vs *Hv*, r^2*=0.92*). Similarly, the correlation between the height of the walls (*Hw*) and the total height of the church *(H)* is also very good (r^2*=0.90*). In addition, the correlation between the total height of the churches (*H*) and the span (*L*) is statically reasonable (r^2*=0.61*) but no other significant statistical correlations between the other geometric key parameters were found (Table 3). Therefore, it should be stressed that the single regression analyses revealed that with the previous mentioned exceptions, no major general evidence about statistical correlations was found between the geometric parameters.

Table 3-1. Coefficient of variation obtained for statistical correlations between different geometric key parameters

	Phase 1		**Phase 2**		**Phase 3**	
Variables	r^2	Data number	r^2	Data number	r^2	Data number
Hv vs ***L***	-	-	0.73	20	0.92	15
Hw vs ***L***	0.20	33	0.08	23	0.35	14
tv vs ***L***	-	-	0.10	10	0.17	8
t***w*** vs ***L***	0.002	41	0.40	19	0.22	11
H vs ***L***	0.38	35	0.19	25	0.61	14
tv vs ***Hv***	-	-	0.55	8	0.55	8
tw vs ***Hw***	0.03	31	0.14	23	0.13	13
tv vs ***tw***	-	-	0.07	10	0.10	8
Hv vs ***Hw***	-	-	0.24	24	0.18	15
Hv vs ***H***	-	-	0.64	24	0.46	15
Hw vs ***H***	0.87	32	0.92	24	0.90	15

On the other hand, by considering the analysis of the histograms defined for each key geometric parameter and the associated statistical distribution (normal or lognormal), mainly considering the results of Phase 2 and Phase 3, it was possible to define the most frequent values and to define the dimensions of the cross section of single span churches and barrel vaults, see Table 3-2. A schematic representation of the typical cross section derived from the analysis of Phase 3 and by considering the minimum, maximum and average values is shown in Figure 3-3.

Table 3-2. Selected frequency range for each phase

	Phase 1			**Phase 2**			**Phase 3**		
Frequencies Variables	Minimum (m)	Maximum (m)	Average (m)	Minimum (m)	Maximum (m)	Average (m)	Minimum (m)	Maximus (m)	Average (m)
Span	Nr[1]	Nr	Nr	9.25	11.71	10.48	9.06	11.26	10.16
Height wall	7.35	10.15	8.75	7.31	10.13	8.72	7.23	9.89	8.56
Height vault	[2]	[2]	[2]	4.43	5.57	5.0	4.47	5.61	5.04
Thickness wall	Nr	Nr	Nr	Nr	Nr	Nr	2.55	3.17	2.86
Thickness vault	[2]	[2]	[2]	0.404	0.556	0.48	0.411	0.559	0.49
Total height at intrados	Nr	Nr	Nr	12.72	15.02	13.87[3]	11.84	15.26	13.55

(1) Nr: normality behaviour rejected; (2) analysis of vaults was not performed; (3) lognormal adjustment was necessary

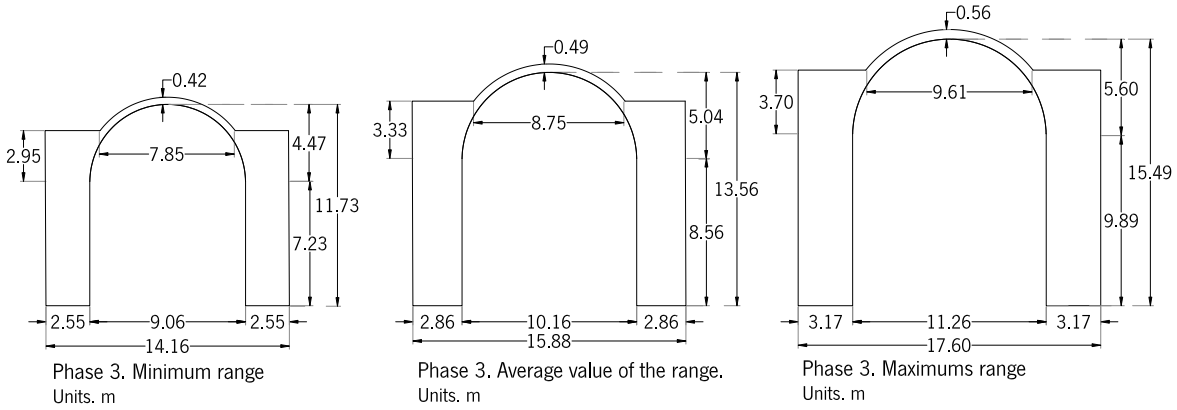


Figure 3-3. Geometrical proposal for semi-circular barrel vaults (image in proportion with dimensions)

3.4 Derivation of empirical relations from statistical analysis

Starting from the results of Phase 3 (database with 16 churches), it was decided to remove data until the statistical correlations were improved so that the coefficient of correlation (r^2) presented a value greater or equal to 0.6, see Figure 3-4a. It is important to note that for this process the outliers and residual values regarding to the key variables were reviewed to take the most accurate decision.

Considering the span of the church (L) as the independent variable, two types of linear correlations between geometric parameters and the span (L) were defined (Figure 3-4), namely: (1) linear correlation of type $y=ax_i+b$; *(2)* linear correlation of type $y=ax_i$ (b=0). The aim is to determine the dependency between both x (independent) and y (dependent) variables that best fits the distribution. A summary of the geometric parameters, the coefficient of correlation (r^2) and linear equations from both types is presented in Table 3-3.

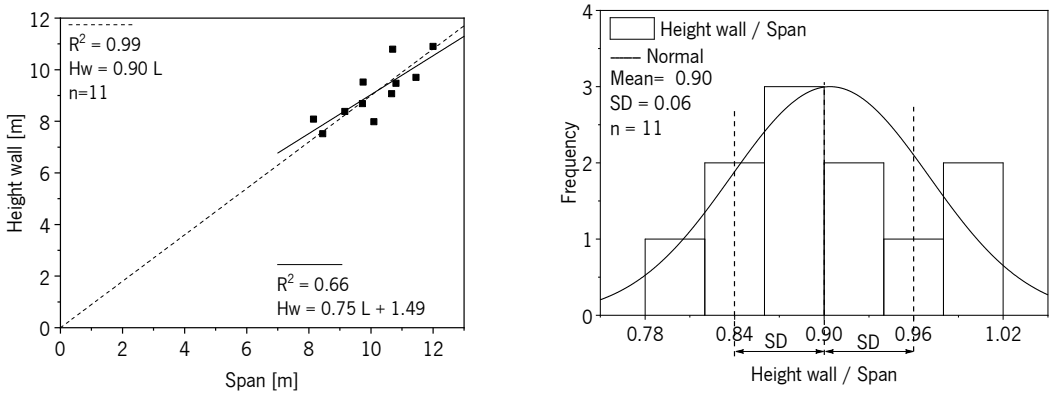


Figure 3-4. (a) Churches with significant statistical correlation between height of the walls and span; (b) histogram for the height wall/span ratio. See Annex 3.2

It is observed that reasonable correlations were found by considering the first type of linear correlation between the span (*L*) and the height of the walls (*Hw*), thickness of the walls *(tw)* and total height of the churches (*H*) and very good correlations were achieved between the span and the height of the vault (*Hv*) and between span and thickness of the vault (*tv*), see Table 3-3. In fact, it is interesting to notice that the thickness of the vault increases as the span increases, as it would be expected, revealing good understanding of the behavior of structures from the builders at that time. On the other hand, by considering the linear correlation passing through the origin (b=0), it is possible to obtain also very good correlations, as can be seen in Table 3-3.

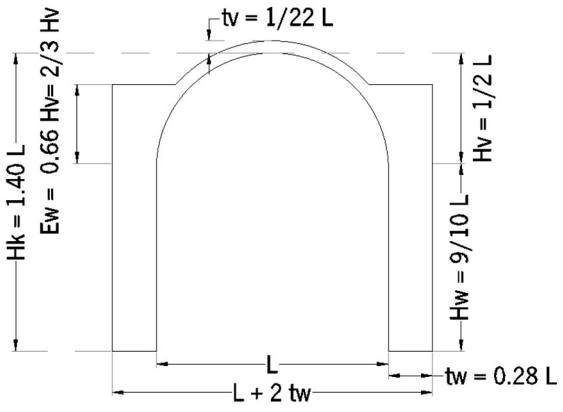
Table 3-3. Significant statistical correlation between geometric variables and span

Variables	**r^2**	**equation with b≠0**	**equation with b=0**
Hw vs ***L***	0.66	*Hw=0.75L+1.49*	*Hw=0.90L*
Hv vs ***L***	0.92	*Hv=0.50L-0.048*	*Hv=0.50L*
tw vs ***L***	0.69	*tw=0.24L+0.43*	*tw=0.28L*
tv vs ***L***	0.93	*tv=0.036L+0.10*	*tv=0.045L*
H vs ***L***	0.60	*H=1.29L+0.67*	*H=1.36L*

A complementary analysis of the most frequent ratio between the key geometric parameters and the span (key parameters/span ratio) was also performed by using histograms and normal distribution diagrams, which allowed to define the intervals including 68% of the data by calculating the minimum and maximum values, see Figure 3-5a. The average values proposed for the ratio between the key parameters and the span of the churches (*L*) are in line with the simple linear expressions used to correlate the key parameters and the span (b=0), see Figure 3-5b.

Selecting range	**Second Campaign**		
	Minimum	Maximum	Average
Ratio	[-SD]	[+SD]	
Hw/L	0.84	0.96	0.90
Hv/L	0.48	0.51	0.495
tw/L	0.26	0.30	0.28
tv/L	0.044	0.048	0.046
H/L	1.26	1.46	1.36

(a)



(b)

Figure 3-5. Statistical information for the ratio between the span (L) and the key geometric parameters; (a) ranges of frequencies selected for geometric parameters to span ratio; (b) proposed parameters to span ratios

3.4.1 Comparison with data of other Mexican churches

Aiming at comparing the results of the empirical relations between the key geometric parameters found for Yucatan churches (single span and barrels vaulst) with other similar churches in Mexico, it was decided to make a literature review in order to enlarge the database of churches. A database with more 35 Mexican churches with available information about the key geometric parameters above mentioned was built (Alejo et al., 2014; García et al. 2008; INAH, 2020b; Kubler, 2009). This database includes Mexican churches from Oaxaca (south, 5 churches), Morelia (west, 12 churches) and Morelos (centre, 18 churches). The typical spans of these churches range from 6m to 13.5m, whereas the typical span of Yucatan churches range from 8m to 13m. The statistical analysis carried out on this additional database was similar to the one developed for the Yucatan Churches. The quality of the data was assessed by analysing the existence of outliers, after which normally tests were carried out. Single regression analysis was derived between the span (*L*) and the other key geometric parameters, namely height of the walls (*Hw*), height of the vaults (*Hv*), thickness of the walls (*tw*), thickness of the vaults (*tv*) and total height of the churches (*H*), see Table 3-4. In addition, the most frequent range for the ratio (Average±SD) between the key parameters and the span (*L*) was also provided by identifying the minimum and maximum values.

The analysis of the statistical single regressions indicates that apart from the thickness of the vaults to span ratio (*tv* vs *L* ratio), linear equation fits reasonably well the data presenting in the majority of the cases very reasonable coefficient of determination (r^2) higher than 0.7.

According to Figure 3-6a, where the minimum and maximum values obtained for the height of the vaults to the span ratios are represented graphically, it can be seen that the barrel vaults of Yucatan and Oaxaca churches range from reduced to high vaults. This is supported by the height of the vaults to span ratios (*Hv/ L*) ranging from 0.43 to 0.57 and from 0.46 and 0.57 for Yucatan and Oaxaca churches respetively. This means that shape approaches the semi-circular barrels vaults (*Hw/ L*=0.5) with a maximum deviation of about 14% corresponding to the high and reduced barrel vaults. Regardind to Morelia churches the deviation of the reduced vauls from the semi-circular vaults is higher, being in the order of 30%, corresponding to the relation *Hv=0.35L*.

Table 3-4. Relationships between key geometric parameters and span for additional churches in Mexico.

Variable	Data	Geometric parameter to *L* ratio			SD	CV	Equation	r^2
Place	number	Minimum	Maximum	Average		(%)		
Hw vs ***L***								
Yucatan	23	0.59	1.01	0.84	0.14	17	-	-
Morelia	11	0.97	1.33	1.13	0.12	11	*Hw=0.79L+2.87*	0.70
Oaxaca	5	0.57	0.69	0.63	0.04	7	*Hw=0.66L-0.20*	0.77
Hv vs ***L***								
Yucatan	19	0.43	0.57	0.49	0.03	7	*Hv=0.37L+1.17*	0.72
Morelia	11	0.35	0.55	0.46	0.11	24	*Hv=0.52L-0.52*	0.74
Oaxaca	5	0.46	0.57	0.50	0.04	8	*Hv=0.37L+0.97*	0.74
tw vs ***L***								
Yucatan	21	0.13	0.32	0.24	0.06	24	-	-
Morelia	11	0.12	0.22	0.18	0.03	16	*tw=0.23L-0.44*	0.75
Oaxaca	5	0.15	0.29	0.24	0.05	22	*tw=0.40L-1.10*	0.62
Morelos	17	0.11	0.19	0.15	0.02	15	*tw=0.15L+0.06*	0.51
tv vs ***L***								
Yucatan	9	0.034	0.058	0.046	0.007	16	-	-
Morelia city	12	0.046	0.097	0.071	0.016	22	-	-
Oaxaca	4	0.050	0.153	0.098	0.042	43	-	-
Morelos	11	0.042	0.086	0.062	0.012	20	-	-
H vs ***L***								
Yucatan	25	1.03	1.67	1.35	0.18	13	-	-
Morelia	9	1.52	1.87	1.61	0.11	7	*H=1.16L+3.84*	0.97
Oaxaca	5	1.06	1.20	1.13	0.06	5	*H=1.03L+0.77*	0.87
Morelos	17	1.10	1.83	1.44	0.22	15	*H=1.98L-5.52*	0.68

Regarding to the thickness of the vaults (*tv*), all churches under analysis present a minimum thickness around *0.05L*. Morelos and Morelia churches have vaults with maximum thickness of *0.09L* to *0.1L* respectively, whereas the vaults of Oaxaca churches present the maximum thickness of about *0.15L* (Figure 3-6b). This difference suggests that the higher thickness of the vaults in Oaxaca churches can be attributed to the higher seismic hazard of this region, see Figure 3-6f. Notice that despite the coefficient of variation found for the thickness of the vaults in Oaxaca churches, there are not outlier on the database. However, it is recommended to expand the database of Oaxaca churches.

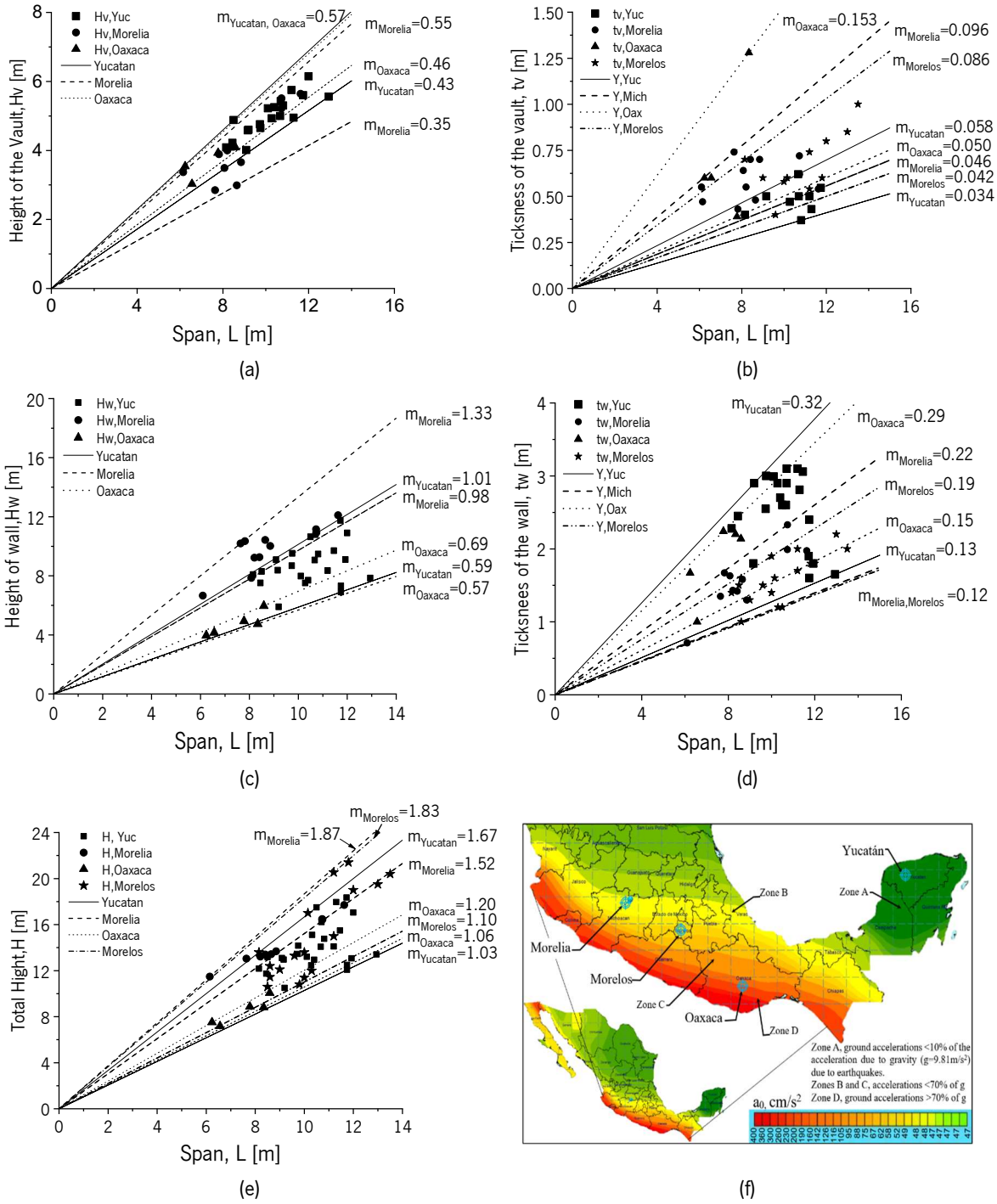


Figure 3-6. Comparison of the variation with the span (*L*) of key geometric parameters of churches with barrel-vaults and single span; (a) *Hv* vs *L*, (b) *tv* vs *L,* (c) *Hw vs L,* (d) *tw vs L,* (e) *H vs L* and (f) rock seismic acceleration map, adapted from PRODISIS (2017)

From Figure 3-6c, it is clear that Morelia churches present the highest walls height to span ratio (*Hw*/ *L*), with an average value of *1.1L*, whereas Oaxaca churches present the lowest values for the highest walls height to span ratio (average value of *0.6L*), see Figure 3-6c. The values of *Hw*/ *L* ratio found for Yucatan churches are mostly between Oaxaca and Morelia churches, ranging from *0.59L* to *1.01L*.

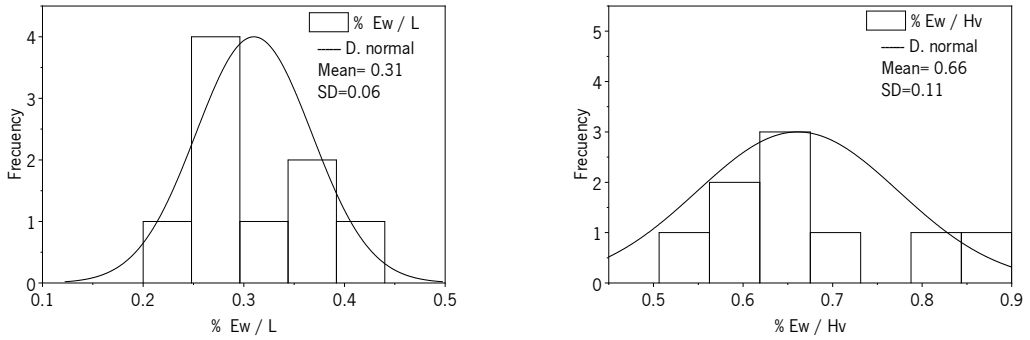
Regarding to thickness of the walls (*tw*), it is observed that the southern churches (Yucatan and Oaxaca) show greater thickness ranging from *0.10L* to *0.30L*, whereas the thickness of the walls in Morelia and Morelos churches ranges from *0.10L* to *0.20L*, see Figure 3-6d.

Finally, the total-height from Mexican churches ranges from *L* to *1.8L*, similarly to what was reported by García (2008), see Figure 3-6e.

3.5 Analysis of the backfill at the extrados of the masonry barrel vaults

The filling of the extrados of masonry vaults has not been considered of much interest by the research community and although there are studies that mention its importance (Gea et al., 2014; Hernandez, 2019; Alejandro Ramos, 2011), most of them are focused on bridges (Conde, Díaz-Vilariño, Lagüela, and Arias, 2016; Gago, Alfaiate, and Lamas, 2011; Molins, 1998). It is considered that the backfill at the extrados of the vaults is an important geometric characteristic, as this leads not only to the reduction of the free span of the vault but also to an additional load, which influence the mechanical behaviour of the vaults. The infill material in the extrados prevents the development of the collapse kinematics and improves the stability of the structure (Huerta, 2004; Ramos and León, 2017). However, if it is in excess, it may overload the vault, increment the permanent vertical deformation, reduce the original curvature and, thus, the bearing capacity. Therefore, its presence on arched structures is still a research open issue (Gaetani et al., 2017).

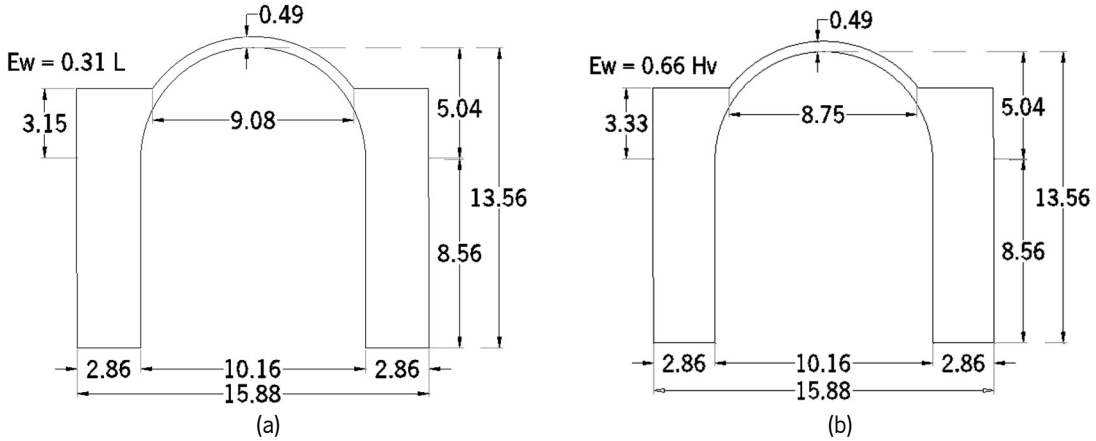
Due to the importance of the backfill at the extrados, the transversal sections of 10 Yucatan churches under analysis have been studied. The reduced number resulted from the absence of information for the remaining churches. Two geometrical ratios were considered for the study, namely: (a) the backfill height versus span of the vault (*Ew/ L*) and (b) the backfill height versus the height of the vault (*Ew/ Hv*). The histograms of these ratios and the description of the data through normal statistical distributions are shown in Figure 3-7. From these, and following the methodology already described in the previous section, the most frequent values were selected in the range centred in the average and length of $\mu\pm$ SD. Thus, it is observed that the backfill height (*Ew*) ranges mostly from 0.25*L* to 0.37*L*, corresponding to a variation from 0.55*Hv* to 0.77*Hv*.



(a) (b)

Figure 3-7. Statistical analysis: (a) backfill height and span ratio (*Ew/ L*) and (b) backfill height to height of the vault ratio (*Ew/ Hv*)

The normal distribution found for the variables geometric ratios under analysis reveals that the average value of backfill height is about 31% of the span and 66% of the height of vault (Figure 3-7), leading to a reduction of the free span ranging from 10.6% and 13.9% (see Figure 3-8). Therefore, there is not a significant difference by using the span of the vaults or height for the definition of the backfill height.



(a) (b)

Figure 3-8. Definition of the backfill height regarding to the; (a) span (*L*) and (b) height of vault (*Hv*)

The same study was carried out on 12 Morelia churches (Alejo et al., 2014) and 5 Oaxaca churches (INAH, 2020). In case of Morelia churches, the backfill height to span ratio (*Ew/ L*) varies from 0.18 to 0.58 and from 0.21 to 0.60 in Oaxaca churches, see Figure 3-9a, which means that the values are relatively close. In comparison to Yucatan churches, it is seen that these churches present wider range of the backfill height variation and considerable higher maximum values, resulting in higher reduction of the free span.

In addition, it is observed that the backfill regarding the total height of the vault (*Hv*) varies from 0.57 to 0.72 in Yucatan churches, from 0.76 to 1.30 in Morelia churches and from 0.46 to 1.27 in Oaxaca churches, which means that the backfill used in Morelia and Oaxaca frequently cover completely the

vaults. The vaults backfill height in Morelia churches is at least 76% of the vault height, while the minimum value found for Oaxaca churches is lower than 46% of the vault height, see Figure 3-9b. Additionally, statistical correlation between variables were achieved and the equations are shown in Figure 3-9. It is observed that the backfill height of the vaults can be reasonably obtained from both the span and height of the vaults (r^2 >0.60).

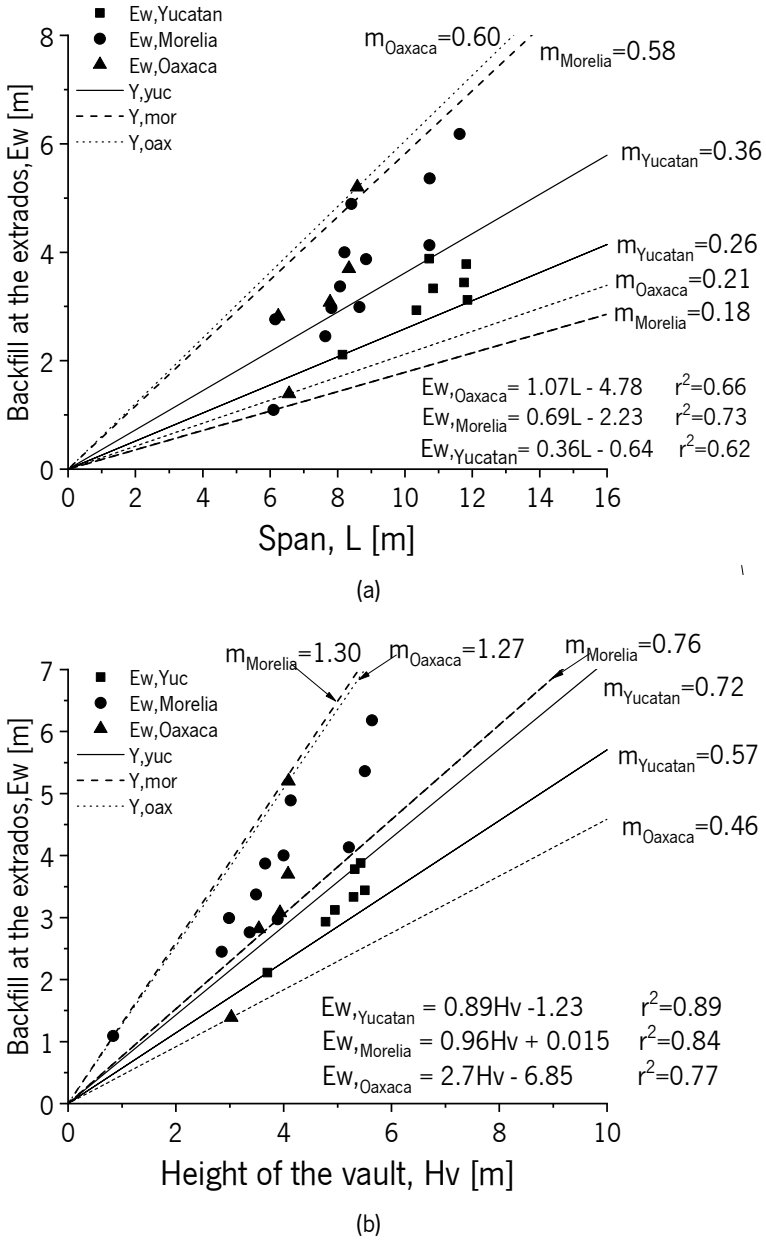


Figure 3-9. Percentage of backfill height found for different churches regarding to the; (a) span (*L*) and (b) height of the vault (*Hv*)

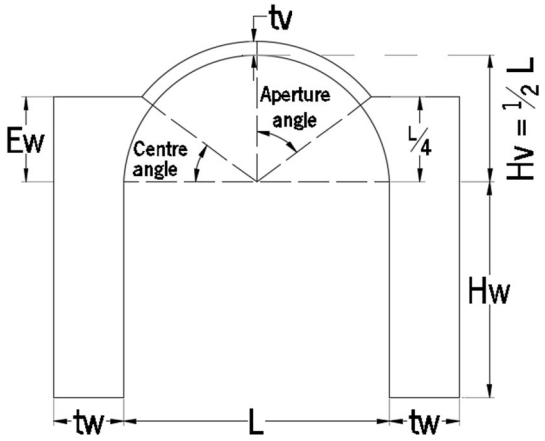


Figure 3-10. Identification of centre angle for barrel vaults

Based on these results, it was decided to correlate the free span of the vault with the centre angle, which can vary from 0° (Ew=0m) to 90° ($Ew \geq Hv$), see Figure 3-10. The aperture angle is the complementary angle of the centre angle.

It is seen that the backfill height in Yucatan churches are associated to a variation on the centre angles from 33° to 46°, in Oaxaca churches the centre angle vary from 22° to 90° and in Morelia churches it varied from 26° to 90°, see Figure 3-11a. It is also possible to observe that a strong concentration of centre angles between 30° and 65°, corresponding to aperture angles of churches between 60° and 25°. In Yucatan churches the aperture angle varied from 57° to 44°, in Oaxaca churches it varied from 68° to 0° and in Morelia churches it presents a variation between 64° and 0°.

Gaetani (2017) carried out a parametric study on masonry cross vaults from which a variation of the centre angles from 40° to 90° was observed. Huerta (2006) studied the reduction of the aperture angle by filling the extrados on semi-circular barrel vaults and concluded that the backfill height of L/4 (Ew=0.25L) correspond to an aperture angle of approximately 62°. The relation between the aperture angle and the backfill height to span ratio (Ew/L) for the Mexican churches with semi-circular barrel vaults under study is shown in Figure 3-11b.

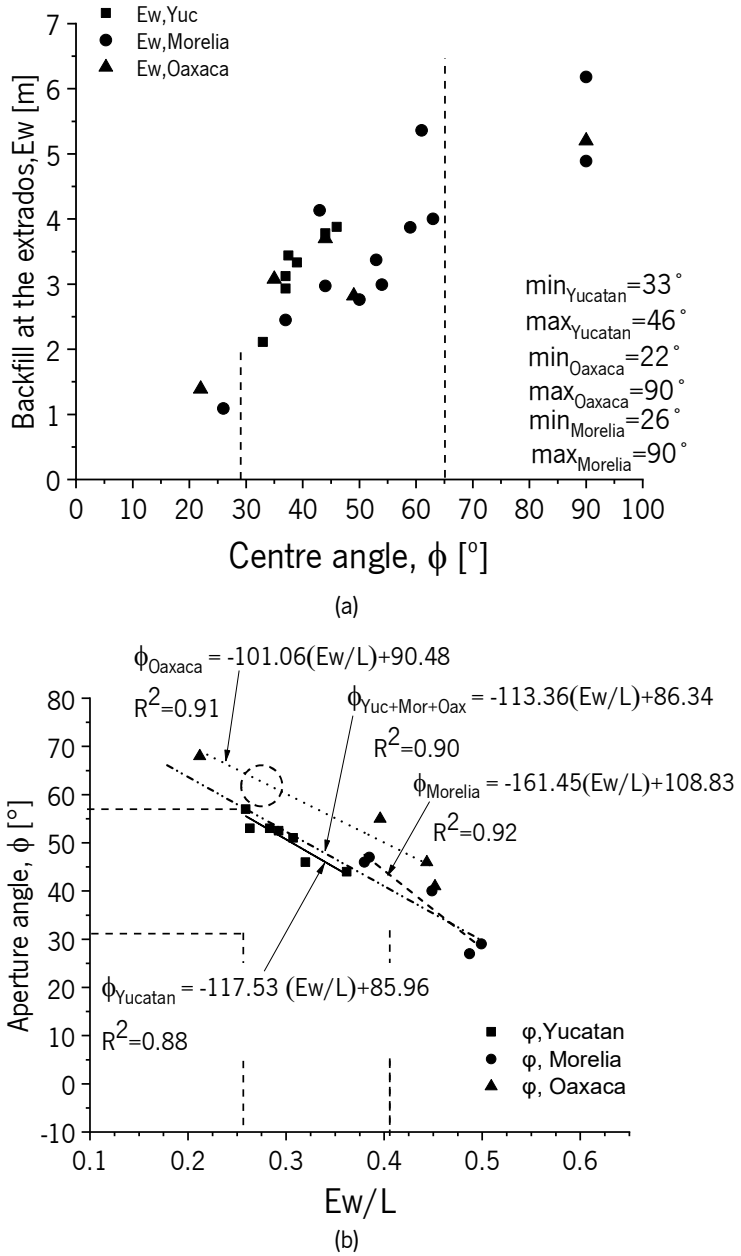


Figure 3-11. Relation between backfill height to span ratio (*Ew/L*) with: (a) central angles, (b) aperture angle

It was observed that the aperture angle decreases linearly as the backfill height to span ratio increases. In Yucatan churches aperture angles vary from 57° to 44° corresponding to a variation of the *Ew/L* ratio from 0.26 to 0.36. In Morelia churches with backfill height to span ratio varying from 0.38 to 0.50 leads to variation of the aperture angles from 47° to 27° and in Oaxaca churches backfill height to span ratios varying from 0.21 to 0.45 corresponds to aperture angles ranging from 68° to 41°. From the linear fitting considering the data of all churches (r^2=0.90), the height to span ratio of 0.25 correspond an aperture angle of 57° (Figure 3-11b), which is close to the one (62°) pointed out by Huerta (2006) for semi-circular vaults.

3.6 Empirical rules from European historical construction treatises

3.6.1 Review of European historical construction treatises

Available European historical construction treatises from sixteenth to eighteenth centuries were analysed to understand possible geometrical rules defining the geometry of structural masonry elements that masons used in the construction of the buildings. It should be mentioned that neither treatises nor manuals are available regarding to Yucatan churches or even to Mexican churches, but it is expected that the influence of Spanish builders can be seen in Franciscan religious buildings. The research was focused on churches with one span and barrel vaults, according to the features of Yucatan churches previously analysed. Therefore, European geometrical rules described in historical manuscripts, manuals and treatises were reviewed. The manuscripts studied were published in the same period of Yucatan churches construction and it is probable that the builders and frails of the Mexican churches did not have access to them. However, it is also possible that the builders of the Mexican churches were aware of the geometric calculations they proposed, since, prior to the treatises and manuscripts, the knowledge was transmitted orally.

Until the fifteenth century, architectural treatises did not provide information on architectural design. The rules were highly protected and were only available orally to guild members, handled secretly from person to person. Until the strict safeguard rules were relaxed, some of that knowledge was gleaned from analysis of old buildings and the historical manuscripts, manuals and treatises were written (Gaetani et al., 2016; Fangary, 2010). From the sixteenth to the eighteenth century several historical manuscripts, manuals and treatises were developed in Europe by different authors aiming at providing empirical and geometrical rules for buildings, see Table 3-5.

Vitruvius (1549) was probably the most famous roman architect since the 1st century BC. He was an architect working to the emperor Augustus and wrote a summary of his own experience in the field of architecture ‘De Architectura’. The first printed edition, consisting of 10 volumes, appeared in Rome in 1486 (Baptista, 1582; Ortiz y Sanz, 1787). Vitruvius observed that the first builders did not have rules for tracing, dividing and ordering their buildings and decided to propose a book that relates the measures of well-proportioned human body to establish the dimensions of the constructive elements such as columns and cornices (Sagredo, 1549).

Table 3-5 – Authors of historical manuscripts, manuals, and treatises from sixteenth to eighteenth centuries.

Century	Treaties
sixteenth century	Vitruvius at 1486 (Sagredo, 1549) Baptista Alberti at 1485 (Loçano, 1582) Lorenz Lechler at 1516 (Sanabria, 1982) Serlio at 1537 (Villalpaldo, 1552) Rodrigo Gil de Hontañón at 1544 (S. García, 1681; Sanabria, 1982) Paladio at 1570 (J. F. Ortiz y Sanz, 1797)
seventeenth century	Hernan Ruiz the Younger at 1560 (Navascués Palacio, 1974) Xines Martinez de Arana (1600b) Fray Lorenzo de San Nicolás(1639) François Derand (1643) Simón García (1681) François Blondel (1683)
eighteenth century	Philippe de La Hire (1695, 1712) Bernard Bélidor (1725, 1729, 1755) Frézier (1737, 1768, 1769) García Berruguilla (1747) Perrault (1761) Gauthier at 1765 (Brencich et al, 2007, Huerta, 1990) Pol y Camin (1767) Ortiz y Sanz (1787) Perronet at 1788 (Huerta, 1990)

De Re Aedificatoria by Alberto Leon Baptista was formally presented to Pope Nicholas V in 1452, but the first edition was printed in 1485 in Florence, after which several copies were written in Latin during the sixteenth century (Figueiredo, 2015; Suárez Quevedo, 2008). The Spanish version consulted for this study was translated in Madrid in 1582 with the name *Los Diez Libros de Architectura de Leon Baptista Alberto* (Loçano, 1582). Baptista did not provide specific rules for structural elements but provided interesting constructive and structural recommendations. In the seventh book, recommendations for religious buildings are provided, namely for the shape of the temples, for relationships between the length and width of the temples and for the use of stone vaulted ceilings resulting from his concern with fire. Regarding to vaults (Book III), it is clear that Baptista understood the importance of the weight of stone vaults for the supporting walls by suggesting using light stones such as pumice or tuff. Another recommendation was to build the backfill at the extrados of the vaults with ordinary, strong and compacting masonry linked to the wall, which suggests the use of connecting stone elements. Serlio (1552) pointed out also recommendations for vaults (without pointing out geometric rules), relating the type of vault with the use of the space. In addition, based on structural safety reasons, it was proposed the placement of iron or bronze tie-rods between supporting beam and both vaults and columns.

Other interesting contribution was from Lorenz Lechler, a German master mason who composed *Instructions*, a book on gothic design at 1516 (Sanabria, 1982). He proposed a rule for the thickness of the walls as a function of the span of the building (*tw=3/10L*), allowing a variation of +1.4% and -

2.4% depending on the stone quality, see Table 3-6. This reveals his understanding on the strength of materials.

At sixteenth century, Rodrigo Gil de Hontañón, the most prolific and versatile Spanish architect and probably the most important Late Gothic master in Spain (Gaetani, 2016), wrote an architectural treatise which was lost and was taken up in 1681 by Simon García (1681). According to Sanabria (1982), the original Hontañon's book was written between 1544 and 1554. Simon García was a Salmantine architect that wrote the manuscript *Compendio de Arquitectura y Simetria de los Templos,* which included the contribution of several authors including Hontañón, but it does not specify which chapters are from Hontañon (S. García, 1681).

Table 3-6. Rules for the thickness of the walls

Geometric Rules	Walls/Buttresses
Lorenz Lechler in 1516 (Sanabria, 1982)	$t_w=3/10L$ (+1.4% -2.4%) (Sanabria, 1982) $t_w=1/10L$ (Huerta, 1990)
Rodrigo Gil in 1544, Rule 1. For buttress (Sanabria, 1982)	$t_w=1/4L$
Rodrigo Gil in 1544, Rule 4. Semicircular Arch Buttress Depth (Sanabria, 1982)	$t_w=\sqrt{(H+P/2)}$
A.Palladio in 1570 (J. F. Ortiz y Sanz, 1797)	$t_w \geq 1/3L$
Fr_Laurencio de San_Nicolas (Fr Laurencio, 1639)	$t_w=1/3L$ (without buttress) $t_w=1/6L$ (with buttress) and $t_{buttress}=1/6L$ $t_w=1/7L$ (with any thrust) $t_w=1/7L$ (brick vaults with buttress) and $t_{buttress}=4/21\ L$ $t_w=1/8L$ (double brick vaults with buttress) and $t_{buttress}=1/4L$ $t_w=1/5L$ (double brick vaults without buttress)
Garcia Berruguilla (1747)	$t_w=1/3L$ (stone vaults without buttress) $t_w=1/6L$ (stone vaults with buttress) and $t_{buttress}=1/6L$ $t_w=1/7L$ (with any thrust) $t_w=1/7L$ (brick vaults with buttress) and $t_{buttress}=4/21\ L$ $t_w=1/8L$ (double brick vaults with buttress) and $t_{buttress}=1/4L$ $t_w=1/5L$ (double brick vaults without buttress)

t = thickness, L = span, H= wall height, P= arch intrados perimeter

However, other studies as Camón Aznar (1941) and Sanabria (1982) attribute the six first chapters to Hontañón's contribution, in which seven formulations for piers, walls and thickness of vaults are provided. The first rule (Rule 1) is an empirical rule for the thickness of the walls ($t_w=0.25L$), Rules 2 and 3 are focused on ribbed vaults, Rule 4 is an arithmetic formulae for walls depth supporting semi-circular arches ($t_w=\sqrt{(H+P/2)}$, where H is the height of the wall and P is the arch intrados perimeter), see Table 3-6. Rules 5, 6 and 7 are three geometric formulations for walls supporting semi-circular

arches, in which the height of the backfill material at extrados was also defined geometrically introducing thus the concept and the importance of the backfill at extrados (S. García, 1681). This rule also suggests that the height of the walls should be equal to the span (*Hw=L*). It is recommended to adjust the thickness of the walls by increasing or decreasing as the height of the walls is higher or lower the span respectively (Huerta, 1990). An example of this construction is given in Table 3-8 for height of the walls equal to *1⅓L* or *1½L* (Sanabria, 1982).

Table 3-7. Thickness of vault (*tv*) and the backfill at the extrados of vaults (*Ew*)

	Thickness of vault	Backfill at the extrados of vaults
Rodrigo Gil in 1544, Rule No. 7. Third geometric formula. Part 1 (Sanabria, 1982)	*tv=1/6L*	
Rodrigo Gil in 1544, Rule No. 7. Tirth geometric formula. Part 2 (Sanabria, 1982)	*tv=1/5L*	
Hernan Ruiz the Younger at 1560 (Navascués Palacio, 1974)	*tv=1/10L*	*Ew=1/2Hv*
Xinés Martínez de Aranda (1600b)	From 5 to 10 ft (approx. 1.40-2.80m) *tv=1/6L* From 10 to 20 ft (approx. 2.80-5.60 m) *tv= 1/8L* From 20 to 40 ft (approx.5.60-11.2m) *tv=1/10L*	
Fr_Laurencio de San_Nicolas (1639)	-	*Ew=1/3Hv* (plus sections of wall to arrive at 2/3 of Hv)
Amédée-Frangois Frézier (1768) (Huerta, 1990)	Along the aperture angle equal to 120° *tv=1/24L* Along the central angle equal to 30° *tv=2x(1/24L)*	
Bélidor (1725, 1729, 1755) (Huerta, 1990)	*tv=1/24L* (semi-circular vault) *tv=1/24L+1ft* (reduced vault)	
Gauthier in 1765 for semi-circular barrel vault (Brencich and Morbiducci, 2007)	*tv=0.32+L/15* (brickwork arches only)	
Jean Rodolphe Perronet in 1750, 1752, 1777 (Huerta, 1990)	*tv=L/24+1–L/144* (for arches of bridges)	
Jean Rodolphe Perronet in 1788 for semi-circular barrel vault (Brencich and Morbiducci, 2007)	*tv=0.325+0.0347L ≈ 0.325+L/30* (brickwork arches only)	
Jean Rodolphe Perronet in 1788 for reduced vaults (Brencich and Morbiducci, 2007)	*tv=0.325+0.0694(L/2) ≈ 0.325+(L/2)/15* *tv=0.325+0.0347L ≈ 0.325+L/30* (brickwork arches only)	
Garcia Berruguilla (1747)	-	*Ew=1/3Hv*
Plo y Camin (1767) stone vaults	-	*Ew=1/2Hv*
Plo y Camin (1767) brick vaults	-	*Ew=2/3Hv*

Note:
ft = roman feet, according to (Gaetani et al., 2016) one roman foot is approximately equal to 0.28 m.
1 foot = 12 inches; 1 inch = 12 lines (Huerta, 1990)

The developments on geometric construction rules by Andres Palladio in 1570 focused on bridges but made important observations about the buttresses and vaults in buildings (Ortiz y Sanz, 1797). It was also considered that for a barrel vault to be stable, the wall thickness should be greater than one third

of the span ($t_w>1/3L$) and proposed a height of the wall equal to the span ($Hw=L$). Five formulations to determine the height of the vault (Hv) were also proposed according to the plan dimensions, see Table 3-9. He described the mode of the collapse of a vault after the formation of three hinges located at the supporting walls and at the keystone of the vault and highlighted that the weight of the vault plus the weight of the backfill at extrados should be lower than the weight of the walls to achieve stability.

Table 3-8. Graphic Rules for piers and walls proposed by Rodrigo Gil de Hontañón

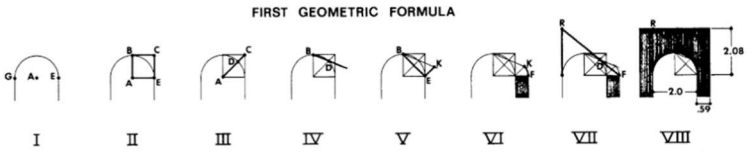
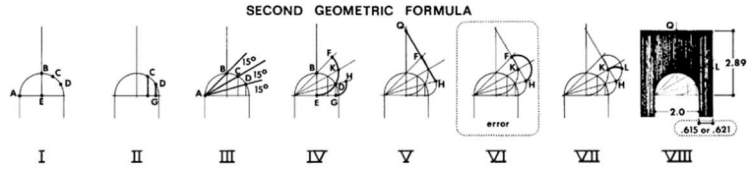
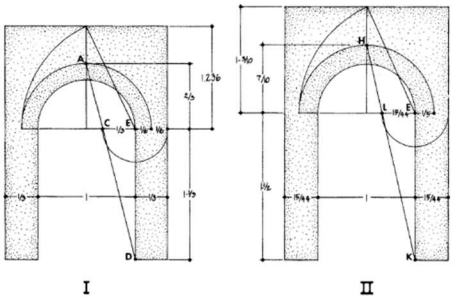
Geometric Rules. Rodrigo Gil de Hontañón in 1544 (Sanabria, 1982)	Walls's thickness	Allowed Backfill height
Rule No.5. First geometric formula 	*L/3.414*	2.081 radii
Rule No.6. Second geometric formula 	*L/3.22* *L/3.25*	2.894 radii
Rule No. 7. Third geometric formula 	Height of the walls *Hw=1 1/3L* *Hw=1 1/2L*	*1/3L* (Part 1) *15/44L* (Part 2)	2.472 radii (Part 1) 2.6 radii (Part 2)

Table 3-9. Paladio's rules to determine the height of the vault (Hv)

Plant	Height of the vault (Hv)
Square (LxL)	*L+1/3*
Rectangular (LxD)	*1/3L* (perimetral hallways and rooms)
Rectangular (LxD)	*(L+D)/2*
Rectangular (LxD)	*√(LxD)*
Rectangular (LxD))	$(LxD)/H_{v1}$
L = span; D = long	Where $H_{v1}=\sqrt{(LxD)}$

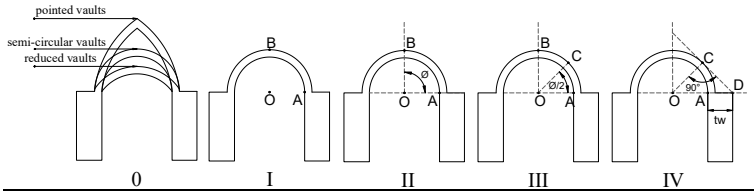
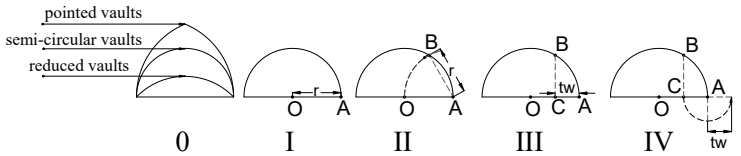
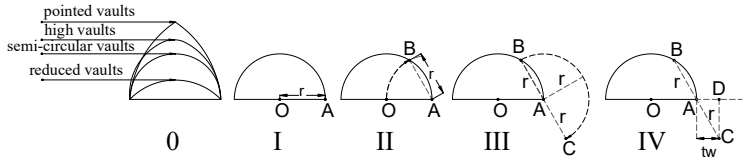
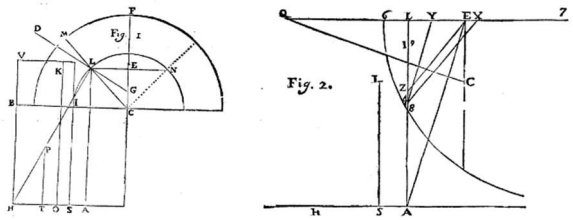
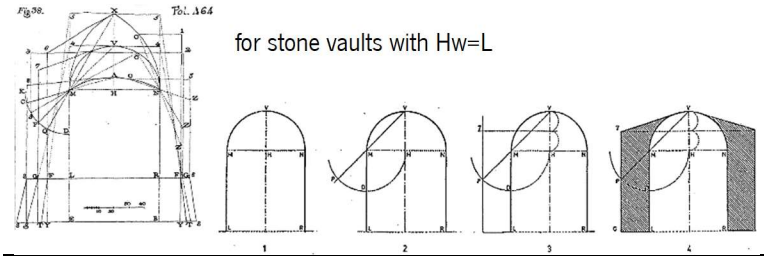
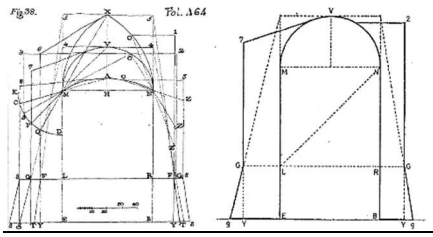
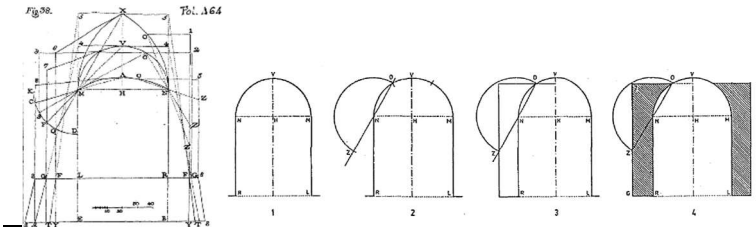
Additionally, he explained the concept of differential settlement due to inadequate foundations and mentioned several times that the walls should increase the thickness for increasing height of the walls (Huerta, 1990; Ortiz y Sanz, 1797).

In spite of Hernan Ruiz the younger wrote a book in 1560 with proposals for the thickness of walls, taking into consideration the thickness of the vaults through geometric procedure indicated in Table 3-10, it was only published at the seventh century. The backfill at the extrados as a stabilizing element was recommended to have half of the height of the vault (E_w=0.5H_v), and the thickness of the vault must be greater than 1/10 of the span (Table 3-7) (Alejo et al., 2014; Gaetani, 2016; Navascués Palacio, 1974). A similar geometric rule to determine the width of the walls was proposed by Xines Martinez de Arana (1600b, 1600a), see Table 3-10. Nevertheless, its greatest contribution was the proposal for the thickness of barrel vaults/arches as a function of the span, see Table 3-7.

Fray Lorenzo de San Nicolás (1639) studied the floor-plan dimensions of temples and proposed two rules for the thickness of the walls receiving the thrust of vaults considering or not the use of buttresses, as well as a rule for the thickness of the buttresses. A rule was also defined for the thickness of walls receiving the thrust of timber-roof (without vaults). Additionally, the width of buttresses added in the longitudinal direction of the churches was defined as 2/3 of the wall thickness and the spacing between buttresses as 1/2 of the span. A classification of the vaults according to the material and construction system was provided, being the barrel vault considered as the most solid and the strongest vault and with the easiest construction system. In spite of no recommendations were provided for the thickness of the vaults, it was suggested to compact alternated backfill material and stone layers until to achieve the second third of the vault height.

François Derand, in the *L'Architecture des voutes* (1643) and François Blondel on the *Cours d'Architecture treatise* (1683) point out the same geometrical rule proposed by Xines Martinez de Arana to define the thickness of the walls supporting barrel vaults, see Table 3-10 (Alejo et al., 2014; Calvo-Lopez, 1999; Gaetani, 2016; Hassan Fangary, 2010; Huerta, 2006).

Table 3-10. Graphic Rules for piers and walls proposed by different authors

Geometric Rules	Walls thickness
Hernan Ruiz the Younger at 1560 (Navascués Palacio, 1974) 	
Xinés Martínez de Aranda, (1600b) 	1/4 L (only for barrel vaults) (Calvo-Lopez, 1999)
François Derand (1643) and François Blondel (1683) 	
La Hire 1712 (1695, 1712) 	
Plo y Camin (1767) and interpretation by Huerta (1990) 	for stone vaults with Hw=L
Plo y Camin (1767) and interpretation by Huerta (1990) 	for stone vaults with Hw>L
Plo y Camin (1767) and interpretation by Huerta (1990) for brick vaults with Hw=L 	

Hw = height of the wall, L = span

At eighteenth century, several studies were carried out on the geometry of vaults with better scientific and static knowledge. An example was Philippe de La Hire, which published the *Traité de mécanique* in 1695 and the book entitled *Sur la construction des voíltes dans les édifice. Mémoires de l'Académie Royale des Sciences de Paris* (La Hire 1695; 1712). He highlighted the difficulty of obtaining the thickness of the wall and he did not deal with this problem until 1712. At this time, from a design of semi-circular barrel vaults (Figure 3-12a) he defined the thrust of the vaults, as the forces exerted by the voussoirs to the walls supporting the vault inducing their out-of-plane rotation. When the walls are weak, two critical-joints located at the quarters of the vault are identified (Figure 3-12a), which divide the vault in three parts, as shown in Figure 3-12b. He also defined the mechanism of the collapse of the vaults through the concept of sliding-wedge, in which by the action of the self-weight, the upper part slides down on the critical-joints producing thrusts to the adjacent ones and causing the wall rotation at point H (Figure 3-12b). It is important to note that the friction at critical joints was not considered, assuming the transmission of loads between the bodies in the vault along the perpendicular direction to the critical-joint and tangent to the intrados (point L), see Figure 3-12a,c.

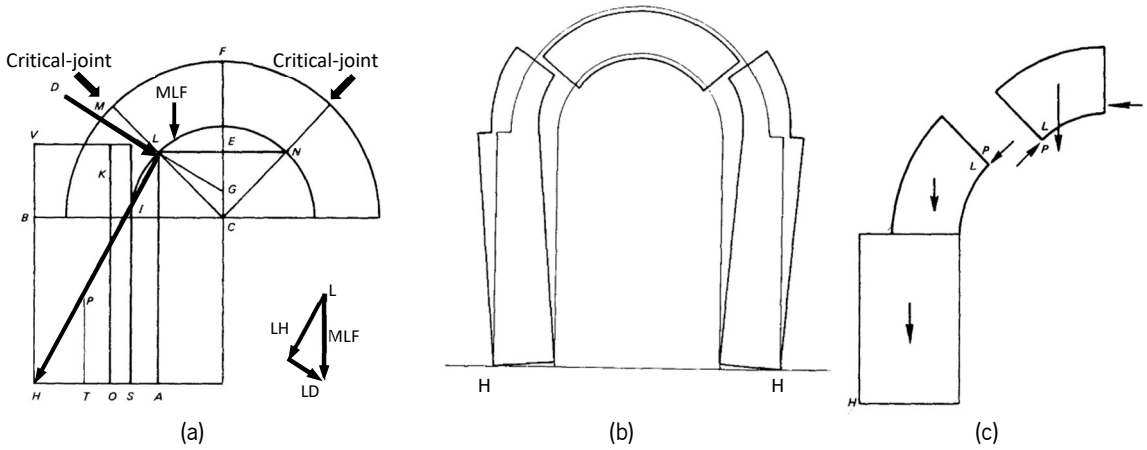
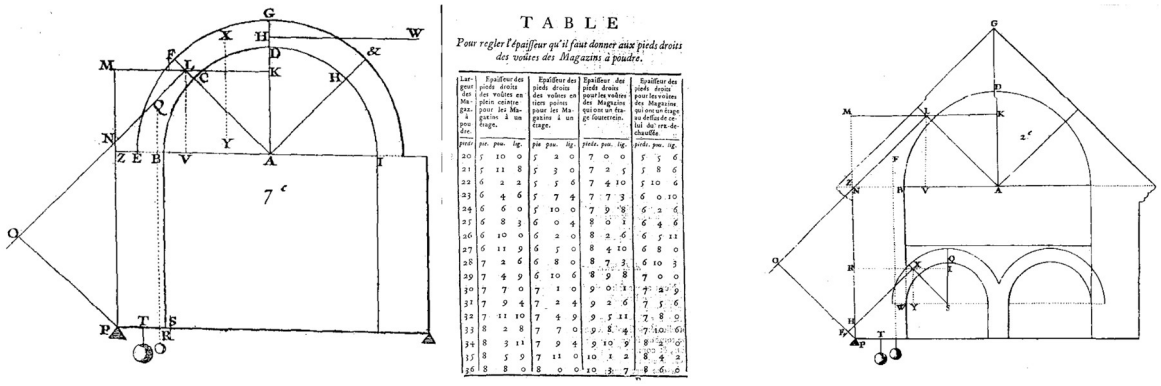


Figure 3-12. (a) La Hire theory: definition of thrust and sliding-wedge concept, (b) mechanism of the collapse and (c) transmission of loads. Adapted from (La Hire, 1712; Huerta and Hemando, 1998)

La Hire determined the thickness of the wall supporting any kind of vault through two procedures, namely analytic and geometric methods (Table 3-10). As both methods become very complicated for practical applications (De Sousa Gago, 2004; Huerta and Hemando, 1998; La Hire, 1695, 1712), Bernard Forest de Bélidor in book *Nouveau Cours de mathématique* (Bélidor, 1725), tried to the solve the mathematic equation proposed by La Hire's by simplifying it assuming that the point of load-transmission between voussoirs is located at midpoint of the vault thickness and is perpendicular to the critical joint (Figure 3-13a). He also recommended to increase the calculated thickness by 5 or 6 inches (12.7 cm or 15.24 cm) or adding buttresses. Because he includes numerous application

examples in his book (Figure 3-13b), this method became the standard for calculating wall thickness (De Sousa Gago, 2004; Huerta and Hemando, 1998).



TABLE

Pour regler l'épaisseur qu'il faut donner aux pieds droits des voûtes des Magazins à poudre.

Largeur des Magazins à poudre.	Epaisseur des pieds droits des voûtes en plein cintre pour les Magazins à un étage.	Epaisseur des pieds droits des voûtes en tiers points pour les Magazins à un étage.	Epaisseur des pieds droits pour les voûtes des Magazins qui ont un étage souterrein.	Epaisseur des pieds droits pour les voûtes des Magazins qui ont un étage au dessus de celui des rez-de-chaussée.
pieds	pie. pou. lig.	pie. pou. lig.	pieds. pou. lig.	pieds. pou. lig.
20	5 10 0	5 2 0	7 0 0	5 5 6
21	5 11 8	5 3 0	7 2 5	5 8 6
22	6 2 2	5 5 6	7 4 10	5 10 6
23	6 4 6	5 7 4	7 7 3	6 0 10
24	6 6 0	5 10 0	7 9 8	6 3 6
25	6 8 3	6 0 4	8 0 1	6 4 6
26	6 10 0	6 2 0	8 2 6	6 5 11
27	6 11 9	6 5 0	8 4 10	6 8 0
28	7 2 6	6 8 0	8 7 3	6 10 3
29	7 4 9	6 10 6	8 9 8	7 0 0
30	7 7 0	7 1 0	9 0 1	7 2 9
31	7 9 4	7 2 4	9 2 6	7 5 6
32	7 11 10	7 4 9	9 5 11	7 8 0
33	8 2 8	7 7 0	9 8 4	7 10 6
34	8 5 3	7 9 4	9 10 9	8 1 0
35	8 5 9	7 11 0	10 1 2	8 4 2
36	8 8 0	8 0 0	10 3 7	8 6 6

(a) (b)

Figure 3-13. (a) First application of simplified La Hire theory by Belidor and (b) application examples on full buildings (Belidor, 1725)

Garcia Berruguilla (1747) inspired in the proposals of Fr Laurencio de San Nicolas(1639) to provide several relations to the thickness of walls supporting vaults according to their span, by considering different types of materials for the vaults (stone or brick masonry), different masonry bonds and by considering or not the existence of buttresses, see Table 9. He carried out a comparative analysis between his proposal and the ones proposed by Blondel-Derald (same formulation) and Palladio and concluded that the collapse of some buildings could be attributed to unsafe rules provided by these authors. Additionally, he proposed to fill the extrados of the vault (*Ew*) until to reach 1/3 of the height of the vault (*Hv*), see Table 3-7.

Amedée François Frézier classified the arches according to their use and loading levels, namely high load levels in bridges and lower load levels in buildings and churches (Frézier, 1768) and suggested a thickness for the vaults and arches in buildings and churches equal to *L/24*. This value could increase twice (*L/12*) from the starting of the vault until reaching a centre angle of 30°, see Table 3-8. For the thickness of the walls, he adopts La Hire's rules.

Plo y Camin (1767) proposed a geometric rule to determine the thickness of the wall (*tw*) considering all types of barrel vaults (hight, semi-circular and reduced) and recommended to the height of the walls a value equal to the span (*Hw = L*). In addition, he included a geometrical adjust of the wall thickness when the height of the wall is greater than the span (*Hw>L*), see Table 3-10. In case of stone vaults the backfill at the vault extrados extends until 1/2 of the height of the vault and then increases linearly until the vault crown (Table 3-7). Additional correlation from Gauthier at 1765 and Perronet

at 1788 for the thickness of barrel vaults was found in recent publications and are summarised in Table 3-7 (Brencich and Morbiducci, 2007, Huerta, 1990).

A summary of empirical rules proposed in European historical construction treatises under review are shown in Figure 3-14 to the: (1) thickness of the vaults, (2) height of the backfill at extrados, (3) thickness of the walls and (4) height of the walls.

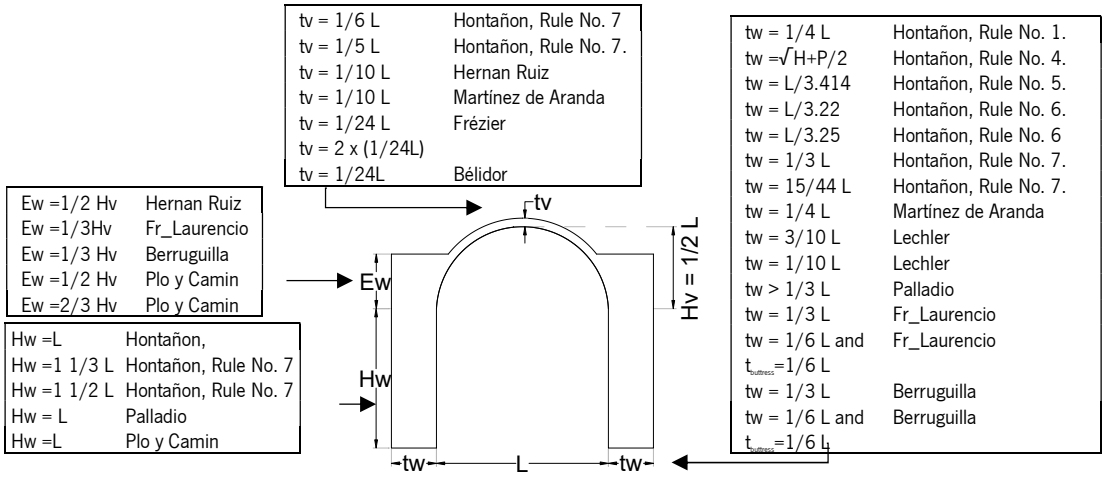


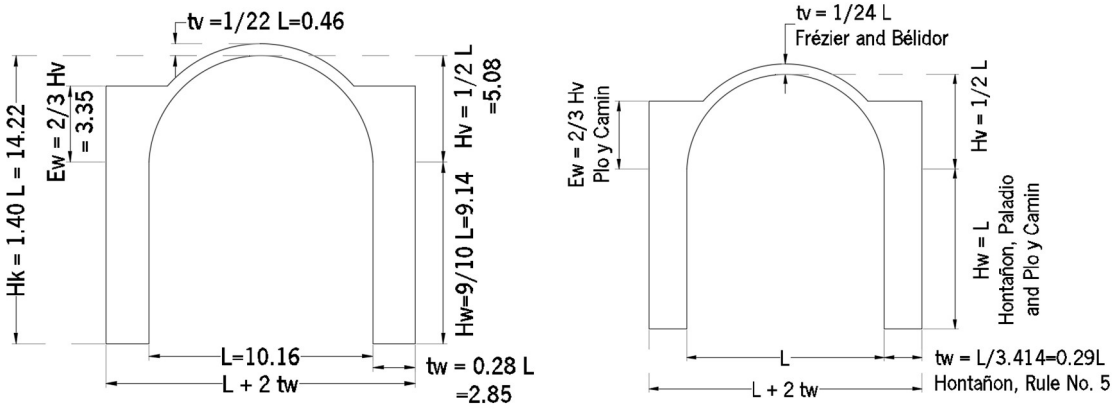
Figure 3-14. Empirical rules from European historical construction treatises

3.6.2 Analysis of the Yucatan churches parameters to the light of the treatises

In this section, a comparison between the key geometrical parameters describing the cross-section of Yucatan churches with single span and the values for the same parameters provided in the different European historical construction treatises is provided. The main aim was to assess if the geometrical key parameters of selected single span Yucatan churches are in the range of the values provided in historical construction treatises. For this, the selected empirical rules derived in section 3.4 for semi-circular vaults (Figure 3-15a) were compared with the closest geometric rules from European historical construction treatises (Figure 3-15b). The comparison reveals that the dimensions characterizing single span Yucatan churches with semi-circular barrel vaults approach reasonably well some proposals provided in treatises.

A statistical analysis to review the scatter of the data regarding to historical rules was also performed. Figure 3-16 shows the graphical representation of the historical rules (from Figure 3-14) for some key geometric parameters as a function of the span (L) as well as the same relations obtained for the

Yucatan churches with semi-circular barrel vaults. It is observed that the thickness of the vaults are close to the minimum thickness provided by historical constructions treatises available for stone vaults (Figure 3-16a).



(a) (b)

Figure 3-15. Geometric profiles of single span churches with barrel vaults; (a) derived empirical rules for Yucatan churches; (b) geometry rules from European historical construction treatises

The geometric rule proposed in this work for the thickness of semi-circular barrel vaults is *L/22* (Figure 3-15a), slightly higher than the one indicated by Frézier and Bélidor (*L/24*). As seen in Figure 3-16b the wall thickness of Yucatan churches presents a very high scatter, being in the range of the several values proposed in the historical construction treatises. In any case, there is a trend for the thickness of the walls approach the rules provide by Hontañon. The height of the walls in Yucatan churches is equal or lower than the span, thus below the relation proposed by Hontañon, Palladio and Plo y Camin, see Figure 3-16c. Finally, the backfill at extrados of barrel vaults (*Ew*) shows values ranging from *0.57Hv* to *0.75Hv* (see Figure 3-16d), which are close to the rules proposed by Hernan Ruiz the Younger and Plo y Camin which varied from *0.5L* and *0.66L*, see Figure 3-16d.

In addition, it was carried out a comparison between the thickness of the walls and vaults as a function of the span for churches from different regions of Mexico, which were reviewed in section 3.4. It is observed that the thickness of vaults of all churches analyzed presents a high scatter and mostly ranges from *L/24* (Frezier Belidor) to *L/10* (Ruiz Martinez), see Figure 3-17a. The values found for the thickness of vaults (*tv*) as a function of the span (*L*) in Yucatan churches exhibit a significant variation from approximately *L/30* to *L/17*. The minimum values for the thickness of the vaults for Morelos, Morelia and Oaxaca churches are *L/24*, *L/22* and *L/20* respectively, which are close to the value proposed by Frezier and Belidor (*L/24*), see Figure 3-17a. On the other hand, the maximum

values of the thickness of the vaults are between *L/10.5* and *L/11.5*, which are in the range proposed by Frezier (*L/12*) and Ruiz-Martinez (*L/10*).

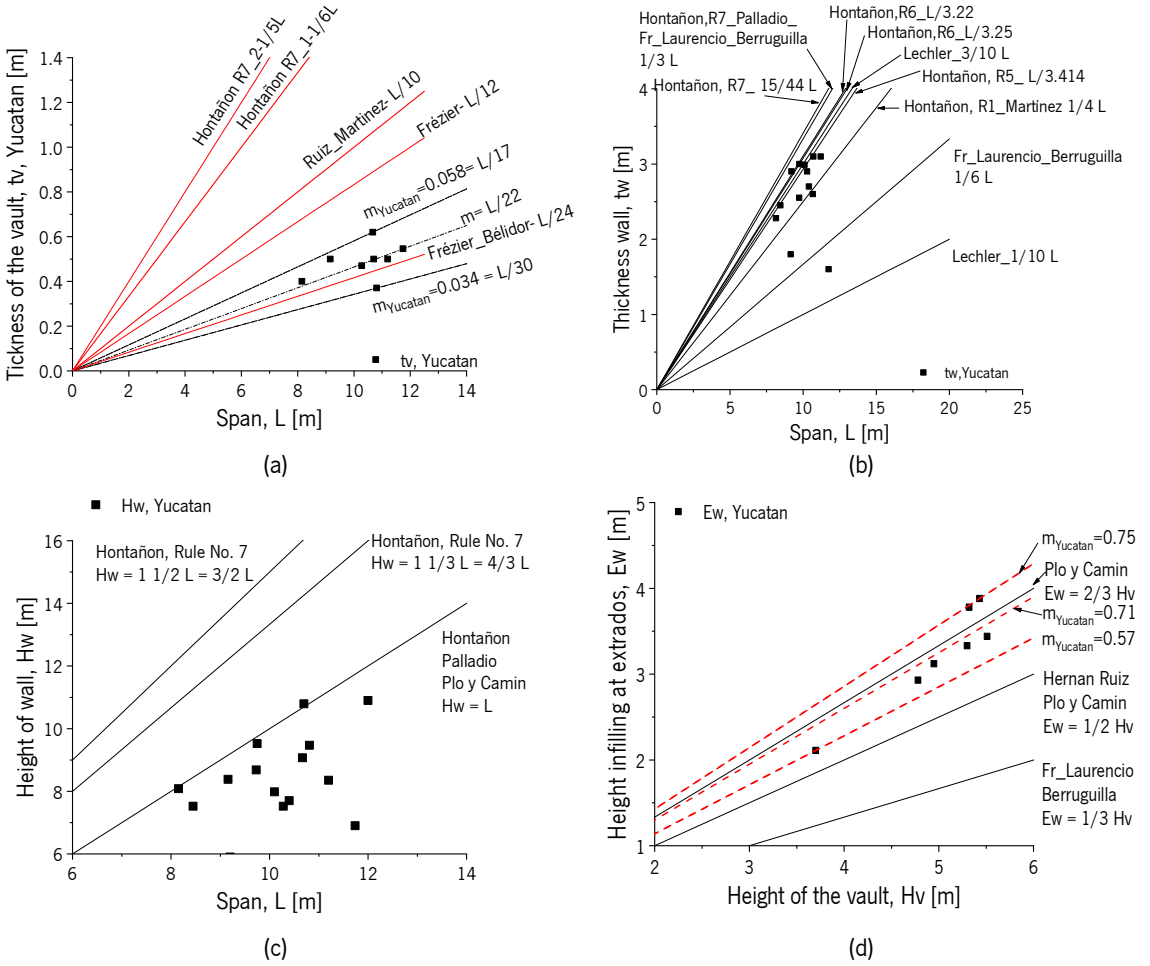


Figure 3-16. Comparison between the Yucatan churches and the historical rules; (a) Thickness of the vault, (b) Thickness of the wall, (c) Height of the wall and (d) Height infill at extrados of vaults

Regarding to the thickness of the walls, in Morelia and Morelos churches, it is around the historical rule proposed by both Fr_Laurencio and Berruguilla (*tw=1/6L*). In case of Morelia churches, the thickness of the walls ranges from *0.12L* to *0.22L* (approximately *L/8* and *L/4.5*) and in Morelos churches it varies from *0.11L* to *0.19L* (approximately *L/9* to *L/5.25)*, see Figure 3-17b. Finally, the thickness of the walls in Oaxaca churches ranges from *0.25L* to *0.29L* and is within the rules 1 and 5 (*tw=L/4* and *tw=L/3.414*) proposed by Hontañon (Sanabria, 1982), see Figure 3-17b.

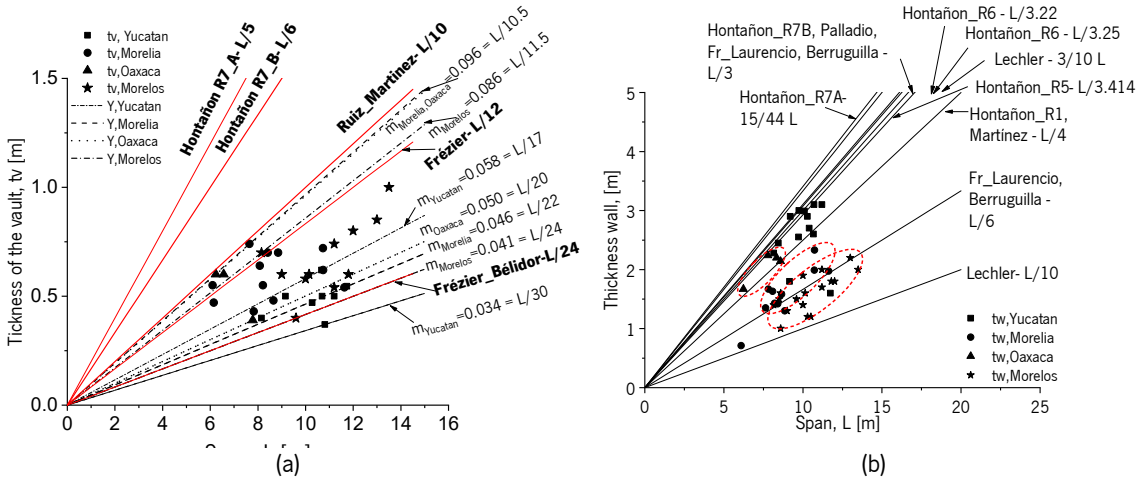


Figure 3-17. Comparative analysis of geometric parameters from churches of Mexico and proposals provided in historic treatises

3.7 Concluding Remarks

A statistical geometrical study comprising a database of 44 churches in Yucatan was carried out aiming at finding significant statistic correlations between selected key geometric parameters describing the cross section of the churches. This study revealed that the height of the walls (*Hw*) was probably governed by the total height of the churches (*H*), being defined approximately as 75% of *H* (±1.8m), independently on the type of vaults adopted.

On the other hand, taking only single span churches with barrel vaults, corresponding to about 60% of the churches in the database, it was possible to derive three statistically significant empirical rules between the height of the vaults (*Hv*) and height of the walls (*Hw*) with the span (*L*): *Hv=0.39L+1.06* (r^2*=0.73*), *Hv=0.28H+1.18* (r^2*=0.64*) and *Hw=0.72H-1.18* (r^2*=0.92*). This appears to indicate that the height of the vaults is related to both the height of the walls and to the span. As expected, when only semi-circular barrel vaults are considered, the correlation between the height of vaults and the span (*Hv=0.5L)* is very significant (r^2*=0.92*). Significant correlations were also found between *Hw* and *H* (r^2 *= 0.90*) and between *H* and *L* (r^2 *= 0.61*) but no other significant statistical correlations between the key geometric parameters were obtained. Based on these results, it was decided to derive empirical rules by considering only the data that resulted in significant statistical data ($r^2 \geq 0.6$). From this procedure, it was possible to derive expressions as a function of the span (*L*) for the height of the walls (Hw), height of the vaults (Hv), thickness of the walls (*tw*) and for the thickness of the vaults (*tv*). Additionally, a comparative analysis was performed between Yucatan churches and other Mexican churches from Morelia, Oaxaca and Morelos. Also for these churches, with single span and barrel

vaults, significant statistical correlations between the key geometric parameters *Hw*, *Hv*, *tw* and *H* and the span of the churches, *L*, were found.

An interesting finding regarding to the backfill height at extrados of the barrel vaults of Yucatan churches is the variation of centre angles from 33° to 46°, which means that the free vault span reduces from 10.6% to 13.9%. The comparisons with other Mexican churches from Oaxaca and Morelia show a strong concentration of backfill height with centre angles between 30° and 65°. However, there are other examples where the backfill covers completely the vaults.

By reviewing empirical rules for key geometric parameters in European historical constructions treatises from sixteen to eighteen century, namely, thickness and height of the walls, thickness of the vaults and backfill height at extrados of the barrel vaults, it was possible to see that the empirical geometric rules found for Yucatan churches can be compared with some geometric rules proposed by different authors. In addition, the analysis of other Mexican churches, which appear to have been built at an empirical or intuitive basis, reveals that geometrical key parameters are in the range of the several values proposed in the historical construction treatises, which indicates that the Mexican builders had incorporated some existing knowledge, possibly introduced by Spanish explorers.

Chapter 4.
Physical-mechanical characterization of limestones from Yucatan churches

Abstract:
This Chapter aims at the characterization of limestones and mortars found in masonry churches from sixteenth to eighteenth centuries located in Yucatan region in Mexico. To achieve the objectives, an experimental campaign was designed with the following steps: (1) identification of churches under ruins and in situ collection of stone specimens and mortar samples, (2) characterization of physical and mechanical properties on the collected stone specimens; (3) evaluation of the mineralogical composition of limestones and mortars and petrography description of stone samples.
It was found that the limestones studied were mainly composed of calcium carbonate ($CaCO_3$) and based on the physical properties, it was possible to group them in three different groups. It was also found that different ranges for the compressive strength and modulus of elasticity were obtained for the limestone belonging to each group defined. Furthermore, the mortars were identified as calcium carbonate ($CaCO_3$) and no mechanic test were possible to perform since the samples were so weak.

4.1. Introduction

As described in Chapter 2, structural elements of Yucatan churches and many others in Mexico were mostly build with limestone and lime mortar. In spite of this, there is neither much information on the mechanical properties of raw materials nor on the stone masonry material as a composite.

From literature review, only few works could be found on the experimental characterization of the mechanical behaviour of limestone. In this scope, studies on the physical, petrographic, and mineralogical properties of limestone have been carried out by Alonzo (2003), Carrillo (1991), Estrada-Medina (2008) and May-Crespo (2012). The influence of high temperatures in the physical properties of four limestone from the Yucatan Peninsula has been addressed by González-Gómez (2015). Environmental degradation of a red and white limestone exposed to a rural tropical atmosphere has been analysed by Maldonado (2011). However, there is no specific information on the types of limestone used in Yucatan historic churches.

Regarding to historical mortars, few studies were also carried out on Mexican historical structures both concerning identification of the raw materials, namely at the level of the binder to aggregate ratios and physical and mechanical characterization. Binder to aggregate ratios of 1:2.5 and 1:3 (in volume) have been point out by Chávez and Meli (2008) and by Chávez et al. (2012). With respect to mortars from Yucatan historical constructions there is no quantitative evaluation of the binder to aggregate ratios. It is important to note that the ratios in volume are different of ratios in mass. As an example, volume ratios from 1:1 to 1:4 correspond to mass ratios of about 1:3 to 1:12 in mass (Veiga, 2015), as it depends on the density of the aggregate and of the binder. At the international level, several research has been conducted in the scope of characterization of historic mortars, such as in Portugal, Italy, Belgium and Spain (Balen and Hendrickx, 2008; Binda et al., 1997; Calderini et al., 2015; Garmendia et al., 2015; Magalhães and Veiga, 2009; Veiga, 2015). These works pointed out binder: aggregate ratios from 1:1,5 to 1:5,5 (in mass).

It is stressed that the knowledge of stone and mortar properties is very important when conservation and repair on materials in historical buildings is required. In addition, when the structural analysis is needed, it is also important to know the mechanical properties of stone masonry (Giaretton et al., 2015; Hatir and Ince, 2021). In the case of experimental research on existing masonry structures, an important challenge is to replicate the old materials to have representativeness of the experimental models, namely at the mechanical level. It should be mentioned that this can be difficult due to (a)

the lack of open quarries to provide similar stone (a) the aging and to decay processes inducing physical and mechanical properties.

Therefore, the main goal of the present chapter is a multi-scale experimental characterization of limestone types and mortars used in the construction of Yucatan churches. For stones the experimental program encompasses: (1) characterization of physical properties at macro-scale, namely open porosity, water absorption at atmospheric pressure and water absorption coefficient by capillarity; (2) obtainment of mechanical properties regarding compressive behaviour, namely compressive strength and elastic modulus; (3) characterization at micro-scale with: (a) chemical and mineralogical identification; (b) petrographic description based on optical microscopy; (c) analysis of micro-structures through scanning electron microscopy. Due to the absence of adequate samples to process with the physical and mechanical characterization of mortars, only the chemical and mineralogical identification campaign was performed.

It should be stressed the output of this chapter is important to select the materials to be used in the experimental model of the barrel masonry vault to be tested and whose results will be presented in Chapter 7.

4.2. Survey of limestone and mortars from historical churches

Aiming at characterizing the stone and mortars used in Yucatan churches, it was decided to collect stone specimens and mortar samples from six partially collapsed churches built from sixteenth to eighteenth centuries located in the Yucatan State, which has an extension of 38,400 Km^2, see Figure 4-1.

The spatial location of the churches in Yucatan region is indicated in Figure 4-2. The churches were selected according to the damage state and major collapsed parts, trying to cover the larger state area with the time, resources, and access permissions available. It is important to notice that the stones and mortars to be characterized have already experienced weathering process and may present some weathering degree.



(a) (b)

Figure 4-1. Examples of partially collapsed churches: (a) San Jose Church from seventeenth century, Petulillo, Peto, (b) San Francisco church from eighteenth century, Kikil, Timizin

From a geological point of view, the Yucatán platform is composed of 3.7 km of massive carbonate sequences down to a granodiorite basement (Gulick et al., 2013; Monroy-Ríos, 2020; Sikora et al., 1996). The lithology of the area is mainly composed of limestone, marlstone, lutite and calcarenite amongst others (Figure 4-2).

The selected buildings are protected according to the Mexican federal law for monuments, archaeological, artistic, and historical areas (Camara de Diputados, 2018). Therefore, the collection of samples from the buildings was supervised by the National Institute of Anthropology and History of Mexico (INAH), which is the main representative of the Federal government for the heritage protection, and by the Commission of Ecclesiastical Properties and Sacred Art of the Archdiocese of Yucatan. Hence, only the samples allowed by both organizations were collected.

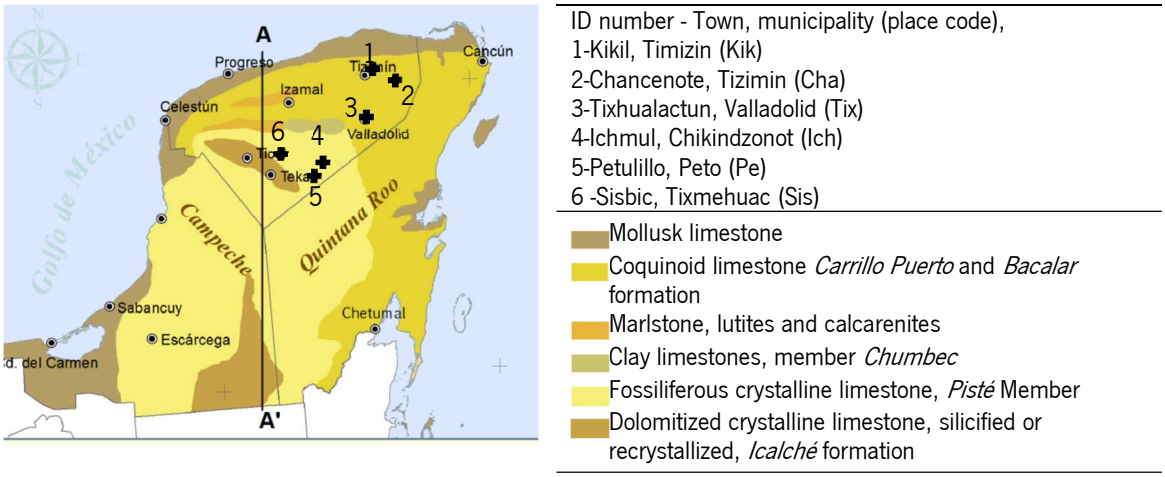


Figure 4-2. Spatial distribution of selected churches as case studies and general lithology of Yucatan state (adapted from (García and Graniel, 2010))

The guidelines for the samples collection were based on the entire respect for the historical value of the monument: (1) dismounted stones from the structure were preferred. The collection of stones in the original position was not allowed; (2) stones with carvings, paintings or drawings were not allowed

to be collected; (3) the samples must be collected with the minimum possible damage to the building. The mortar samples were collected from 7 mortar joints and 6 rendering mortars, whereas the stone blocks were picked up from the collapsed walls and vaults. About 12 wall units and 4 vault units were collected as stone samples. All samples were identified with an initial letter (P- stones, Ar-mortar) and with a code based on numbers (number of sample) and letters (location defined according to Figure 4-2), see Table 4-1 and Table 4-2.

Table 4-1. Identification code of stone blocks

sample	Town	case of study	ID Code	sample	Town	case of study	ID Code
1	Sisbic	wall	P1SIS	10	Kikil	wall	P10KIK
2	Sisbic	wall	P2SIS	11	Kikil	vault	P11KIK
3	Petulillo	wall	P3PE	12	Chancenote	wall	P12CHA
4	Petulillo	wall	P4PE	13	Chancenote	wall	P13CHA
6	Ichmul	wall	P6ICH	14	Tixhualactun	vault	P14TIX
7	Ichmul	wall	P7ICH	15	Tixhualactun	vault	P15TIX
8	Kikil	wall	P8KIK	16	Tixhualactun	wall	P16TIX
9	Kikil	vault	P9KIK	17	Tixhualactun	wall	P17TIX

Note: The sample number 5 was not in good conditions to be considered.

Table 4-2. Identification code of mortars

Sample	Town	case of study	ID Code	sample	Town	case of study	ID Code
1	Sisbic	render	AR1SIS	8	Kikil	render	AR8KIK
2	Sisbic	joint	AR2SIS	9	Kikil	joint	AR9KIK
3	Sisbic	joint	AR3SIS	10	Chancenote	joint	AR10CHA
4	Petulillo	render	AR4PE	11	Chancenote	render	AR11CHA
5	Petulillo	joint	AR5PE	12	Tixhualactun	render	AR12TIX
6	Ichmul	joint	AR6ICH	13	Tixhualactun	joint	AR13TIX
7	Ichmul	render	AR7ICH				

In order to carry out the characterization, both stone and mortar samples were transported at laboratory to be process. It was necessary to collect at least 30 gr of mortar in order to do possible the chemical characterization. While, the stone blocks were cored according to the standard ASTM-D4543 (2001). Due to the condition of the stone blocks, it was not possible to identify the bedding planes at the first glance. Therefore, it was decided to core the samples in two directions according to the parallel and vertical directions to the bed joints in the original position of each block. The cores were called vertical (*V*) or horizontal (*H*) according to the extraction direction, see Figure 4-3a.

After coring, it was possible to identify the bedding planes by visual inspection. The orientation of the bedding planes (β) was defined as the angle between the loading direction and the bedding plane (Figure 4-3b): (1) $\beta = 0°$ when the bedding plane is parallel to the loading direction (//), (2) $\beta = 90°$ when the bedding plane is perpendicular to the loading direction ($\perp$). It should be mentioned that in few times it was not possible to easily identify the bedding plane due to the random or absence of

pigmentation. In these cases, some uncertainty in the definition of the bedding planed needed to be assumed, see Figure 4-4.

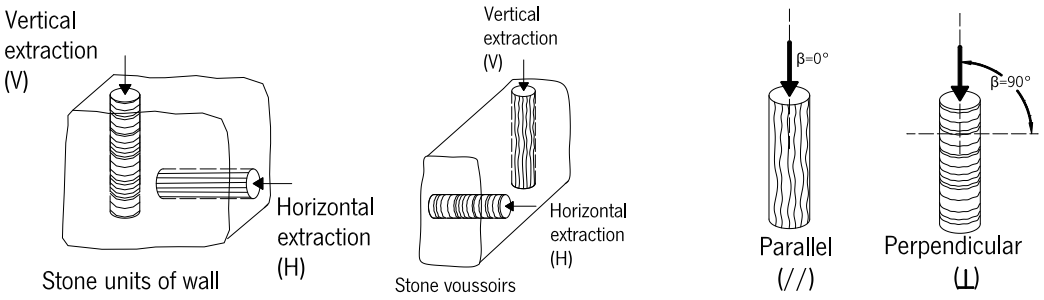


Figure 4-3. Cylindrical specimen: (a) extraction direction, (b) orientation of the bedding planes (β)



Figure 4-4. Limestone samples: (a) stone block, (b) view of some prepared core samples (c) defined bedding planes, (d) random or absence of clear bedding planes

In total, 16 masonry stone units were collected from the existing buildings, from which 111 cylindrical stone specimens were cored. The total number of core sample tested for each limestone sample and the number of specimens in each direction is summarized in Table 4-3. The distinct number of specimens is related to the variable dimensions of the original limestone blocks sampled since they had different dimensions.

Table 4-3. Core samples tested for each limestone block and the number of specimens according to the bedding planes

ID Code	Total	Parallel (//)	Perpendicular (⊥)	ID Code	Total	Parallel (//)	Perpendicular (⊥)
P1SIS	8	5	3	P10KIK	6	3	3
P2SIS	9	4	5	P11KIK	7	4	3
P3PE	6	3	3	P12CHA	6	3	3
P4PE	5	2	3	P13CHA	6	3	3
P6ICH	8	4	4	P14TIX	8	4	4*
P7ICH	7	3	4	P15TIX	7	3	4*
P8KIK	7	3	4	P16TIX	8	4	4
P9KIK	7	3	4	P17TIX	6	3	3
∑	57	27	30	∑	54	27	7

* these were not considered in the mechanical tests.

The core samples were extracted with two different diameters, namely 5.70 cm and 5.08 cm. According to the Standard previously mentioned, the specimens shall have a length/diameter ratio of 2.0 to 2.5 and a diameter not lower than 47 mm. Nevertheless, as some stone units have limited size dimensions and the experimental conditions were not ideal, the specimens were cut with height to diameter ratios of 1:1 and 1:2, see Figure 4-4b.

4.3. Experimental campaign

For the characterization of limestone from Yucatan churches, a detailed experimental analysis was designed at two different scales: (1) at macro-scale to obtain the petrographic features, physical and mechanical properties. At this scale, the anisotropy induced by the bedding planes was also analysed and discussed; (2) at micro-scale to obtain the chemical, mineralogical and micro-structure features. This section presents the description of the different experimental tools used for stones and mortar characterization.

4.3.1. Petrographic and mineralogy characterization

Polished thin sections of the different collected stone samples were prepared and examined under a polarized microscope to carry out the petrographic characterization of the limestone. A LEICA DMEP microscope coupled with a JVC colour video camera was used for taking micrographs of the samples.

Scanning electron microscopy with energy dispersive X-ray spectroscopy (SEM-EDS) was used as a first approximation for elemental chemical analysis. Additionally, X-ray diffraction (XRD) was used to identify the crystalline phases of the stone samples.

Stone fragments, previously coated with a high conductance thin film (gold film) were examined by scanning electron microscopy (SEM) associated with X-ray energy dispersive spectroscopy (EDS), using a PHILIPS ESEM XL30 electron microscope with a detector type sutw-sapphire using an electron bombardment with 25 KeV, under a vacuum of 1 Pa. The SEM micrographs of the samples were obtained at magnifications of 20X, 100X, 200X, 500X 1000X and 2000X. The EDS elemental analysis of the samples was performed in specific regions of the micrographs where a change in the appearance and colour of the particles was identified. Additionally, some pore size measurements were performed.

Mineral phase identification was carried out by X-ray diffraction (XRD) for both mortars (13) and stones (11) hereinafter called “natural samples”. Furthermore, the mineral phase identification was

performed with the obtained sample fraction after acid attack (hereinafter called "mineral traces"). After grinding the whole rock to an approximate particle-size <63 μm the samples were submitted to an hydrochloric acid attack (HCl-5% v/v) to eliminate the carbonates and to identify the clay and associated minerals. The XRD patterns were recorded with a Bragg-Brentano geometry at room temperature with CuKα radiation (λ = 1.5418 Å) at 40 KeV 30 mA in a D8 Advance diffractometer (Bruker). Diffractograms were recorded from 5 to 60° (2θ) at a speed of 0.02° through an aperture and a passage time of 0.5s and 0.1s, for natural and mineral traces samples, respectively. EVA software (Bruker AXS, Karlsruhe, Germany) was used to identify mineral phases with the ICDD database (International Centre for Diffraction Data, PDF2, 2003).

4.3.2. Physical and mechanical characterization

The physical characterization of limestone was performed on cored samples according to EN-1936 (2006) and NP-EN-13755 (2008) to obtain key physical properties such as apparent density (ρ), open porosity (η) and water absorption by immersion at atmospheric pressure (Ab). Capillarity water absorption tests were also performed according to standard NP-EN-1925 (2000) from which kinetics of the capillary rise and the water capillary absorption coefficient were evaluated. The specimens were dried until constant mass at 60±5 °C in a ventilated oven. The amount of water absorbed by the specimen per unit area, Q_i (kg/m²), at time t_i(s) was calculated as:

$$Q_i = \frac{(m_i - m_0)}{A} \quad (1)$$

Where:
m_i is the mass of the specimen (in kg) at time t_i,
m_0 is the mass of the dry specimen (in kg)
A is the area of the specimen in contact with water (in m²).

The diagrams of the capillary water absorption (Qi) as a function of the square root of time ($t_i^{1/2}$) were defined to obtain the capillary water absorption coefficient (Cw) as the slope of the linear regression considering at least 6 successive points in the ascending branch (EN 15801, 2008). As the capillary water absorption was obtained for the parallel and perpendicular direction to the bedding planes, it was decided to consider a factor relating the capillary coefficient in both directions. This factor was called Fwc and was calculated by dividing the coefficient of capillary obtained in the parallel direction to the coefficient of capillary obtained in the perpendicular direction to the bedding planes.

The mechanical characterization was based on uniaxial compression tests and was performed in two stages: (1) in the first stage, the specimens were tested until 30% of the predicted average compressive strength to obtain the elastic modulus, considering 4 load cycles (BS EN 14580, 2005). All cyclic tests were performed under loading control. The linear elastic load threshold to be considered in the cyclic procedure was estimated based on preliminary two monotonic tests carried out until failure, being fixed in 30% of the predicted average compressive strength. The modulus of elasticity was calculated by dividing the variation of stress by the variation of displacement in the last load cycle; (2) in the second stage, complete uniaxial compression tests were carried out, from which the stress-strain diagrams were obtained (NP EN 1926, 2000).

The testing equipment and the control system represent the major factors for a successful compression test conducted on stiff rocks. In the present work, the uniaxial compression tests were carried out in a very stiff frame connected with an appropriate closed-loop control system at the Structural Laboratory of University of Minho. The capacity of the hydraulic jack was 300 kN. In order to obtain the Young's modulus, *E*, two steel rings were placed at the thirds from the top and bottom sides of the specimen, to which three LVDTs were attached at 120° apart to measure the vertical displacement (Figure 4-5a). The length of measurement is about one third of the height of the specimen. For the complete uniaxial compression tests, axial displacement of the specimens was measured by means of three LVDTs placed 120° apart between the lower and upper platens according to the configuration indicated in Figure 4-5b. These LVDTs have a linear field of 25 mm with a sensitivity of 150 (± 5) mV/V/mV and a resolution of 0.09%. The compression test was performed by displacement control at a rate of 0.002 mm/s.

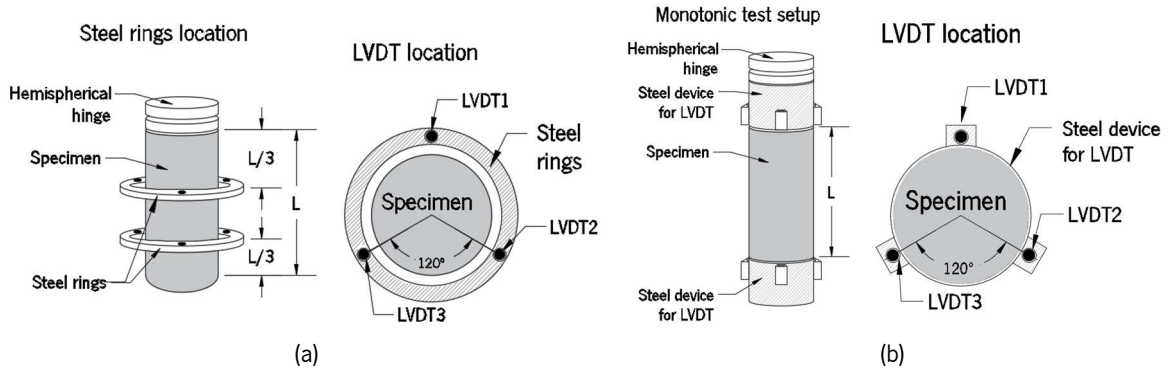


Figure 4-5. Devices used for the mechanical characterization; (a) under cyclic tests, (b) under monotonic tests

The compressive strength of each specimen was calculated by the ratio between the maximum load obtained during the uniaxial compression tests and the average cross-sectional area. The average displacement and corresponding strain were calculated based on the displacements measured by the

three LVDTs. In samples in which the height to diameter ratio differs from one by 25 % or more, the experimental compressive strength (*fe*) was corrected to the real compressive strength (*fc*) according to the standard ASTM C170 (1999).

Following the recommendations of Singh (1983), Ramamurthy (1993) and Saeidi (2014), the strength anisotropy index can be calculated according to the equation:

$$I\sigma_c = \frac{f_{c90°}}{f_{cmin}} \tag{2}$$

Where:
$I\sigma_c$ is the strength anisotropy index.
$f_{c(90)}$ is the uniaxial compression strength to perpendicular to the planes of anisotropy.
$f_{c(min)}$ is the minimum value of f_c.

In this research, as there is no information on the minimum value of the compressive strength as only two loading directions were considered, it was decided to calculate the strength anisotropy index ($I\sigma_c$) by the ratio between the compressive strength in parallel direction (*fc*//) and the compressive strength obtained in perpendicular direction (*fc*⊥). At the same time, it was decided to classify the strength anisotropy based on the classification pointed out by (Ramamurthy et al., 1993; Saroglou and Tsiambaos, 2007), see Table 4-4**.**

Table 4-4. Classification of strength anisotropy index

Strength anisotropy index, $I\sigma c$	Class
1.0-1.1	Isotropic
>1.1-2.0	Low anisotropy
>2.0-4.0	Medium anisotropy
>4.0-6.0	High anisotropy
>6.0	Very high anisotropy

Additionally, an anisotropy index based on the modulus of elasticity was also calculated as (Amadei, 1996; Nasseri et al., 2003; Saeidi et al., 2014; Worotnicki, 1993):

$$I_{aE} = \frac{E_{max}}{E_{min}} \tag{3}$$

Where:
I_{aE} is the degree of anisotropy by modulus index.
Emax is the maximum modulus of elasticity.
Emin is the minimum modulus of elasticity.

The classification of the stones based on the modulus anisotropy index was carried out following the recommendation of Worotnicki (1993), see Table 4-5.

Table 4-5. Classification of index by modulus anisotropy

Classification	Modulus anisotropy index (I_{ae})
Low anisotropy	<1.3
Mean anisotropy	<1.7
High anisotropy	< 4.0

4.4. Microscopic and mineralogical analysis

As previously mentioned, an attempt was carried out to identify the masonry stone and mortar existing the selected Yucatan churches. The results of petrography, X-ray and electronic microscopic analysis are presented and discussed herein. It should be mentioned that regarding to the mortars removed from the buildings, only mineralogical results are presented. An attempt was made to carry out petrographic analysis of mortars to possibly define the binder to aggregate ratio, but is was not successful because no other particle other than lime binder were identified: (a) as mentioned in Chapter 2, the mortars should be composed of lime binder and limestone aggregates; (b) due to the possible low size of the aggregates, it was not possible to obtain any contrast with the lime binder. Based on this, it was decided not to proceed also with the electronic microscopic analysis of the mortars.

4.4.1. Petrography

In a first phase a macroscopic analysis of the limestone was carried out based on visual inspection of the 16 research samples, see Figure 4-6. The samples present different combinations of beige, red and brow colours, and brownish tones, which their colour is most of the times non homogenous, except for P1SIS and P4PE, that are very homogeneous light beige and light-yellow limestone. The different combination on beige, red and brown colours enabled to clearly identify the bedding planes in most samples.

Moreover, these lithotypes present different textures (e.g., Figure 4-5: P4PE vs P15TICH), different macrofossils content (e.g., Figure 4-6: P7ICH vs P1SIS) and occurrence, in certain cases, of stylolites (e.g. Figure 4-6: P3PE) and also randomly distributed macropores visible to naked eye (e.g. Figure 4-6: P2SIS, P4PE, P6ICH, P11KIK, P13CHA, P16TIX). These voids in randomly coloured samples (e.g., Figure 4-6: P14TIX P15TIX P16TIX P17TIX) generally contained low cohesion material, which was, at least superficially, lost during the preparation of the specimens.

Figure 4-7 and Figure 4-8 illustrates the microstructure of these lithotypes observed under an optical microscope. For the classification of these lithotypes, the compositional scheme of Folk (1959, 1962) and the textural features of Dunham (1962) were used. The examination of the polished thin sections of the different samples (Figure 4-7and Figure 4-8) allowed their subdivision into 4 groups, based on the mineralogical composition, compositional texture, structure, and bioclasts content:

- **Group A**, corresponding to samples P2SIS (Figure 4-7b), P8KIK (Figure 4-7g) and P10KIK (Figure 4-8a) which are micrite limestones (mudstones) with interparticle porosity made up of relatively large pores (areas with darkest color). Indeed, bioclasts were not observed in these samples.
- **Group B**, corresponding to samples P1SIS (Figure 4-7a), P4PE (Figure 4-7d), P6ICH (Figure 4-7e), P7ICH (Figure 4-7f) and P9KIK (Figure 4-7h), which are biosparite limestones (grainstones). Sparry calcite cement is made of clear transparent crystals. Remains of different bioclasts were found, which included gastropods, bivalves, benthic foraminifera, green algae, ostracodes and corals, among others. Inter and intra-particle pores (areas with darkest color) are observed, being the first the dominant.
- **Group C**, corresponding to samples P3PE (Figure 4-7c), P11KIK (Figure 4-8b), P12CHA (Figure 4-8c), P13CHA (Figure 4-8d), P14TIX (Figure 4-8e) and P16 TIX (Figure 4-8g), which corresponds to porous micrite limestone with scattered sparite calcite, with almost absence of bioclasts.
- **Group D**, corresponding to samples P15TIX (Figure 4-8f) and P17TIX (Figure 4-8h), which corresponds to biomicritic limestones (wackstone and mudstone, respectively), with recrystallized calcite patches and inter and intra-particle pores. The remains of bioclasts included gastropods, bivalves, and corals.

In samples P3PE (Figure 4-7c) and P15TIX (Figure 4-8f) it also must be mentioned the occurrence of several spots of orange-brownish material probably associated to the presence of iron oxides-oxyhydroxides.

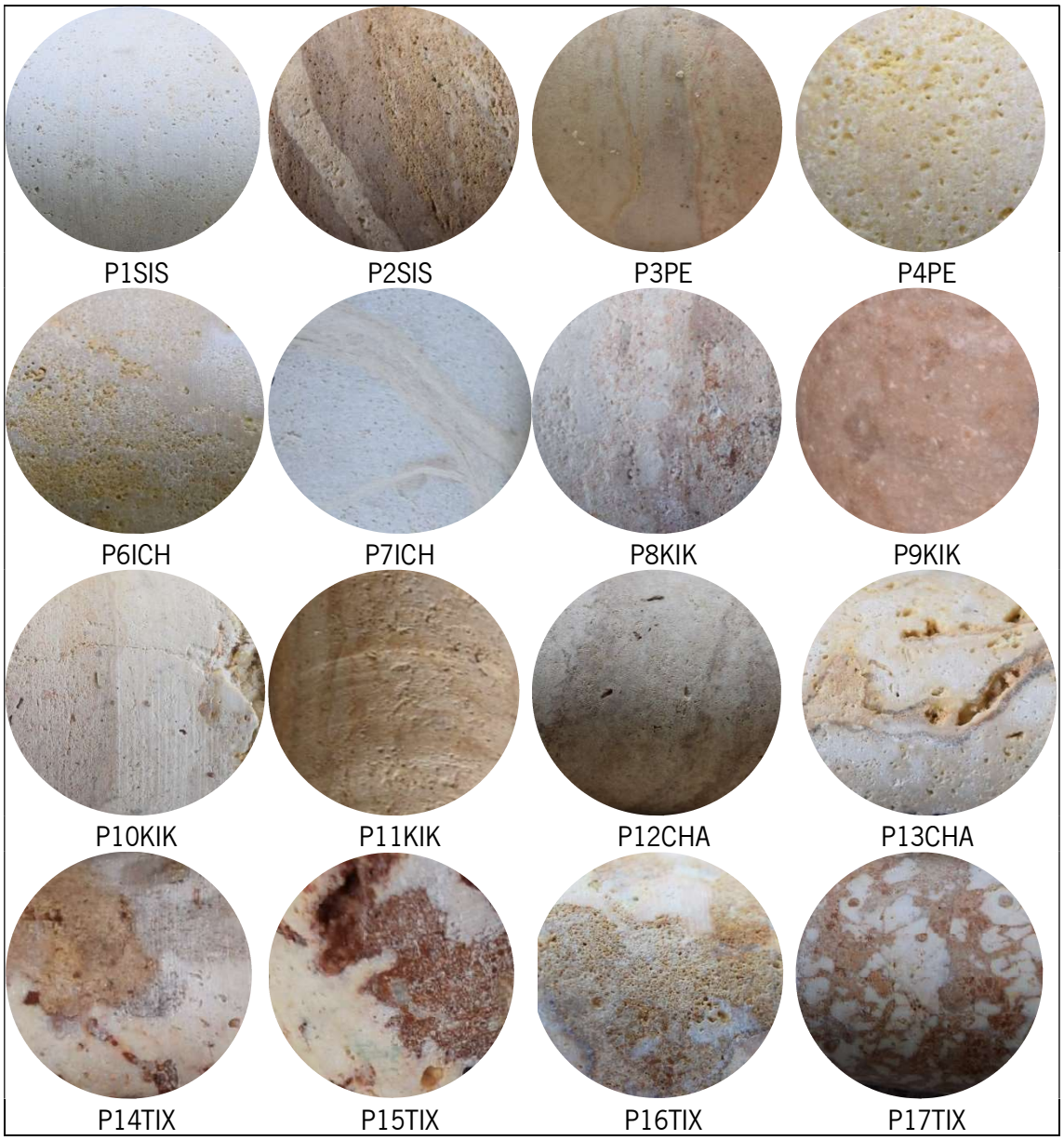


Figure 4-6. Macroscopic image of the 16 studied lithotypes

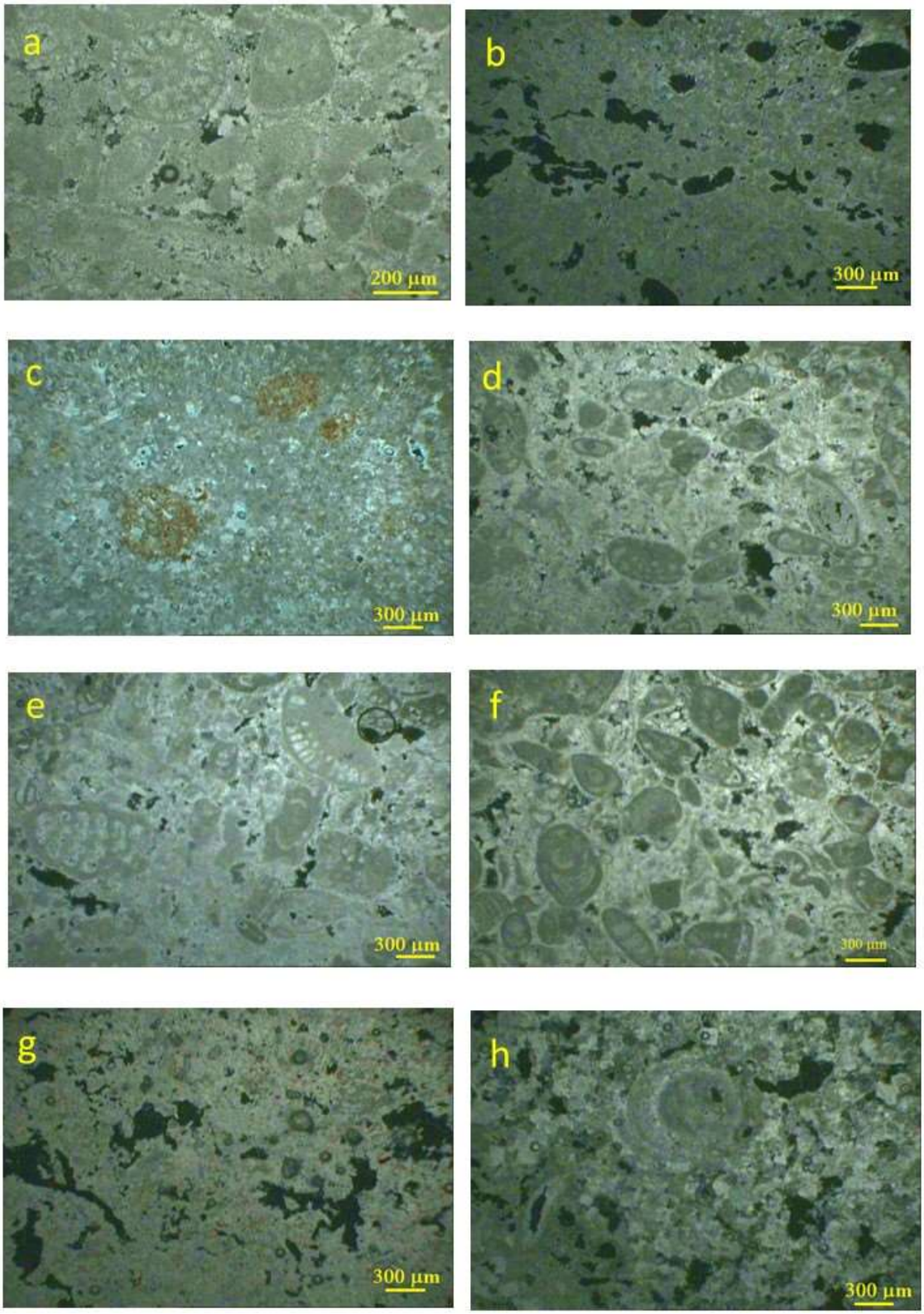


Figure 4-7. Micrographs of the studied lithotypes: a) P1SIS; b) P2SIS; c) P3PE; d) P4PE; e) P6ICH; f) P7ICH; g) P8KIK; h) P9KIK (cross polarized light)

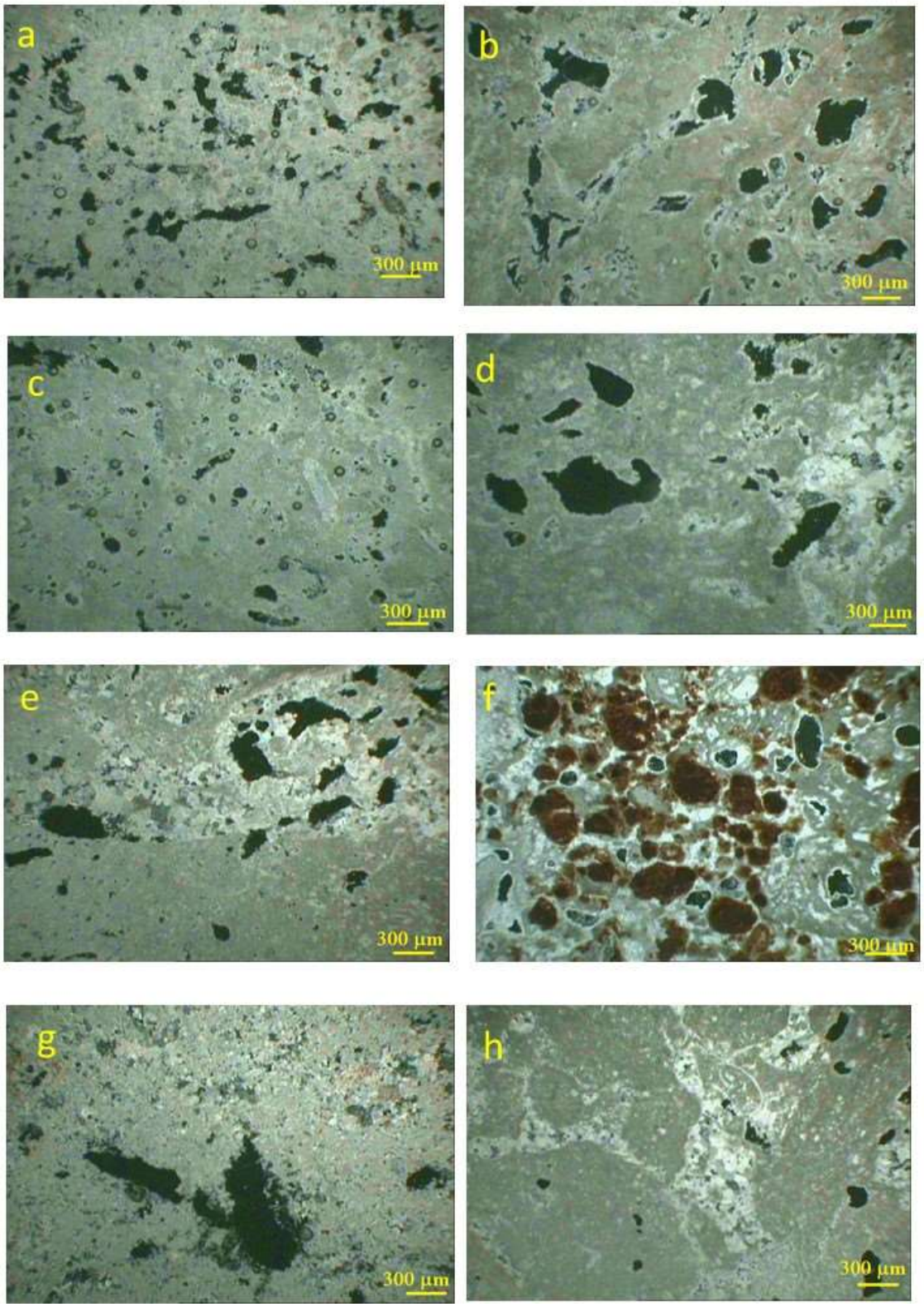


Figure 4-8. Micrographs of the studied lithotypes: a) P10KIK; b) P11KIK; c) P12CHA; d) P13CHA; e) P14TIX; f) P15TIX; g) P16TIX; h) P17TIX (cross polarized light)

4.4.2. Mineralogic analysis

4.4.2.1. Mortars

From visual inspection, different colours were identified in the mortar samples. The most frequent was the yellowish, but whitish, light brown, dark brown and reddish colours were also observed in the samples. Among the samples analysed, the render mortars are white (2AR1SIS, 17AR8ICH, 32AR12TIX, 22AR8KIK) and yellow (10AR4PE, 30AR11CHA) (Table 4-6). On the other hand, joint mortars exhibit yellow (12AR5PE, 29AR10CHA, 14AR6ICH, and 33AR13KIK), brown (light 5AR2SIS and dark 6AR3SIS) and red (23AR9KIK) colours (Table 4-7). The identification of mineral phases in each mortar sample by X-ray diffractogram analysis was carried out both in render and joint mortars. Figure 4-9 shows the diffractograms obtained in rendering and joint mortars.

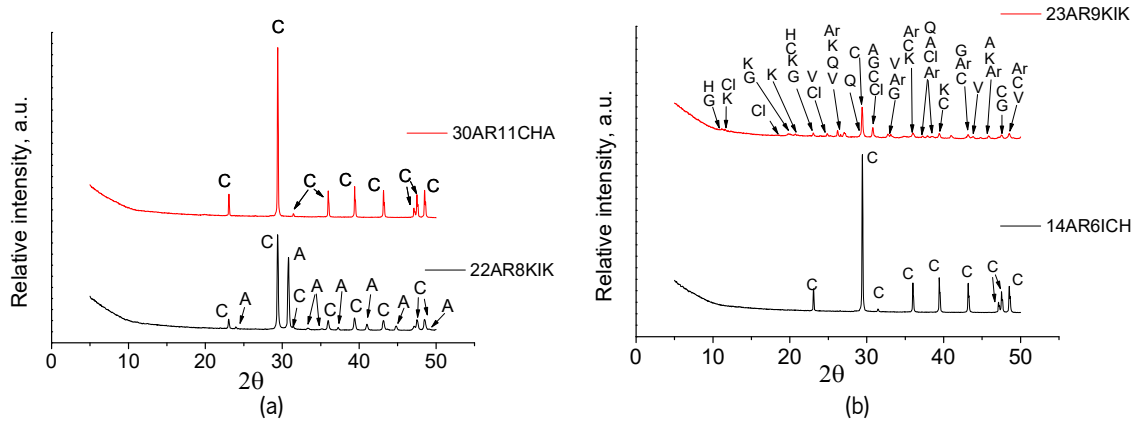


Figure 4-9. Examples of typical diffractogram from natural mortar samples. (a) render mortars, (b) joint mortars. C=Calcite, A=Ankerite, H=Hydrotalcite, G=Gypsum, K=Kaolinite, Ar=Aragonite, Q=Quartz, Cl=Clinochlore, V=Vaterite

Render mortars

The X-Ray analysis of natural samples taken from render mortars revealed only the presence of calcite and ankerite minerals, being both compounds classified as carbonates. The calcite mineral exhibits a rhombohedral structure of calcium carbonate ($CaCO_3$) and was recorded in six render mortars (AR1SIS, AR8ICH, AR12TIX, AR8KIK, AR4PE, AR11CHA). The ankerite mineral is a calcium carbonate polymorph with some traces of manganese and iron ($Ca(Mg0.67Fe0.33+2)(CO_3)_2$) and was recorded in only one sample (AR8KIK). This means that the samples AR8KIK have both calcite and ankerite in percentages of 56.8% and 43.2% respectively (Table 4-6). The presence of this mineral (ankerite) in the mortar can be justified if the aggregates used in the preparation of the mortar come from stones with a high content of ankerite,

As the predominant crystalline phase is carbonate in almost 100% of all render mortars analysed, the samples were decarbonized and further analysed aiming at identifying the mineral clay phases. From the mineral traces, clays such as kaolinite and montmorillonite calcian were detected in white colour render mortars. Quartz mineral was identified in the traces of 3 of 4 mortars with white colour. Minerals such as stilbite and phyllosilicates with micas such as muscovite (only in AR12TIX) and vermiculite (only in AR8KIK) were recorded as unique cases in white colour render mortars. According to Özkahraman and Işık (2003) quartz is a common associated mineral with limestone as binder and limestone aggregates.

In yellow render mortars (AR4PE, AR11CHA): (a) clay minerals as montmorillonite 2-0009, kaolinite-montmorillonite, saponite and hematite could be seen in AR4PE; (b) kaolinite, tosudite, palygorskite and halloysite clay mineral were identified in sample AR11CHA. According to González-Gómez (2015) and Maldonado (2011a), red coloration in the mortars is attributed to the presence of hematite. Probably the small amount of hematite brings the yellowish coloration to AR4PE sample.

Table 4-6. Mineral phases identified in render mortar samples

Render mortars		Natural mortars (%)		Mineral traces													
ID Code	Colour	Calcite	Ankerite	Kaolinite	Montmorilonite Calcian	Tosudite	Montmorillonite 2-14	Montmorilonite 2-0009	Kaolinite-Montmorilonite	Saponite	Palygorskite	Halloysite	Muscovite	Chlorite-vermiculite-montmorilonite	Quartz	Stilbite	Hematite
AR1SIS	whitish	100		X	X	X	X								X		
AR7ICH	whitish	100		X	X	X									X	X	
AR12TIX	whitish	100		X	X								X				
AR8KIK	whitish	56.8	43	X	X									X	X		
AR4PE	yellowish	100						X	X	X							X
AR11CHA	yellowish	100		X		X					X	X					

Joint mortars

X-ray diffraction analysis of natural samples of joint mortars revealed a composition based on carbonates in almost all samples, meaning that the predominant crystalline phase is calcite ($CaCO_3$) with very high concentrations (almost 100%). Only the mortar identified with a reddish colour (AR9KIK) presents clay phyllosilicates minerals, as well as quartz and gypsum. Additionally, regardless to the colour of mortar, all samples presented traces of kaolinite clay mineral.

Nevertheless, in two of the four yellow mortars (AR6ICH and AR13KIK) and in those identified in brown colour (both light and dark), tosudite, montmorillonite calcian and quartz mineral were identified. The difference in colour between them can be attributed to presence of calcite in yellow samples, and of rutile (TiO2) in brown coloured samples. Rutile (TiO2) is a mineral found in nature in red blood, bluish, brownish yellow, reddish brown or violet colours. The mortar sample AR6ICH sample presents also traces of rutile mineral (dark colours) in addition to the calcite (colourless or white, grey, yellow or greenish colours).

In spite of the similarities between joint mortars described above, there are two cases of yellowish joint mortars with specific characteristics. The first corresponds to the sample AR5PE, which only contains clay minerals as montmorillonite 2-0009, palygorskite, ilite and kaolinite. The other sample (AR10CHA) contains only kaolinite and another phyllosilicate named clinochlore. Finally, the particular case of the reddish-coloured mortar (AR9KIK) presents kaolinite and nacrite, as well as other two phyllosilicates: muscovite and chlorite-vermiculite-montmorillonite.

Table 4-7. Mineral phases identified in joint mortar samples

Joint mortars		Natural mortars (%)									Mineral traces												
ID Code	Colour	Hydrotalcite	gypsum	Kaolinite	Clinochlore	Aragonite	Quartz	Vaterite	Ankerite	Calcite	Kaolinite	Tosudite	Montmorilonite Calcian	Montmorilonite 2-0009	Palygorskite	Ilite	Nacrite	Clinochlore	Muscovite	Chlorite-vermiculite-montmorilonite	Calcite	Quartz	Rutile
AR5PE	yellowish									100	X			X	X	X							
AR10CHA	yellowish									100	X									X			
AR6ICH	yellowish									100	X	X	X					X			X	X	X
AR13KIK	yellowish									100	X	X	X								X	X	
AR2SIS	light brown									100	X	X	X									X	X
AR3SIS	dark brown									100	X	X	X									X	X
AR9KIK	reddish	2.5	3.7	3.9	1.2	7.3	4.1	8.2	24.5	44.5	X						X		X	X			

4.4.2.2. Stones

Three main mineralogical phases were identified in limestone samples: calcium carbonates (namely calcite CaCO3), magnesian calcite ($Mg_{0.03}Ca_{0.97}$)(CO_3) and ankerite ($Ca(Mg_{0.67}Fe_{0.33}^{+2})(CO_3)_2$), see Figure 4-10. The mineral phases identified after the decarbonation showed traces of (1) clay minerals as kaolinite ($Al_2Si_2O_5$), tosudite ($(K,Ca)_{0.8}Al_6(Si,Al)_8O_{20}(OH)_{10}$ $4H_2O$), nacrite ($H_4Al_2Si_2O_9$) and montmorillonite

calcian ($Ca_{0.2}(Al,Mg)_2Si_4O_{10}(OH)_2\ H_2O$); (2) muscovite ($(H,K)AlSiO_4$), Gypsum ($CaSO_4\ 2H_2O$), quartz ($SiO_2$) and salt halite (NaCl), see Table 4-8.

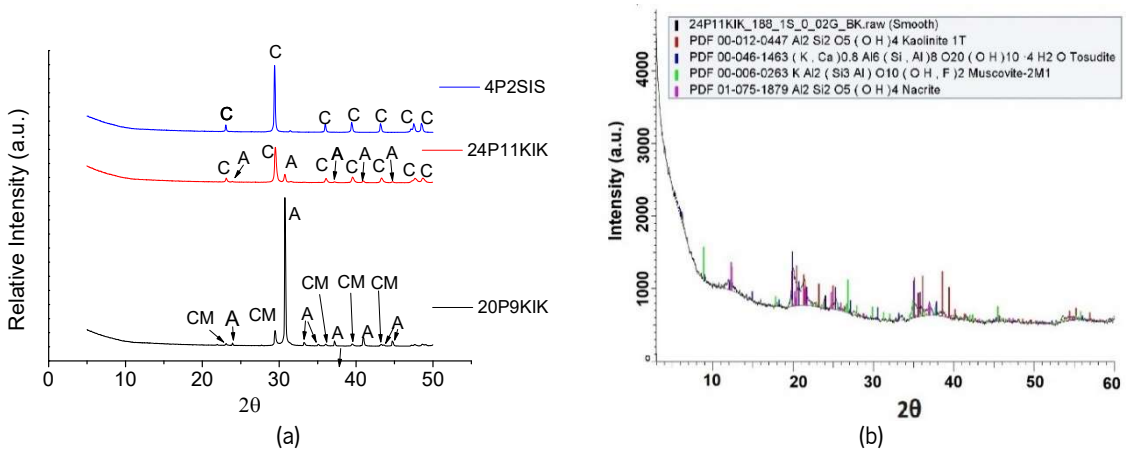


Figure 4-10. (a) Typical diffractograms of natural samples and (b) diffractograms of mineral phases after decarbonation. C=Calcite, A=Ankerite, CM= Calcite Magnesia

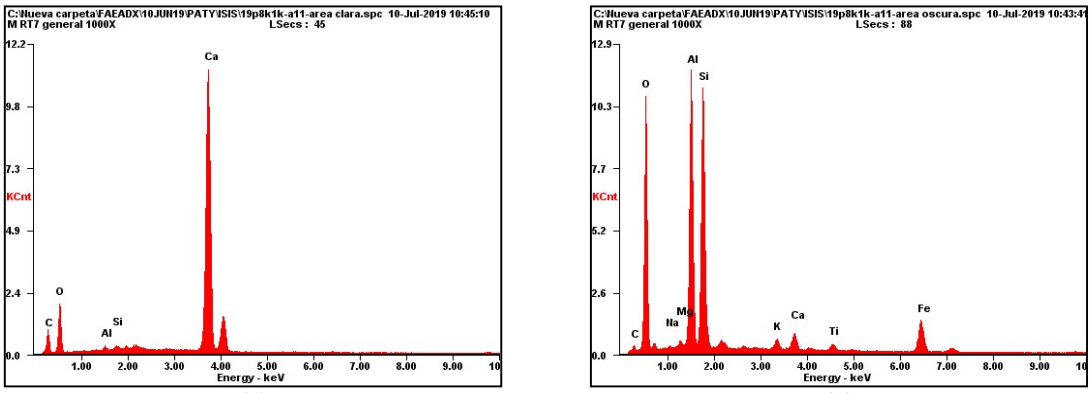
The results revealed that the studied rocks are carbonates (CO3) and some of them have traces of additional minerals. Since they are in a lower percentage (<10%), it is considered they have no impact on the physical and mechanical behaviour of the stone (Bissell and Chilingar, 1967). Calcite ($CaCO_3$) and dolomite [$CaMg(CO_3)_2$] are the most abundant carbonate minerals in the Earth. Most calcite is relatively pure, but sometimes have impurities as ions of magnesium, iron and manganese (Sun et al., 2014). In 1935, Cayeux developed a classification of carbonate rocks, according to their mineral content (%). This classification is composed by five rock typologies: (1) pure limestone (>95% calcite and <5% dolomite), (2) magnesian limestone (90-95% magnesian calcite and 5-10% dolomite), (3) dolomitic limestone (50-90% calcite and 10-50% dolomite), (4) calcitic dolostone (10-50% calcite and 50-90% dolomite) and (5) dolostone (<10% calcite and >90% dolomite) (Bissell and Chilingar, 1967; Pettijohn, 1975). Moreover, ankerite stone is a sedimentary rock that in comparison with dolomite are isomorphous, have similar optical properties and crystalline structures. Substituting Fe for Mg, ankerite forms a solid solutions series with dolomite. Ankerite stone is thereby defined as having a Fe/Mg ratio of greater than 1/4 otherwise is namely ferroan dolostone (Ellwood et al., 1989; Hendry, 1978). Therefore, from the mineral composition point of view, identified three rocks were identified: (1) limestones, (2) ankerite stone (P9KIK) and (3) magnesian limestone with ankerite stone (P11KIK).

Table 4-8. Mineral phases identified in the stone samples

	Natural stones (%)			Mineral traces									
	Calcite	Magnesian calcite	Ankerite	Kaolinite	Tosudite	Nacrite	Montmorillonite Calcian	Muscovite	Quartz	Gypsum	Halite	Calcite
Vault stones												
P15TIX	100			X	X	X						
P9KIK	0	10	90	X	X	X			X	X		
P11KIK	0	79.7	20.3	X	X	X		X				
P14TIX	100			X	X		X	X			X	X
Wall stones												
P4PE	100											
P6ICH	100											
P2SIS	100			X								
P7ICH	100			X			X					
P12CHA	100			X					X			
P8KIK	100			X	X				X			
P10KIK	100			X	X				X			
P1SIS	100			X	X			X				
P16TIX	100			X	X	X		X				
P17TIX	100			X	X			X				

4.4.3. Scanning electronic microscopic analysis

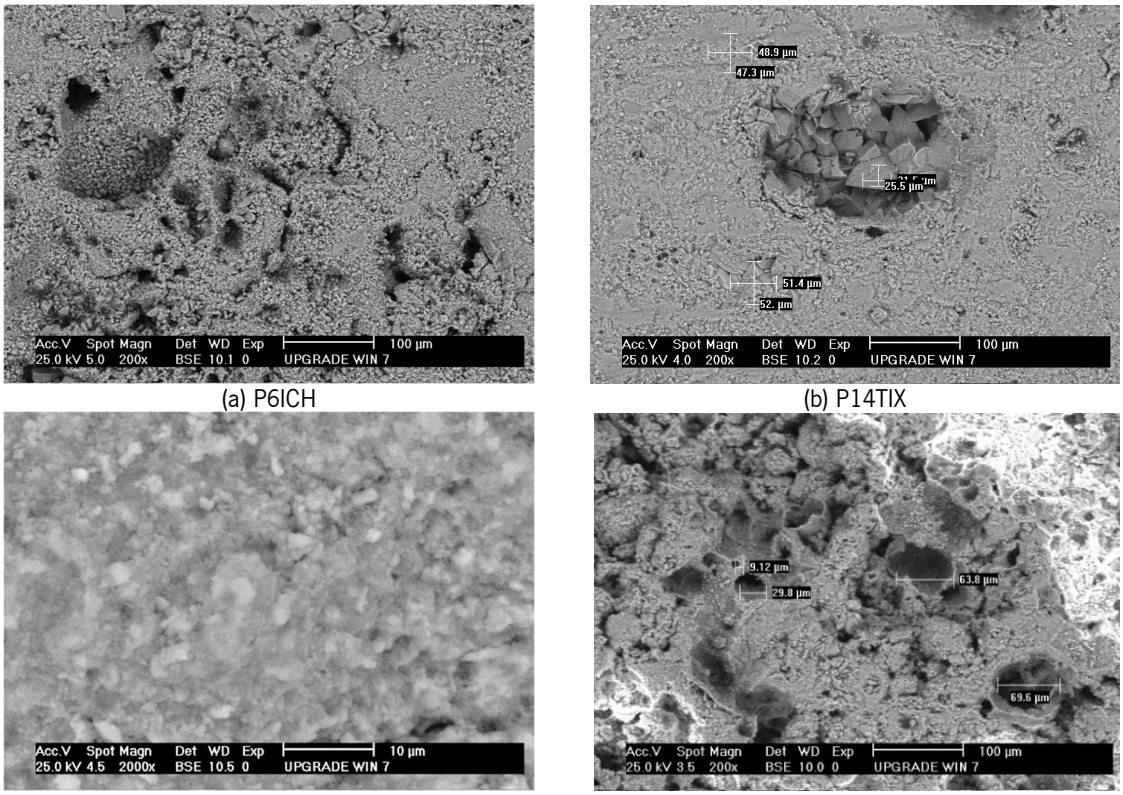
The SEM-EDS analysis (energy-dispersive X-ray spectroscopy, EDS) of the limestone samples revealed mostly three chemical elements: (1) calcium (from 28.85% to 41.34%), (2) carbon (from 19.04% to 23.35%) and (3) oxygen (from 37.57% to 47.8%). Traces of other elements were also identified, such as magnesium (from 0.51% to 2.11%) silica (around 1.45%) and alumina (around 0.55%), see Figure 4-11a and b.



(a) (b)

Figure 4-11. EDS analysis from sample P8KIK; (a) clear zone, (b) dark zone

Scanning electron microscopy photomicrographs show the samples had both compact and porous areas (Figure 4-12a and b both magnified at 200X). In the microscopy photomicrographs the voids or pores are identified in black. The predominance of the compact or porous areas makes possible the classification as a compact or porous sample. Figure 4-12c shows the P10KIK sample magnified at 2000X where is possible to observe the absence of voids or pores, contrary to the sample P11KIK (Figure 4-12d) magnified at 200X, which shows a clear presence of pores.

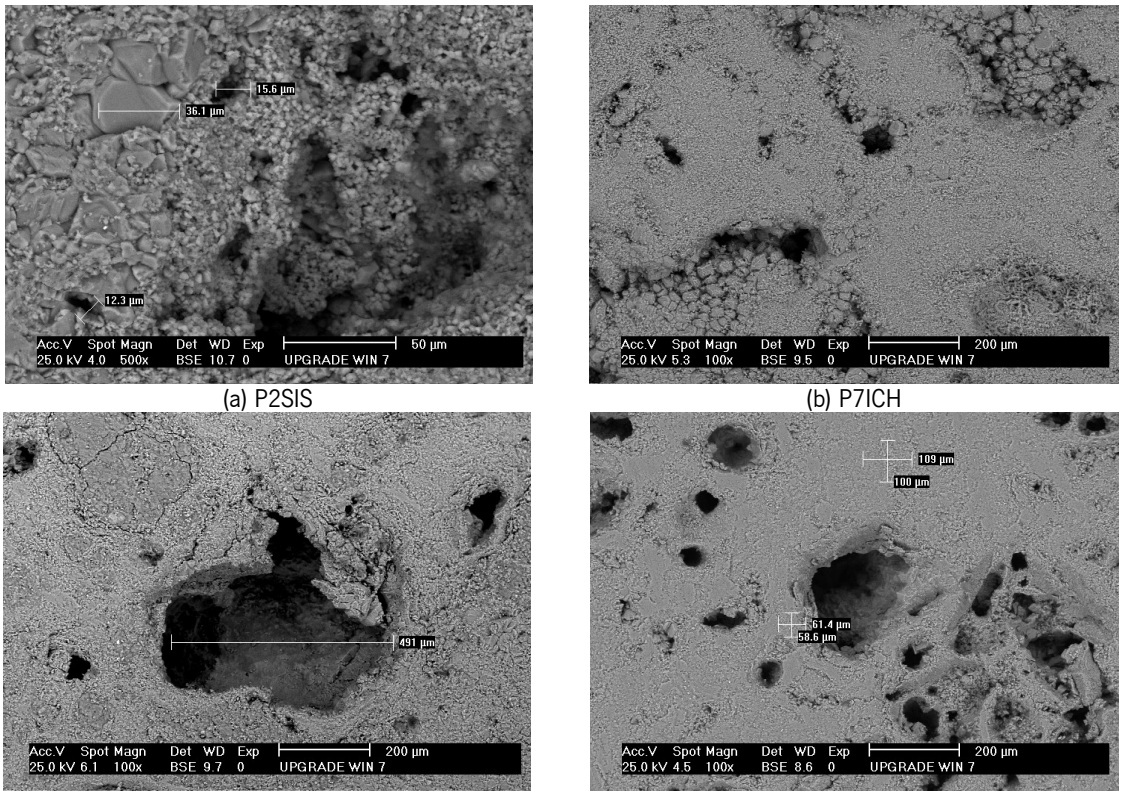


(a) P6ICH (b) P14TIX

(c) P10KIK (d) P11KIK

Figure 4-12.Scanning electron microscopy photomicrographs; (a) compact samples, (b) porous samples

The voids were measured from microscopy photomicrographs at different magnifications. The microscopy photomicrographs reveal voids with sizes from 10µm to 500µm with different densities. Figure 4-13a shows the P2SIS sample magnified at 500X and voids sizes from 12.3µm, while Figure 4-13b, c and d show samples magnified at 100X and pores from 50µm to 500µm. The voids show irregular geometries and there are randomly placed.

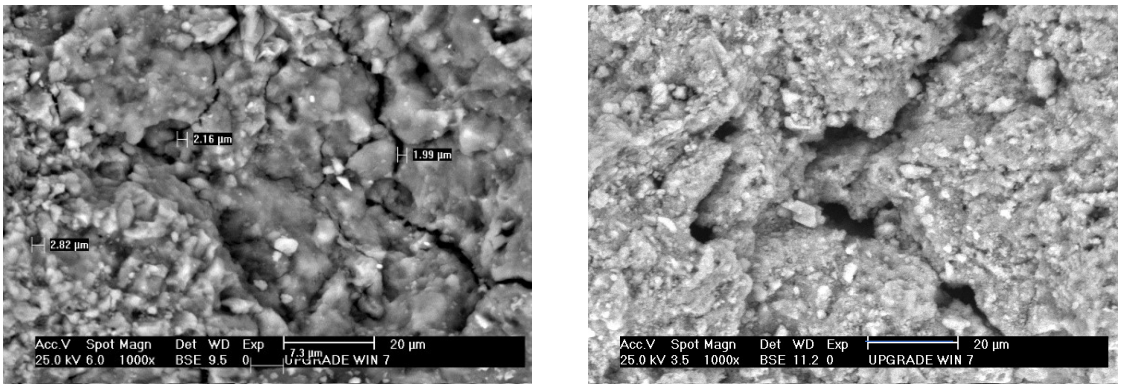


(a) P2SIS (b) P7ICH

(c) P8KIK (d) P15TIX

Figure 4-13. Scanning electron microscopy photomicrographs; voids

Some samples additional the voids show microcracks at greater magnifications. Figure 4-14a and b show microcracks on samples magnified at 1000X, P8KIK and P11KIK respectively. The microcrack thickness ranges from 1µm to 10µm and P11KIK sample shows grater microcrack thickness than P8KIK sample.

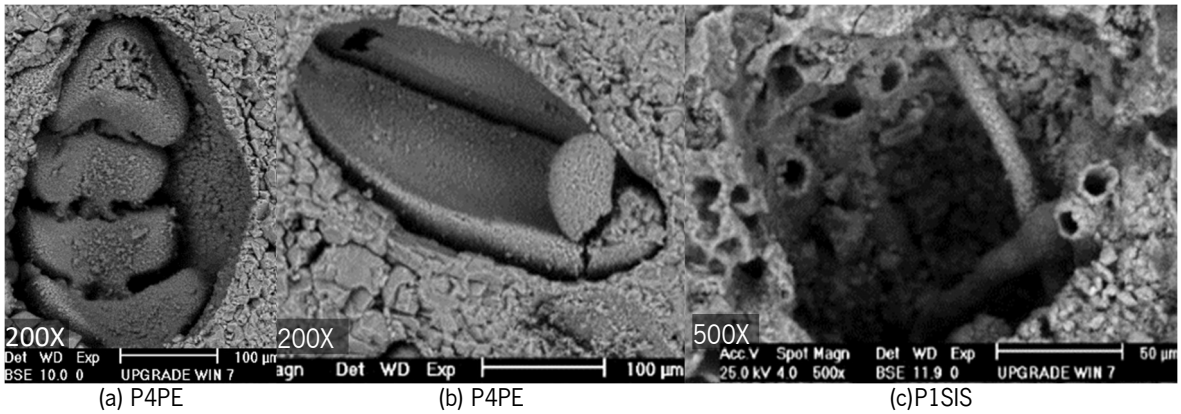


(a) P8KIK (b) P11KIK

Figure 4-14. Scanning electron microscopy photomicrographs; Microcracks

Fossil microorganisms, probably of marine origin, were identified on samples P11K1K, P8KIK, P6ICH, P4Pe and P1SIS. Figure 4-15a and b show the microscopy photomicrographs of P4Pe and P8KIK samples magnified at 200X, while Figure 4-15c the P1SIS sample magnified at 500X. The EDS

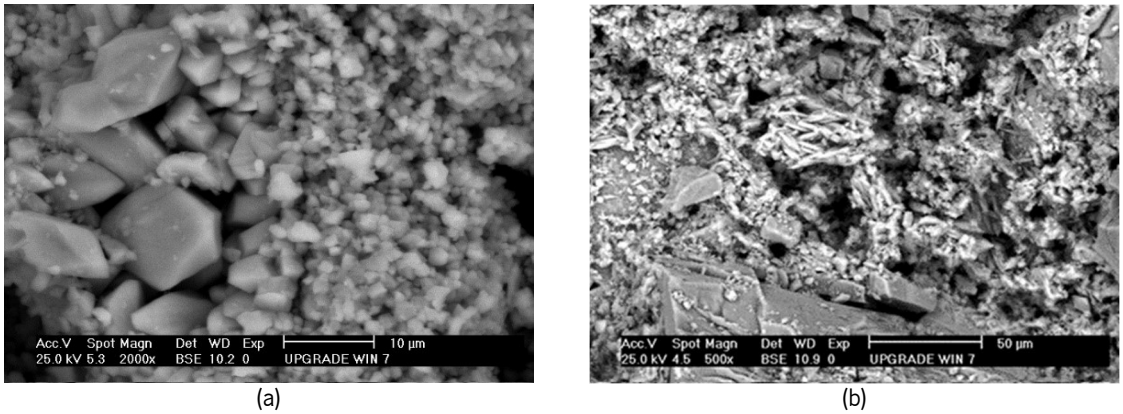
analysis (energy-dispersive X-ray spectroscopy) reveals a composition based on calcium, carbon and oxygen suggesting they are calcium carbonate (CaCO3).



(a) P4PE (b) P4PE (c)P1SIS

Figure 4-15. Scanning electron microscopy photomicrographs; Fossil microorganisms

The microscopy photomicrographs on Figure 4-16 show (a) hexagonal structures and (b) thin and elongated crystals. EDS analysis carried out on punctual elements reveals a composition based on calcium, carbon and oxygen suggesting they are calcium carbonate (CaCO3). However, the hexagonal shape suggests this structure belong to calcite, while the fibrous crystal shape suggests that there are related to aragonite.



(a) (b)

Figure 4-16. Scanning electron microscopy photomicrographs; (a) hexagonal structures and (b) thin and elongated crystals

4.5. Physical properties

4.5.1. Apparent density, open porosity and water absorption by immersion

As mentioned in Section 4.2, the physical characterization of limestone was performed in 111 stone specimens in parallel and perpendicular directions to bedding planes. Three key physical properties were obtained, namely apparent density (ρ), open porosity (η) and water absorption by immersion at atmospheric pressure (A_b). The apparent density (ρ) varies from 1577.68 to 2471.37 kg/m^3. The

greater frequency of apparent density is comprised between 1857.61 and 2471.37 kg/m³. Open porosity (η) ranges from 3.72% to 39.62% but the lower values are more frequent. Finally, the water absorption by immersion at atmospheric pressure (A_b) ranges from 1.54% to 25.04%, but low absorption predominates. These results indicate a wide range of variation of the physical properties for the limestone samples under analysis.

The relationships between these 3 parameters (open porosity, water absorption by immersion and apparent density) were analysed based on the scatterplots between pairs of variables. A single regression analysis, based on power regression models, was carried out and strong correlations between the parameters were observed, being the coefficients of determination (r^2) greater than 0.9 (Figure 4-17). Based on these scatter diagrams, it was possible to divide the limestones into three groups according to the ranges of values for open porosity and apparent density.

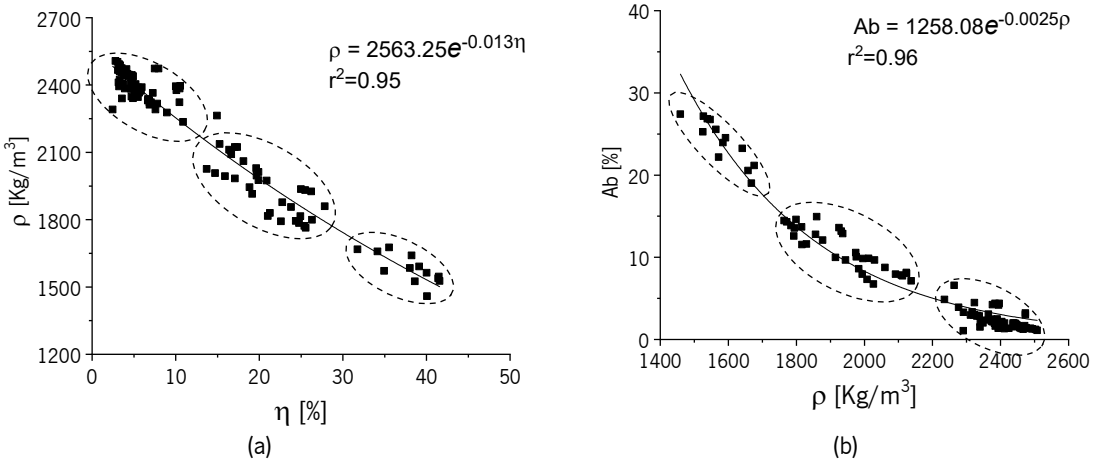


Figure 4-17. Power regression model analysis; (a) porosity vs density and (b) density vs water absorption

This assumption if confirmed by the results found for the box plots defined for all specimens of the same stone block shown in Figure 4-18. This allowed to distribute the stone samples contained in each group. Group 1 includes samples P8KIK and P10KIK, group 2 includes samples P2SIS, P3PE, P7ICH, P11KIK AND P12CHA and group 3 includes stone samples P1SIS, P4PE, P6ICH, P9KIK, P13CHA, P14TIX, P15TIX, P16TIX AND P17TIX.

This classification reveals that the Tixhualactun churches were built with stones from group 3, whereas Kikil churches have samples mainly belonging to group 1. Churches from Sisbic, Petulillo, Ichmul and Chancenote show a preference of stones from group 2 and 3. It should be stressed also that Group 1 encompasses stones belonging to the petrographic group A, but it is not possible to associate to the Group 2 and 3 a unique petrographic classification. The stones from Group 2 belong to petrographic groups A, B and C and stones from Group 3 belong to the petrographic groups B, C and D. The

limestone in group 1 combines the lowest apparent density with the highest porosity and water absorption by immersion. Stones from group 3 present the highest apparent density and the lowest porosity and water absorption by immersion.

The results shown in Figure 4-18 reveal the low to high scatter of the physical properties analysed, variable skewness and one outlier value, corresponding to the result obtained in specimen P9KIK-7V.

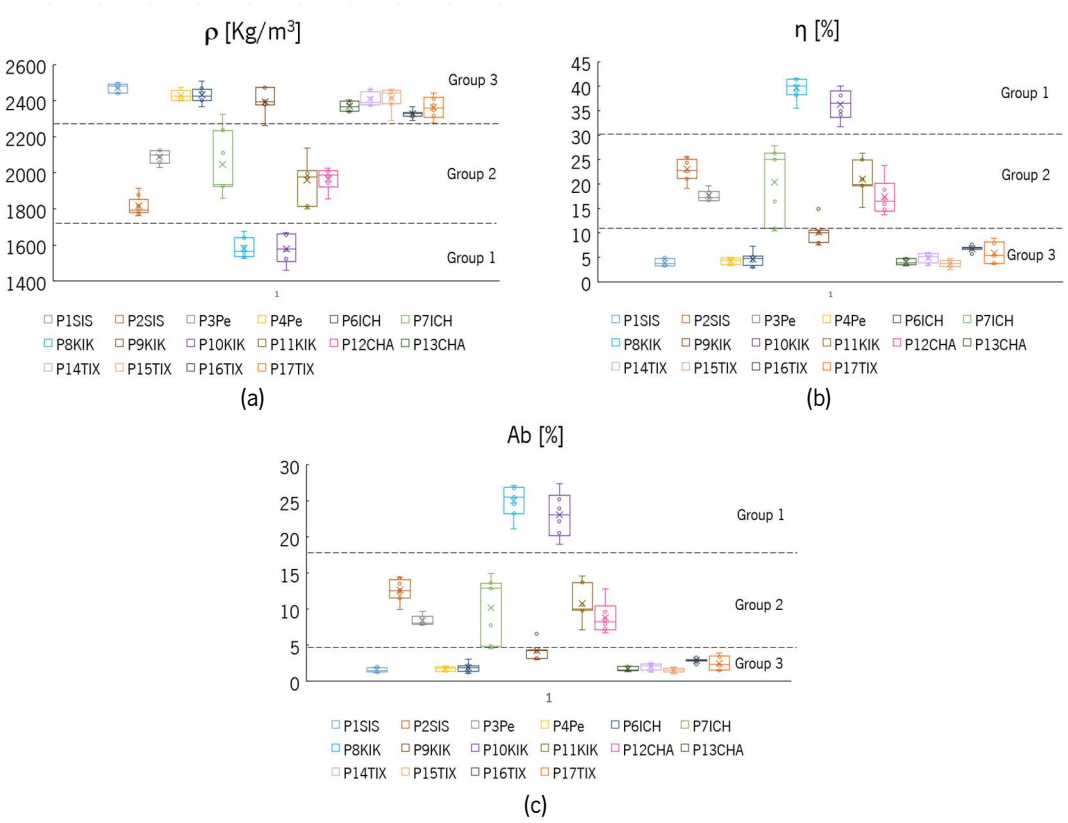


Figure 4-18. Box plot for each stone type; (a) apparent density, (b) open porosity and (c) water absorption by immersion

Figure 4-19 illustrates the statistical features of physical properties regarding each group by using histograms and corresponding normal distributions. It was found a small overlapping of ranges between group 2 and 3. In case of apparent density (ρ), group 2 has an upper extreme of 2323.48 kg/m^3 and the group 3 has a lower extreme of 2263.61 kg/m^3 (Table 4-9). In case of open porosity (η), group 2 has a lower extreme of 10.45% and group 3 has an upper extreme of 14.94 %. Regarding to water absorption by immersion (Ab), group 2 has a lower extreme of 4.49% and group 3 has an upper extreme of 6.59%, see Figure 4-19. With the histograms, it is possible to confirm the clear grouping of limestones according to different ranges of variation of the physical properties. According to the previous analysis, group 1 should present the stones with higher water absorption and porosity and lower density, which tends to be less durable and less resistant (Alves, Faria, and Simão, 2017).

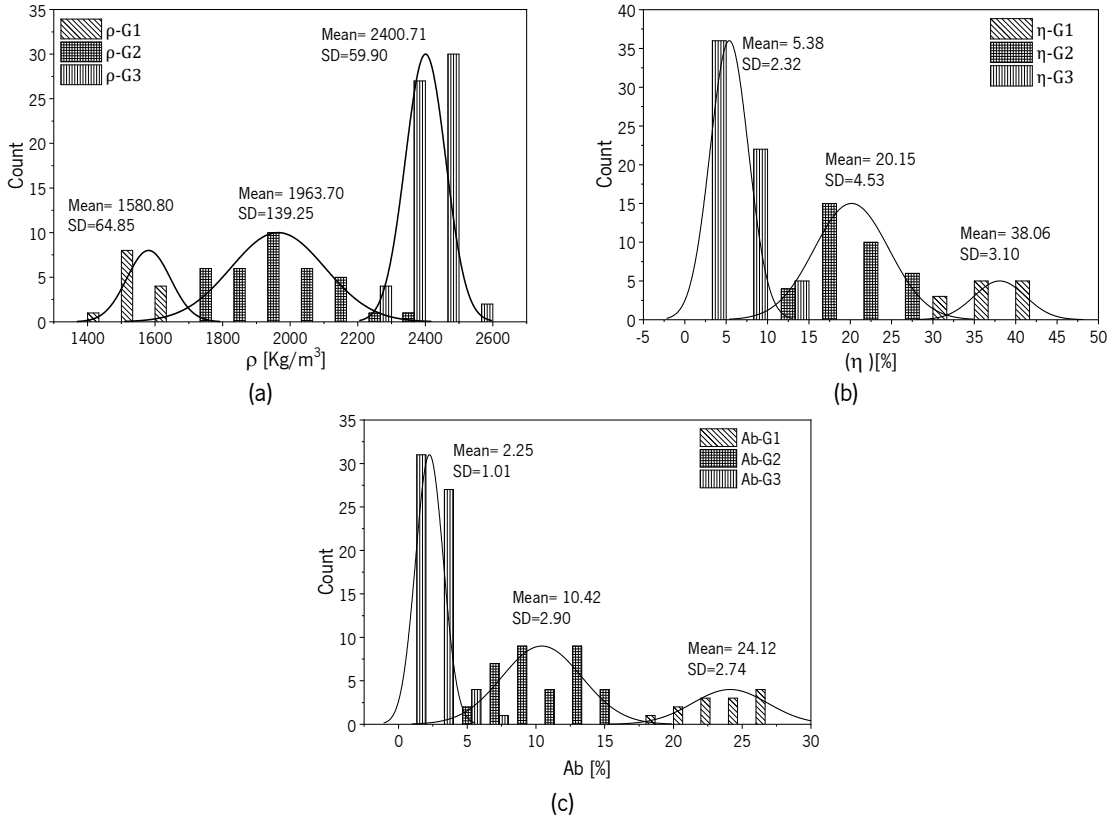


Figure 4-19. Grouping the limestones according to values of; (a) apparent density; (b) open porosity and (c) water absorption by immersion

The physical properties obtained for these Yucatan limestones (Table 4-9) can be compared with the physical properties obtained by different authors also for limestone (Table 4-10). According to Bednarik (2014), Leitha stone, one of the most important and popular historical building materials in Eastern Austria and adjacent areas, was also analysed according to different ranges of porosity and water absorption, namely low porosity (from 2.5% to 5.0%), medium porosity (from 7.9% to 12.0%) and high porosity (from 16.5% to 30.8%), which is comparable to values of group 2 (G2).

Table 4-9. Limestone values of; (a) apparent density, ρ; (b) open porosity, η and (c) water absorption by immersion *Ab*

	G1			G2			G3		
	ρ	η	*Ab*	ρ	η	*Ab*	ρ	η	*Ab*
	[kg/m3]	[%]	[%]	[kg/m3]	[%]	[%]	[kg/m3]	[%]	[%]
Minimum value:	1459	31.76	19.00	1763	10.45	4.49	2263	2.46	1.07
Maximum value:	1676	41.56	27.41	2323	27.82	14.93	2507	14.94	6.59
Average:	1580	38.07	24.13	1963	20.16	10.43	2400	5.38	2.25
Standard deviation:	64.86	3.11	2.74	139	4.54	2.90	59.90	2.32	1.02
Coefficient of variation:	4.10%	8.16%	11.37%	7.09%	22.50%	27.82%	2.50%	43.17%	45.10%

Other studies point out a wide range of porosities, either very high such as those provided by Pappalardo (2016) for Italian limestones, varying between 28% -38%. Much lower values of porosity varying from 0.5% to 0.7% are reported Karakul (2013) on limestone from Turkey. Values of porosity

close to 10 % and 30% were recorded by Torok (2003) to Hungarian limestone and by Bell (1993) for limestone from United Kingdom, respectively.

Table 4-10. Physical properties of limestones

Property	η (%)			*Ab* (%)		
Reference. Identification of Stone	Maximum	Minimum	Average	Maximum	Minimum	Average
Bednarik (2014). Burgenland and Styria, Austria						
Low	2.5	4.99		0.67	2.08	
Medium	7.85	11.96		1.57	3.55	
High	16.53	30.85		4.85	13.00	
Karakul (2013). Turkey						
Golbası-Haymana Highway limestone	0.5	0.7		0.14	0.36	
Torok (2003)						
Oolitic limestones	21.0	31.0				
Al-Omari (2015). Chambord, France						
Tuffeau			45.20			
Richemont			29.00			
Bell (1993).						
Magnesian Limestone - Kiventon Park. U.K.			10.40			
Ancaster. U.K			19.3			
Stamford. USA			24.00			
Pappalardo (2016)						
PS			28.60			12.00
D-NS			37.30			17.50
B-NS			38.60			18.70
Minimum	0.50	0.70	10.40	0.14	0.36	12.00
Maximum	21.00	31.00	45.20	4.85	13.00	18.70

4.5.2. Water absorption by capillarity

The capillary water absorption coefficient is a physical parameter that is dependent on the porous structure of a material and thus it can provide some qualitative data about it. As stated by Tomašić et al. (2011), the capillary water absorption is conditioned by several parameters such as shape and size of pores, along with the petrographic and structural textural characteristics of the stones. Higher values of coefficient of capillary are associated to the ability of a porous material to absorb liquid water due to the capillary force and it is an indirect measure of its vulnerability to moisture induced decay processes.

The average values of the capillary water absorption coefficient for the limestone of each group and according to the two loading directions are shown in Table 4-11. The loading directions relate also with the direction of the bedding planes. The coefficient of determination (r^2) regarding to linear fitting defined for the calculation of the capillary coefficient was always higher than 0.97 (Table 4-11).

Table 4-11. Average values of capillary water absorption coefficient (*Cw*) [kg /(m².s$^{1/2}$)] and factor F_{wc}.

Stone ID	*Cw* Parallel	r²	*Cw* Perpendicular	r²	F_{wc}
G1-P8KIK	0.168	0.9981	0.148	0.9980	0.88
G1-P10KIK	0.232	0.9946	0.152	0.9991	0.66
G2-P2SIS	0.097	0.9975	0.147	0.9787	1.52
G2-P3Pe	0.033	0.9963	0.066	0.9840	2.00
G2-P7ICH	0.088	0.9995	0.015	0.9900	0.17
G2-P11KIK	0.086	0.9949	0.049	0.9955	0.57
G2-P12CHA	0.019	0.9980	0.014	0.9960	0.74
G3-P1SIS	0.004	0.9967	0.003	0.9961	0.75
G3-P4Pe	0.016	0.9843	0.003	0.9892	0.19
G3-P6ICH	0.025	0.9851	0.015	0.9814	0.60
G3-P9KIK	0.021	0.9950	0.038	0.9907	1.81
G3-P13CHA	0.008	0.9920	0.009	0.9935	1.13
G3-P14TIX	0.006	0.9973	0.001	0.9948	0.17
G3-P15TIX	0.002	0.9920	0.003	0.9780	1.50
G3-P16TIX	0.016	0.9943	0.013	0.9935	0.81
G3-P17TIX	0.008	0.9976	0.094	0.9953	11.75

It is observed that the limestone samples show significant differences in capillary water absorption. The highest capillary water absorption coefficient (Figure 4-20) was found for stones from group 1, whereas very low values are recorded in limestone from group 3. This is the result of the very different curves describing the water capillary absorption kinetics among the limestone groups induced by differences in their porous media.

The water absorption capillary diagrams found for limestone belonging to group 1 are composed of two branches: the first branch is linear and describes the capillary water absorption and the second branch is composed of a plateau and defines the saturate condition of the samples. This behaviour is close to other building stones, namely porous granites (Martins et al., 2015). In limestone of group 2, and particularly in limestone from group 3, the water capillary diagrams exhibit a very different shape, which is characteristic of stones with low ability for capillary water absorption (Çobanoğlu, 2015). In these cases, it is difficult to achieve the water absorption stabilization, even after long time of absorption. In case of limestone from group 3, the curves reflect the very low ability for capillary water absorption, resulting in the low values of the capillary coefficient, as already presented in Table 4-11. The great differences on the water absorption capillary behaviour among the limestone under study should be justified not only by the different values of porosity, but also differences on structural and textural features of the pore dimensions and its distributions. With this respect, it is important to underline that the stones belonging to group 1 present micrite texture with inter-particle porosity made of relatively large pores, which can justify the clear differences regarding to capillary kinetics when

compared with stones from group 2 and group 3. It is also seen that the open porosity found for the stones from group 3 is much lower than the porosity found for limestone of group 1, which helps also to explain the very different values of water capillary coefficient.

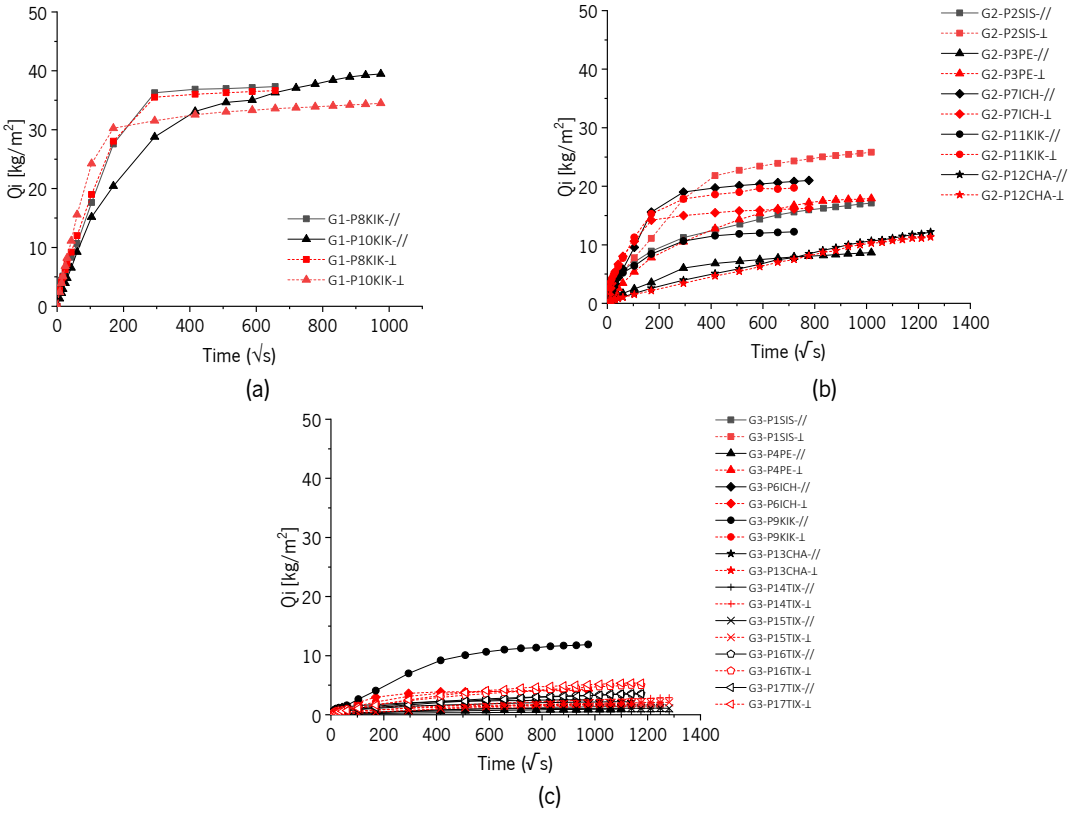


Figure 4-20. Capillary water absorption kinetics for the different limestone groups; (a) group 1, (b) group 2, (c) group 3

The average capillary coefficients for groups G1, G2 and G3 are 170 g/(m².s$^{1/2}$) (CV=14%), 60 g/(m².s$^{1/2}$) (CV=62.9%) and 10 g/(m².s$^{1/2}$) (CV= 79.90%) respectively. According to the capillary water absorption classification proposed by Çobanoğlu (2015), limestone samples from group 3 are classified as "low to medium absorbing rocks" (5 g/(m².s$^{1/2}$) < water absorption coefficient < 14 g/(m².s$^{1/2}$)), limestones from group 2 as "medium to high absorbing rocks" (14 g/(m².s$^{1/2}$) < absorption coefficient < 147 g/(m².s$^{1/2}$)) and limestone from group 1 as "very high absorbing rocks" (absorption coefficient >147 g/(m².s$^{1/2}$)). It should be also mentioned that the carbonate rocks as limestones are widely recognized to have pore geometry that is significantly more complex than other sedimentary rocks. One of the reasons of the pore geometric complexity is the formation environment: (a) sedimentation cycles; (b) variable depths of marine sedimentation; (c) deposition of additional calcareous material which often contains fragments of marine organisms; (d) diagenesis, which exerts significant genetic influence over the development of texture and fabric of a carbonate rock (Bednarik

et al., 2014; Bell, 1993; Folk, 1980; Zhu et al., 2010). This is associated with variability in the rock's composition and porosity.

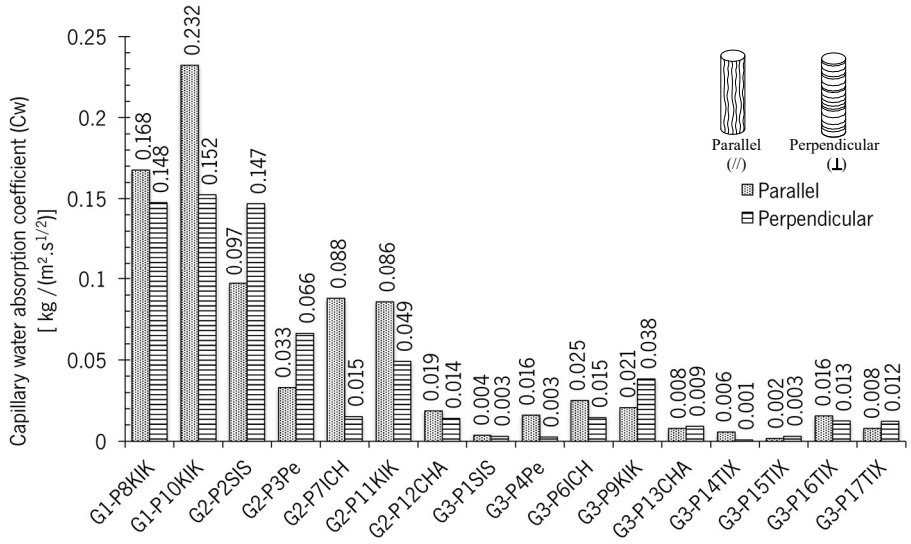


Figure 4-21. Capillary water absorption coefficient (*Cw*) [kg/(m².s$^{1/2}$)] by groups and bedding planes

By comparing the capillary water absorption coefficient obtained in the direction parallel and perpendicular to the bedding planes (Figure 4-21), it is seen that there are differences between both directions and these are reflected by the factor F_{wc} that relates the water capillary coefficient obtained in parallel and perpendicular direction to the bedding planes. It would be expected that greater absorption could be measured along the parallel direction to the bedding plane when compared to the direction of perpendicular to the bedding plane. There is a preferred capillary water absorption along the parallel direction to the bedding plane, but it appears not to be a rule, because the contrary also happens in some cases. Higher values of capillary water absorption coefficient were found in the parallel direction to the bedding plane in group 1, but in group 2, the value of capillary coefficient is not always higher in the parallel direction to the bedding plane. From the six stones belonging to this group, two of them present the bedding planes clearly defined (P2SIS and P3PE) but the other four have a random pigmentation. In case of limestone from group 3, there are no consistent conclusion because all values of capillary absorption are very low. It is interesting to notice that considering that water is one of the main agents of stone decay, stones belonging to group 1 should be more vulnerable to decay processes, particularly in case of capillary absorption direction coincides with the parallel direction to bedding planes.

4.6. Compressive behaviour and key mechanical properties

4.6.1. Static Elastic modulus

Table 4-12 shows the results of the average values of the static elastic modulus for each limestone and considering the foliation planes for the two loading directions. The index of modulus anisotropy (I_{aE}) and the anisotropy classification according to Worotnicki (1993) are also included.

The values of the static elastic modulus (E) of limestone stones varied from 6035.4 MPa to 70877 MPa. There is a considerable difference on the modulus of elasticity in limestone belonging to different groups defined previously.

Table 4-12. Static modulus of elasticity (E) and index of modulus anisotropy (I_{aE})

	ID Sample	Perpendicular (⊥)		Parallel (//)		
		E (MPa)	CV (%)	E (MPa)	CV (%)	I_{aE}
Group 1	P8KIK	6035	(3)	7404	(-)	1.23
	P10KIK	11945	(21)	8950	(-)	1.33
Group 2	P7ICH	21975	(70)	17086	(-)	1.29
	P2SIS	16100	(33)	23607	(4)	1.47
	P3PE	25785	(-)	30052	(2)	1.17
	P11KIK	-	(-)	34018	(4)	-
	P12CHA	26132	(9)	36100	(-)	1.38
Group 3	P9KIK	43140	(27)	-	(-)	-
	P16TIX	52255	(11)	48809	(6)	1.07
	P6ICH	58109	(7)	53227	(17)	1.09
	P17TIX	44860	(19)	53716	(5)	1.20
	P13CHA	53071	(3)	55773	(7)	1.05
	P4PE	48223	(11)	60421	(-)	1.25
	P1SIS	62992	(2)	62342	(6)	1.01
	P15TIX	-	(-)	66203	(14)	-
	P14TIX	-	(-)	70877	(9)	-

Limestone from group 1 presents the lowest values of static modulus of elasticity, whereas limestone from group 3 has the greatest values of modulus of elasticity (Table 4-12). It is also observed that following the recommendation of Worotnicki (1993), the stones are classified mostly as low anisotropic since the modulus anisotropy (I_{aE}) is lower than 1.3. Only two stones from group 2 (P2SIS, P12CHA) and one stone from group 1 (P10KIK) can be classified as medium anisotropic. With this respect, there is also a trend, at least in average, for the elastic modulus presents higher values in the parallel direction to the bedding planes, particularly in case of group 2 and group 3, see Figure 4-22.

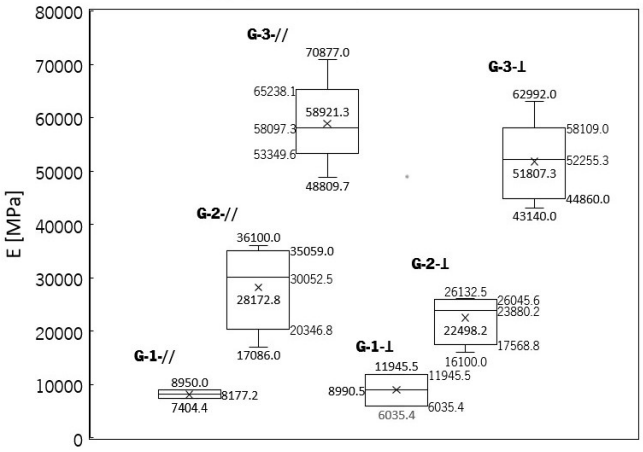


Figure 4-22. Box diagram of Static Elastic modulus (E) by limestone group and by bedding planes

From the box diagram (Figure 4-22), it is seen that there is no possibility to assess the dispersion and symmetry in case of limestone from group 1 due to the low number of samples. On the other hand, groups G-2// and G-2⊥ show lower dispersion from 50% to 75% (3rd quartile), group G-3// presents dispersion between 25% to 50% (2nd quartile) and group G-3⊥ show a symmetric behaviour. Additionally, there is no overlapping values among the groups. About 50 % of samples from group G-2// have the elastic modulus ranging from 20346 to 35059 MPa, from 17568 to 26045 MPa in group G-2⊥, from 53349 to 65238 MPa in group G-3// and from 44860 to 58109 MPa in group G-3⊥.

Table 4-13. Modulus of elasticity of limestones

Property	E [MPa]		
	Max	Min	Average
Al-Omari ((2015)). Chambord, France			
Tuffeau			1624
Richemont			2599
Yasar, E. (2003). Turkey			
Adana/Ceyhan			26500
Adana/Karaisali			14400
Hatay/Iskenderum			43100
Adana/Pozanti			45400
Adana/Kozan			15000
Pappalardo ((2016)). Sicily, Italy			
PS	5170	3780	4330
D-NS	3600	1730	2670
B-NS	3950	1170	2230
Karakul (2013) Turkey			
Golbası-Haymana Highway limestone	22480	9340	
Bell (1993).			
Magnesian Limestone - Kiventon Park. U.K.			41300
Ancaster. U.K			19500
Stamford. USA			18400
Min	3600	1170	1624
Max	22480	9340	45400

A comparison between the values of the static modulus of elasticity of limestone obtained in this research with values given in literature was carried out, see Table 4-13. All the values of static modulus of elasticity pointed out on literature for limestone are within the range of variation obtained for limestone belonging to groups G1 and G2 defined in this study. It is also seen that the average values of modulus of elasticity obtained for group 3 are higher than any value pointed out for the different authors.

4.6.2. Stress-strain diagrams and compressive strength

Table 4-14 shows the compressive strength obtained in the experimental tests (*fe*) and the compressive strength corrected according to the standard ASTM C170 (1999) (*fc*) for each group and for the two loading directions (perpendicular and parallel to the bedding planes). In addition, information about the strength anisotropy index ($I\sigma_c$) is also provided. The analysis of results enables to observe that very different values of compressive strength are obtained for the limestone belonging to the three groups. The limestone belonging to group 3 present considerably higher values than the limestone belonging to group 2 and particularly regarding to limestone of group 1.

Table 4-14. Compressive experimental strength (*fe*), corrected compressive strength (*fc*) for parallel (//) and perpendicular (⊥) direction to the bedding planes and strength anisotropy index ($I\sigma c$)

	ID Sample	Perpendicular (⊥)		Parallel (//)		$I\sigma_c$	Strength anisotropy classification
		fe (MPa)	*fc* (MPa)	*fe* (MPa)	*fc* (MPa)		
Group 1	P8KIK	7.8045	8.5526	12.2838	13.2131	1.54	Low anisotropy
	P10KIK	10.6462	11.928	15.1163	15.6354	1.31	Low anisotropy
Group 2	P7ICH	17.5247	19.2019	20.1838	20.9107	1.09	Isotropic
	P2SIS	16.5804	17.311	26.3043	29.6157	1.71	Low anisotropy
	P3Pe	39.5912	41.9363	49.6301	52.9418	1.26	Low anisotropy
	P11KIK	22.5641	22.5641	31.025	34.872	1.55	Low anisotropy
	P12CHA	39.1097	43.9525	38.055	42.5657	0.97	Isotropic
Group 3	P9KIK	52.2197	58.8113	63.8056	63.8056	1.08	Isotropic
	P16TIX	55.5385	60.3516	60.8223	68.3731	1.13	Low anisotropy
	P6ICH	62.6412	67.238	64.2197	68.7523	1.02	Isotropic
	P17TIX	61.2179	67.5244	74.839	83.7871	1.24	Low anisotropy
	P13CHA	48.584	54.6724	52.3539	56.7023	1.04	Isotropic
	P4Pe	61.9652	66.4883	78.9146	84.6638	1.27	Low anisotropy
	P1SIS	81.4844	91.5155	78.913	88.6978	0.97	Isotropic
	P15TIX	22.3714	-	56.0337	62.6933	-	
	P14TIX	47.8866	-	70.6114	93.4151	-	

According to the classification suggested by Ramamurthy et al. (1993) and Saroglou and Tsiambaos (2007), and taking into account the strength anisotropy index, the stones can be classified as isotropic or low anisotropic. It is also seen that in average the compressive strength is higher in the samples

loaded in parallel direction to bedding planes. This trend is confirmed by the box diagrams presented in Figure 4-23, where average values of the compressive strength and corresponding statistical features (dispersion and symmetry) are illustrated for each limestone group and for the parallel and perpendicular direction to the bedding planes. It is seen that among the groups there is no overlapping of the average and range values. Given the low number of limestone samples belonging to group 1 (G-1), it is not possible to observe important dispersion and symmetry, but in groups 2 and 3 (G-2 and G-3) it is possible to evaluate these statistical features. The boxplot obtained for group G-2//, G-2⊥ and G-3// show lower dispersion between 25% to 50% (2nd quartile), whereas group G-3⊥ shows lower dispersion between the 50% to 75% (3rd quartile). Additionally, it is possible to observe that 50% of the samples in group G-2// present compressive strength between 25.6 to 47.75 MPa, in group G-2⊥ it varies from 18.26 to 42.94 MPa, in group G-3// it ranges from 63.25 to 86.68 MPa and in G-3⊥ it varies from 58.81 to 67.52 MPa.

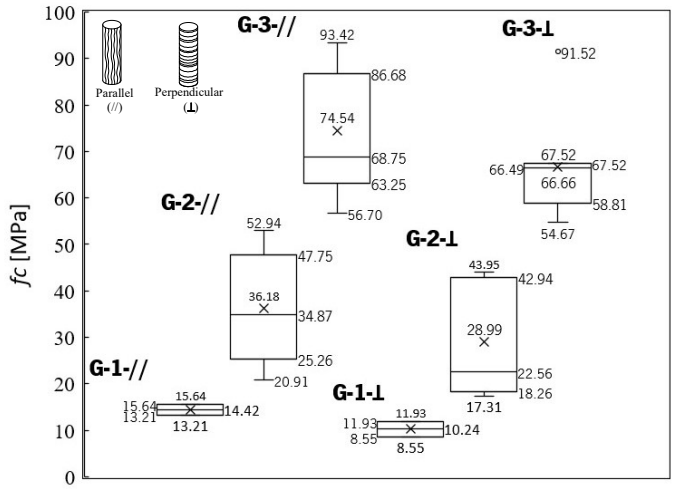


Figure 4-23. Box diagram of uniaxial compressive strength (*fc*) for the limestone groups considered and according to bedding planes

Figure 4-24 shows the stress-strain diagrams for each limestone group considering also the two different loading directions. From the analysis of diagrams it is possible to confirm that limestones from the three groups present a very different compressive behavior, not only at the level of the compressive strength and modulus of elasticity as already analyzed, but also regarding behavior after post-peak strength. Higher strength and higher initial stiffness are attributed to group 3 but contrarily to limestone of group 1 and group 2, they present higher brittleness. In the latter cases, the post peak branches are rarely obtained.

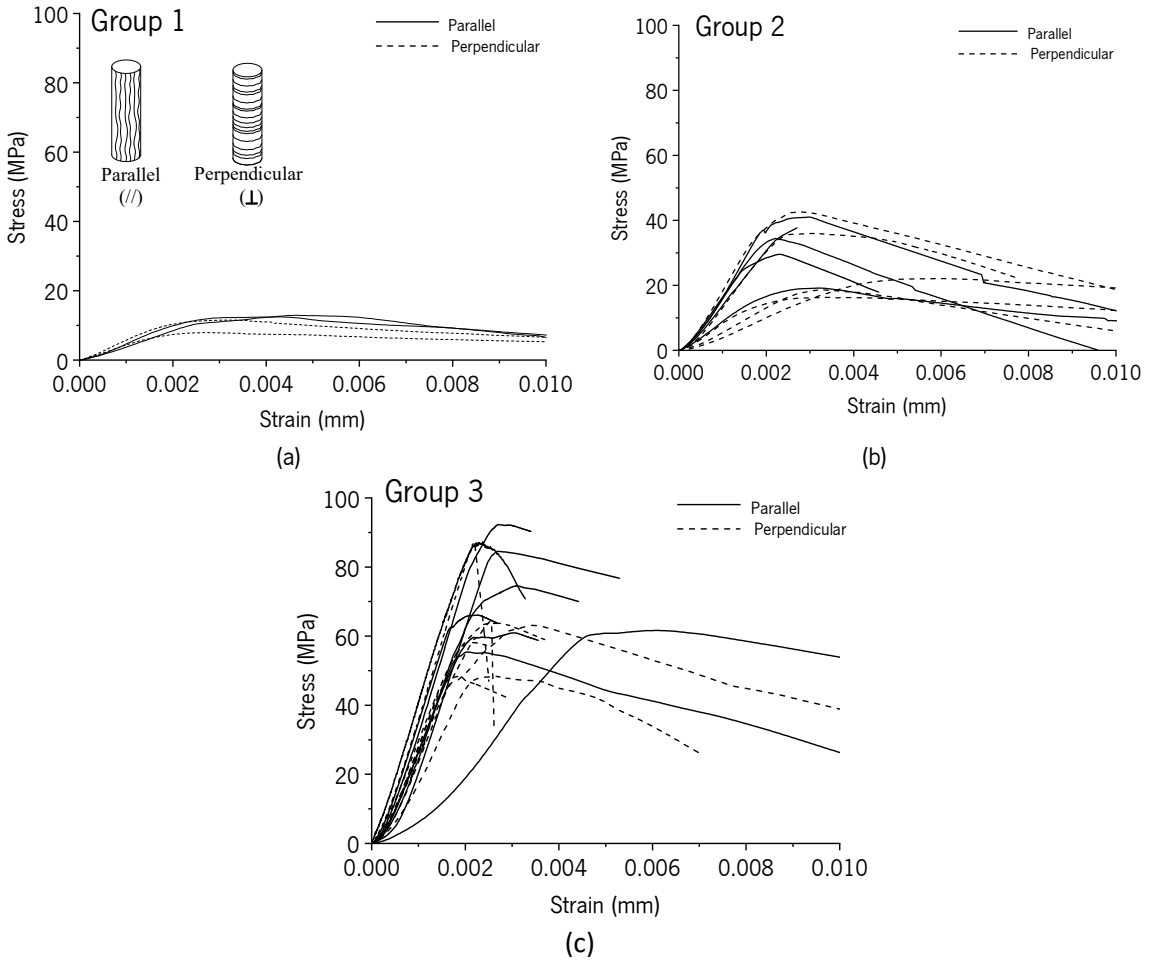


Figure 4-24. Stress-strain behaviour of limestones; (a) group 1; (b) group 2; (c) group 3

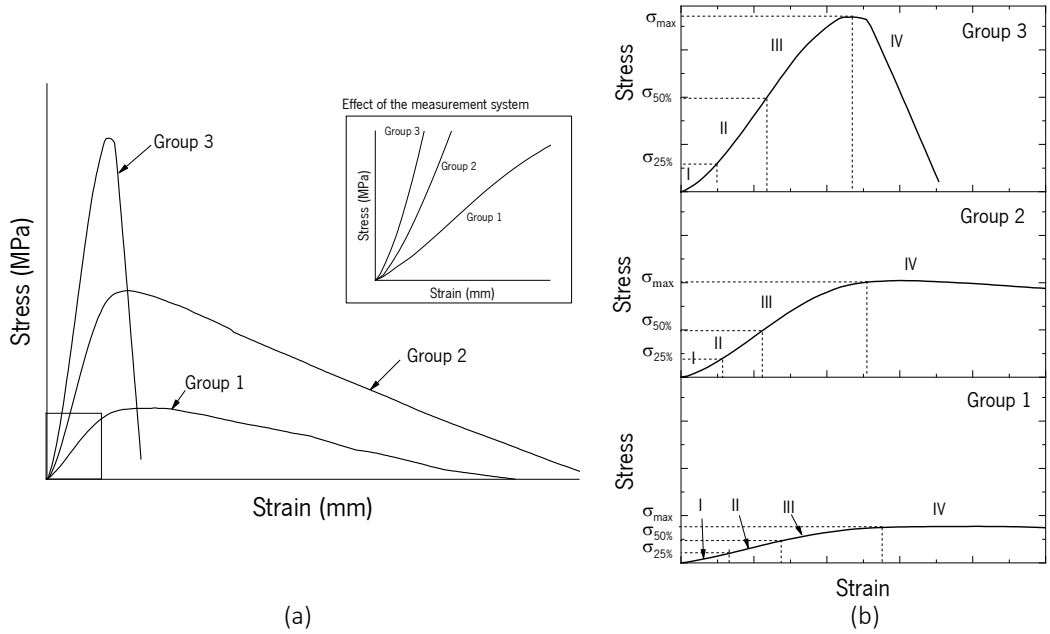


Figure 4-25. Stress-strain behaviour of limestones; (a) general behaviour of limestone, (b) four distinct stages of the curves strain-stress for each group

The stress-strain diagrams of the limestone shown in Figure 4-25 exhibit an initial upward concave shape, which is attributed to the effect of the measurement system, the closure of pre-existing flaws or voids and the structural characteristics of the material (Korinets and Alehossein, 2002; Vasconcelos, 2005). This behaviour extends until almost the 25% of the maximum stress of the sample (phase I), which is followed by a linear elastic response (phase II), initiation and propagation of stable cracks (phase III) and crack damage, unstable crack growth and post-peak behaviour (phase IV).

Compressive strength varies in group 1 from 10.55 to 13.78 MPa (G1), in group 2 (G2) from 19.93 to 48.54 MPa and in group 3 (G3) from 55.69 to 93.42 MPa (Table 4-15). Based on these ranges and considering as an example the classification of ASTM C 568 (ASTM, 2010), it was decided to classify limestone from group 1 as low strength, limestone from group 2 and medium strength, and limestone from group 3 as high strength.

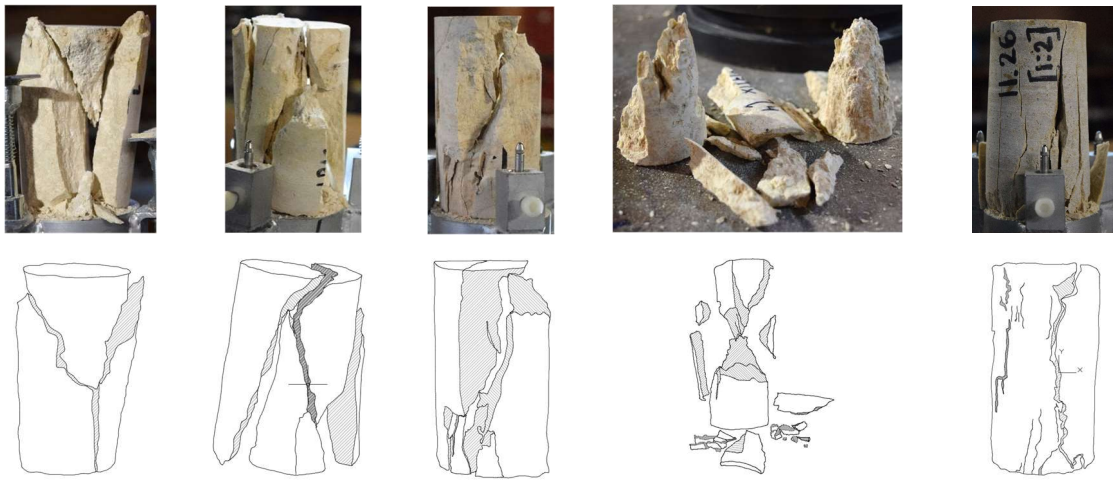
Table 4-15. Results of compressive strength, density and open porosity by groups

	Group 1			Group 2			Group 3		
	fc [MPa]	η [%]	ρ [Kg/m^3]	*fc* [MPa]	η [%]	ρ [Kg/m^3]	*fc* [MPa]	η [%]	ρ [Kg/m^3]
Minimum	10.55	31.76	1459.09	19.93	10.45	1763.96	55.69	2.46	2263.61
Maximum	13.78	41.56	1676.05	48.54	27.82	2323.48	93.42	14.94	2507.70
Average	12.17	38.07	1580.81	32.68	20.16	1963.71	71.64	5.38	2400.72

Similar classification was also pointed out by Bednarik (2014) (Leitha limestones) according to different ranges obtained for the compressive strength (*fc*), namely low strength from 8.32 to 26.55 MPa (open porosity ranging from 16.53% to 30.85%), medium strength from 45.59 to 55.19 MPa (open porosity ranging from 7.85% to 11.96%) and high strength from 92.14 to 105.96 MPa (open porosity ranging from 2.5% to 5%). Based on these results, it is also possible to observe the role of open porosity in the compressive strength of these studied limestones. High strength limestones have associated low values of porosity, whereas low strength limestone has considerably high values of porosity. Low strength limestone has been also pointed out by Pappalardo (2016) with the compressive strength varying from 9 to 21MPa (for porosity variation from 28% to 39% and ρ from 1600 to 1900 kg/m3) and medium to high strength limestone has been characterized by Yasar (2004) being the compressive strength in the range between 35 and 120 MPa (density ranging from 2400 to 3000 kg/m^3). From the classification of limestone into groups, the stones from Tixhualactun church are classified as group 3 (high strength), stones from Kikil church range from group 1 to group 3 (from low to high resistance), whereas churches from Sisbic, Petulillo, Ichmul and Chancenote have stones from groups 2 and 3 (stones of medium to high resistance).

4.6.3. Crack patterns

Given that the mechanical behavior of rocks is dependent on the mineralogy, the arrangement of the particles, voids, porosity and microcracks (Basu et al., 2009; Hudyma et al., 2004; Szwedzicki, 2007), the rock failure modes are difficult to predict. A comprehensive study on rock failure modes at laboratory scale is potentially important to predict the behaviour of the rock under stress, especially when used as construction material (Basu et al., 2013; Pappalardo et al., 2016). From works carried out in the past, it could be seen that the main failure modes in rocks under uniaxial compression are mostly tensile and shear (2013) (Hudyma et al., 2004) (Szwedzicki, 2007): (1) single shear failure involves one or more parallel shearing planes developing at an oblique angle to the vertical direction; (2) multiple shear mode is defined by two or more planes that intersect and develop in an oblique direction regarding to the vertical load; (3) axial splitting mode (also identified as vertical splitting or axial cleavage) consists of failure along planes parallel to the vertical direction; (4) mixed shear-tensile (Y shaped) mode characterized by the connection of diagonal shear cracks with vertical tensile cracks (Basu et al., 2013).



Shear (Y shaped failure, single shear and double shear) Tensile - splitting

Figure 4-26. Failure modes under uniaxial compression observed in this study

In the evaluation of the crack patterns, it has been widely recognized that microcracks that initiate and propagate before the peak stress is reached are predominantly tensile cracks and develop in the direction parallel to the applied loading (Vasconcelos, 2005). According to Carpinteri (2014), in uniaxial tests the macroscopic cracks essentially starts parallel to the direction of the axial loading, being explained by the heterogeneity due to pre-existing microcracks, pores and voids acting as stress concentrators. In addition, Lajtai (1998) refers that shear fractures do not form before failure and represent a post-failure phenomenon.

In this research, the failure modes recorded at the end of the uniaxial compression tests can be integrated in the four types previously mentioned, see Figure 4-26.

As shown in Figure 4-27, the predominant failure mode is shear mode with 68% of the total failures, whereas the tensile splitting mode represent 32% of the failures. It is important to notice that: (1) the same boundary conditions were considered for all specimens; (2) both shear and tensile failure occurs in cylindrical specimens with different height to length aspect ratios.

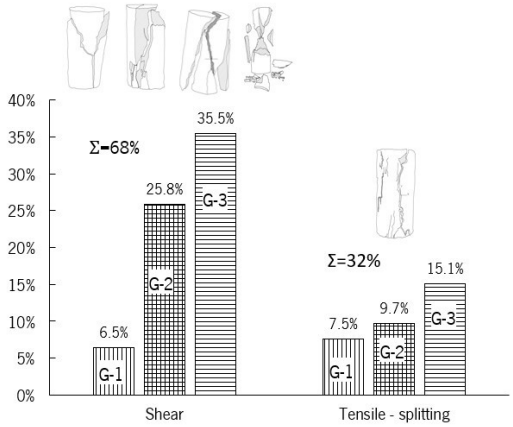


Figure 4-27. Percentage of specimens by failure mode

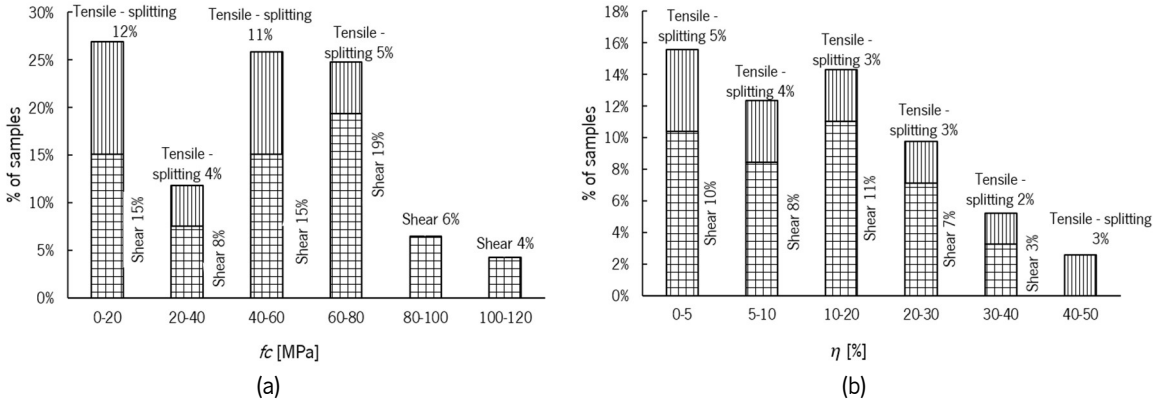


Figure 4-28. Percentage of specimens by mode of failed regarding to (a) *fc* and (b) η

It is also interesting to mention that there are not very significant differences in terms of failures modes when a comparison is made among the three groups of limestone, see Figure 4-27 and Figure 4-28: (1) both shear and tensile failure modes occurred in the three groups; (2) shear failure mode clearly predominated in limestones from group 2 and group 3; (3) in group 1 both shear and tensile splitting play practically the same role. Therefore, there is a trend for the shear failure mode predominates on samples with porosities lower than 40%, whereas in samples with porosities higher than 40% only develops tensile splitting failure mode. In addition, for samples with compressive strength $fc < 80$ MPa

both failure modes predominate, whereas in samples with fc > 80 MPa, only shear failure mode develops.

4.7. Concluding Remarks

In this research mortars and stone units from both masonry walls and vaults of historical churches from sixteenth to eighteenth centuries located in Yucatan region were studied. The churches are located on a lithological area mostly of Coquinoid limestone and Fossiliferous crystalline limestone.

The results from mineralogical analysis revealed that: (1) in mortar samples, the mineral phase of calcite ($CaCO_3$) was the most abundant compound. Additional studies are needed to identify the binder to aggregate ratio and possible additives on the mortar; (2) the stones studied are limestones with some traces of others additional minerals. The SEM, X-ray and petrography revealed that there is no clear dependence of the anisotropy of the stones on the mineralogical and textural varieties.

The limestone samples under analysis were arranged in three groups according to the physical properties, namely open porosity, water absorption by immersion at atmospheric pressure and apparent density. Based on this, it was possible to define group 1 with limestone samples with high porosity (31.8%≤η≤41.6%), group 2 encompassing limestone with porosity ranging from low to medium values (10.5%≤η≤27.8%) and group 3 with limestone of low porosity (2.5%≤η≤14.9%) Regarding to this grouping: (1) it was possible to clearly observe that group 1 is associated with petrographic group A. However, it was not possible to associate only one petrographic group to the limestone groups 2 and 3; (2) distribution of the water absorption by capillarity (Cw) is also coherent with the grouping carried out mostly on the other physical parameters. This is justified by the strong correlations (r^2 > 0.9) among the physical properties; (3) the mechanical properties, namely compressive strength and modulus of elasticity, are also very well distributed among the limestone groups. In term of compressive strength, it was possible to observe that group 1 can be classified as low strength (10.6 MPa ≤ fc ≤ 13.8 MPa), group 2 can be classified as average strength (19.9 MPa ≤ fc ≤ 48.5 MPa), and group 3 can be classified as high strength (55.7 MPa ≤ fc ≤93.4 MPa); (4) from the classification of limestone into groups, it was also seen that stones from Tixhualactun churches are considered as high strength stones, stones from Kikil churches range from low to high resistance, whereas churches from Sisbic, Petulillo, Ichmul and Chancenote were built with stones of medium to high resistance.

From the results it is also possible to conclude that: (1) it was noticed that higher water capillary coefficients were obtained mostly for the parallel direction to the bedding planes; (2) if strength anisotropy index is considered, the stones are mostly classified as low anisotropic and most of the stones present higher compressive strength in the parallel direction to the bedding planes; (3) most of the samples tested under uniaxial compression failed in shear, even if both shear and tensile-splitting failure modes could be recorded in stone belonging to the three groups. As expected, high strength stone presented a brittle failure, being not possible to record the post-peak behaviour;

It should be also mentioned that the results obtained in this Chapter aims at defining a range of the mechanical properties of materials to be used in the experimental model of the barrel masonry vault to be tested to imposed vertical displacement (Chapter 7). It is considered that this is achieved for limestone. In case of mortar, the mineralogical results are clear about the origin of the binder and aggregates, but it was not possible to characterise the physical and mechanical properties due to the very low size specimens gathered form the case study buildings.

Chapter 5
Simple NDT evaluation of limestone and Statistic correlations between physical and mechanical properties

Abstract:
This chapter intends to evaluate the effectives of two non-destructive tests performed (Schmidt hammer (N) and ultrasonic pulse velocity (UPV)) to predict physical and mechanical properties of limestone from Yucatan churches. It aims also at understanding the influence of factors such as anisotropy and moisture content in the values of UPV. For this, a statistical study is carried out on statistic correlations between NDT indexes and physical and mechanical properties. In addition, the relation between physical and mechanical properties is also analysed by a set of statistic correlations.

5.1 Introduction

In the diagnosis and inspection of the stone masonry heritage buildings the biggest challenge is to evaluate the structural and material condition, particularly in cases in which the possibility of sampling material cores is reduced or forbidden. For these reasons, simple and more sophisticated non-destructive techniques have been developed to apply in-situ in order to obtain more accurate information about masonry materials and masonry as a composite. Some non-destructive techniques like the ground probe radar and the sonic tests have been used in the definition of the morphology of masonry walls cross section and estimate the dynamic elastic modulus of masonry respectively. Other tests like controlled micro-drilling, ultrasonic pulse velocity (UPV) and Schmidt hammer are commonly used for the material characterization. The controlled micro-drilling can be correlated with the elastic and strength properties of bricks (Fernandes and Lourenço, 2007). The UPV method is an useful and reliable non-destructive tool of assessing the mechanical characteristics of stones, such as the modulus of elasticity and the compressive strength (Azimian and Ajalloeian 2015; Selçuk and Nar 2016; Uyanık et al. 2019; Kurtulus et al. 2016). The Schmidt hammer was developed by E. Schmidt in 1948 for non-destructive testing of concrete hardness and only later applied to estimate rock strength (Goudie, 2006; Torok, 2003). Nowadays, Schmidt hammer test had been used to evaluate the quality of concrete and by several authors to estimate the compressive strength of the rocks. It is considered an expedite and economical non-destructive technique (Katz et al. 2000; Fener et al. 2005; Yilmaz and Sendir 2002). Sharma (2011) presented correlations between P-wave velocity, Impact strength index and Slake durability index for sedimentary, metamorphic and igneous stones.

Different correlations were proposed by Sharma (2011) between ultrasonic pulse velocity (UVP) and the rebound hardness number for granite, basalt, andesite, sandstone and quartzite stones. Yasar (2004) proposed correlations between UVP and uniaxial compression strength (fc) of stones, elastic modulus, E, and density, ρ, for limestones, marbles, dolomitic limestones, dolomites and gravelled limestones. Pappalardo (2016) proposed relations between η, fc and E as a function of UPV for fine-grained limestone. All these proposals considered several lithotypes, which have important differences on densities, compressive strength and elasticity modulus. Thus, despite the coefficient of correlation is good, probably the accuracy is weak.

Others authors pointed out also statistical correlations between mechanical and physical properties, engineering geological properties and textural features, between non-destructive indices and weathering degree (G. Pappalardo et al. 2015; Bednarik et al. 2014; Basu et al. 2009; Giovanna

Pappalardo 2014; G. Pappalardo et al. 2016; Kahraman and Yeken 2008; Karakul and Ulusay 2013; Yasar and Erdogan 2004; Liu et al. 2019).

In line with the works presented in the literature, the mechanical and physical properties obtained in Chapter 4 were correlated with the ultrasonic pulse velocity and Schmidt's hammer results. It is considered that these simple and economical non-destructive techniques can give good indications about the quality of the limestone and can help in the prediction of the mechanical properties. In addition, extensive statistical correlations were also defined between physical and mechanical properties for the limestone obtained in Chapter 4. A discussion about the factors that influence variations on the velocity measurements is also provided, namely with respect to moisture content and anisotropy direction.

The relevance of the proposed statistical correlations is based on the possibility of estimating the mechanical properties of limestones from non-destructive techniques. This reduces the need for sampling material cores and makes the stone masonry conservation assessments less invasive.

5.2 Non-destructive testing (NDT)

Two non-destructive tests were performed, namely Schmidt hammer and ultrasonic pulse velocity (UPV), aiming at correlating the results (NDT indexes) with the physical properties. The Schmidt Hammer test was carried out according to the standard ASTM-D5873 (1995), see Figure 5-1. This test was performed directly on the 11 masonry stone units collected from the existing buildings and not on the cylindrical specimens. This procedure was adopted due to the possibility to induce some type of damage in the individual specimens, which could influence the physical and mechanical properties. The exposed surface was treated by mechanical means to avoid to have weakened rock material by weathering. The measurements were made on an uniform surface, see Figure 5-1 (b,c). Ten representative locations on the specimen were considered in positions separated at least by the diameter of the piston and only impact one test was taken at each point. The average of the ten readings were calculated and all readings differing by more than seven units were discarded and the average of the remaining readings was considered. No correction factor was applied to the average value since the calibration readings fall within the range provided by the manufacturer (80 ± 2).



(a) (b) (c)

Figure 5-1. Details of NDT: a) Schmidt hammer, b) stone surface treated, c) perpendicular readings at surface

The ultrasonic test was conducted using the Pundit Lab PROCEQ equipment according to standard EN14579 (2005) considering the direct transmission method for the measurement of the P-wave velocities in the stone specimens (Figure 5-2). Piezoelectric transducers of natural resonance frequency of 54kHz and 150kHz were used in the measurements (Vasconcelos et al. 2008).

The samples were tested in both dry (0 % saturation) and saturated conditions (100 % saturation). The surface of the specimens was sufficiently smooth but to achieve adequate coupling between the specimen and the transducer, a coupling material was used. The mean values of the ultrasonic pulse velocity were obtained by averaging three measurements of the transit time (t). Additionally, the specimen's length (L) was measured and the values of the velocity (v) were calculated.

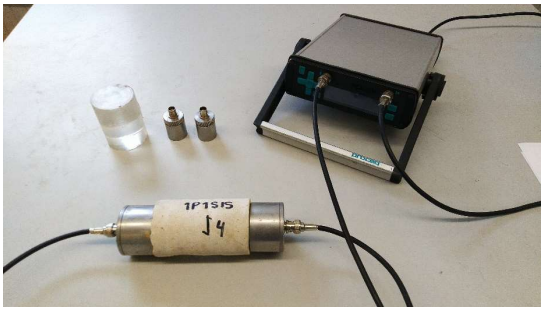


Figure 5-2. Ultrasonic test conducted using the Pundit Lab PROCEQ equipment

5.3 Physical and mechanical properties

The physical characterization of limestone was performed on the stone cylinders according to EN-1936 (2006) and NP-EN-13755 (2008) to obtain key physical properties such as apparent density (ρ), open porosity (η) and water absorption by immersion at atmospheric pressure (Ab).

Table 5-1. Average values of apparent density (ρ), open porosity (η), water absorption by immersion at atmospheric pressure (A_b), Rebound hardness number by Schmidt hammer (M), uniaxial compression strength (fc) and static elastic modulus (E)

Sample	η	Ab	ρ	fc	E
	[%]	[%]	[Kg/m³]	[N/mm²]	[N/mm²]
P1SIS	3.88	1.57	2471.37	89.75	62558.7
P2SIS	22.99	12.67	1816.17	21.93	20604.6
P3Pe	17.56	8.40	2089.57	48.54	28630.0
P4Pe	4.19	1.73	2428.04	73.76	52289.33
P6ICH	4.64	1.91	2430.38	68.10	55668.25
P7ICH	20.33	10.24	2046.19	19.93	20753.0
P8KIK	39.62	25.04	1583.48	10.55	6491.7
P9KIK	10.22	4.29	2394.41	61.31	43140.0
P10KIK	36.26	23.06	1577.68	13.78	10947.0
P11KIK	20.98	10.82	1958.76	29.60	34018.0
P12CHA	17.34	8.85	1968.69	43.40	29455.0
P13CHA	4.01	1.69	2368.19	55.69	54422.5
P14TIX	4.89	2.03	2405.94	93.42	70877.0
P15TIX	3.72	1.54	2413.66	62.69	66203.5
P16TIX	6.78	2.91	2326.64	64.36	50532.5
P17TIX	5.84	2.49	2360.77	75.66	49288.0

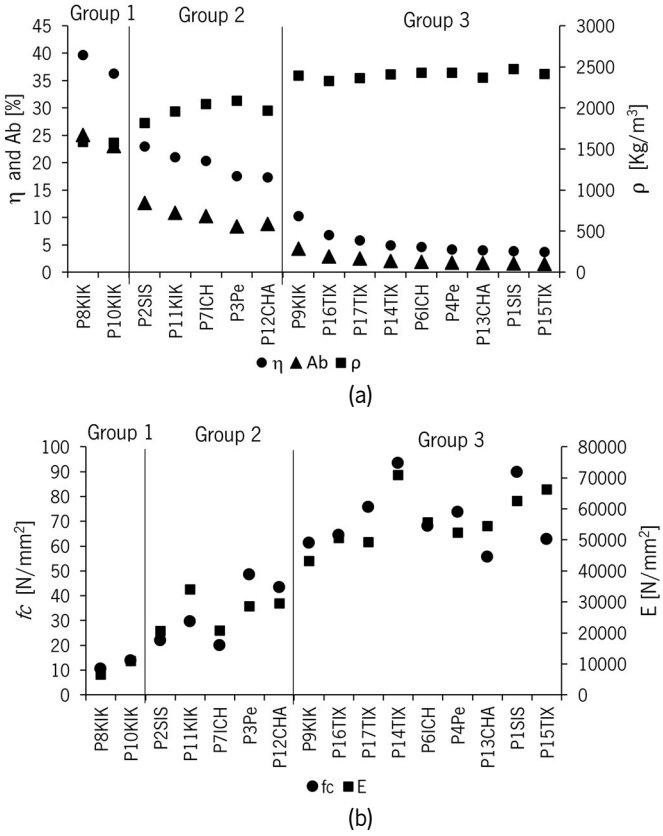


Figure 5-3. (a) Physical properties namely: apparent density (ρ), open porosity (η), water absorption by immersion at atmospheric pressure (Ab) and (b) mechanical properties namely. compression strength (fc) and static elastic modulus (E)

The mechanical characterization was based on uniaxial compression tests according to the standards BS-EN-14580 (2005) and NP-EN-1926 (2000), from which it was possible to obtain elastic modulus (*E*) and the uniaxial compressive strength (*fc*) respectively . Table 5-1 presents a summary of the physical and mechanical properties discussed in detail in Chapter 4. The limestone samples were arranged in three groups according to the ranges found for physical and mechanical properties as discussed in detail in Chapter 4, see Figure 5-3. As expected, porosity and water absorption by immersion present the same trend, while density exhibits different behaviour from porosity and water absorption. Moreover, high values of compressive stress are associated with high levels of modulus of elasticity and low values of porosity.

5.4 Results from NDT

5.4.1 Rebound hardness number (N)

The average rebound hardness found for all stone blocks are presented in Table 5-2. It is observed that the average rebound hardness present low dispersion, which is reflected by the values of coefficients of variation (CV), mostly lower than 10%. The analysis of results reveals also that the ranges of rebound numbers follow the grouping of limestone based on physical properties (Group 1 - G1, Group2 - G2 and Group 3 - G3), see Figure 5-4. Although the number of samples is small, it is possible to observe a clear increasing trend of the rebound values from group 1 to group 3, varying from 17 to 41. Increasing values of Rebound hardness number obtained in group 3 should be associated with denser limestone.

Table 5-2.Average values of the rebound hardness number (*N*) and coefficient of variation (CV)

Sample	N	CV [%]
P1SIS	40	1.6
P2SIS	24	13.7
P3PE	30	0.7
P4PE	36	1.9
P6ICH	41	3.0
P7ICH	22	1.6
P8KIK	17	1.8
P12CHA	29	0.2
P13CHA	40	1.2
P16TIX	36	5.3
P17TIX	41	1.6

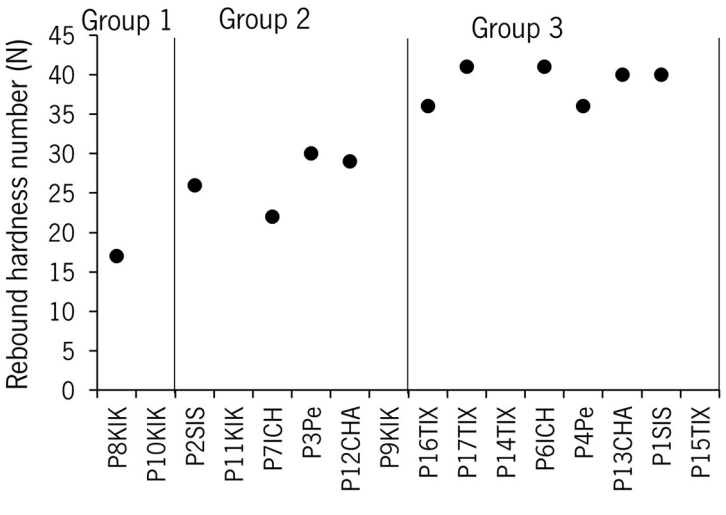


Figure 5-4. Rebound hardness number (*N*) by groups

From an analysis of data available in literature, it was found that Rebound hardness number range from 12.5 to 56.4 for limestone, meaning that the values found in this research are within this range (Table 5-3).

Table 5-3. Rebound hardness number (*M*) found for limestone

Reference, provenance and identification of Stone		N
This study. Yucatan, Mexico Limestones from churches		
Group 1		17
Group 2		22-30
Group 3		36-41
Fatz (2000). USA Indiana limestone		50.6
Day and Goudie (1977). Bahrain Limestone aeolianite		14.5
Day (Michael J. Day, 1980). Puerto Rico Aymamon limestone		12.5
Day (Michael J. Day, 1980). Yucatan, Mexico limestone Carillo Puerto		35.9
Lyew-Ayee (2004). Jamaica Montpelier Limestone		20.5
Day (Michael J. Day, 1980). Mulu, Malasia Melinau limestone		56.4
Day and Goudie (1977). Mallorca, Spain Limestone with pinnacles		52.7
Torok (2003). Budapest, Hungary Miocene oolitic		18-23
	Maximum	12.5
	Minimum	56.4
	Average	32.95

5.4.2 Ultrasonic pulse velocity (*UPV*)

The values of the ultrasonic pulse velocity are shown in Table 5-4. The results are also organized according to the groups identified previously and the average values were obtained for the different anisotropy planes and for different moisture content (dry and saturated). It is important to mention that in some cases the anisotropy plane was not clear, mainly in group 3, according to what was discussed in Chapter 4. The lowest values of *UPV* are obtained for limestone samples in Group 1 (2788m/s<*UPV*<2942m/s) and the highest values are found for the limestone samples belonging to Group 3 (4860m/s<*UPV*<5758m/s). The last column in the Table 5-4 shows the ratio between ultrasonic pulse velocity measured under dry and saturated conditions, being the largest ratio equal to 11%.

Table 5-4. Ultrasonic pulse velocity (*UPV*)

		Dry specimens			Saturated specimens			Ratio
	UPV	Average	Parallel	Perpendicular	Average	Parallel	Perpendicular	Dry/Sat
	ID Sample	[m/s]	[m/s]	[m/s]	[m/s]	[m/s]	[m/s]	
Group 1	P8KIK	2788.07	3019.52	2614.47	**3122.37**	3444.66	2907.50	0.89
	P10KIK	2942.68	3108.46	2832.16	**3239.25**	3398.05	3133.39	0.91
Group 2	P2SIS	3878.42	4250.30	3580.93	**3995.29**	4304.47	3747.95	0.97
	P3PE	4471.61	4636.00	4225.02	**4518.96**	4637.49	4341.16	0.99
	P7ICH	3623.91	3544.76	3683.27	**3934.92**	3920.51	3945.73	0.92
	P11KIK	4003.55	4569.74	3248.64	**4340.61**	4752.20	3791.83	0.92
	P12CHA	4442.76	4682.91	4282.66	**4500.30**	4773.73	4318.01	0.99
Group 3	P1SIS	**5758.02**	5651.72	5935.18	5662.20	5561.88	5829.40	**1.02**
	P4PE	5415.07	5506.93	5353.82	**5634.65**	5848.43	5492.13	0.96
	P6ICH	**5549.89**	5478.51	5645.06	5549.17	5507.06	5605.33	**1.00**
	P9KIK	4860.38	4838.77	4876.59	**5560.32**	5816.62	5368.10	0.87
	P13CHA	5350.93	5352.97	5348.90	**5616.18**	5761.12	5471.24	0.95
	P14TIX	**5303.28**	5356.66	5249.90	5032.56	4792.03	5273.08	**1.05**
	P15TIX	5550.57	5550.57	-	**5853.98**	5853.98	5325.85	0.95
	P16TIX	5327.61	5281.95	5373.28	**5786.85**	5658.63	5915.07	0.92
	P17TIX	5223.15	5341.50	5104.79	**5443.25**	5490.79	5395.71	0.96

Figure 5-5 shows the trend of ultrasonic pulse velocity (*UPV*) in limestone with different moisture conditions namely (a) dry samples and (b) saturate samples and both anisotropy planes. It is observed that ultrasonic pulse velocity appears to have higher values in the parallel direction to the anisotropy both in dry and saturated conditions. Additionally, the values of UPV are higher in saturated samples when compared to dry samples for almost all stones (see ratio column from Table 5-4 and Figure 5-5). These results are in agreement with other results found in literature that suggests significant increase in *UPV* in porous saturated samples (Al-Omari, Beck, Brunetaud, Török, and Al-Mukhtar, 2015; Vasconcelos, Lourenço, Alves, and Pamplona, 2008). In this research, the exception is seen in two samples with low porosity but the difference ranges from 2% and 5% (Table 5-4).

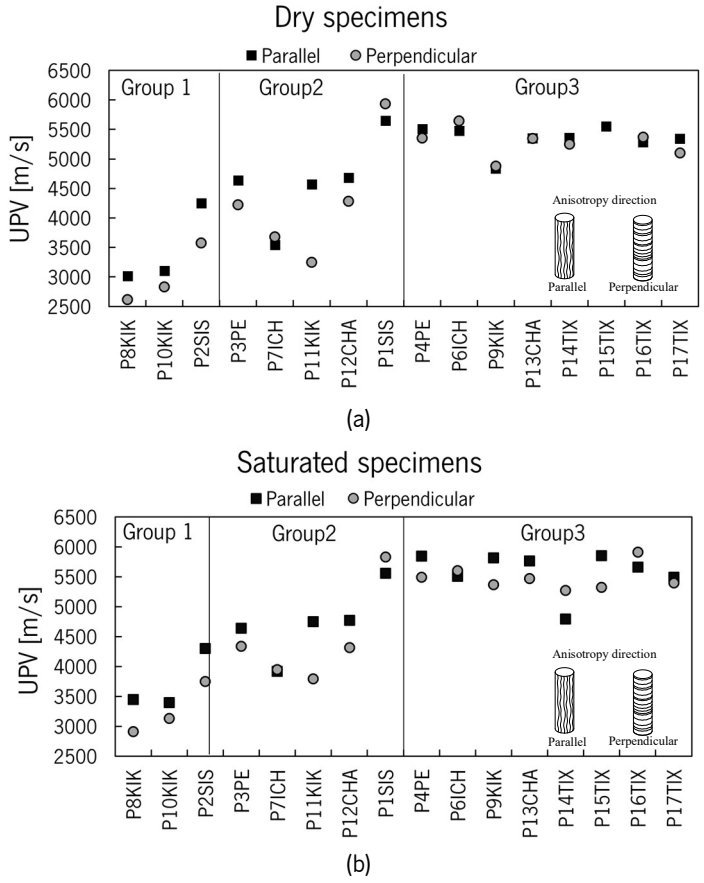


Figure 5-5. Ultrasonic pulse velocity (*UPV*). (a) dry samples and (b) saturate samples

Table 5-5.Ultrasonic pulse velocity recorded in limestone worldwide

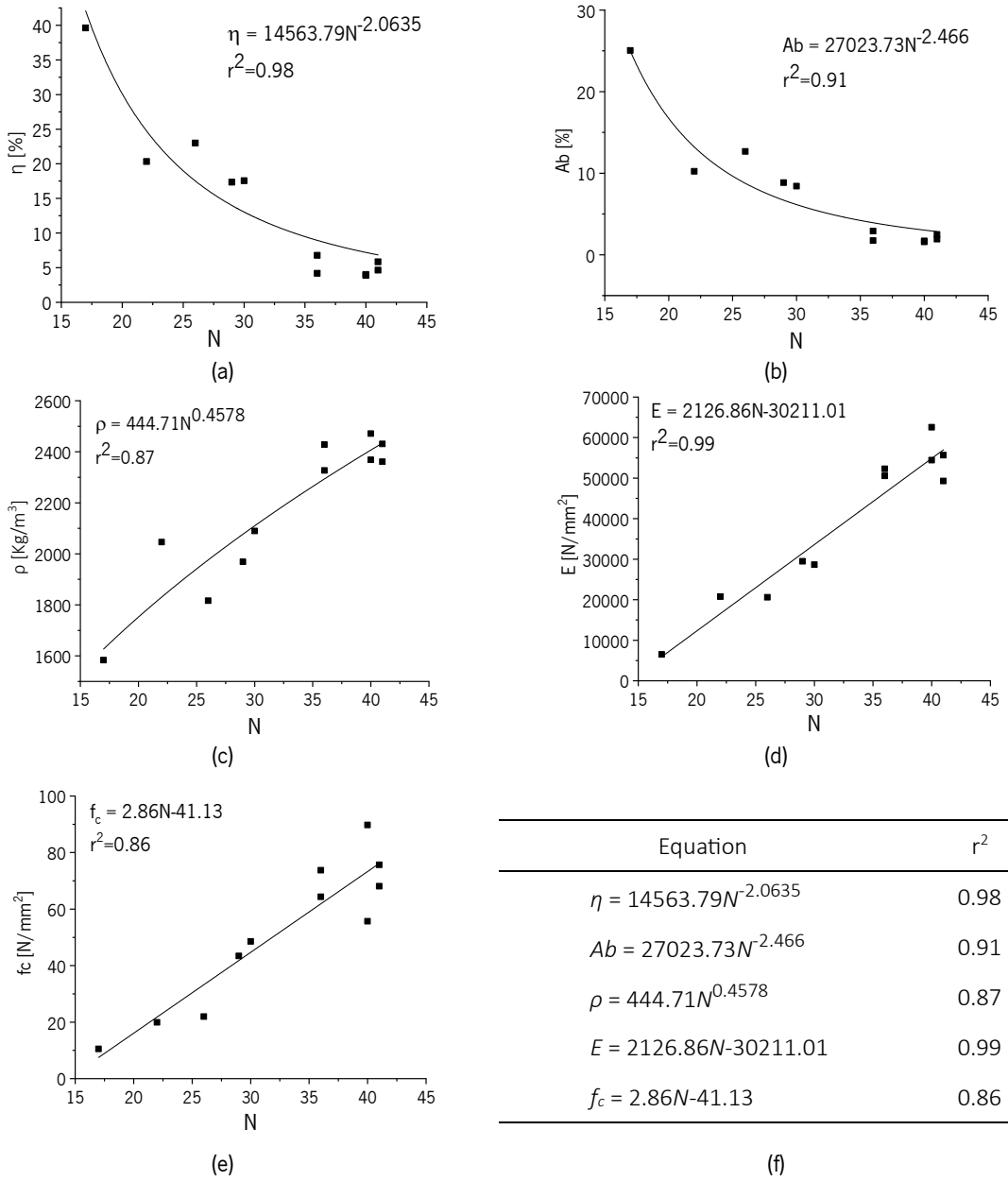
Reference, provenance and identification of Stone		*UPV* [m/s]
Al-Omari (2015). Chambord, France		
Tuffeau		1624
Richemont		2599
Yasar (2004). Turkey		
Adana/Ceyhan		4900
Adana/Karaisali		2900
Hatay/Iskenderum		5600
Adana/Pozanti		5800
Adana/Kozan		3000
Pappalardo (2016). Sicily, Italy		
PS		3490
D-NS		2850
B-NS		2790
Karakul (2013). Turkey		
Golbası-Haymana Highway limestone		6300-6160
Bell (1993).		
Magnesian Limestone Kiventon Park. United Kingdom		3600
Lincolnshire Limestone Ancaster. United Kingdom		2900
Lincolnshire Limestone Stamford. USA		2800
	Minimum	1624
	Maximum	6160

Several studies recorded the ultrasonic pulse velocity in limestone throughout the world (France, Turkey, Italy, United Kingdom and USA) and some indicative values are presented in Table 5-5. According to the values measured, *UPV* ranges from 1624m/s to 6160m/s. In this work, it is observed that *UPV* measured in limestone from Group 1 is in concordance with values of French limestone pointed out by Al-Omari (2015). The *UPV* range found in limestone from Group 3 is comparable with the values provided by Turkey by Karakul (2013) and by Yasar (2004). Finally, the limestone belonging to Groups 2 presents values of *UPV* close to the ones provided in Yasar et al., (2004), Pappalardo (2016) and Bell (1993). This means that the ranges of *UPV* found in this research are in accordance with the ranges previously point out also for limestone.

5.5 Prediction of physical and mechanical properties from NDT

As previously mentioned, the ultrasonic pulse velocity and Schmidt hammer non-destructive techniques can be useful methods for estimating the mechanical properties of different building stones found in ancient masonry structures. The prediction of physical and mechanical properties of building stones can be achieved through single regression analysis between non-destructive indexes and the physical and mechanical properties. These empirical correlations can be of great value in a preliminary phase of the diagnosis and inspection of the structural and material condition, particularly in cases in which the possibility of sampling material cores is reduced.

In this section, the variables Rebound hardness number obtained through Schmidt hammer (*N*) and Ultrasonic pulse velocity (*UPV*) were correlated with physical and mechanical properties, namely apparent density (ρ), open porosity (η), water absorption by immersion at atmospheric pressure (A_b), uniaxial compressive strength (f_c) and Elastic modulus (E). All correlations were adjusted to obtain the best fit to the experimental data and the regression equations, and the coefficient of determination (r^2) were calculated.



Equation	r^2
$\eta = 14563.79N^{-2.0635}$	0.98
$Ab = 27023.73N^{-2.466}$	0.91
$\rho = 444.71N^{0.4578}$	0.87
$E = 2126.86N\text{-}30211.01$	0.99
$f_c = 2.86N\text{-}41.13$	0.86

(f)

Figure 5-6. Relationship of Rebound hardness number (*N*) with physical and mechanical properties and equations of empirical correlations

Figure 5-6 illustrates the empirical correlations between the physical (porosity, η, water absorption by immersion, *Ab,* and density, ρ) and mechanical properties (E, f_c) with the Rebound hardness number (*N*). In all statistical relations the coefficients of determination (r^2) were greater than 0.85. It is observed that the increase on the porosity and water absorption results in decreasing values of surface hardness, whereas high values of density, elasticity modulus and compression correspond to higher values of rebound hardness number. It should be mentioned that the Rebound hardness number is particularly well correlated with the elastic modulus, as the coefficient of determination is approximately 1.0.

Several authors have been used the Rebound hardness number (N) as a tool to estimate the density, elastic modulus and uniaxial compression strength of building stones (Fatz et al., 2000; Saptono et al., 2013; Torabi et al., 2011; Yaşar and Erdoğan, 2004), see Table 5-6.

Table 5-6. Correlation between Schmidt hammer hardness with uniaxial compressive strength (fc), Elasticity modulus (E), density (ρ) and open porosity (η)

Expression	r2	Rock type / lithology	Reference
$fc = 2N$	0.72	Sandstone, siltstone	Singh (1983)
fc=0.4N-3.6	0.70	Coal	Shorey (1984)
fc = 0.994N-0.383	0.84	Coal	Haramy (1985)
fc = 0.88N-12.11	0.87	-	Ghose (1986)
fc = 702N-1104	0.77	Sandstone	O' Rourke (1989)
N=0.2329fc+15.7244	0.81	Marble, limestone, dolomite	Sachpazis (1990)
fc=exp(aN+b) a, b coefficient depends on rock type	0.91	Mica-schist, prasinite, serpentinite, gabbro, mudstone	Xu et al. (1990)
$fc = 0.0001N^{3.2658}$	0.84	Marl	Gökçeoglu (1996)
fc = 2.22N-47.67	-	Gabbro and basalt	Aggistalis (1996)
fc=1.31N-2.52	0.55	Gabbro and basalt	Aggistalis (1996)
$fc = 2.208e^{0.067N}$	0.96	Marble, limestone, granite, sandstone, chalk and syenite	Katz (2000)
fc =exp (0.818+0.059N)	0.98	Gypsum	Yilmaz (2002)
fc = 4E-06$N^{4.2917}$	0.80	Limestone, marble, basalt and sandstone	Yasar (2003)
fc = 2.75N-36.83	-	Andesites, basalts, tuffs	Dinçer (2004)
fc=4.24 $e^{0.059N}$	0.81	Basalt, granite, andesite, metagabbro, granodiorite, quartzite, marble, limestone, and travertine.	Fener (2005)
fc=0.0137$N^{2.2721}$	0.94	Diorite, quartzite, limestone, sandstone, granodiorite, basalt, marble, trachyte, travertine, andesite and tuff	Kiliç (2008)
fc=0.0465N^2-0.1756N+27.682	0.86	Siltstone, sandstone, argillaceous sandstone, shale, fossiliferous shales, argyle and tabular argyle	Torabi (2011)
fc=0.308$N^{1.327}$	0.9	Coal	Saptono (2013)
E=0.00013$N^{3.09074}$	0.99	Marble, limestone, granite, sandstone, chalk and syenite	Katz (2000)
E =exp (1.146+0.054N)	0.91	Gypsum	Yilmaz (2002)
ρ = 1308.2/n(N)-2873.9	0.99	Marble, limestone, granite, sandstone, chalk and syenite	Katz (2000)
ρ = 0.9377/n(N)-1.0299	0.84	Limestone, marble, basalt and sandstone	Yasar (2003)
η=0.1999(N) + 11.21	0.8	Limestone, marble, basalt and sandstone	Yasar (2003)

Some of these researches considered the same lithology (Haramy and DeMarco, 1985; O'rourke, 1989; Yilmaz and Sendir, 2002) but in others, the correlations were obtained from data including several lithologies (Fener et al., 2005; Kiliç and Teymen, 2008). Furthermore, different equations have been pointed out for the empirical correlations between N and uniaxial compression strength, namely linear, exponential and power functions. Also in this research, a linear fit between N and uniaxial compression strength was found (r^2=0.86), see Figure 5-6e. On the other hand, some researchers multiplied N by density to improve the correlation with uniaxial compression strength (Aufmuth, 1973; Beverly et al., 1979; Deere and Miller, 1966; Haramy and DeMarco, 1985; Kidybiński, 1981).

The empirical correlation summarized in Table 5-6 were plotted and compared with the relations found between N and uniaxial compression strength for Yucatan limestones, see Figure 5-7.

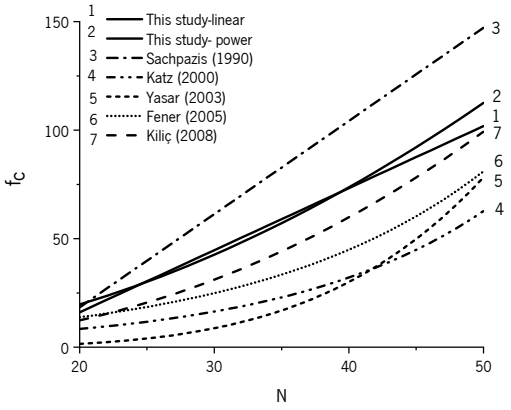


Figure 5-7. The relationship between Schmidt hammer hardness and *fc* for limestones and sedimentary stones from different researchers

Most of the coefficients of determination (r^2) for limestone and sedimentary stones present reasonable accuracy ranging from 0.70 to 0.96, similar to Yucatan limestones which present a determination coefficient of 0.86. Despite the curve shape of all these equations is similar, Yucatan limestones showed greater values of f_c than most equations from literature. In summary, the nature of the material, as sedimentary stone, shows a clear scatter when empirical relations from different locations. This means that for the same N number, different values of the uniaxial compression strength are predicted according to each equation. Probably, if these sedimentary stones were studied specifically by lithotype, the dispersion would decrease.

The rebound hardness number (N) has also been correlated with the properties E, ρ and η thought exponential, logarithmic and linear fit functions, see Table 5-6. The mechanical and physical properties are strongly connected and depend on the characteristics of each lithologic type, for this reason the

use the same equation for different lithological groups makes the results not very accurate. Since this research focuses only on limestone, it is expected that the provided equations will be more representative and reliable for studies with same lithology, contrarily to the previous ones that consider different lithologic groups.

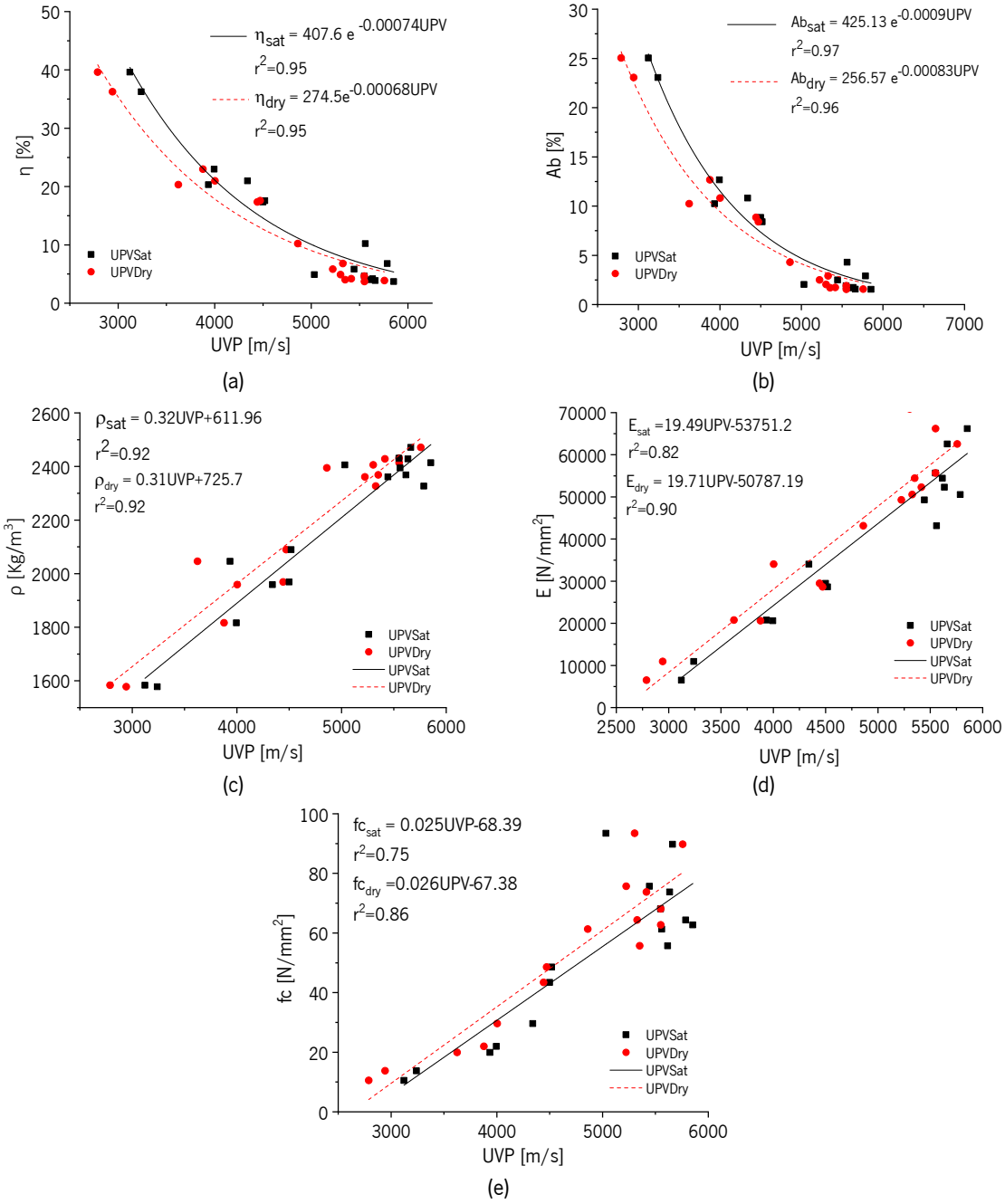


Figure 5-8. Relationship between ultrasonic pulse velocity (UPV) and physical and mechanical properties

Ultrasonic pulse velocity analysis (UPV) was also correlated with physical and mechanical characteristics by considering the best fit to the experimental results. Figure 5-8 shows the correlations between variables, for both dry and saturated conditions. Coefficients of determination (r^2) from 0.75 to 0.97 were achieved for the different empirical correlations. The results reveal that UPV increases

for increasing values of open porosity (η) and water absorption at atmospheric pressure (*Ab*), being the statistical correlation between the variable well described by exponential functions. On the other hand, UPV increases linearly with density (ρ), elasticity modulus (*E*) and uniaxial compressive strength (*fc)*. This results are in agreement with the findings reported by (Kahraman and Yeken, 2008; G. Pappalardo et al., 2015; Yasar and Erdogan, 2004). Additionally, it was observed that the moisture content also influences the correlations between the variables. From which, faster UPV values were recorder for saturated samples than dry samples.

The UPV results achieved in this work were compared with data from literature. A summary of different empirical correlations found in literature between UVP, and uniaxial compressive strength is presented in Table 5-7. The empirical correlations include different lithologies, from which were selected specified the correlations for limestone to compare the linear correlation between *fc* and *UPV.* It is seen that the correlations from this research are in the range of previously limestone defined in the literature (Figure 5-9a).

Table 5-7. Empirical statistical correlations between uniaxial compressive strength (*fc)* and ultrasonic pulse velocity (UPV)

Correlation	r^2	Rock type / lithology	Reference
$fc = (UPV - 0.0195)/0.032$	0.81	Limestone, marble, dolomite	Moos A. V. (1948)
$fc = 35.54UPV - 55$	0.8	limestone	D'Andrea D. V. (1964)
$fc = 9.95UPV^{1.21}$	0.83	Marl, limestone, dolomite, sandstone, hematite, serpentine, diabase and tuff	Anon (1979), Christaras B (1997), Kahraman S (2001)
$fc = 2.21e^{(0.07 \times N)}$	0.96	Chalk, limestone, marble, granite	Katz O (2000)
$fc = 2.304UPV^{1.43}$	0.97	Diorite, quartzite, limestone, sandstone, basalt, marble, trachyte, andesite and tuff	Kılıç & Teymen (2008)
$fc = 56.71UPV - 192.93$	0.81	Sandstone and limestone	Cobanoğlu & Celik (2008)
$UPV = 966.22e^{0.0262N}$	0.96	Sandstone, Siltstone, Conglomerate, Sandstone, Schist, Quartzite, Gneiss, Granite, Basalt and Andesite	Sharma (2009)
$fc = 49.4UPV - 167$	0.89	Travertine, limestones, schist	Yagiz S (2011)
$fc = 0.012UPV - 5.95$	0.89	Limestone	Babacan (2012)
$fc = 0.033\ UPV - 34.83$	0.87	Quartzite, granite, dolomite, sandstone, limestone, shale, marble	Khandelwal M (2013)
$fc = 22.18UPV - 30.32$	0.83	Gypsum, ignimbrite, sandstone, limestone, andesite, dacite and basalt	Selçuk (2014)
$fc = 12.746UPV^{1.194}$	0.79	Limestones, sandstone, travertine, marl, dolomite, mudrock shale, slate, siltstone	Azimian (2014)
$fc = 0.018UPV - 18.405$	0.93	Limestone	Kurtulus (2016)
$fc = 10.57UPV - 19.9$	0.84	Limestone	Pappalardo (2016)
$fc = 0.043\ UPV - 136.8$	0.932	Basalt rock	Aldeeky (2018)

Furthermore, the empirical correlations between UVP and elastic modulus (*E*) proposed by other authors are listed in Table 5-8. All empirical correlations are described by linear equations as found also in this research, see Figure 5-9b. The correlation found for limestone from Yucatan churches show a similar slope found for granites point out by Vasconcelos (2007) and a mixture of 4 lithologies by Yagiz (2011), which means they have similar increments with close coefficients 19.87, 24.19, 19.71 for Vasconcelos et al. (2007), Aldeeky (2018), and this experiment respectively. The mixture of 4 lithologies maybe is close because they are mostly limestones. (Figure 5-9b and Table 5-8).

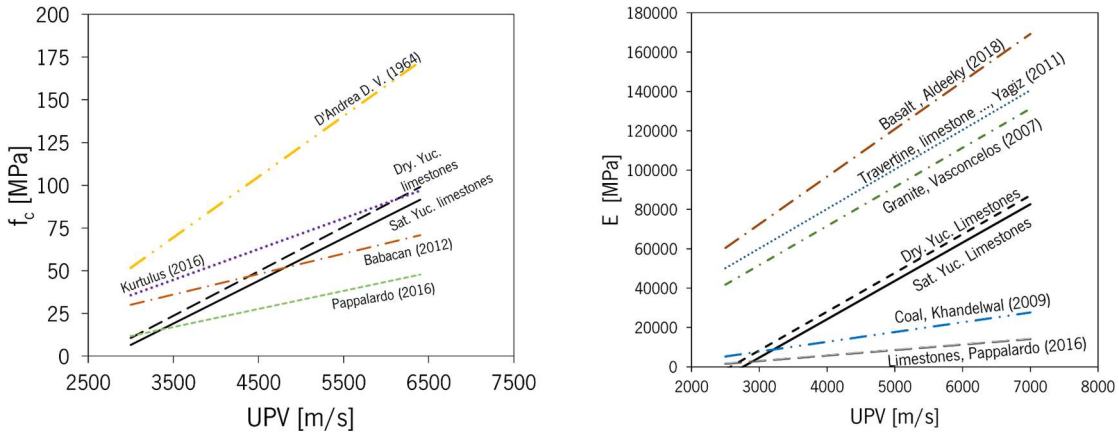


Figure 5-9. Comparison of the regression equation of the current study with those equations from the literature review: (a) fc vs UPV of limestones, (b) E vs UPV

Table 5-8. Empirical equations correlating modulus of elasticity (E) and ultrasonic pulse velocity (UPV)

Expression	r^2	Rock type / lithology	Reference
E = 19.87UPV-27813	0.84	Granite rock	Vasconcelos et al. (2007)
E = 4.9718 UPV - 7151	0.97	Coal rock	Khandelwal and Singh (2009)
E = 0.041 UPV - 264.15	0.81	Peridotites	Diamantis et al. (2011)
E = 0.0015 UPV - 2.516	0.74	Granite rock	Kurtulus et al. (2011)
E = 20.1 UPV - 53	0.95	Four types of travertine, three types of limestone, and two types of schist.	Yagiz (2011)
E = 0.919(UPV)1.9122	0.79	Sedimentary rock	Altindag (2012)
E = 0.01286UPV - 32.8773	0.72	Basalt rock	Karakuş et al. (2013)
E=2.784UPV-5.434	0.73	Limestone	Pappalardo (2016)
E = 24.19 UPV - 71.98	0.83	Basalt rock	Aldeeky (2018)
Esat=19.49UPV-53751.2	0.82	Limestones	This research- saturated
Edry=19.71UPV-50787.19	0.90	Limestones	This research-dry

Table 5-9. Empirical equations correlated dry density (ρ) and ultrasonic pulse velocity (UPV)

Expression		r^2	Rock type / lithology	Reference
ρ = (UPV+7.707)/4.3183	[Kg/m³]	0.80	Limestone, marble, dolomite	Moos A. V. (1948)
ρ = 0.2316UPV+1.785	[Kg/m³]	0.80	Carbonate rock	Yasar (2004)
ρ = 0.2136UPV+1.256	[Kg/m³]	0.82	Carbonate rock	Kahraman (2008)
ρ = 0.19UPV + 1.61	[Kg/m³]	0.58	Travertine, limestone and schist	Yagiz S (2011)
ρ = 0.0002UPV+1.7752	[g/cm³]	0.87	Granite rock	Kurtulus (2011)
ρ = 0.0003098UPV+1.0058	[g/cm³]	0.89	Basalt rock	Karakus (2013)
ρ = 0.802UPV-1.6065	[Kg/m³]	0.85	Calcarenite rock	Rahmouni (2013)
ρ = 0.00038UPV+0.91	[g/cm³]	0.89	Basalt rock	Chen (2015)
ρ = 0.0002UPV+1.2447	[g/cm³]	0.91	Volcanic rock	Canbay (2016)
ρ= 0.002UPV + 1.339	[g/cm³]	0.90	Limestone	Kurtulus (2016)
ρ = 0.000081 UPV + 2.241	[g/cm³]	0.88	Basalt rock	Aldeeky (2018)
ρ_{sat} = 0.32UPV+611.96	[Kg/m³]	0.92	Limestone	This research-saturated
ρ_{dry} = 0.31UPV+725.7	[Kg/m³]	0.92	Limestone	This research-dry

Table 5-10. Empirical equations correlated open porosity (η) and ultrasonic pulse velocity (UPV)

Expression	r^2	Rock type / lithology	Reference
$UPV = -0.021\eta + 4.3239$	0.89	Travertine, limestone and schist	Yagiz S (2011)
$\eta = 6x10^{-5}UPV+0.0366$	0.67	Granite rock	Kurtulus (2011)
$\eta = -0.00006814UPV+0.4802$	0.747	Basalt rock	Karakus (2013)
$\eta = 1332.7e^{0.001UPV}$	0.67	Andesite	Siratovich (2014)
$\eta = -0.004UPV + 3.1465$	0.85	Limestone	Kurtulus (2016)
$\eta = -0.000064UPV+4.409$	0.832	Basalt rock	Aldeeky (2018)
$\eta_{sat} = 407.6e^{0.00074UPV}$	0.95	Limestone	This research-saturated
$\eta_{dry} = 274.5e^{0.00068UPV}$	0.95	Limestone	This research-dry

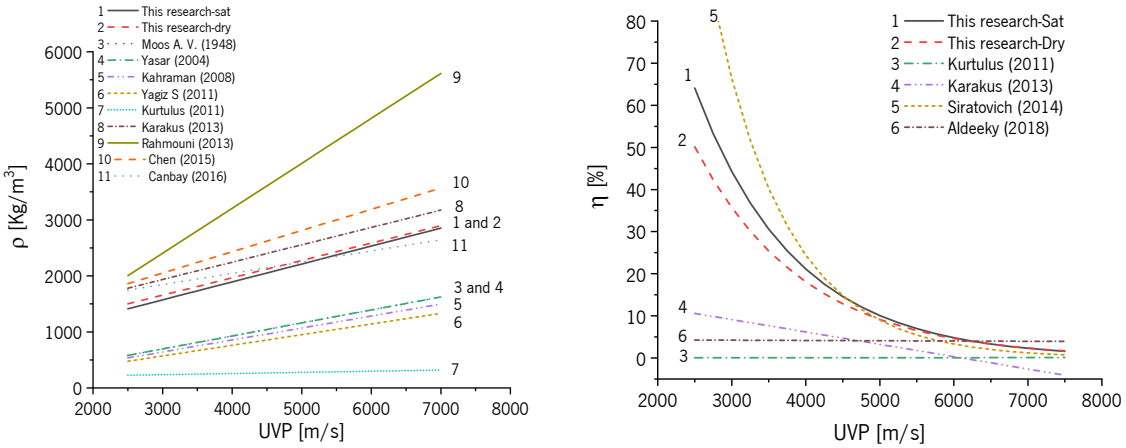


Figure 5-10. Comparison of the regression equations of the current study with those equations from the literature review: (a) ρ vs UPV, (b) η vs UPV

Similar analysis was carried out between UPV and density and open porosity. The correlations found in literature are listed in Table 5-9 and Table 5-10, while the comparative analysis in Figure 5-10. The density of stones can be obtained from the ultrasonic pulse velocity through linear functions (Figure 5-8c and Table 5-9. The correlation between open porosity and ultrasonic pulse velocity is described by both linear and exponential functions. In case of limestone from Yucatan churches, the correlation is described by an exponential function (Figure 5-8a), like Andesite stones as pointed out by Siratovich (2014).

5.6 Relations between physical and mechanical properties

Several authors had studied statistic correlations between mechanical and physical properties, engineering geological properties and textural features (Basu et al., 2009; Bednarik et al., 2014; Liu et al., 2019; G. Pappalardo et al., 2016; Pappalardo, 2014). Nevertheless, the variation in the physical and mechanical properties among lithotypes result in different regression equations and sometimes these do not totally represent the stone lithotype of other regions. Particularly with limestones, which present a remarkably complex porous system, namely regarding to the geometry of pores, which is attributed to the complex genesis. In these rocks, the genesis of pores normally has a long and complex history, due to the chemical mobility of their minerals. Furthermore, once the materials have been deposited, in the final stage of the sedimentary cycle (diagenesis) the limestones suffer chemical and physical alterations that generally cause their compaction (Basu et al., 2009; Bednarik et al., 2014; Liu et al., 2019; G. Pappalardo et al., 2016; Pappalardo, 2014). Therefore, it is important to identify the stone physical characteristics of the stone regarding to which the estimation of the mechanical properties is required. In this section was carried out a statistical study to assess the possible relation between physical and mechanical properties based on single regression analyses.

The physical properties were statistically analysed to understand the dependence between them by defining meaningful statistical correlations, see Figure 5-11. Regression analysis was performed aiming at obtaining the best-fit with coefficients of determination (r^2) greater than 0.9, when possible.

The physical properties namely, open porosity (η), density (ρ), absorption capacity by immersion (Ab) and by capillarity (Cw) are closely correlated, which is confirmed by the good coefficient of determination (r^2). The water capillary coefficient increases with increasing open porosity. This appears to indicate that in the limestone under study, the open porosity controls definitely the behaviour of

limestone to water absorption. This means also that in low porosity stone, the capillary action has much lower effect (Bednarik et al., 2014), which can be beneficial in terms of its durability.

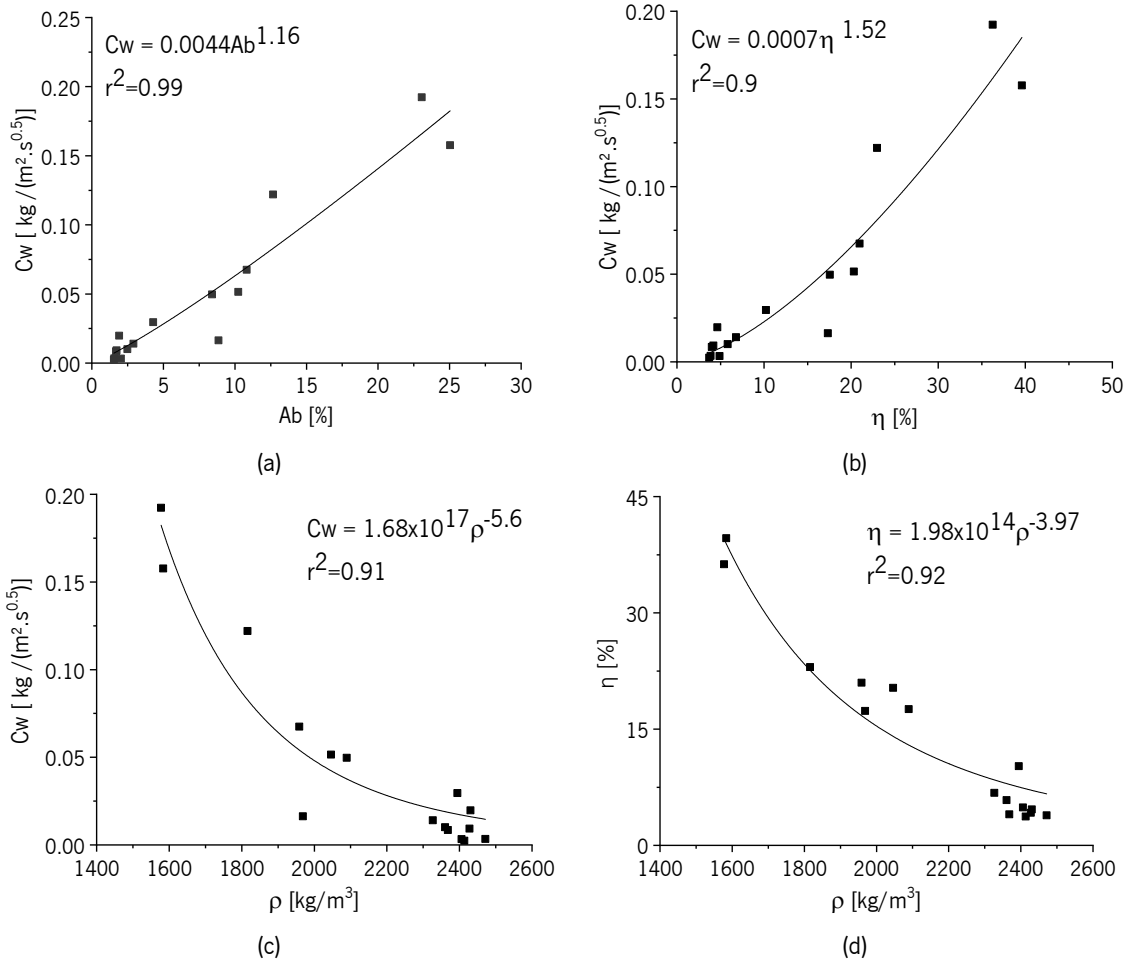


Figure 5-11. Correlations between physical properties; (a) *Cw* vs *Ab*; (b) *Cw* vs η; (c) *Cw* vs ρ; (d) η vs ρ

As mentioned previously (Chapter 4), high values of compressive strength and modulus of elasticity are characteristic of more brittle stones and are also an indication of the quality of the material. Usually, higher values of compressive strength are associated to higher values of modulus of elasticity. This trend is confirmed for the limestone analysed herein through the statistical correlation found between both variables characterized by a very good coefficient of determination (r^2=0.99), see Figure 5-12.

Correlation between compressive strength and modulus of elasticity for limestone and other rocks, including marble, limestone, sandstone, granite and volcanic rocks have been also pointed out in literature, being clear that rocks with low values of compressive strength have also low values of modulus of elasticity (Basu et al., 2009; Chang, Zoback, and Khaksar, 2006; Karakul and Ulusay, 2013; Liu et al., 2019; G. Pappalardo et al., 2016; Ündül, 2016; Vasconcelos and Lourenço, 2009)

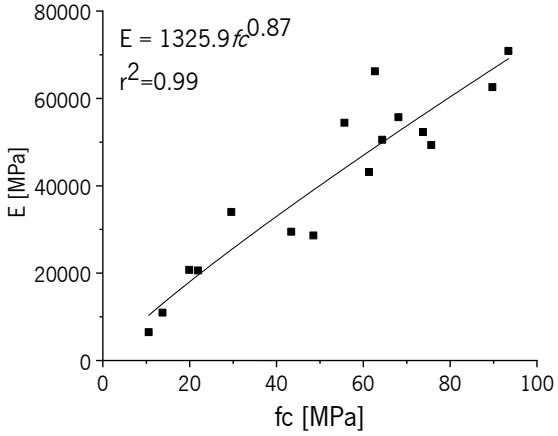


Figure 5-12. Correlation between compressive strength and modulus of elasticity

The dependence of mechanical properties on the physical properties was also investigated. The dependence of the modulus of elasticity (E) on the physical properties of limestone is illustrated in Figure 5-13. The physical properties used for the statistical analysis were the open porosity (η), water absorption by immersion (A_b), density (ρ) and water absorption by capillary (Cw). The modulus of elasticity of limestone highly depends on the physical properties, namely open porosity, as shown by the coefficients of determination (r^2) of 0.92, see Figure 5-13a. It is seen that the limestone from group 1 (G1) present high values of porosity between 31.75 to 41.56%, corresponding to the lowest range of the modulus of elasticity between 1459.09 to 1676.05 MPa. The average values of porosity found for Group 2 (G2) ranging from 10.45 and 27.82% have associated a variation on the modulus of elasticity between 20604.6 to 34018 MPa and the low porosity limestone from Group 3 (G3) present the highest values of modulus of elasticity ranging from 43140 to 70877 MPa.

The modulus of elasticity strongly depends also on water absorption by immersion, on the capillary coefficient and density, which is confirmed by the nonlinear statistical correlations, to which high values of coefficient of determination have been found (r^2 higher than 0.84). The modulus of elasticity increases in denser limestone and decreases in limestone with high water absorption coefficient, both by immersion and capillarity (Figure 5-13 c,d). This is in agreement with the results pointed out by Pappalardo (2016), Karakul (2013) and Bell (1993).

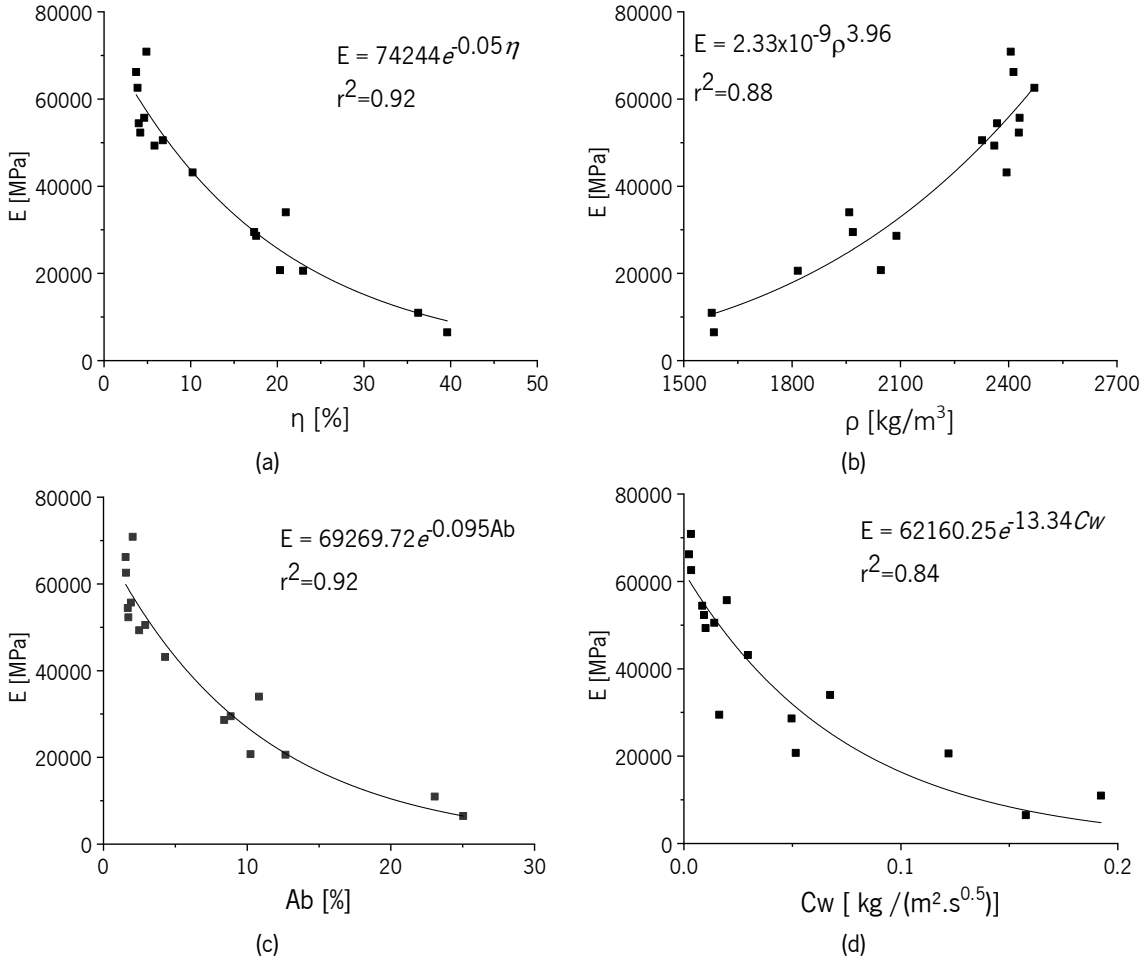


Figure 5-13. Statistical correlation between modulus of elasticity (*E*) and physical properties; (a) *E* vs. open porosity; (b) *E* vs. density; (c) *E* vs water absorption by immersion; (d) *E* vs capillary coefficient

The statistical correlations between the compressive strength and the physical properties of limestone are illustrated in Figure 5-14. The dependence of the compressive strength on the physical properties is similar to the one observed for the modulus of elasticity. This is justified by the good correlation between compressive strength and modulus of elasticity as discussed previously.

Denser limestone has higher compressive strength. On the other hand, more porous limestone present lower values of compressive strength. Several authors discussed the influence of porosity on the mechanical features of stones, highlighting that more porous skeleton results in the reduction of the compressive strength (Andriamihaja et al., 2016; Di Benedetto et al., 2015; G. Pappalardo et al., 2016; Vasconcelos and Lourenço, 2009).

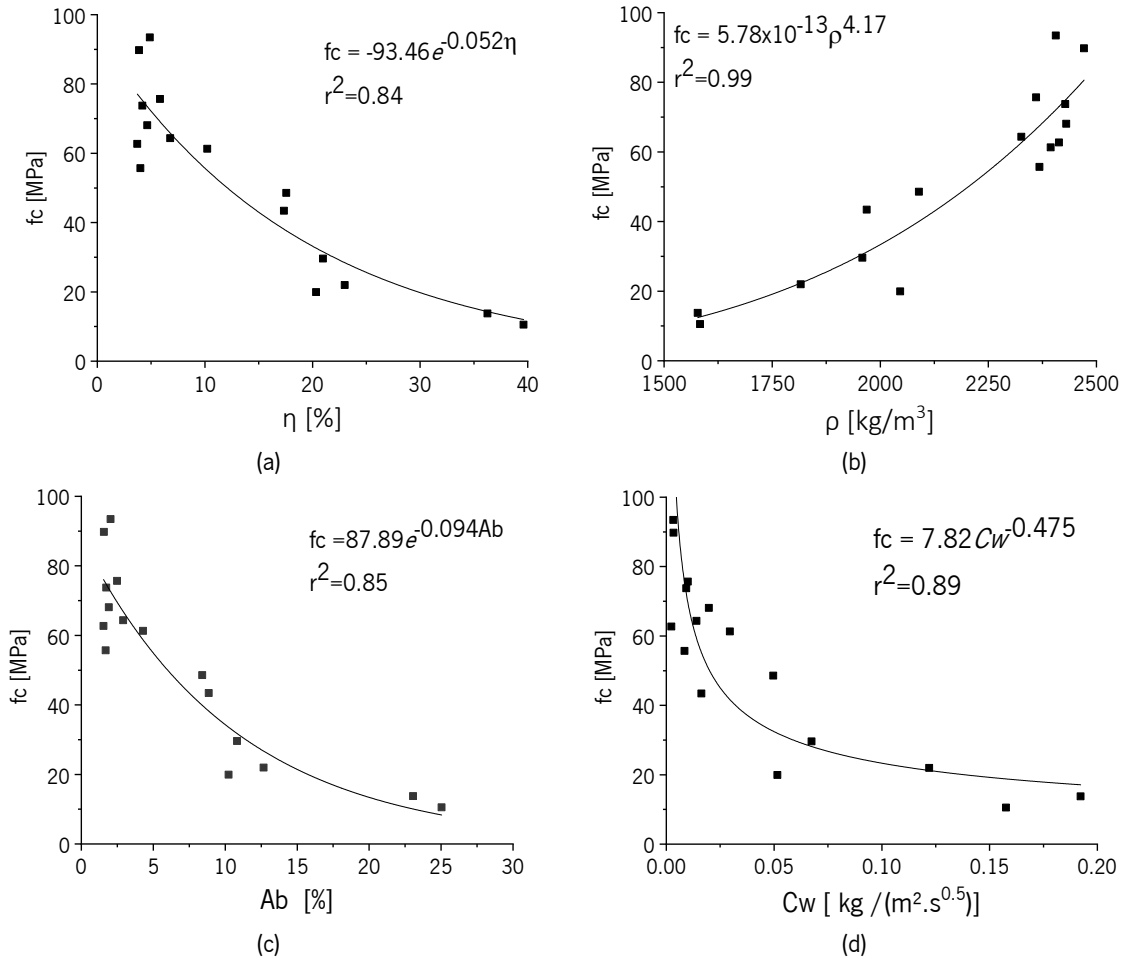


Figure 5-14. Statistical correlation between compressive strength (*fc*) and physical properties; (a) *fc* vs. open porosity; (b) *fc* vs. density; (c) *fc* vs water absorption by immersion; (d) *fc* vs capillary coefficient

The compressive strength in limestone naturally decreases with the increase on the ability of limestone to absorb water, both through immersion and capillarity (Figure 5-14c,d). Notice that both physical properties regarding the water absorption are influenced by the open porosity and increase with increasing porosity.

The results proposed in this work are consistent with the results presented by Chang (2006), Pappalardo (2016) and Zhu (2010) as in these works the physical properties (η, *Ab, Cw*) also show similar negative exponential relationship with the compressive strength (*fc*).

5.7 Concluding Remarks

This Chapter intended to obtain possible correlations between physical and mechanical properties with indexes given from two simples non-destructive techniques extensively used for in situ materials assessment, namely Schmidt hammer and Ultrasonic pulse velocity. In addition, further statistical

correlations between physical and mechanical properties were analysed, taking the data obtained in Chapter 4.

The results indicated very good statistical correlations found among the physical properties. Furthermore, the statistical correlations, to estimate the mechanical properties from the physical properties, revealed very reasonable coefficients of determination (r^2>0.9).

Non-destructive indexes based on Schmidt hammer (N) and ultrasonic pulse velocity (UPV) on limestone showed reasonably accurate to predict mechanical and physical properties. Influencing factors as anisotropy and moisture content were also reviewed. For both dry and saturate conditions, higher values of UPV were recorded along the stratification's layers (when the anisotropy plane was in the same direction of measurement of the ultrasonic pulse velocity). The denser samples show higher velocities than samples with low density. Also, the saturated samples have mostly higher velocities than the dry samples. Higher values of Rebound hardness number (N) were clearly associated with denser and consequently low porosity limestone.

The results appear to confirm that the UPV and Schmidt hammer tests can be effectively used as non-destructive methods for a preliminary prediction of mechanical and physical properties, for which equation of correlation are provided in this research. It is considered that these results can be used for the estimation of physical and mechanical properties of limestone belonging to the Yucatan churches in Mexico.

Chapter 6
Description of the experimental model and experimental test

Abstract:
This chapter presents the description of the experimental model representing the cross section of single nave Yucatan churches with barrel vaults, the design of the teste setup and the main results of the experimental testing of the model submitted to differential vertical settlements.

6.1 Introduction

Masonry vaults have been an efficient roofing construction technique, revealing high strength to vertical uniform loads but usually show damage mostly related to displacements of the walls abutments, which support them. In historical constructions, the supporting walls of the vaults were generally built on superficial foundations with the same construction system used for the walls and in the best of cases by using slightly larger stones. At that time, not much attention was paid to soil characteristics since the science of soil mechanics was developed after 1925 (Nash, 1961).

Besides the damage caused by seismic events, historical constructions show damages and crack patterns due to: 1) ageing of material, 2) lateral displacements due to lateral wall instability, 3) settlement of the foundations due to soil degradation or non-uniform soil stratigraphy and 4) support failure due to poor foundations, stress concentrations or flooding phenomena, among others. In addition, although the effects of an ongoing process of deformation are clear on vaults throughout visible cracks, the origin of causes such us the ongoing settlement can be difficult to identify.

The understanding of the causes of damages and the proposal of adequate intervention is a great challenge in structural engineering. In particular, it should be mentioned that few works have dealt with the influence of foundation settlement in the crack patterns masonry arches. It has been seen that hinge configurations depend mainly on the angle of the settlement, the slenderness and stiffness of the vault or arch (Acikgoz et al., 2017; Cascini et al., 2020; D'Altri et al., 2020; De Guglielmo et al., 2015; Portioli and Cascini, 2016, 2017; Torres et al., 2019; Tubaldi et al., 2018; Zampieri et al., 2017; Zampieri et al., 2019; Zampieri et al., 2018; Zhang et al., 2018). Thus, despite the settlements are the origin of many common structural damages on historical masonry constructions, it is important to mention that vertical settlements are much more difficult to simulate in laboratory environment than horizontal displacement and thus few research focused on this topic. As consequence, the effect of settlement on the structural behaviour of masonry vaults and arches was not yet explored in detail (Zampieri et al., 2018). The importance of experimental testing is also attributed to the data generated to calibrate numerical models and further perform parametric analysis that can enhance the understanding of the structural behaviour of masonry structures. Based on the experimental results, it is also possible to define retrofit interventions according to different retrofitting techniques assess it structural performance (Garmendia et al., 2014; Girardello et al., 2013; Ramaglia et al., 2016).

Following the identification of a research gap in the scope of the experimental analysis of masonry vaults submitted to vertical settlements, it was decided to perform an experimental campaign on stone

semi-circular barrel vaults supported on stone masonry walls when subjected to an imposed settlement, representing the typical cross section of single nave Yucatan churches with barrel vaults. These vaults can be seen commonly in churches of Yucatan region in Mexico from the 16th to the 18th century. The main aim was the assessment the mechanical behaviour of the vault-wall system under vertical settlements identifying the main crack patterns and failure mechanisms in order define possible interventions and strengthening. Since it was not possible to carry out tests on real scale in the laboratory, the experimental model was scaled at 30%. The morphology and constructive processes were defined according to the deep survey developed and presented in Chapter 2 and the geometric characteristics of the experimental model of the cross section of Yucatan churches were defined according to the statistical analyses presented in Chapter 3. The materials used for the experimental model were selected according to the physical-mechanical characterization presented in Chapter 4. Furthermore, numerical analyses were performed to predict the mechanical behaviours and the positions of the hinges, taking into account materials properties data taken from literature and from the results of uniaxial compression tests carried out on stone masonry representing both the bond of masonry walls and vaults bonds of the experimental model.

6.2 Behaviour and collapse mechanisms of masonry vaults

An arch is stable and in equilibrium under a certain external loading state when the thrust line can be drawn in vault's thickness. The cracks appear when the thrust line touches the edges of the vault thickness, revealing the hinges' location. The collapse develops when the number of hinges increase until the development of a mechanism. The position of the hinges depends on the shape of the arch and on the thrust line. In vaulted masonry structures the hinges appear usually between the stones or brick units.

An arch with fixed supports (six degrees of freedom) is statically indeterminate because the static equilibrium equations ($\Sigma Fx=0$, $\Sigma Fy=0$ and $\Sigma M=0$) are insufficient to determine the internal forces and reactions. Thus, the structure is considered to be a hyperstatic structure of third grade. To achieve a statically determined arch (isostatic), three hinges are necessary. If the arch develops fourth hinges, then it will become a mechanism. The collapse of vaulted masonry structures occurs due to the formation of mechanisms.

A masonry arch begins to exert thrusts on the supporting walls immediately after the formwork is removed. In turn, the walls inevitably develop displacements, which will increase or reduce the span.

Due to this movement, the thrust line moves adopting higher or lowered positions while touching the edges resulting in the formation of hinges. To avoid the collapse, the thrust line should keep inside of the thickness vault.

Regarding to the collapse mechanism, Parland (1982) establishes that the structure is unsafe if there is the possibility of a slip failure mechanism, although it is possible to find a line of thrust inside the arch or vault. It is well known that masonry vaults are usually prone to flexural failure and the sliding failure is often neglected. In fact, shear or sliding failure in the joint is prevented by the friction between the stone units, which generally is high (Heyman, 1966; Huerta Fernández, 2007; Parland et al., 1982). Regarding to settlement conditions, if the masonry vault-wall system is considered as hyperstatic structure with two degrees of redundancy, three hinges are necessary to transform the structure into a mechanism and achieve the collapse (Zampieri et al., 2019), see Figure 6-1. In case of a unreinforced vault, failure mechanism activates by the formation of four hinges, alternated at the intrados and at the extrados. The presence of the reinforcement modifies the failure mode because the thrust line can lie away from the thickness of the arch, increasing its deformability capacity and delaying its collapse. The failure of the arch occurs also when four hinges are formed but the strengthening delay the development of hinges, besides additional failure mechanisms must be considered as a combination of crushing, sliding, debonding or rupture (Boem and Gattesco, 2021; Borri et al., 2011; Cancelliere et al., 2010; De Santis et al., 2018; Garmendia et al., 2015a; Tanriverdi, 2023).

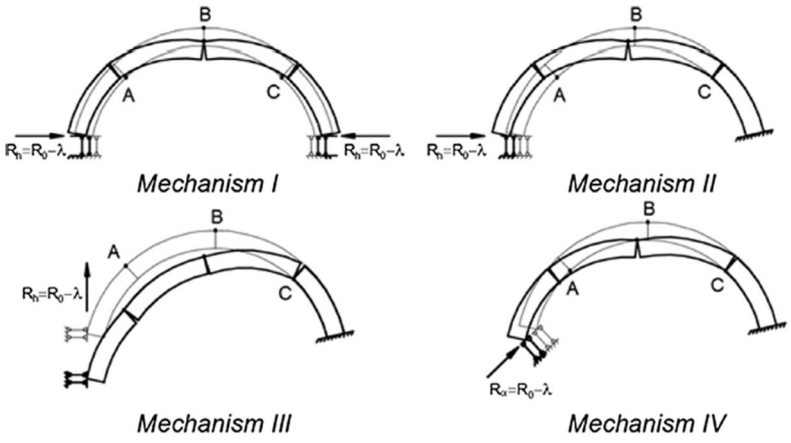


Figure 6-1. Main collapse mechanisms of masonry arch due to supports settlement according to Zampieri (2018)

Different studies are available on vault structures under settlement conditions. These studies focused on: 1) multi-span masonry arch bridges subjected to scour (Tubaldi et al., 2018), 2) collapse mechanisms due to horizontal loads on masonry arches (Gaetani et al., 2017; Masciotta et al., 2020;

Michiels and Adriaenssens, 2018; Zampieri et al., 2017; Zhang et al., 2018), 3) collapse mechanisms considering different settlement configurations (D'Altri et al., 2020; Zampieri et al., 2019; Zampieri et al., 2018), 4) software tool development for collapse mechanism analysis (Cascini et al., 2020) and 5) development of numerical models and methods of analysis. (Acikgoz et al., 2017; Portioli and Cascini, 2017)

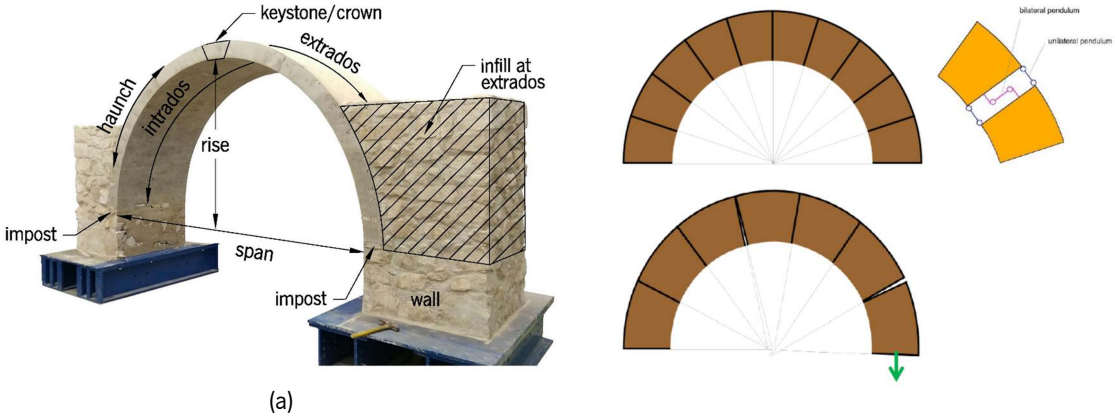


Figure 6-2. (a) parts of the vault and (b) De Guglielmo model and hinges on arches (De Guglielmo et al., 2015)

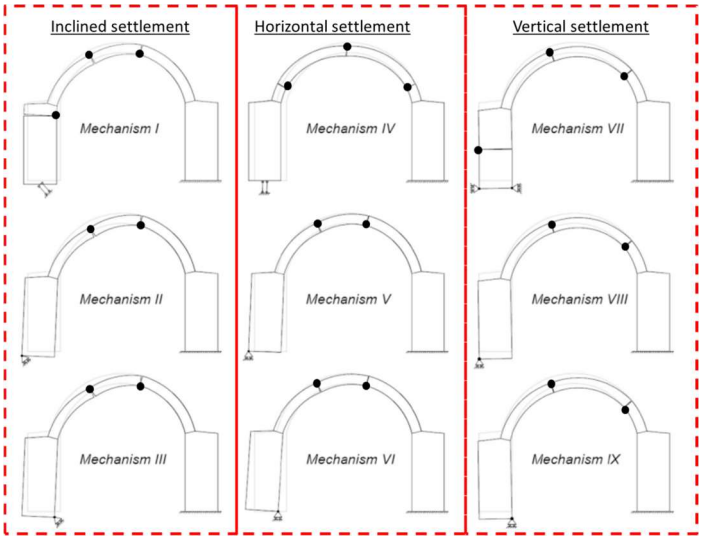


Figure 6-3. Main theoretical collapse mechanisms of masonry buttressed arches considering three types of support settlement (horizontal, vertical and inclined) (Zampieri et al., 2019b)

The local failure mechanisms developed in vaults compromising the structural stability are related to the rotations of the walls due to the thrust of the vault, low stiffness of arched structures or differential vertical settlements at the supports (D'Altri et al., 2020; Zampieri et al., 2018a; Zampieri et al., 2018b). The vault-wall systems are more vulnerable to horizontal displacement than inclined or vertical displacement (Zampieri et al., 2019). According to De Guglielmo (2015), in a barrel vault, cracks commonly open at the keystone, on the haunches or at the imposts (Figure 6-2a), because these are the points where the thrust line tends more easily to exit from the volume of the structure and tensile

stresses appear, see Figure 6-2b. According to Zampieri et al. (2019) there are nine main theoretical collapse mechanisms of masonry vault when this is supported by walls and considering three types of support settlement (horizontal, vertical, and inclined), see Figure 7-3.

6.3 Brief review on past experimental research

Aiming at developing a proper design of the experiment model representing a typical masonry vault of Yucatan churches, an extensive overview of experimental studies on arches and vaults has been performed, including: (1) scale and representative geometry for experimental models, (2) load conditions, (3) instrumentation design, (4) support conditions, (5) failure mechanisms.

6.3.1 Scale and geometry for experimental models

The experimental studies of vaults have been mostly performed on experimental models representing only part of the vault. It is considered that the behaviour of barrel vaults is very close to the behaviour of arches because long barrel vaults can be obtained as a series of adjoining arches of unit width (Giuriani et al. 1999). Nevertheless, this assumption should be used with caution since this behaviour is valid only in the middle of the total length, because the influence of edge effects (Rodriguez, 2006).

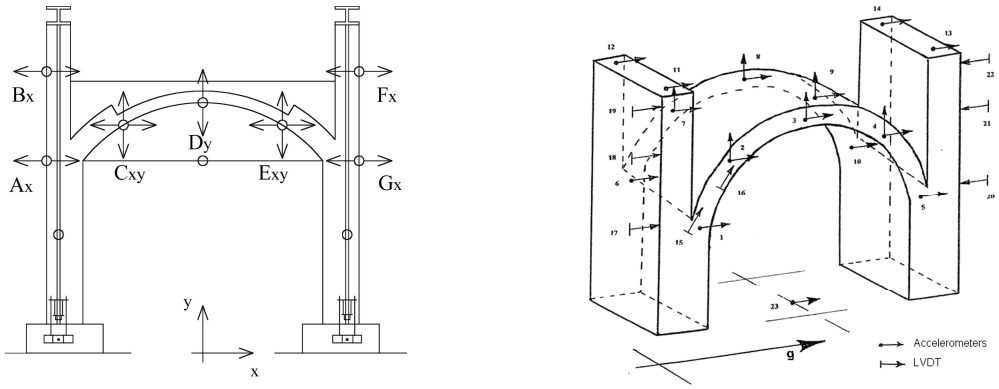
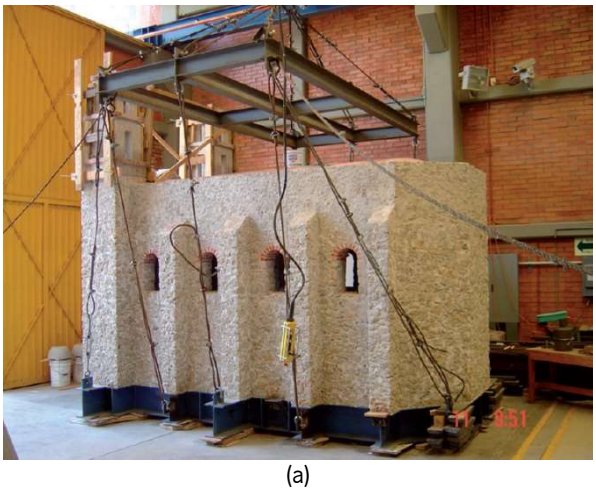


Figure 6-4. Full experimental models; (a) model proposed by (Marini, Giardina, Riva, and Giuriani, 2008); (b) model proposed by Baratta et al. (2008)

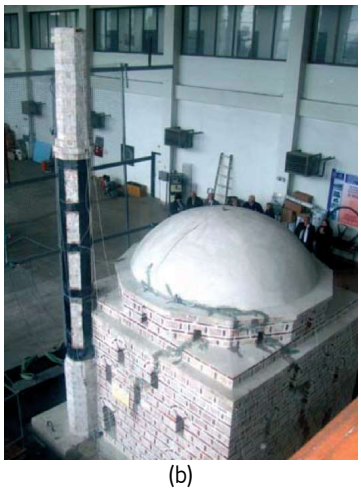
The behaviour of arches and vaults and its interaction with supporting masonry walls has been investigated experimentally (Baratta et al., 2008; De Canio and Ranieri, 2009; A. Marini, et al., 2008), see Figure 6-4. The experimental models composed of vaults and arches supported by masonry walls have been often used when horizontal loads are applied to represent seismic actions. In this scope, Marini et al. (2008) determined the rocking mechanism experienced by barrel vaulted structures undergoing horizontal loading, while Baratta et al. (2008) correlated the theoretical vibration frequency

with in situ dynamic identification and dynamic experimental tests executed on masonry arches placed on a shaking table.

Due to high amount of resources needed, complete models representing masonry structures including masonry vaults or timber floors represent a very reduced group of models tested experimentally. The interest of preserving historical buildings in seismic prone areas has motivated the study of their dynamic behaviour and their seismic vulnerability (Chávez and Meli, 2008; Krstevska et al., 2008; Peña and Chávez, 2016, Ramaglia et al. 2016). Therefore, the full scale models are mainly used with two main aims; (1) to improve the reliability of the numerical models implemented by enabling its calibration or (2) to evaluate the seismic stability and response of the structure, namely by obtaining the global response, assessment of critical components, identifying collapse mechanisms (Chávez and Meli, 2008; Krstevska et al., 2008). Despite of the complete structural models can provide the most realistic results, often it is decided to select individual structural elements to test.



(a)



(b)

Figure 6-5. Monumental buildings models at reduced scale. (a) Typical colonial temple of central Mexico from 17th and 18th (M Chávez and Meli, 2008). (b) Mustafa Pasha Mosque from 15th century (Krstevska et al., 2008)

In the selection of the experimental scale, the laboratory size, available space, and equipment facilities available often guide the selection of the scale of the experimental models to be tested. Examples of reduced scale experimental models are the ones representing typical colonial temple of central Mexico from 17th and 18th Centuries with barrel vaults (reduced scale 1:8), see Figure 6-5a. The walls and buttresses were built with a heterogeneous masonry constituted by small stones bonded by a lime-sand mortar, while vaults and bell towers were built with bricks (M Chávez and Meli, 2008). A reduced scale model (1:6) was also used to represent the Mustafa Pasha Mosque (15th century) in Skopje in which the Minaret was built with the same materials as those of the real building (stone, bricks and lime mortar) (Krstevska et al., 2008), see Figure 6-5b.

6.3.2 Load conditions

In scientific literature different loading conditions have been considered on masonry vaults aiming at representing critical loading conditions and at assessing the structural behaviour to these specific actions: (i) static monotonic or cyclic forces; (ii) displacements aiming at simulating soil settlements and movements of supports, or inducing lateral load coming from seismic events. Fewer researchers consider static loads to reproduce seismic actions, but these can be more effectively simulated in the shaking table.

When vaults and arches are studied, experimental models can be subjected to a wide variety of loading types such as: (1) self-weight (always); (2) additional weight applied as punctual vertical load or as distributed (full or partially) vertical load at extrados. The extrados can be also filled to emphasize the vault crown or increase the vertical stresses on the walls (Baratta et al., 2008; Cescatti et al., 2018; Paolo Girardello et al., 2013; Ramos and Lourenço, 2008); (3) vertical load applied over the walls or abutments to induce pre-compression stresses on the supports (Castellano et al., 2021a; Marini et al., 2008), see Figure 6-6; (4) horizontal loads or displacement to simulate the seismic action (force or displacement) controlled experimental tests (Masciotta et al., 2020). These forces can be applied directly on the arch or vaults by considering one or two equal forces on the abutments, supported by the hypothesis that they move in-phase and experience the same acceleration during the earthquake (Marini et al., 2008), see Figure 6-7. The horizontal motions is generally applied on the vault plane because it is the most unfavourable direction in the vaults (Candeias et al., 2004; Chávez and Meli, 2008; Krstevska et al., 2008; Mendes and Lourenço, 2009); (5) vertical displacement to reproduce differential settlements induced by exceeding the load capacity of the soil or the loss of foundations' strength (Castellano et al., 2021; Ferrero et al., 2021; Ferrero et al., 2022; Silva et al., 2006; Torres et al., 2019; Zampieri et al., 2018; Zampieri et al., 2018; Zampieri et al., 2017). Notice that settlements are the origin of many common structural damages in historical masonry constructions. Nevertheless, compared with horizontal displacement, vertical settlements are much more difficult to simulate in laboratory tests, see Figure 6-8; (6) combination of some simultaneous loads as horizontal and vertical loads in Quasi-static tests (Bolis et al., 2017; Marini et al., 2008); (7) dynamic loads induced through shaking tables, where the seismic action is simulated through seismic records (acceleration time-histories) derived from real record of earthquake or from codes specifications. It is recommended that the seismic records had been modified in their scales in the order to enhance their effects in the model according to the similitude laws.

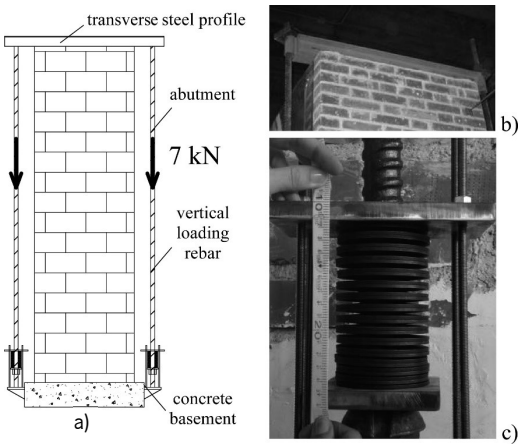


Figure 6-6. Vertical load application system: (a) side view of the loading apparatus, (b) load distribution at the wall to edge, (c) cup-springs at the base reducing the vertical bar stiffness (Marini et al., 2008)

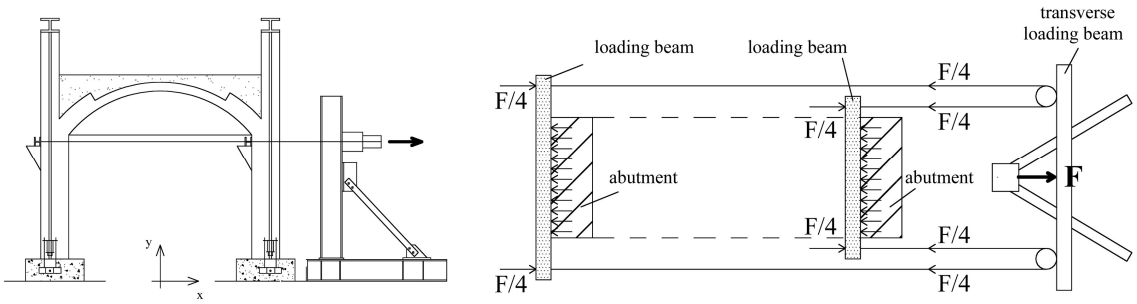


Figure 6-7. Load application system (Marini et al., 2008)

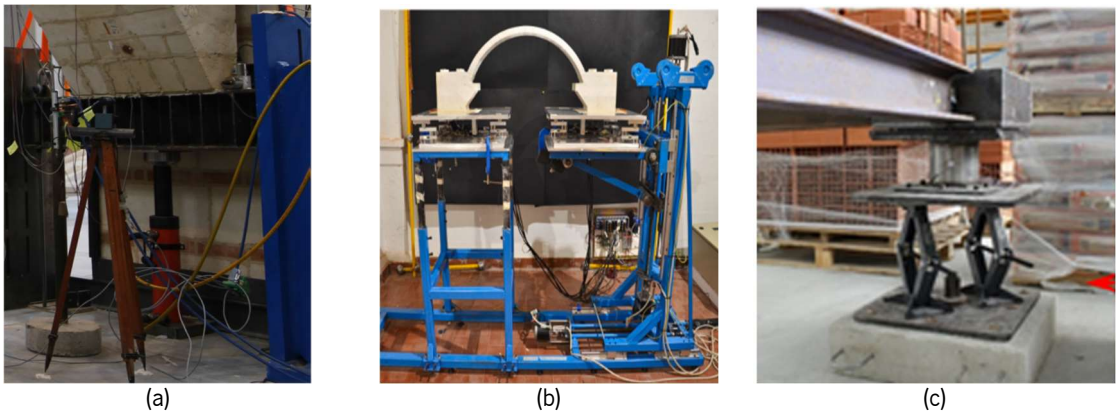
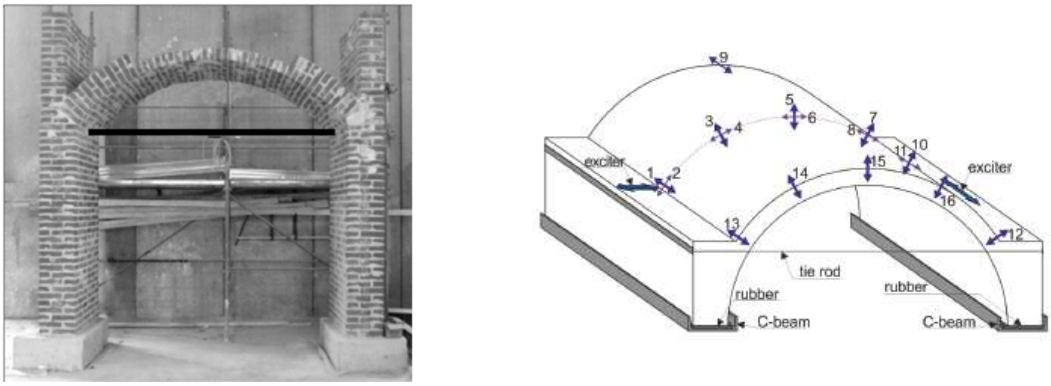


Figure 6-8. Vertical displacement to reproduce the differential settlements: (a) displacement applied on full scale model using hydraulic jacks (Castellano et al., 2021b), (b) displacement applied on small scale model using hydraulic jacks (Ferrero et al., 2022)and (c) displacement applied using mechanical jacks(Torres et al., 2019)

Both load and displacement are usually applied through hydraulic jacks instrumented with a load cell (Figure 6-8a and b), regardless of the experimental approach. In experimental tests intending to simulate vertical settlements, the induced displacement is usually applied by hydraulic jacks instrumented with a load cell (Castellano et al., 2021a; Ferrero et al., 2022) but when these are not available , it is also possible to use mechanical jacks (D'Altri et al., 2020; Torres et al., 2019; Zampieri et al., 2018). The main difference between both instruments would be the precision and control, see Figure 6-8.

6.3.3 Support conditions

Foundations and anchor conditions to reproduce the real structural constraints depends on the aims of the research which can be focused only on the structural element or also in the interaction between them and the other structural elements to which they are attached. In traditional foundation systems, it is usual to use simple contact supports which constrain the vertical displacement but not necessarily the horizontal displacements or rotations. This kind of restrain is possible to reproduce in the laboratory if the prototype is built on a monolithic reinforced concrete foundation, which should be laid over a strong floor (Baratta et al., 2008; Bolis et al., 2017; Giuriani et al., 2009; Hojdys and Krajewski, 2014; Krajewski and Hojdys, 2015; Marini et al., 2008; Ramaglia et al., 2016; Valluzzi et al., 2001), see Figure 6-9a.

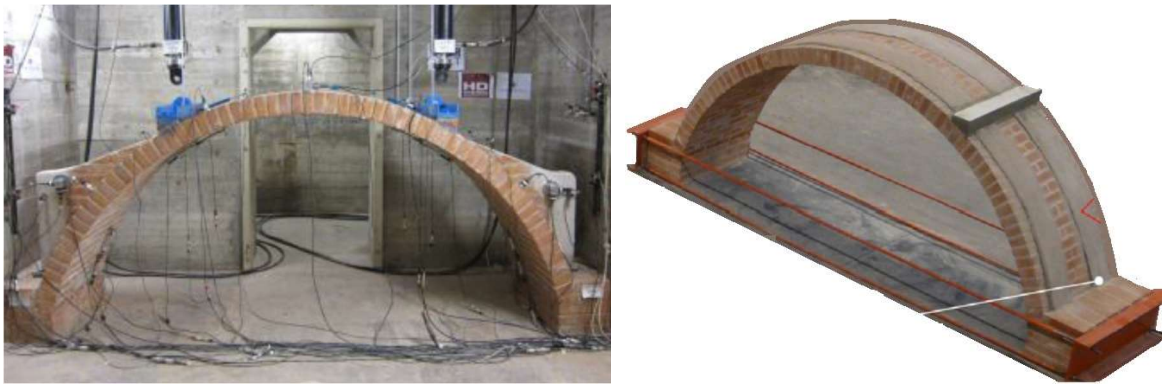


(a) (b)

Figure 6-9. Boundary conditions: (a) support conditions to allow rotations at the base (Giuriani et al., 2009) and (b) C-beam steel to avoid horizontal displacements (Golebiewski et al., 2017)

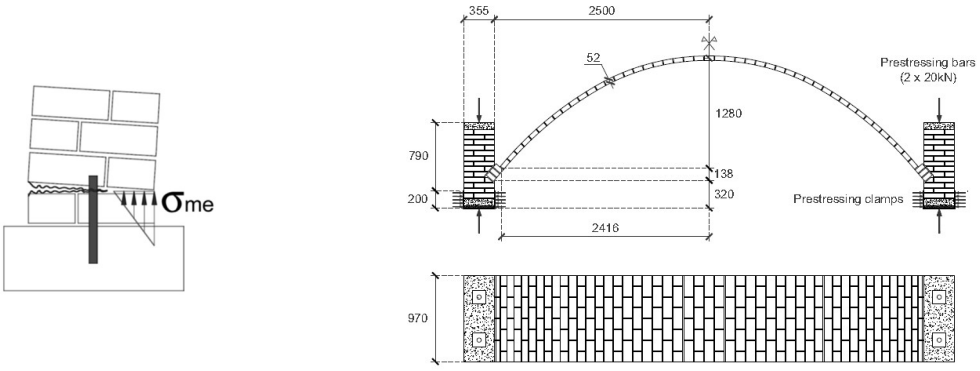
To constrain the horizontal movement of the supports or walls: (1) specific devices can be foreseen as C shape steel beam (Golebiewski, 2017) see Figure 6-9b; (2) to build the experimental model between two reaction walls (Girardello, 2013) (Figure 6-10a); (3) to use two metallic profiles located at both abutments and tied with four rods (Garmendia (2015b), see Figure 6-10b.

To constraint the vertical displacement but inhibiting any shearing sliding and releasing rotations, it is possible to fix the support with vertical rebars (Marini et al., 2008), see Figure 6-11a. In addition, to avoid possible rotations, prestressing clamps and anchoring bars can be also used (Marini et al., 2017), see Figure 6-11b.



(a) (c)

Figure 6-10. Boundary conditions: (a) experimental arch between two reaction walls (Paolo Girardello et al., 2013) and (b) metallic profiles and tied with four rods (Garmendia et al., 2015b)



(a) (b)

Figure 6-11. (a) support with vertical rebars (Marini et al., 2008); (b) prestressing clamps and anchoring bars (Marini et al., 2017)

6.4 Characterization of stone masonry

This section presents the experimental characterization of stone masonry representing the masonry bond of walls and vaults of the experimental model of the barrel vault under uniaxial compression load. For this, masonry wallets were built with the constructive system used in Yucatán churches for both vault and walls. after that, monotonic compressive strength tests on panels were performed. The main aim was to determine the mechanical characteristics as compressive strength (*fc*) and modulus of elasticity (*E*) of the masonry,

6.4.1 Geometric and morphological characteristics of wallets

Both walls and vault masonry wallets were built according to the Yucatan masonry typology described in Chapter 2. The wall stones dimensions range from 0.20m to 0.60m with roughly worked edges, whereas the flat stones vault voussoirs have thickness (*t*) ranging from 0.10m to 0.15m, the height (*h*) varies from 0.30m to 0.40m and the depth (*d*) ranges from 0.40 m to 0.60 m.

Since it was not possible to build and test masonry wallets at real scale, the unit stones masonry were scaled. Thus, the wall stones were scaled at 50% and the maximum dimensions of vault stones were selected and scaled at 33%. The wall's stones range from 10cm to 30cm, while the vault's stones sizes are in average 5cm x 13cm x 20cm, see Table 6-1. For both wall and vault wallets, the ideal scale was 33% since the full experimental vault model developed in this chapter was scaled at 33%. However, at that scale, the dimensions of the wall stones turn out very small and it was decided to increase.

Table 6-1. Scaled stone sizes

Scale	Wall Stones			Stone vault voussoirs					
%	Average dimension cm	minimum dimension cm	maximum dimension cm	b	x	h	x	d	cm
100	30	20	60	15		40		60	
50	**15**	**10**	**30**	7.5		20		30	
33	9.9	6.6	19.8	**4.95**		**13.2**		**19.8**	

Figure 6-12a shows the thickness of the wall, which is a tree-leaf, whereas Figure 6-12b illustrates the masonry wallet intended to represent the masonry bond of the masonry vault. It should be noticed that the wallets intended to simulate the lack of stone interlocking along the axis of the vault.

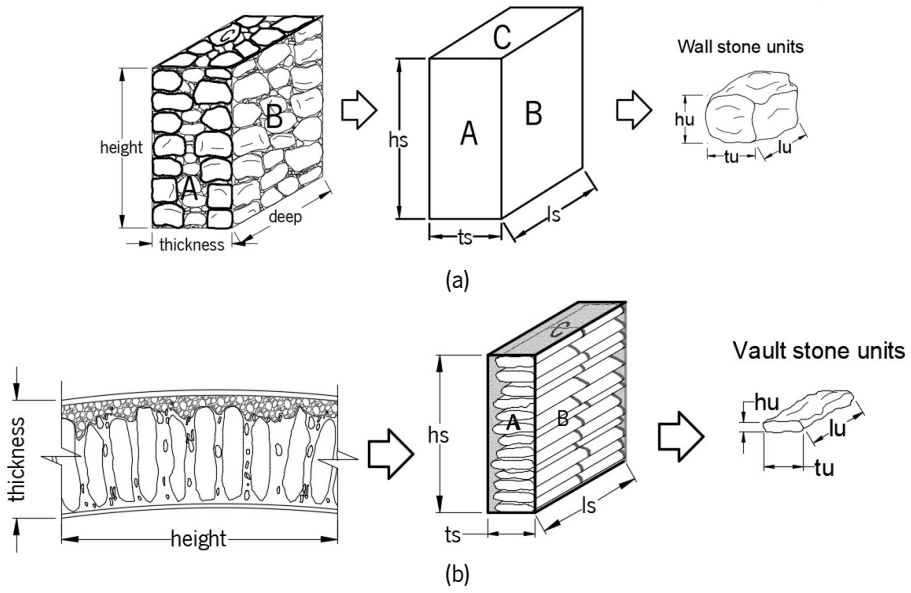


Figure 6-12. Masonry wallets with a rectangular base proposed to represent (a) walls and (b) vaults

Since the wallets are tested under compressive load, in a first stage the wallet dimensions were defined according to the standard BS EN 1052-1 (1999) and using the dimension of the stones units as shown Figure 6-12. According to the standard the wallets must size (1) the walls samples: ts= 450mm, ls=400mm and hs = 1350mm and (2) the vaults samples: ts= 130mm, ls=400mm and hs = 400mm. From those analyses, main critical aspects were observed (1) on wall samples the thickness is bigger

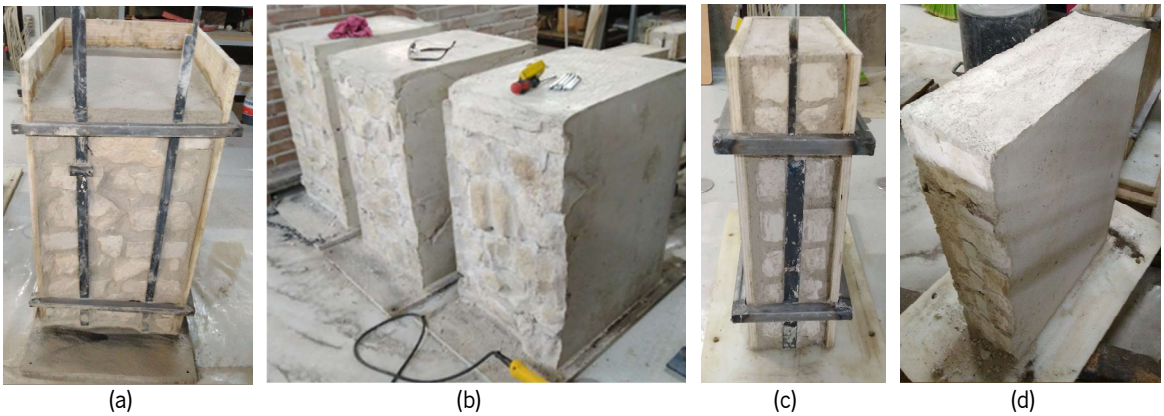
than the length and (2) in vault samples the length and height are the same. Additionally, the proposed height of the wall samples was 1350mm, which was bigger than the available dimensions in the load frame (850mm). According to above new restriction were considered in order to define the wallet dimensions (1) the unit masonry numbers should be selected according to the standard (2) the height of the wallet must be smaller than 850mm, (3) the wallets must satisfy an aspect ratio where thickness must be smaller than length and the length must be smaller than height (4) the analytical load request to carried out the compressive strength must be smaller than 900kN (according to the capacity of the actuator). Thus, Table 6-2 shows the final wallets dimensions.

Table 6-2. Vault and wall wallet dimensions

Stone sizes			Panel sizes					
Thickness	length	Height	Variables		Dimensions [mm]	Courses	Ratio	
Wall panels								
tu	lu	hu	thickness	ts	**450**	3.0	ls/ts	1.3
mm	mm	mm	length	ls	**600**	4.0	hs/ls	1.3
150	150	150	height	hs	**800**	5.3		
Vault panel								
tu	lu	hu	thickness	ts	**150**	1.2	ls/ts	2.7
mm	mm	mm	length	ls	**400**	2.0	hs/ls	1.5
130	200	50	height	hs	**600**	12.0		

6.4.2 Construction of the experimental wallets

Following the recommendation of the European standard, three panel samples were built for both wall and vaults. The geometry was controlled by using prefabricated wooden as formwork with the specified dimensions defined in Section 6.4.1 (see Figure 6-13a and c). All technical specifications were provided in detail in drawings to the masons (Annex 6.1).



(a) (b) (c) (d)

Figure 6-13. Construction of the walls' and vaults' wallets (a) formwork for wall samples (c) wall samples, (b) formwork for vault samples and (d) vault samples

The specimens were built over rigid plates to make the stable transport to the test site possible. The quality of the materials was controlled by mechanical tests carried out on stones and mortars. Casting of mortars specimens for further testing under compression and flexural loading was carried out. The

final aspect of the masonry wallets is shown in Figure 6-13b and d, for both wall and vault respectively. As it is possible to observe, the wallets show an excessive mortar layer in three faces, in contrast to the four face which look with visible and more organized stones. Based on this aspect, it was decided to remove some mortar in excess by using sand blasting. In this process, it was assured that no damage was induced to the specimens. The objective was to expose the stones of the external layers. In this process, it was found out that some no uniform distribution of the stone along the length and thickness of the wallets, which revealed some problems with workmanship. This put some limitations to the representativeness of masonry bonds used in the vault's experimental models.

6.4.1 Experimental setup and loading protocol

The masonry samples were tested under uniaxial compression load according to standard BS EN 1052-1 (1999). The experimental tests were varied out on a stiff steel frame Figure 6-14a. The load capacity of the vertical actuator was about 1000 kN. In order to make the load records possible an additional load cell was attached to the actuator. The experimental uniaxial compression test was performed under displacement control at a rate of 0.35 mm/s. The displacement-time history was composed of a continuous ramp until the failure of the specimen was reached. In order to apply a uniform load on the cross section of the masonry wallet, stiff steel beams were put at the top of the specimens, see Figure 6-14a, b and d.



(a) (b) (c) (d) (e)

Figure 6-14. Setup arrangement (a) load frame, (b) wall's wallets setup, (c) LVDTs placed on wall samples, d) vault's wallets setup and e) LVDTs placed on vault samples

The control system was performed using the Dyna tester V3 program. The data acquisition of the deformation of the walls' wallets was performed through six vertical LVDTs placed on all faces of the wallet and through 2 LVDTs measuring deformations along the thickness of the wallets, see Figure 6-14c. In case of the vault's wallets, four LVDTs were placed on the lateral faces of the panel as shown in Figure 6-14e. The stress-strain diagrams were obtained by: (1) calculating the compression stress

as the ratio between the vertical load measured in the load cell and the cross section area of the masonry specimen; (2) averaging the vertical displacement measured by the LVDTs and divide this displacement by the measurement distance. The secant elasticity modulus was obtained at 33% of the maximum compression stress according to BS EN 1052-1 (1999) and ASTM D 3148(2002).

6.4.2 Uniaxial compression behaviour of the masonry

In this section the analysis and discussion of results of the experimental test on wallets is provided. The results were evaluated with respect to: (1) mechanical properties, namely compressive strength and secant modulus of elasticity; and (2) developed crack patterns. Figure 6-15 shows the force-displacement and corresponding stress-strain diagrams for masonry wallets. Table 6-3presents the compression mechanical properties, namely compression strength and secant modulus of elasticity. Figure 6-15a indicates that the sample Wall 2 recorded the maximum load with 913kN, whereas the Wall 1 samples recorded lowest load. Also, it is possible observe the superposition of the three plots from the beginning to approximately 350kN. The force-displacement diagram for Wall 1 and Wall 3 samples shows a really close behaviour almost during all the test. As shown in Table 6-3, the average compressive strength was 2.96Mpa and the average secant elasticity modulus at 33% was 4349MPa.

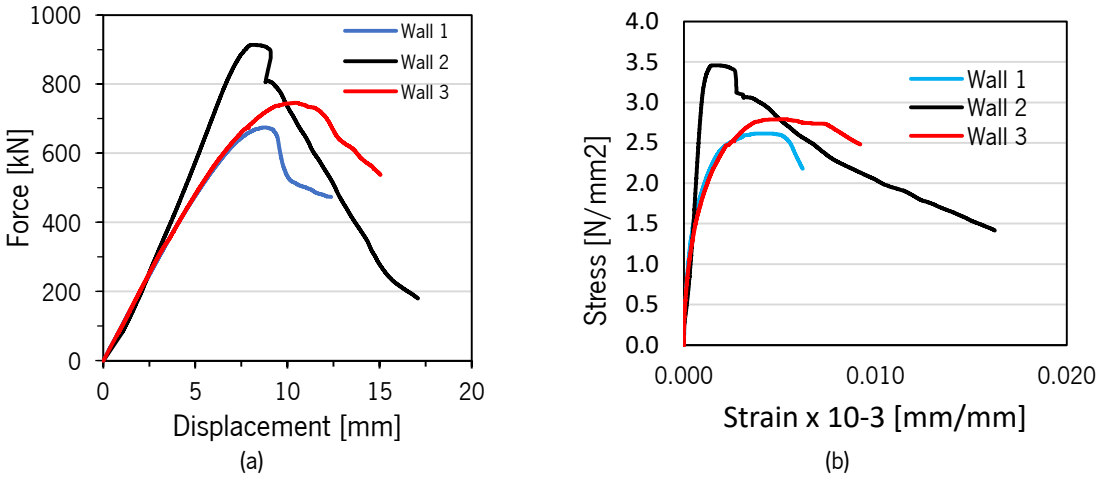


Figure 6-15. Wall samples behaviour. (a) Development of the experiment, force-displacement diagram and (b) stress-strain diagrams

Table 6-3. Mechanical characteristics of masonry wall wallets

Test number	Sample	Load	Compressive Stress	Elasticity modulus Secant (Es)
		kN	MPa	MPa
1	Wall 1	674.85	2.62	5108
2	Wall 2	913.63	3.46	4023
3	Wall 3	746.508	2.796	3915
	Average	778.33	2.96	4349
	SDev	122.529	0.445	660
	Co.V.	16%	15%	15%

Figure 6-16a shows that the masonry sample Vault 1 recorded the maximum load with 538kN, whereas the sample Vault 3 recorded lowest load equal to 315kN. Also, it is possible observe the superposition of the three plots from the beginning to approximately 220kN. Samples Vault 1 and Vault 2 shows a really close behaviour until the Vault 2 achieves the maximum load. From Table 6-4, it is seen that the average of the compressive strength was 7.3MPa and the average secant elasticity modulus at 33% was 3565MPa.

Despite the plots for both walls and vaults shown a really good superposition, it was observed that throughout the experiment some differences in the displacement measured at the different points of the masonry wallets faces were found, which are attributed to the uneven distribution of stones through the cross section of the wallets. This aspect is particularly relevant in masonry wallets and be reason that justifies the high value of the secant modulus of elasticity found in these wallets. Indeed, the ratio between the secant modulus of elasticity and the compression strength is clearly out of the range suggested by some authors in literature for old masonry (Eurocode 6, 2011; Vasconcelos, 2005).

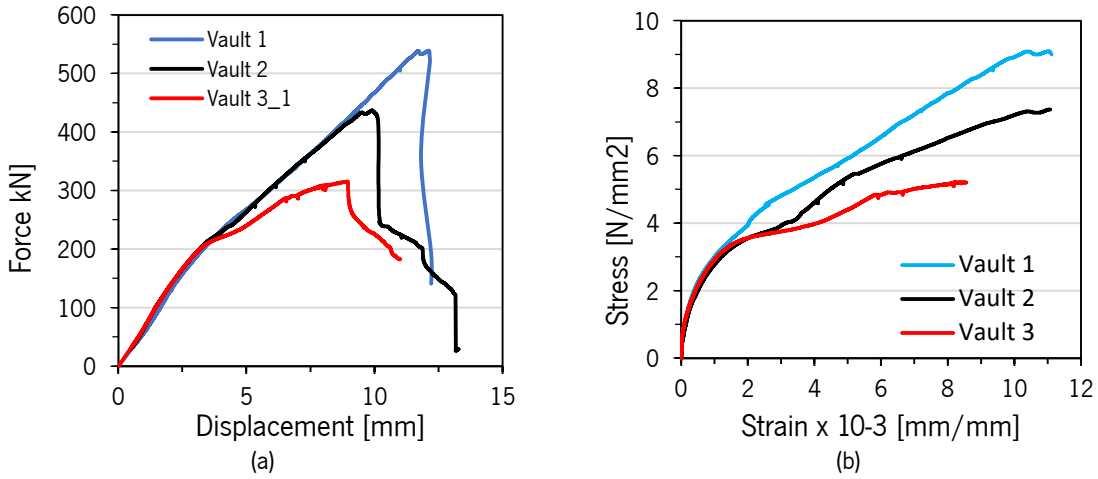


Figure 6-16. Vault samples behaviour. (a) Development of the experiment, force-displacement diagram and (b) stress-strain diagrams

Table 6-4. Mechanical characteristics of masonry vault wallets

Test number	Sample	Load	Compressive Stress	Elasticity modulus Secant (Es)
		kN	MPa	MPa
4	Vault 1	538.93	9.10	2973
5	Vault 2	436.75	7.37	3269
6	Vault 3	315.48	5.32	4455
	Average	430.39	7.3	3565
	SDev	111.858	1.9	784
	Co.V.	26%	26%	22%

6.5 Experimental model of the barrel vault

As aforementioned, one of the main objectives of this work is to assess the mechanical behaviour of masonry vaults that are typical of Yucatan churches under differential vertical settlements. For this and given the scale of the Yucatan churches with barrel vaults, a major challenge is to define a representative experimental model. In this scope, besides the geometry and scale, the use of adequate materials that are close to the existing ones is also an issue. This section provides the most important information regarding to the design of the experimental model both at geometrical and materials levels. In addition, the loading configuration and instrumentation plan are also provided and discussed.

6.5.1 Geometry

The geometry of the barrel vault of the experimental model was decided from the statistical analysis carried out on the main geometric parameters characterizing the cross section of Mexican churches, namely in Yucatan region. The most representative range of the different dimensions (minimum, medium and maximum values) characterizing the cross section of Yucatan churches with semi-circular barrel vaults were provided in Chapter 3. The values corresponding to the lower bound of the range (minimum values) were selected for the experimental model. These dimensions were used to obtain a reduced scale model to use in the experimental tests, given the limitation of the laboratory facilities at University of Minho, the dimensions were further scaled to 30% of the real prototype, see Figure 6-17a.

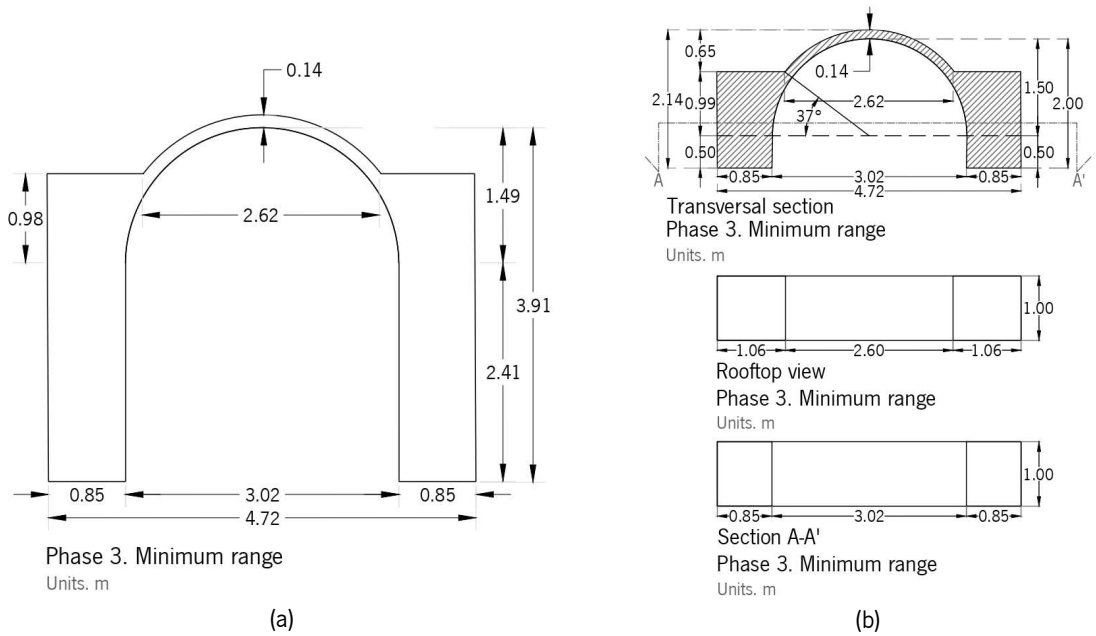


Figure 6-17.Representative cross section. (a) reduced scale model at 30%, (b) experimental cross section, rooftop view and cut section A

As was stated before, the real walls in Yucatan churches have thickness ranging from 2.50m to 3.00m. Therefore, the walls of the reduced scale cross section have 0.85m of thickness, whereas the vault has 0.14m of thickness, the full free span is about 3.02m and of height fill at extrados is 0.99m. Assuming that there is no important lateral displacement of the supporting walls, as it will be induced a vertical displacement, ir was decided to represent the wall y a short length of 50cm. This short length is extended over 0.99m to assure the representativeness of the vault infill according to visual evidences found during in situ inspection of the Yucatan churches (Chapter 2). Figure 6-17b shows the final cross section selected for the experimental test.

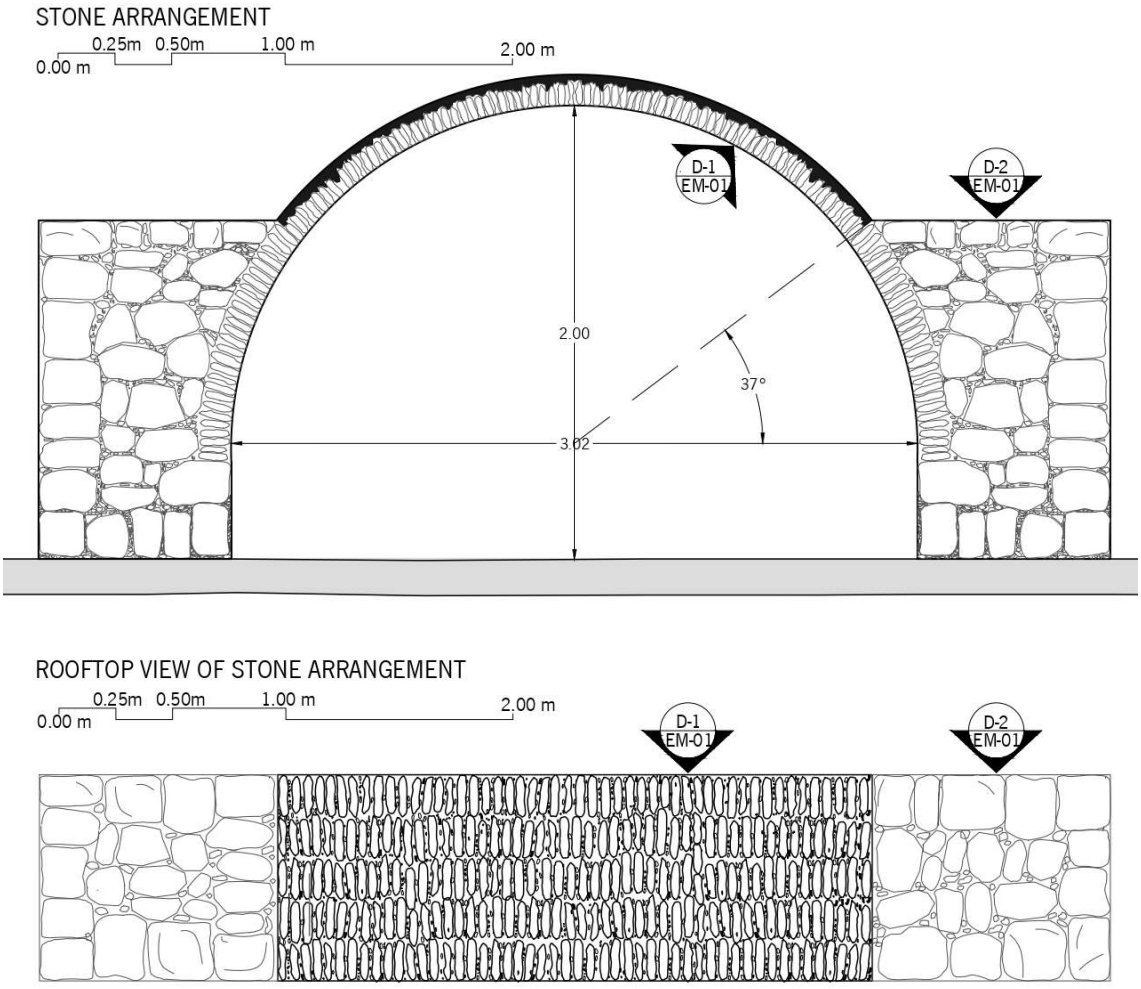
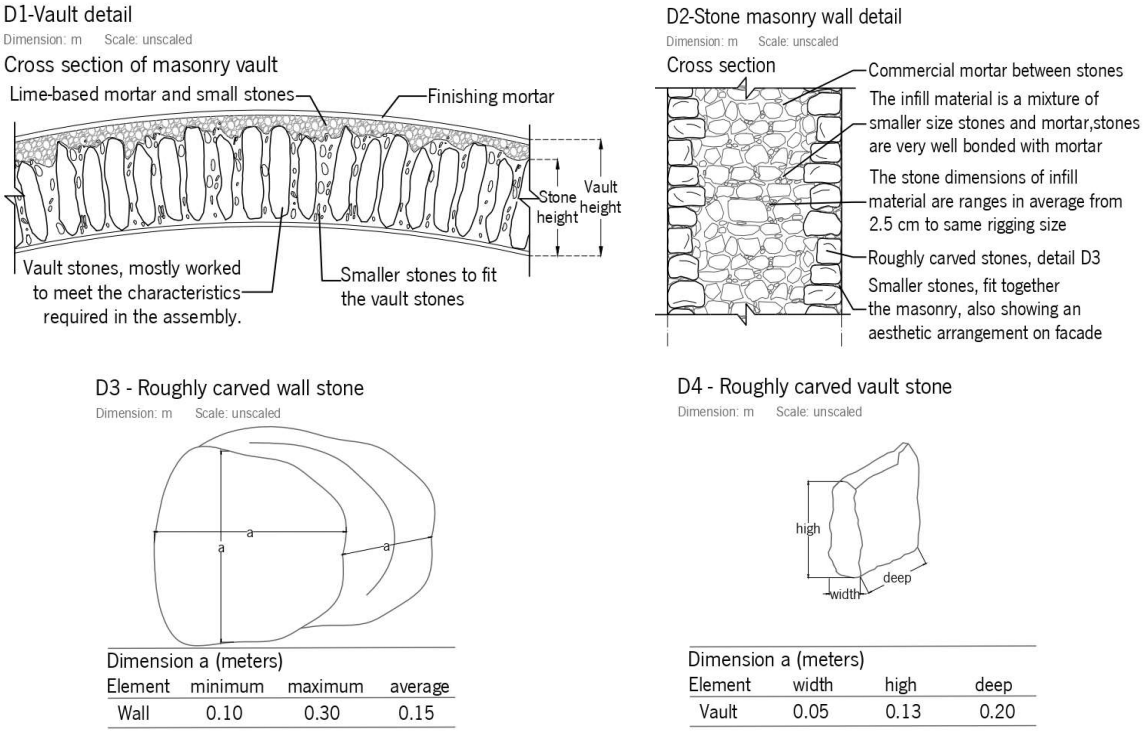


Figure 6-18. Morphological characteristics of walls and vault masonry bonds, rooftop and elevation

The masonry walls and vaults were built according to the morphological characteristics already discussed in Chapter 2, see Figure 6-18 and Figure 6-19. Therefore, the walls intended to represent the typical morphology of walls composed of three leaves: (i) the outer leaves with higher size of stones and more regular arrangement; (ii) inner leaf composed of more irregular and rounded stones and with lower dimensions, see Figure 6-19. The barrel vault is composed by lamellar stones, arranged

vertically bonded with lime-based mortar and smaller stones. Additionally, the extrados has a layer of composite material resulting from the combination of lime-base mortar and small stones as compression and a finishing layer (Figure 6-19).



Dimension a (meters)

Element	minimum	maximum	average
Wall	0.10	0.30	0.15

Dimension a (meters)

Element	width	high	deep
Vault	0.05	0.13	0.20

Figure 6-19. Morphological characteristics of walls and vault masonry bonds, cross section of wall and vault, stones shape and stone dimension

At real scale, the average dimensions of the stone masonry units of walls were defined as 30cm per side with roughly worked edges. The voussoirs stones of the vaults showed an average dimension of 12.5cm x 35cm x 50cm. Following the scaling of the model´s geometry, the dimension of the stones needed also to be scaled so that a proportional experimental model could be built. Therefore, it was decided to scale the dimension of stone at 50%, a little bit more than the geometrical model due to the reduced real dimension of stones (Table 6-5). The decision was also taken to make the construction of the experimental model easier. The shape of the stones defined for the masonry walls and vaults are presented in Figure 6-18.

Table 6-5. Scaled stone sizes

Scale	Wall Stones			Stone vault voussoirs								
%	Average dimension	minimum dimension	maximum dimension	Maximum dimension [cm]					Average dimension [cm]			
	cm	cm	cm	b	x	h	x	d	b	x	h	x	d
100	30	20	60	15		40		60	12.5		35		50
50	15	10	30	7.5		20		30	6.25		17.5		25
33	9.9	6.6	19.8	4.95		13.2		19.8	4.16		11.6		16.65

6.5.2 Selection of materials for masonry walls and vaults

The representativeness of the experimental model relies on the geometry but also on the materials composing the structural elements existing in real buildings. As this research focuses on the mechanical behaviour of masonry vaults, the mechanical properties of stone used to build the experimental model should be close to the ones existing in the prototype buildings. In this way, it is feasible to reproduce better the mechanical behaviour and the governing failure modes (M Chávez and Meli, 2008; De Canio and Ranieri, 2009; Krstevska et al., 2008). According to the chemical characterization presented in Chapter 4, the stones from Yucatan churches are mainly sedimentary rocks composed of calcium carbonate (CaCO3 at 90% or greater), being mostly calcite. For this reason, a review of Portugal lithology was conducted, and two main areas of limestone were identified in centre and south regions of Portugal, see Figure 6-20a. The centre region was identified as the greater limestone concentration and as the most important limestone extraction area in Portugal and thus, it was decided to use limestone supplied by one of the quarries in the area, see Figure 6-20b.

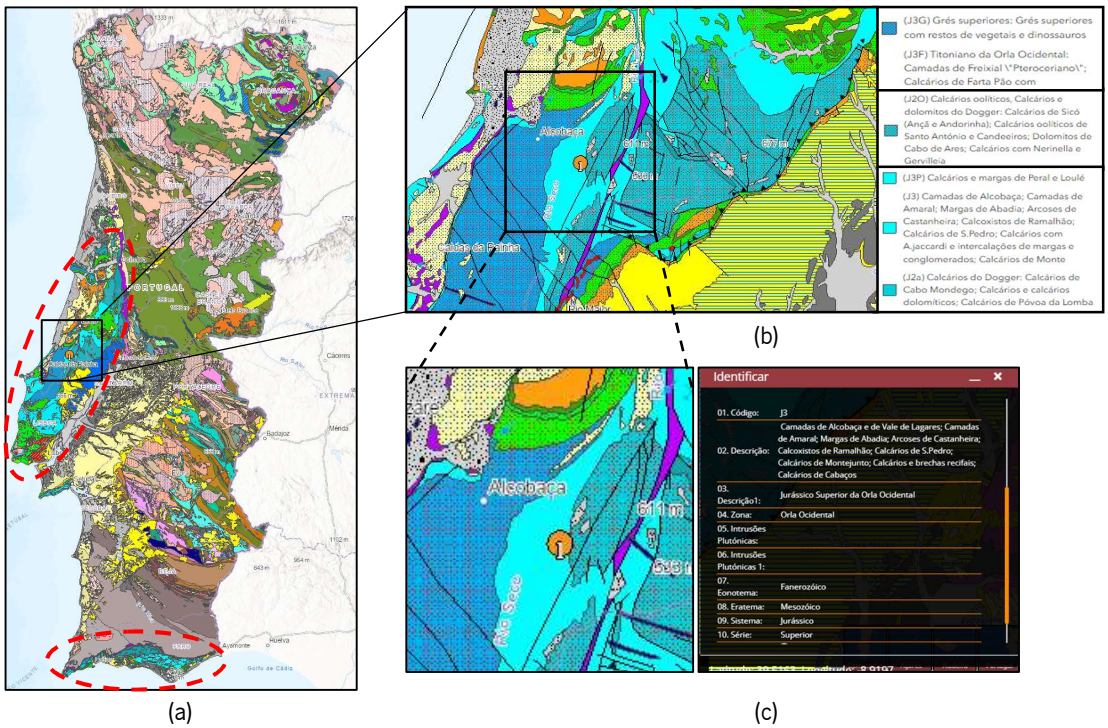


Figure 6-20. (a) Lithology of Portugal, (b) calcium carbonates area and (c) limestones area and location of quarry selected for the delivery of stone for the experimental model. (Direção-Geral do Território, 2022)

From physical and mechanical analysis carried out on Yucatan limestone, three groups were identified according to different physical and mechanical properties (see Chapter 4). Since limestone from groups 2 and 3 were the most predominant, it was decided to request limestone rocks with characteristics close to these groups, see (Table 6-6).

Table 6-6. Most important mechanical and physical properties of limestone from Yucatan churches

Average values of:	G1	G2	G3
ρ [kg/m3]	1580	1963	2400
η [%]	38.07	20.16	5.38
Ab [%]	24.13	10.43	2.25
f'c [MPa]	12.17	32.68	71.64
Ec	8583.8	25335.5	55364.3
Calcite [%]	100	100	100

Note: apparent density, ρ; open porosity, η and water absorption by immersion, Ab.

Therefore, the limestone for the experimental model was delivered by Farpedra quarry located in Alcobaça Portugal (Figure 6-20c). As part of the quality control of the stone provided, uniaxial compression tests were carried out to obtain the effective compression strength and modulus of elasticity of the limestone. Stones were selected randomly from the provided material and 9 cylindrical specimens with a diameter of 50 mm and a height of 100 mm were extracted from them. The compression strength was obtained through uniaxial compression tests carried out on six samples according to ASTM C170 (1999) and ASTM D 3148 (ASTM D 3148, 2002), see Table 6-7. Additionally, the elastic modulus (Ec) was obtained on three samples according to BS EN 14580 standard (2005). The specimens were subjected to 3 cycles of loading and unloading. The loading branch attained about 1/3 of the average compression strength obtained in the previous six samples. The mechanical properties are presented in Table 6-7. According to results, the mechanical properties of the limestone provided to build the experimental model are close to the ones obtained from stones gathered in Yucatan churches (Chapter 3).

Table 6-7. Compressive strength and tangent modulus in limestone

	Compression strength (*fe*)	Corrected stress due to dimensions (*fc*)	Static elastic modulus by cycles (Ec)
	MPa	MPa	MPa
Maximum	107.64	119.95	47287.00
Minimum	64.28	73.77	31502.00
Average	**81.33**	**91.63**	**36599.29**
Standard deviation:	19.01	20.44	5766.28
Coefficient of variation (CoV):	23%	22%	16%

The masonry mortar had to simulate an aged historical mortar and for this purpose it was decided to use a commercial mortar with low mechanical strength of about 1.5 and 5 N/mm^2, being from class CS II, according to (EN 998-1, 2010). In addition, it should be mentioned that using a pre-mixed mortar the control of quality is easier. Thus, it was selected the Natural Hydraulic Lime (NHL) to build the experimental model. The volumetric mass of the mortar is about 1850±150kg/m^3.

6.6 Construction of the experimental model

The experimental model was built over two steel rigid platforms, working as the support for the walls and being part of the experimental setup. The vault construction was supported by a curved steel formwork with the accurate dimensions according to the drawings of the experimental model delivered for the contractor. Special attention was paid to any movements that could occur during the construction. Therefore, to avoid vertical displacements the curved formwork was supported by three metal struts on the keystone position. The horizontal movements of the vault were prevented by horizontal steel bars placed at starting of the vault formwork as shown in Figure 6-21a.

The construction of the vault model started with the construction of the walls. The outer layer of the masonry walls was built with larger stone pieces and mortar, following an irregular masonry bond previously decided. The void spaces between stones were filled with smaller stones as a wedge and mortar. The inner part of the walls was built with cyclopean concrete composed of smaller stones with different dimensions, see Figure 6-21b.

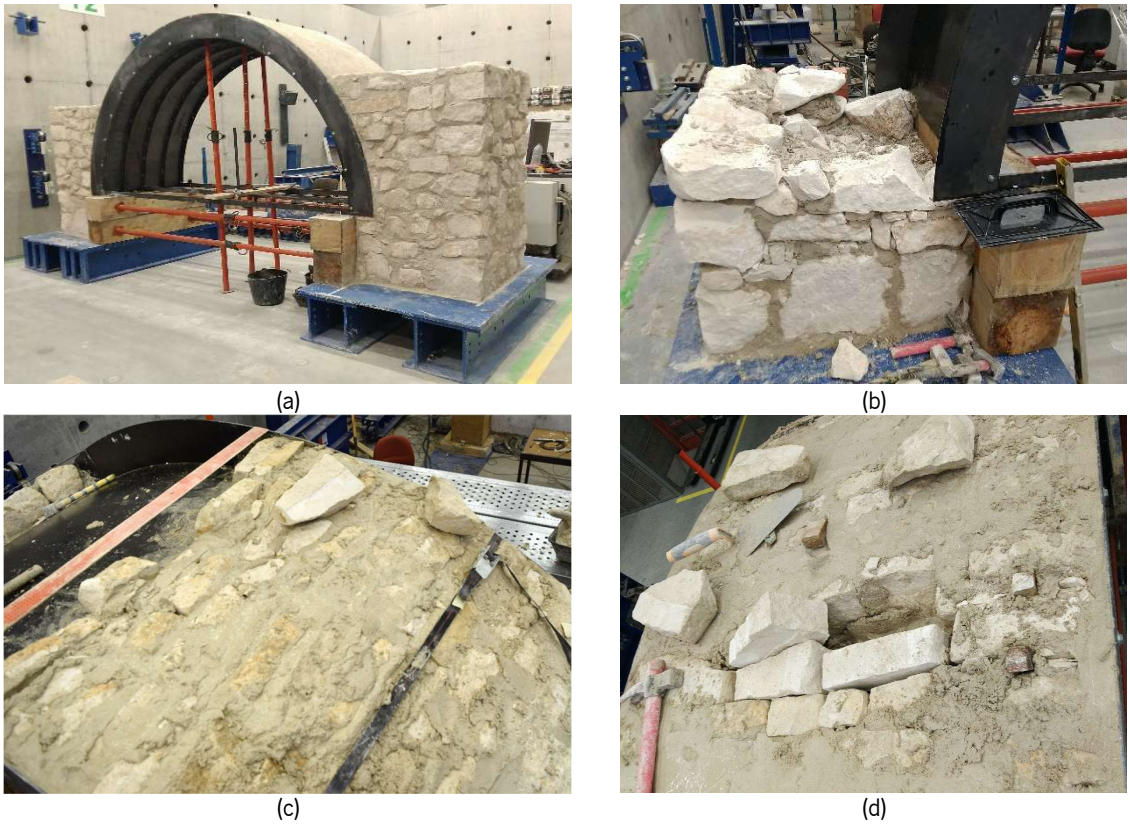


Figure 6-21. Construction of the experimental model. (a) curved steel formwork, (b) construction of the walls, (c) vault construction and (d) placement of the key stone of the vault

The construction of the vault was carried out from the vault-wall connection to the keystone position at the top. Special attention was paid to the wall-vault connection. At the beginning of the vault

construction, the support and arrangement of the vault stones were carefully settled. Following the masonry arrangement previously defined, the vault was built with thin vertical voussoir stones in a Roman-type arrangement practically aligned joints in both directions, without almost no interlocking, see Figure 6-21c. The key stone on the top must be placed with much care. It was introduced under pressure in the available space, see Figure 6-21d.

The so-called wall extension on the vault can be placed in two moments: 1) at the end of the vault construction or 2) built simultaneously with the vault. In this work, it was decided to build the walls' extension simultaneously with the vault.

The overload on the extrados had to reach a height equivalent to a central angle of 37°, see Figure 6-18. According to the dimensions of the experimental model, a central angle of 37° corresponds to a 1m high wall, meaning 1m above the level of the start of the vault, see Figure 6-22a.

Finally, the extrados was covered with a thin layer of mortar to achieve a regular surface that allowed the attachment of instrumentation. The formwork was removed after 28 days. Figure 6-22b shows the experimental model ready to be instrumented and tested.



(a) (b)

Figure 6-22. Final view of the experimental model. (a) wall extension on the extrados and (b) full experimental model

6.7 Prediction of the experimental behaviour of the vault

A Finite Element (FE) model was used to predict the possible location of damage on the vaults and also to have an idea for which vertical induced displacements the damage develops. The numerical model was built with 6 and 8 nodded plane strain elements in DIANA (2020) FE package. To simulate the nonlinear behaviour of masonry a nonlinear analysis by steps was performed. The simulation tried to represent a monotonically increasing vertical displacement applied in one support until the collapse (push down). It should be stressed that the results were qualitative, and they were useful only to predict the possible crack location.

To define the material's mechanical properties, both experimental tests' results from wallets and values from literature and standards were taken into account. The experimental value from wallets were the compressive strength (*fc)* equal to 7.26 MPa and 2.96 MPa for the vault and walls, respectively. In the absence of more experimental values, all other mechanical parameters were selected from the literature: (1) tensile strength (*ft*) ranges from 0.02MPa to 0.182MPa (Borriet al., 2015; Kržan et al., 2015a; Magenes et al., 2010; Manos et al., 019; Silva et al., 2008) worldwide and from 0.1MPa to 0.8MPa from Mexican studies (Chavez et al., 2010; Chávez et al., 2012; Chávez and Meli, 2012a; Peña and Chávez, 2016). For this study, a value for *ft* equal to 0.15MPa, (2) elasticity modulus (*E*) ranges from 200MPa to 3290MPa (Borri et al., 2015; Chavez et al., 2010; Chávez et al., 2012; Chávez and Meli, 2012b; Kržan et al., 2015a; Magenes et al., 2010; Manos et al., 2019; Peña and Chávez, 2016; Silva et al., 2014) but Eurocode 6 proposes the relation E = 500fc to E = 1000fc(Lourenço et al., 2013; UNE -EN 1996-1-1, 2011). Therefore, this study adopted the relation E = 750fc, (3) specific weight (ρ) commonly ranges from 1600kg/m^3 to 2243 kg/m^3 (Chavez et al., 2010; Chávez et al., 2012; Chávez and Meli, 2012b; Kržan et al., 2015a; Peña and Chávez, 2016) and for this study it was selected ρ=1800kg/m3, and (4) Poisson modulus (ν) ranges from 0.20 to 0.3 and the value adopted was ν=0.25 (Chavez et al., 2010; Chávez et al., 2012; Chávez and Meli, 2012b; Manos et al., 2019; Peña and Chávez, 2016)

The most difficult parameters to identify were the compression factor energy (*Gl*) and tensile fracture energy (*Gt*) because there is not enough information about them. Since the average ductility index (*du*) is defined as the ratio between fracture energy and strength, *Gl* and *Gt* were defined from this definition. The average ductility index in compression (*du,c*) is suggested to be equal to 1.6mm for *fc* values lower than 12N/mm^2 (P. Lourenço, 2009). This relation was used for this study taking into account the values of the experimental compressive strength presented previously. The ductility index in tension (*du,t*) found for brick ranges between 0.018mm and 0.040mm. In the absence of more information is the average, 0.029mm, could be considered (Angelillo et al. , 2014; P. Lourenço, 2008), otherwise Gt could be proposed equal to 10% of the tensile strength (in N/mm) (Ramos, 2007). For this study, the relation Gt =1%fc=0.01fc was adopted.

Then, the vault was modelled as a continuous and homogeneous material with a modulus de elasticity equal to 5400 MPa, a Poisson coefficient equal to 0.25, a mass density equal to 1800 kg/m^3, a tensile strength (*ft*) equal to 0.15 MPa, a compressive strength (*fc*) equal to 7.26 MPa, a Mode-I of tensile fracture energy (Gt) equal to 0.0726 N/mm and compressive fracture energy (G_I) equal to 11.6

N/mm. The walls were also assumed with nonlinear behaviour with a modulus of elasticity equal to 3660 MPa, a Poisson coefficient equal to 0.25, a mass density equal to 1800 kg/m^3 a tensile strength ft equal to 0.15 MPa, a compressive strength (*fc*) equal to 2.96 MPa, a Mode-I of tensile fracture energy (Gt) equal to 0.029 N/mm and compressive fracture energy (G_I) equal to 4.73 N/mm.

Since plane strain elements were used, regarding to boundary conditions two considerations were applied: (1) at the right support a fixed support was assigned restringing the displacements (horizontal X and Vertical Y) and one rotation (in Z axis); (2) in left support a vertical free support was created by avoiding the horizontal displacement (X) and rotation Z, see Figure 6-23.

Regarding loading configuration, two conditions were considered: (1) the self-weight and (2) the prescribed displacement on the left support. The self-weight was applied as dead weight load in 10 steps by increasing of 0.1. The prescribed vertical displacement was applied as deformation load at the left support, at a constant rate of 0.3, simulating a pushdown. The convergence criterion for each equilibrium state was based on the internal energy, with a convergence criterion of 10^{-3}. A standard Secant (Quasi-Newton) iterative method was used. And increasing of displacements were applied on left support by steps until the cracks appear and the collapse.

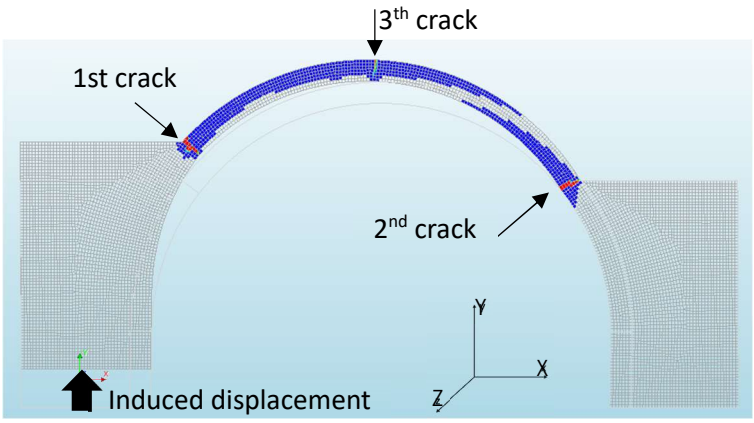


Figure 6-23. Numerical crack prediction

Figure 6-23 summarizes the results of the analyses, which shows three cracked zones, indicating potentially the hinge's location. Firsts two cracks appear at 1mm and 2 mm of induced displacement. The first crack appeared at extrados in the vault-wall connection corresponding to the support where the induced displacement was applied. The second crack appeared at intrados in the vault-wall connection near to fixed support. The third crack appeared at 140 mm of induced displacement at extrados near to keystone position.

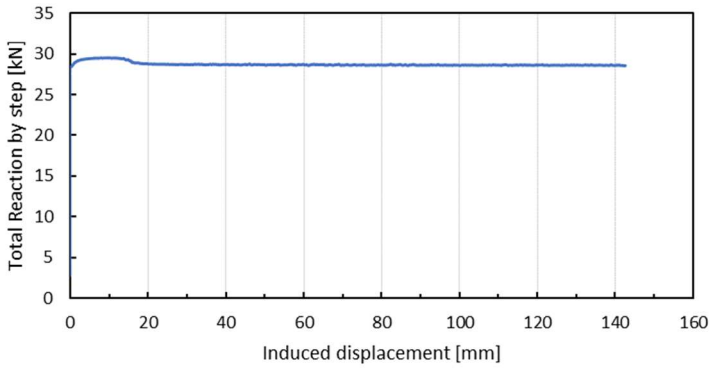


Figure 6-24. Induced displacement and vertical reaction from displaced support

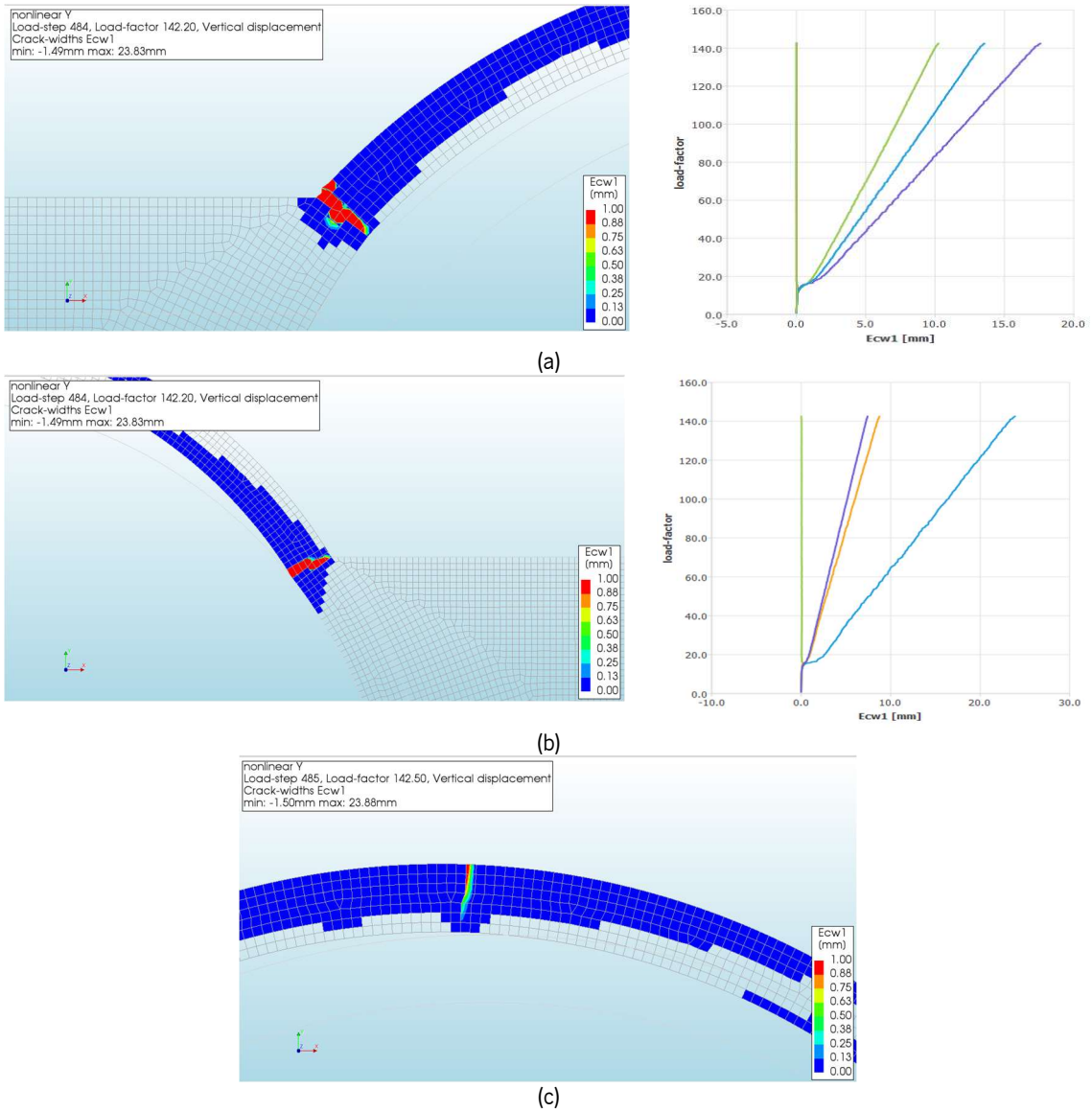


Figure 6-25. Crack widths Ecw1. a) Vault-Wall connection closes the displaced support, (b) Vault-Wall connection closes the fixed support and (c) keystone position

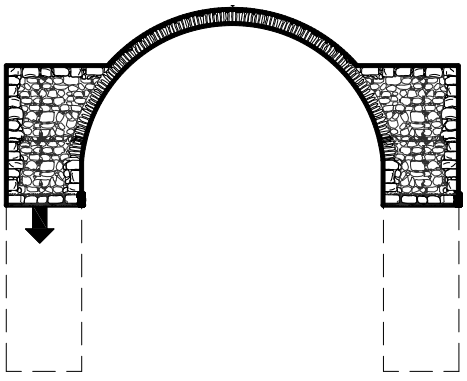
Additionally, the induced displacement and vertical reaction of displaced support were plotted to predict the collapsed moment. Figure 6-24 shows that the induced displacement started when the reaction in the support achieves approximately 30kN and remains constant as the induced vertical

displacement increased until 140 mm. Additionally, Figure 6-25 shows the crack widths for the three identified hinges. At last step in the analysis, the first crack placed in the extrados of left vault-wall connection displayed a crack width of approximately of 18mm (see Figure 6-25a). The second crack placed at intrados of the right wall-vault connection displayed approximately 23mm (see Figure 6-25b). The three cracks shown a increasing almost at total thickness of the vault.

6.8 Experimental setup and loading protocol

Yucatan churches are submitted mostly to self-weight and negligible live load. Notice that in most cases masonry vaults have only a thin layer of lime mortar above serving as rendering and finishing, which does not contribute in any way to the strength of the vault. The walls exhibit tilting which should be attributed at aging of the material, soil settlements or to defects of the construction processes, see Chapter 2. The Yucatan Peninsula is not considered an earthquake hazard zone since it is classified as Seismic zone A, where ground accelerations greater than 10% of the gravity acceleration are not expected. There are no historical records of earthquakes, or no earthquakes have been reported in the last 80 years (INIFED, 2014).

Based on this, it was decided to analyse the structural behaviour of masonry barrel vaults under a combination of the self-weight and imposed vertical displacements simulating movements corresponding to soil settlements, see Figure 6-26.



(a)

Figure 6-26. Load conditions of experimental model submitted to self-weight and differential settlement

In order to simulate a settlement, the experimental tests were carried out under displacement control. For this, a rigid steel platform was designed to enable that the displacement applied is uniform at the base of the left wall. The rigid base, composed of HEB steel profiles, was connected to two L shape steel profiles to which two actuators were attached symmetrically. The actuators were placed in contact with the reaction slab. As the experimental test was carried out in displacement control, a

displacement law was defined for the internal transducers of the actuator. The uplift of the base of the left wall begins after the reaction measured by the two actuators is equal approximately to half weight of the model. The actuator had two load cells that enabled to record the reaction force, see Figure 6-27. The placement of two actuators is symmetric regarding to the vault to ensure the symmetry of the displacement time history and to avoid out-of-plane rotation of the model, see Figure 6-27. In addition, to avoid in-plane rotation of the wall where the induced displacement is applied, a horizontal restriction was considered by means of a simple support. A steel profile was placed in contact with the reaction wall of the laboratory and other steel profile that was instead connected to the rigid steel base. In between the two steel profiles, two Teflon sheet and oil in between were applied to avoid the friction between the steel profiles and thus avoid any restriction to vertical movement, see Figure 6-28. However, after testing, it is important stress that probably a displacement roller supports on both sides of the vertical displacement platform could perform better than the simple supports used, since it would prevent any in-plane rotation and avoid any friction stress.

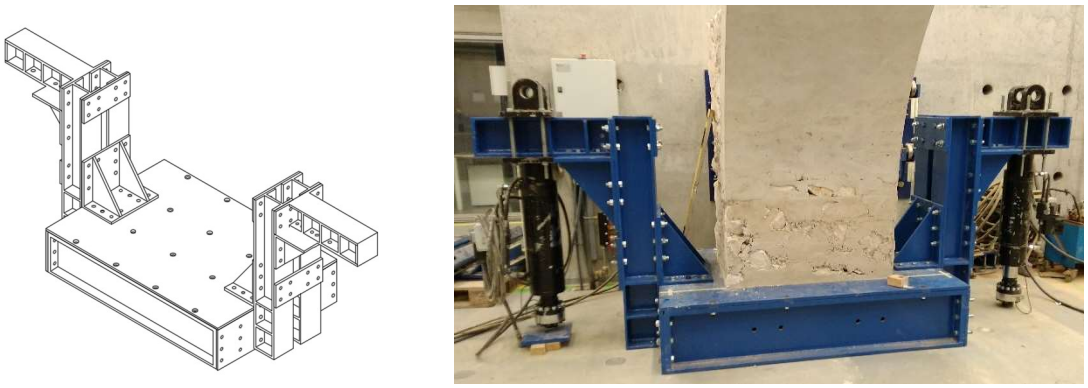


Figure 6-27. Vertical displacement rigid device

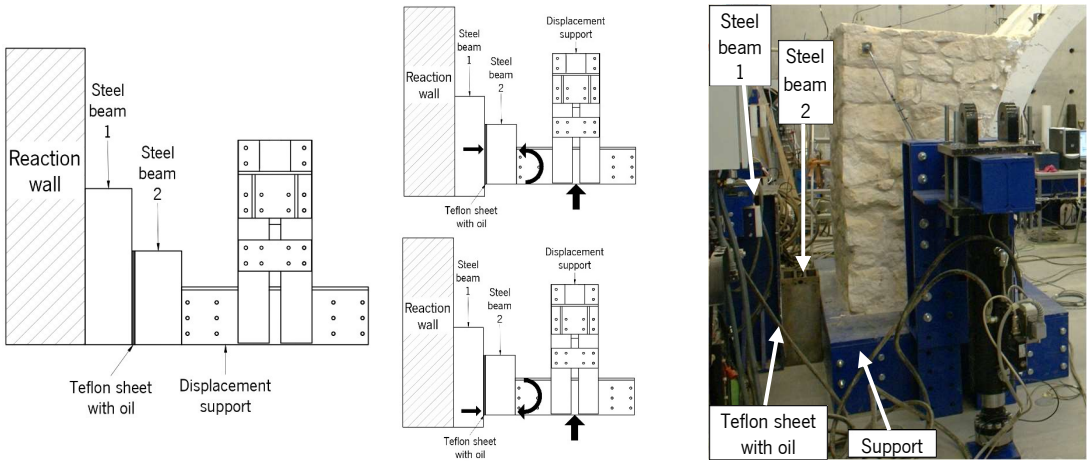
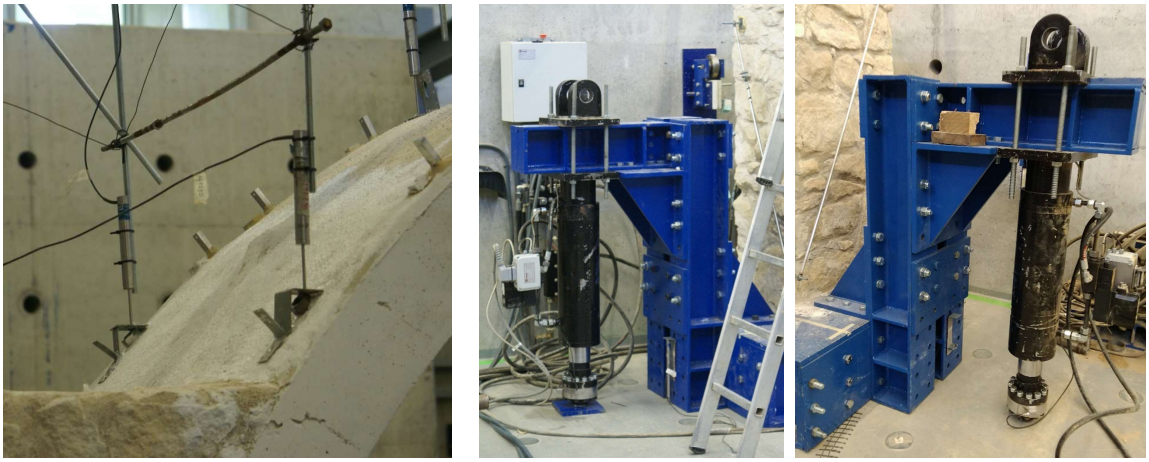
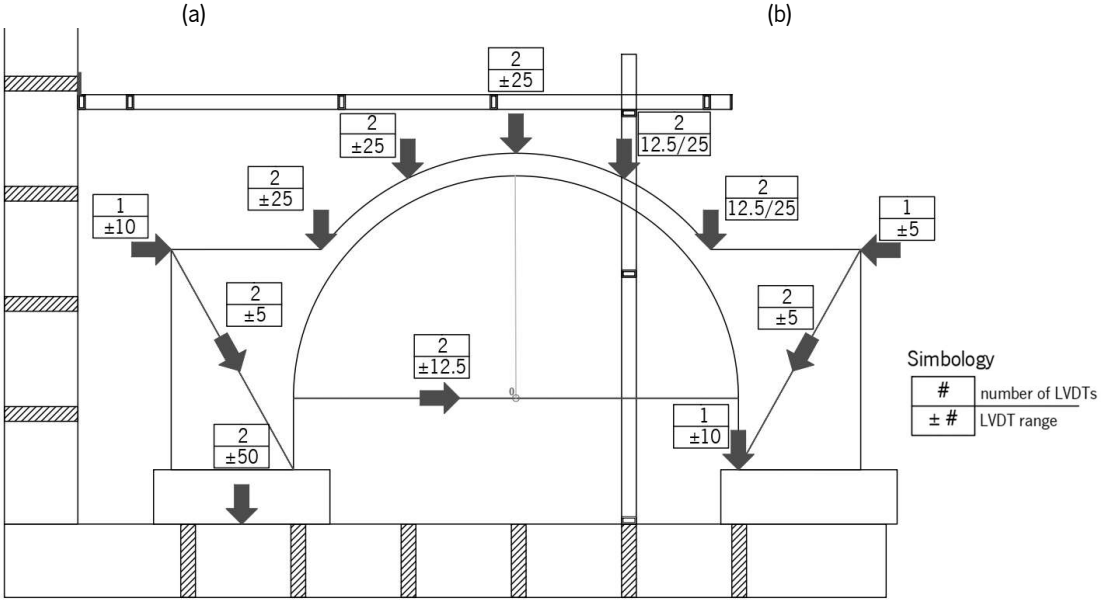


Figure 6-28. Support rotation constraint

The test was designed in control of displacement by means of the two hydraulic jacks. Progressive and controlled damage was applied by increasing displacement, for which both actuators must displace simultaneously at 0.008 mm each second. The displacement was applied with linear ramps until achieve the 3 hinges foreseen in the numerical model.



(a) (b)



(c)

Figure 6-29. Acquisition data setup (a) LVDT device, (b) actuators and (c) LVDT displacement range (in mm)

The data acquisition design was performed by 21 LVDT (Figure 6-29a), 2 computers, 2 actuators with 300kN of capacity (Figure 6-29b) and complement elements as cables, aluminium bars and others. The LVDT had a displacement range as shown the Figure 6-29c. Both actuator and 9 LVDT were controlled by computer 1, while the computer 2 controlled 12 LVDT. The experiment started simultaneously in both computers under control of two operators. The control system was performed using the Dyna testerV3 program and NI LabVIEW FPGA Xilinx 10.1.

6.8.1 Instrumentation of the experimental model

The instrumentation to record the structure's response to a loading configuration is composed generally of linear variable displacement transducers (LVDT), load cells and strain gauges (Girardello et al., 2013; Hojdys and Krajewski, 2014; Golebiewski et al., 2017). Some examples of their use are: (1) during the loading and unloading steps, vertical and horizontal displacement can be recorded using linear variable displacement transducers (LVDT) to measure the opening and closing displacement of the vault/dome. The LVDTs can be placed at the base and on the top of the model, as well as at different heights of the model (Baratta et al., 2008, Krstevska et al., 2008); (2) the applied load can be measured by a load cell placed between the jack and the load application point in the structure (Bolis et al., 2017; Marini et al., 2008). The locations of these instrumentations elements should be decided acording to the needs.

When the availability of measuring devices is limited, its position should be selected balancing two criteria, namely: (1) to consider the most relevant points, (2) to try to obtain a global response of the structure. The use of excessive measurement devices will never be the most successful solution since excessive instrumentation can create excessive noise and confusion in the analysis of the results.

In this test, the induced vertical displacement was measured by the internal LVDTs of the two actuators, see Figure 6-27. For the definition of the displacement measurements layout, the preliminary prediction of the deformation and location of the cracks were taken into account (Section 6.7). The evaluation of the numerical model showed four relevant points to control: (1) the induced vertical displacement, (2) the longitudinal rotation of the model, (3) the behaviour of the walls and (4) the behaviour of the vault.

For this reason, the LVDTs were grouped according to the task to be performed and nomenclature was assigned based on numbers and letters, as shown in Table 6-8. The position and name of each LVDTs are shown in Figure 6-30.

Table 6-8. Nomenclature code description

Objective of measurement	Code of control	Identification symbol	Position	Code of position
Rotation control	R	○	Centre	c
Settlement control	S	△	Side A	a
Vault	V	⬠	Side B	b
Wall	W	▭		

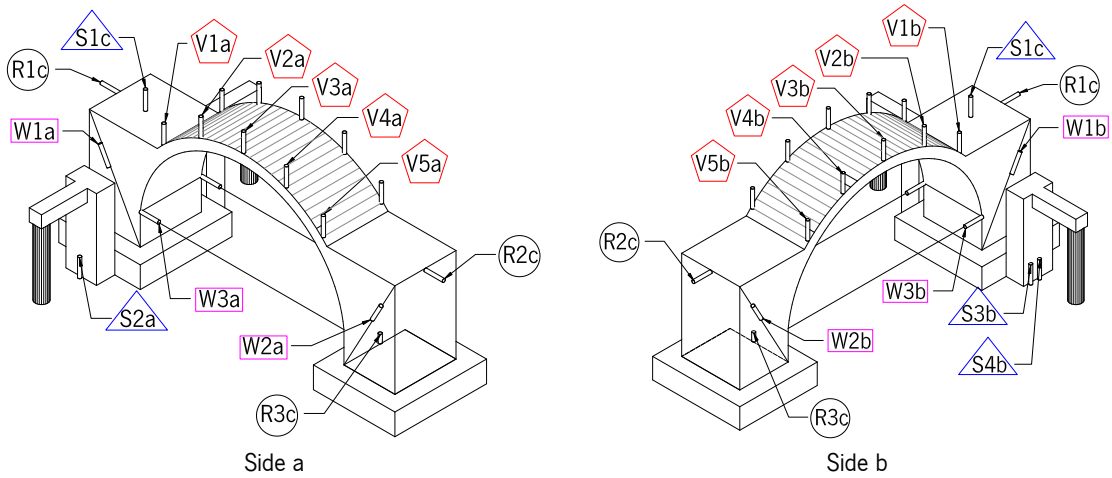


Figure 6-30. LVDT location

Since some LVDTs should measure the vault behaviour, it was necessary an instrumentation frame, which needed to be independent of experimental test model. For this reason, an instrumental frame was designed as shown the Figure 6-31.

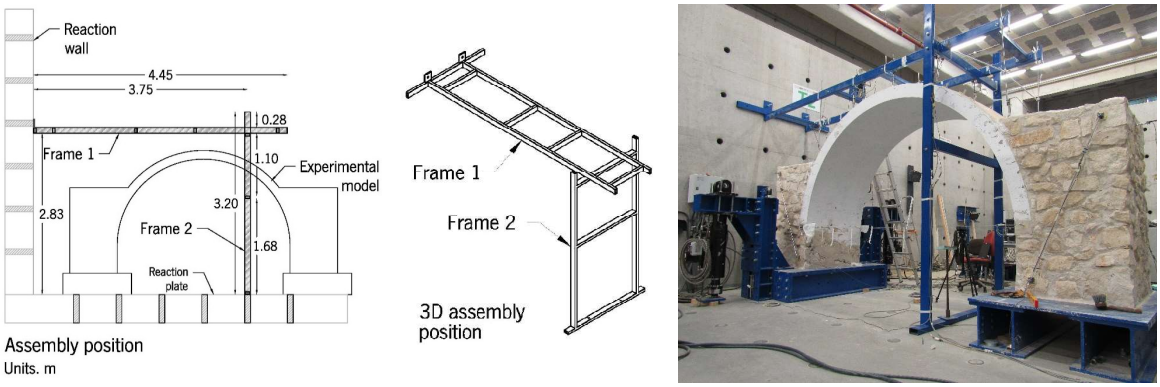


Figure 6-31. Auxiliary frame to support the vaults LVDTs

6.8.2 Photographic record design

A photographic and video recording system based on 8 cameras was designed to record movements of the experimental model and helps in the identification of the cracks location and crack opening time. The place of each device was decided based on the numerical prediction of crack locations and on need of acquire a global vision of the model. Cameras 1, 2, 3, and 4 were placed to record the damage in the theoretical places of the hinges and were programmed to capture a photo every 2 seconds, see Figure 6-32.

Cameras 1 and 2 were simultaneously controlled with the open-source program called digiCamControl V 2.1.2.0 (Istvan, 2018) , whereas cameras 5 and 6 were controlled with the open-source Open Camera V1.48.3 (Harman, 2007). Cameras 5 and 6 recorded videos of the full view of the model. Finally, cameras 7 and 8 were mobile cameras to record additional details (Figure 6-32).

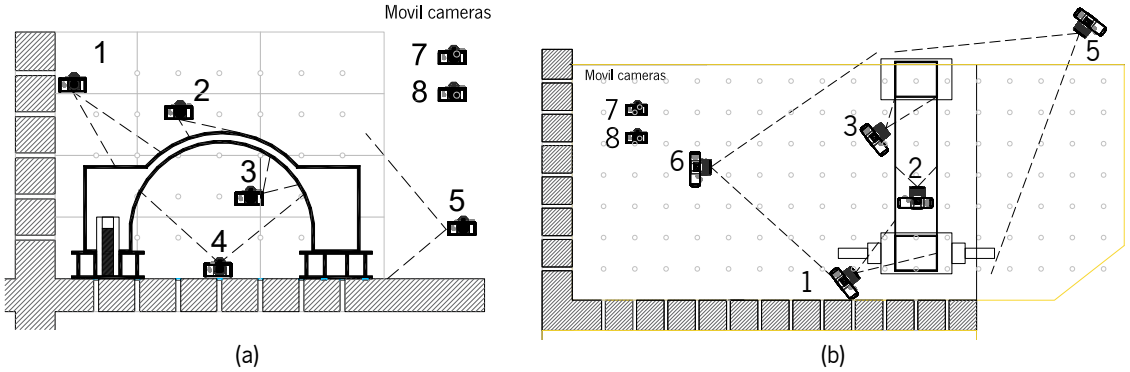


Figure 6-32. Photographic device positions

6.9 Stone masonry vault analysis and discussion of experimental results

In this section the analysis and discussion of results of the experimental test are include. The experimental test simulates a differential settlement under controlled laboratory conditions carried out in the ISISE laboratories of University of Minho. As a fist phase, the results were evaluated with respect to: (1) validation of the test setup; (2) assessment of deformations and analysis of crack pattern and definitions of collapse mechanism and (3) analysis of crack pattern and definition of collapse mechanism.

These different aspects will be presented and discussed in detail in the next sections.

6.9.1 Validation of the experimental model

The experimental test lasted 58 minutes and the maximum displacement induced was 25.99 mm. The validation of the experimental system was carried out by evaluating the evolution of the control displacement inside the vertical actuators as well as the forces measured by the load cells attached to each actuator. In addition, analysis of the displacements measured in the displacement transducers attached to the steel base of the left walls was also carried out. The first task was to define the signs to consider in the displacement based on the movements experienced by the experimental model. As shown in Figure 6-30, the front of the experiment was defined as face A, whereas face B is the back face of the experimental model. The definition of the signs used in the analyses and diagrams were defined according to the Cartesian plane, according to what is defined in Figure 6-33.

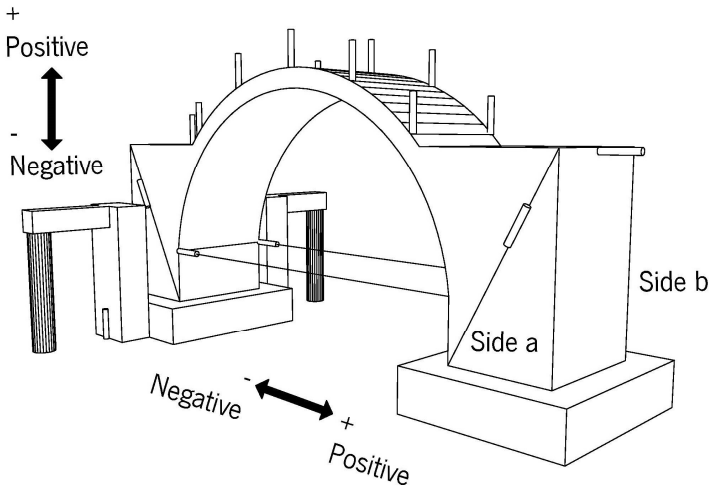
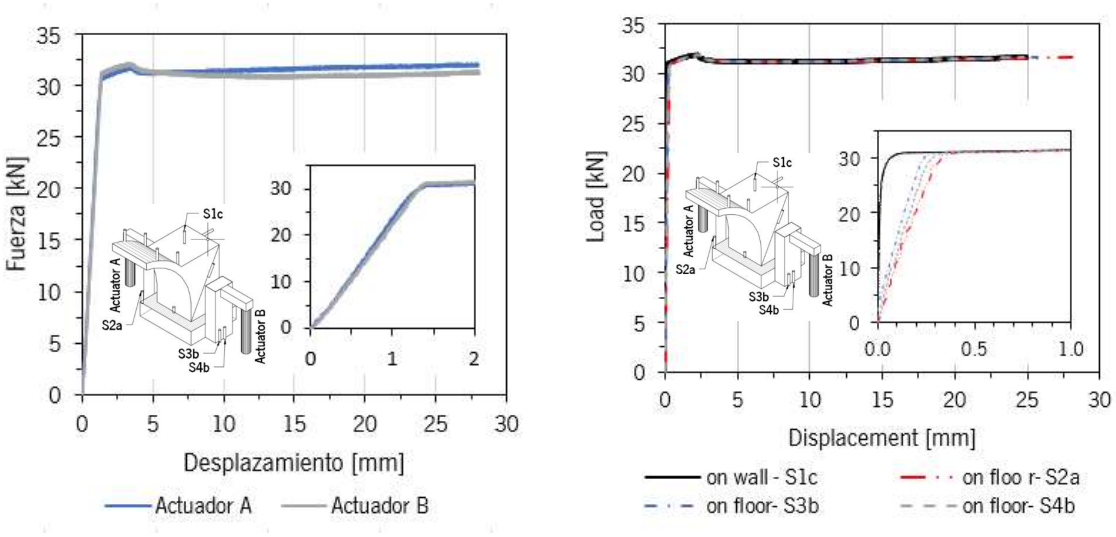


Figure 6-33. Definition of displacement signs for use in graphs

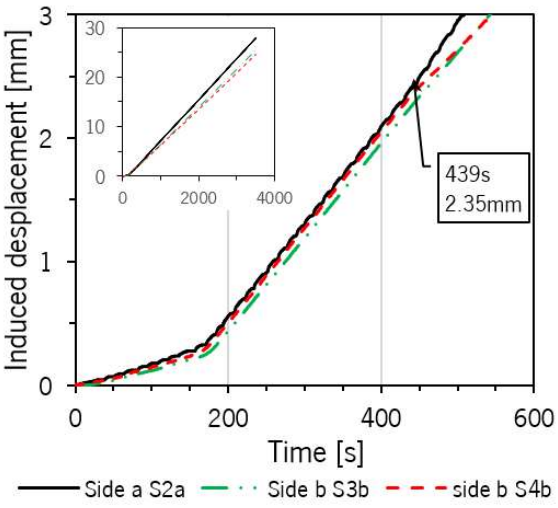
Figure 6-34a presents the relation between the force measured in the load cells and the vertical displacement measured by the internal displacement transducers of the actuators. It is observed that at the beginning of the experimental test, the load increased from zero to approximately 31 kN in few seconds and kept constant until the end of the test. This maximum load reached is identified as approximately the half weight of the vault. The vertical displacement at the left support of the masonry vault started to be induced after the attainment of the recorded load level. It is important to note that the lifting of the left support is recorded simultaneously by the internal transducers of both actuators until the 8mm. After this level of displacement, the actuator on side b recorded a little more displacement (0.35%). It was important to assure that the steel base of the left wall moves in the vertical direction in a uniform way. Transducers S2a, S3b, and S4b were attached to the steel base. LVDT S2a was located on face A and LVDTs S3b and S4b were located on face B (see Figure 6-30). A comparison of the displacements measured in the LVDT at the top of the wall (S1c), and the displacements measured by the LVDTs attached to the steel base is presented in Figure 6-34b. The evolution of displacements indicates that differences recorded between the LVDTs attached to the steel base in both sides was maximum of 2.9mm (11.89%), which indicate that out-of-plane rotation at the base is minor (see Figure 6-35a), Figure 6-34b. It is also observed the displacement recorded at the top of the left wall (S1c) confirms that the induced vertical displacement started to be applied once the weight of the structure on the support is exceeded (Figure 6-34b).



(a) (b)

Figure 6-34. Validation of the experimental system. (a) analysis of vertical displacement applied at the uniform way by comparing the force and the internal transducer displacement from the actuators, (b) evolution of the displacement at the top of the left wall

The steel base was raised horizontally for the first 440 seconds, which is equivalent to 2.34mm of vertical induced displacement, after which a small inclination of the platform was recorded, probably because some damage occurred, see Figure 6-35a.



Moment	Time (s)	Review of out-of-plane rotation	
A	150	0.000000012	0°0'0.10"
B	260	0.000000017	0°0'0.13"
C	341	0.000000020	0°0'0.15"
D	440	0.000000023	0°0'0.17"
E	529	0.000000061	0°0'0.49"
F	645	0.000000100	0°0'0.77"
G	774	0.000000127	0°0'0.98"
H	3508	0.000000626	0°0'4.82"

(a) (b)

Figure 6-35. Evolution of displacement with time (a) displacement measured at the steel base and (b) rotations of the steel base

The out-of-plane rotation angle was evaluated in different stages throughout the duration of the experimental test (3508 seconds). Figure 6-35b shows the slope angle of the steel base at different moments of the experimental test. The equation applied to calculate the inclination angle of the steel base was Rotation=Arctan(h/L), where h is the difference between transducers displacements at sides A and B and L is the horizontal distance between displacement transducers. At the end of the

experiment, the platform had a rotation angle of 0.000000626 (0°0'4.82"), which is considered to be significantly small and practically negligible for the scale and movements that were induced.

6.9.1 Deformation analysis

The analysis of the deformations exhibited by the experimental model includes: (1) the in-plane deformations of the model, (2) the deformations of the vault and (3) the deformations of the walls. The displacements in the different transducer displacement were analysed through time, which enabled to defined critical phases characterizing the global behaviour of the experimental model.

6.9.1.1 In-plane deformations of the experimental model

The in-plane deformation of the experimental model is mostly characterized through three main points, namely R1c, R2c placed at the top of the left and right walls respectively and R3c placed at the base of the right wall, Figure 6-30. The relation between the displacements measured at these points with the induced vertical displacement over time is presented in Figure 6-36a.

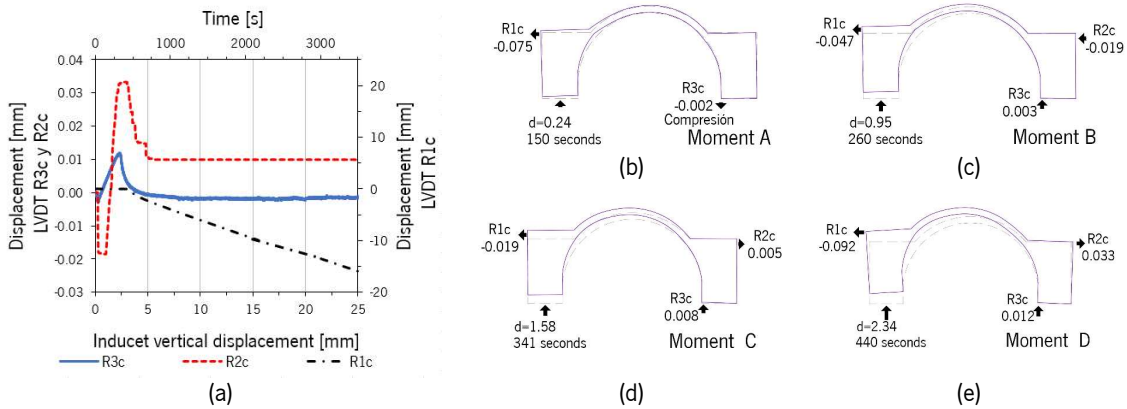


Figure 6-36. (a) Analysis of model deformations in the plane and displacement at key points at an induced vertical displacement (b) Moment A with 0.24mm, (c) Moment B with 0.95mm, (d) Moment C with 1.58mm, and (e) Moment D with 2.34mm

The model stared to exhibit deformations at approximately 150 seconds when the force recorded in the actuators was 27 kN. At this time, the load support has not been exceeded, and the induced vertical displacement was about 0.24mm (Figure 6-36b). The displacement measured in the wall's base by LVDT R3c was about -0.002mm, whereas the horizontal displacement measured at the top of the right walls (R1c) was about -0.075 mm. Probably, the compression observed in R3c can be attributed to the redistribution of the loads on the supports because of the lifting of the platform.

When the induced vertical displacement reached approximately 1mm at the time of 260s, the left wall horizontal movement decreases (R1c), and the right wall horizontal movement (R2c) showed a

displacement of about 0.019mm of displacement also to the left. At the same time, the displacement measured at the base of the wall (R3c) was now positive with a value of 0.003mm, see Figure 6-36c. This appears to indicate that the right wall exhibited a little rotation over the right corner.

Another key phase in the analysis of the in-plane deformation of the experimental models is identified when the vertical induced displacement achieved the value of 1.58mm (Figure 6-36d). The displacement measured at R1c was closest to zero (-0.019mm), the displacement recorded at R2c exhibit an inflexion point, being now positive (0.005mm), being considered very small and close to zero. At this moment, the displacement recorded in R3c achieved a positive displacement equal to 0.008mm, confirming the trend for the right wall to rotate over the right corner.

When the induced displacement reached the value of 2.34mm at approximately 440s, it is observed that both support walls (R1c and R2c) move horizontally in opposite directions. In fact, this represents the key phase on the experimental testing corresponding to the almost linear increasing of the horizontal displacement at the top of the left wall. At the same time, the left corner of the right walls exhibits an uplift equal to 0.012mm (R3c), see Figure 6-36e. This trend is kept until the induced vertical displacement reach the value of 3mm of displacement at 529s, when apparently the structure is divided into two large blocks, see Figure 6-37a.

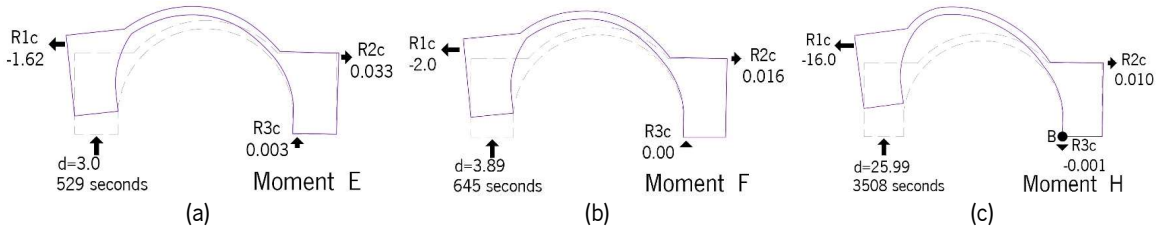


Figure 6-37. In-plane deformations at different stages (a) Moment E with 3.0mm. (b) Moment F with 3.89mm, and (c) Moment H with 25.99mm

The top left wall continues to move to the left, as displacement measures in the top horizontal displacement is increasing linearly (R1c) and the horizontal displacement at the top of the right walls approaches to zero, recovering the initial positions, see Figure 6-37b,c.

The experimental test stops when the induced displacement reached 26mm. At this stage the left wall (R1c) reaches a maximum displacement of 16 mm and the values of displacement at the top (R2c) and base (R3c) of the right wall presents residual values.

6.9.1.1 Analysis of deformations in the vault

The deformation of the vault was monitored by using 10 displacement transducers placed at extrados of the vault, see Figure 6-30. The displacements measured fall in two very distinct ranges: displacement transducers V1, V2 and V3 recorded displacements in the range millimetres (mm), whereas displacement transducers V4 and V5 recorded displacements in microns (μm). This difference is associated to the location of the LVDTs. LVDTs V1, V2 and V3 were located on the left side of the vault, close to the support with induced displacement, and transducers V4 and V5 were located close to the fixed support or right side.

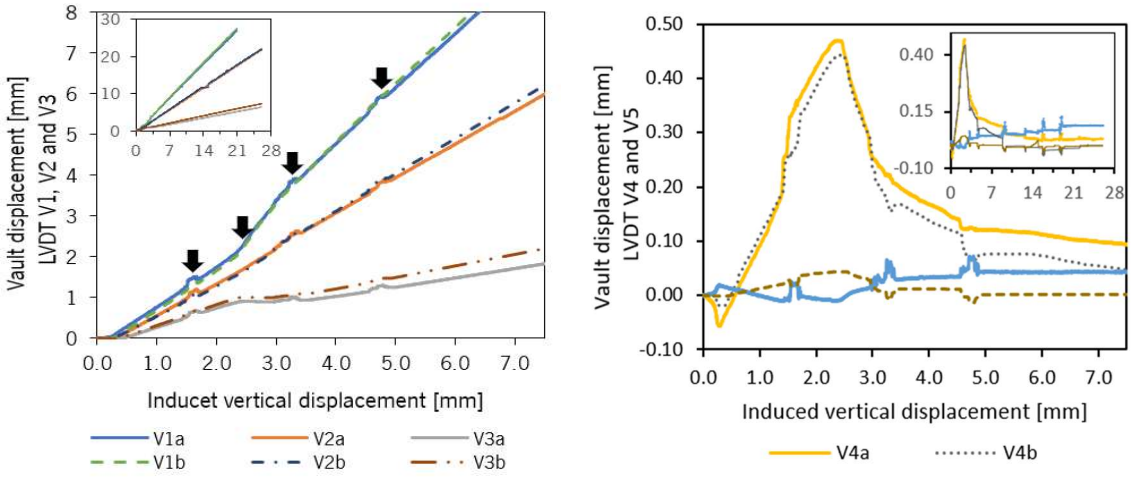


Figure 6-38. Vertical vault deformations regarding to the induced vertical displacement, which shown different displacement ranges: (a) LVDT V1, V2 and V3 in mm, while (b) LVDT V4 and V5 in microns

In general, the left side of the vault (LVDTs V1, V2 and V3) recorded irregularities and slope changes throughout the experiment (Figure 6-38a). The LVDTs placed in the right part of the vault increased until the induced vertical displacement reached the value of 2.34mm. After this stage the displacement started to reduce until stabilize in the residual displacement very close to zero, see Figure 6-38b.

From more detailed analysis of the displacements measured in LVDTs V1, V2, and V3 in the diagram shown in Figure 6-38a , it is observed that: (a) small disturbances occurs when induced displacement achieves the values of 1.5mm, 3mm and 4.86mm, which can be attributed to adjustments, movements, or damages in the experimental model, see Figure 6-38a; (b) the displacement profile measured in LVDTs V3 exhibits a reduction of the slope when the induced vertical displacement reaches 1.5mm until 3.0mm, after which in increases, even if it is keeps lower the initial slope. The displacement measured at LVDT V3 increases at a much slower rate when compared with displacement measured in LVDT V1 and LVDT V2; (c) LVDT V1 presents a linear slope until the induced

vertical displacement reaches the value of 2.34mm, the slope increases between 2.34mm and 3.0mm and after this value reduces but keeps linear until the end of the test; (d) LVDT V2 presents a linear slope until the induced vertical displacement reaches the value of 3.0mm. After these values keeps linear but with a little smaller slope. This means that when the induced vertical displacement reaches the value of 2.34mm some cracking, it appears that a change on the global behaviour of the model occurs. It is also seen that after the induced vertical displacement reaches 3 mm the LVDT V3 begin to record little difference in sides A and B, meaning that a small out-of-plane rotation occurs. This difference is not seen on the other LVDTs. After the induced vertical displacement reaches 4.86 mm any other change on the slope of the LVDTs is recorded.

6.9.1.1 Analysis of deformation in the walls

The recording of diagonal displacement in the walls was made on both faces A and B in positions W1, W2 and W3 (see Figure 6-30). The displacements recorded in LVDT W1 and W2 were in the order of microns and the presence of cracks or any damage in the walls were not observed. The LVDTs W3a,b recorded the horizontal relative displacement between walls supporting the vault. The relative horizontal displacements present an increasing step at 440 seconds for an induced vertical displacement of approximately 2.34mm. After this value the increasing of the spacing between walls keeps linear at the same rate. In the final of the experimental tests, the horizontal distance between the supports increased a total of 6.5 mm.

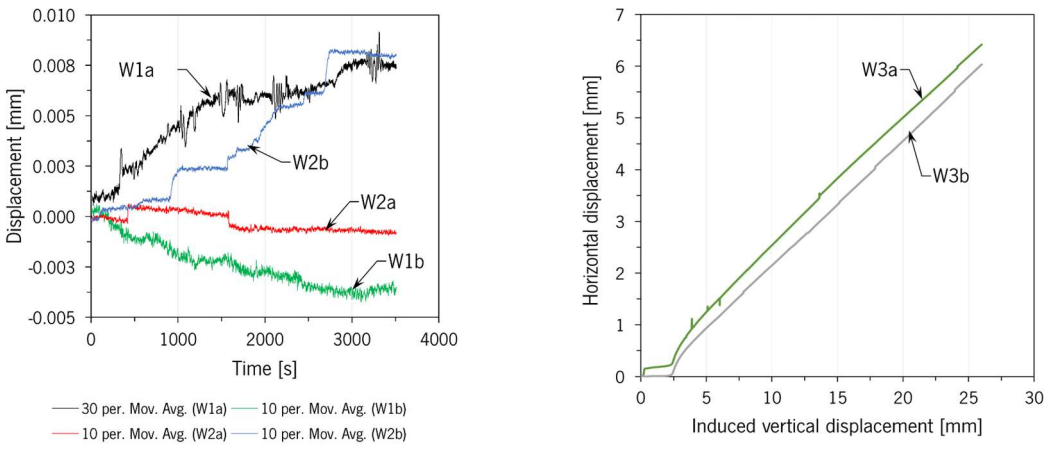


Figure 6-39. Evaluation of the behaviour of the supporting walls. (a) diagonal displacement in the walls and (b) relative horizontal displacement between supporting walls

6.9.1 Analysis of crack pattern and definition of collapse mechanism

In this section, the crack pattern and collapse mechanism are analysed and discussed. For this, the displacement records of LVDTs on walls and vault are analysed together, see Figure 6-36a and Figure 6-38. The evolution of displacements measured in the different LVDTs, namely points corresponding to change in the increasing rate allow to identify with accuracy the crack location and opening. Throughout the experimental test, eight critical moments were identified, which were named from A to H and explained below.

The moment A is achieved at 150 seconds, when induced vertical displacement reached 0.24mm, the reaction load is 27 kN and the displacements in the key points are shown Figure 6-40a. At the beginning of the experimental test, the model does not present any damage or crack, for that reason, it behaves like a monolithic body. Based on the displacements measured at key points R1c and R3c, two hinges seem to be instantaneously formed, see Figure 6-40b. Both walls are connected to the steel base through mortar joints and in right wall, it appears that mortar compresses at the left toe. It should be also noticed that as the walls are simply supported, the bases are not prevented to rotate.

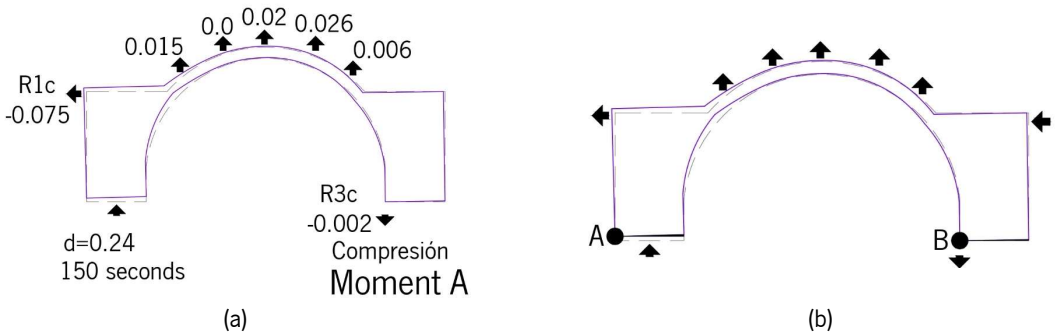


Figure 6-40. Displacement at key points at an induced vertical displacement of 0.24mm. (a) LVDTs records and (b) proposal of global movement of the experimental model

The moment B occurs when the induced vertical displacement reaches approximately 1mm (260 seconds), see Figure 6-41a. At that moment the load on the support is overcome and the hinge A in the left wall begins to close, which is confirmed by the decrease displacement in R1c. The model continues showing a monolithic behaviour since R2c start to record horizontal displacements to the left and R3c begins to register positive values which signal a lift, these seem to indicate that hinge B change the position at hinge B', see Figure 6-41b. The model shows a monolithic behaviour since all control points describes movements towards the centre and upwards, see Figure 6-41b.

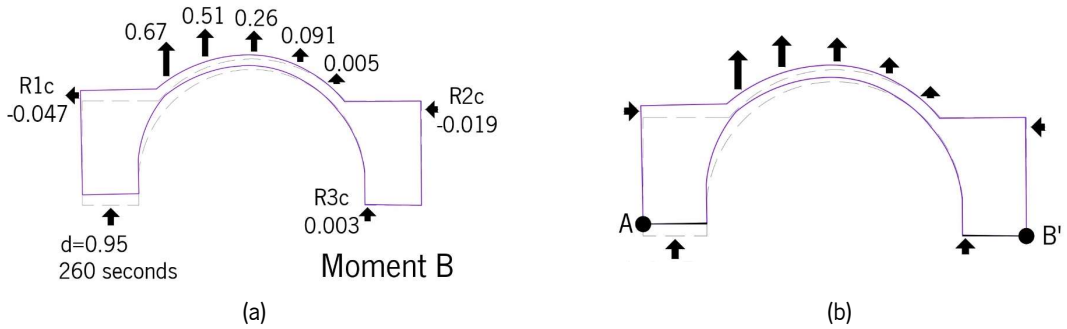


Figure 6-41. Moment B at 0.95mm of induced displacement. (a) LVDTs displacement records and (b) proposal of global movement of the experimental model

The moment C is achieved when of induced displacement reached 1.58 cm at 341 seconds. The displacement at R1c continues to decrease at 158 seconds it was -0.090mm, at 260 seconds it reached -0.047mm and at 341 seconds it reached -0.019mm. Therefore, the displacement recorded in R1c is very small and suggests that hinge A is closing. Consequently, the vault thrusts are redistributed and change the behaviour of the experimental model. The readings on R2c change from negative to positive and point R3c is now uplifting, which suggest a rotation of the right wall at hinge B', see Figure 6-42b. In addition, due to the closing of hinge A, the LVDTs V1, V2 and V3 register some small curves in the graphs, see Figure 6-38a.

At this point, Moment C, two hinges have been clearly identified, however no cracking is still observed in the experimental model.

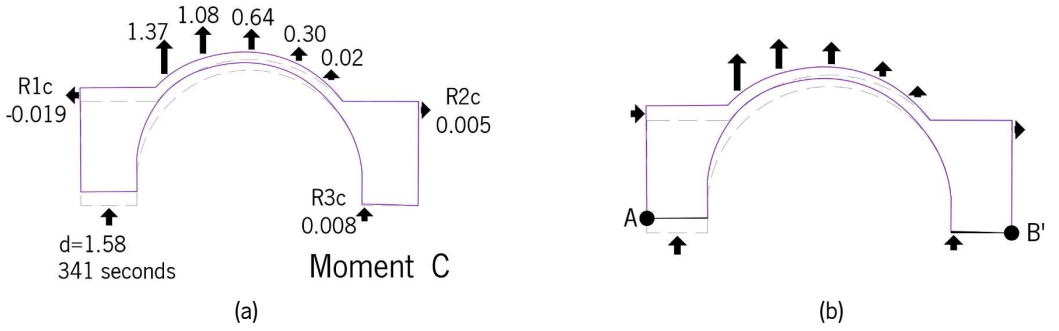


Figure 6-42. Moment C with 1.58mm of induced displacement. (a) LVDTs records and (b) behaviour description

For an induced vertical displacement of 2.34 mm (440 seconds), the LVDTs R1c, R2c and R3c records inflection points, which corresponds to abrupt change of the model's behaviour. Before the Moment D, R1c had shown movements very close to zero, but at this stage a significant increase of displacement at this point was recorded. Moreover, R2c and R3c record their maximum displacement with 0.033mm and 0.012mm respectively (Figure 6-43a). Additionally, the vault records inflection points in the graphs of LVDT V1 and V3, which change remarkably the displacement rate (change on the slope of displacement evolution). Displacement in point V1 begins to register larger displacements

(steeper slope), while V3 record a slope practically equal to zero (horizontal). Moreover, V4 records its maximum displacement (Figure 6-38). That means that at this stage (Moment D), the structure beaks is two rigid blocks that rotate outwards. On the left wall, hinge A located on the support is reactivated and the wall rotates counter-clockwise direction. At hinge B, at the right wall reaches its maximum clockwise rotation, see Figure 6-43b.

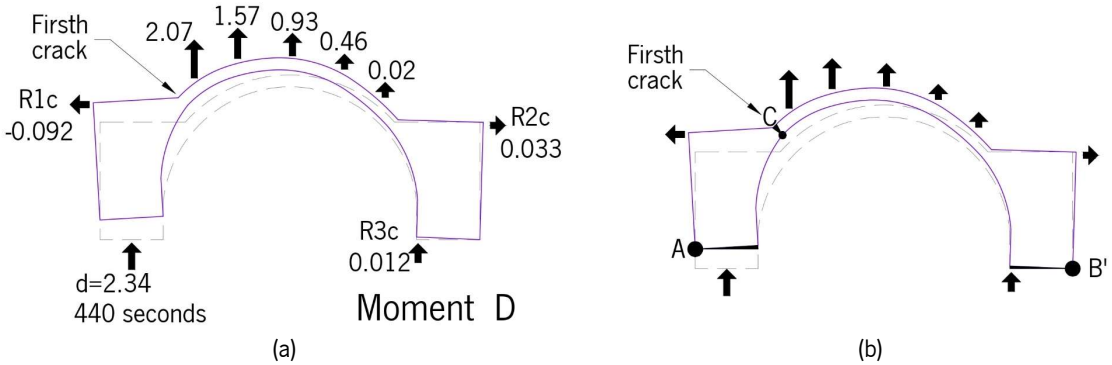


Figure 6-43. Moment D with 2.34mm of induced displacement. (a) LVDTs records and (b) behaviour description

It is assumed that the first crack in the vault opened at its connection with the left supporting wall. It was not visually identified but as the vertical displacement increased it started to be seen at 1:55 minutes later, probably because its thickness was not visible to the human eye and the quality of the photograph was not enough. The crack is the hinge number three identified as hinge C (see Figure 6-43b and Figure 6-44). The position of this crack agrees with the numerical simulation prediction (Figure 6-23,) even if the time of opening is not in agreement with the numerical model (crack opening at 1mm vertical displacement).



Figure 6-44. First crack in the vault at extrados located at the wall-vault connection

The Moment E is achieved when the induced vertical displacement was equal 3mm (529 seconds). Figure 6-45a shows the displacement at the key points at this stage. The increase in R1c indicate that the hinge A in left support is clearly active. The left wall rotates outwards and the crack in the wall-

vault connection is fully visible. AT this stage the displacement recorded at point R3c exhibits significant reduction and approximates to zero, which indicates that the hinge B in the right support is beginning to close. Finally, displacement at point V4 presents a steep decrease, with a tendency to return to its initial position. Displacements at points V1 and V2 register small disturbances, seeming that is undergoing adjustments. This displacement trend is compatible with the opening of a crack at the vault between points V3 and V4, becoming visible until 1:47 minutes later (see Figure 6-46). This crack was identified as hinge D and after this stage the experimental models breaks in three rigid blocks: (1) block between hinge A and C, (2) block between hinge C and D and (3) block at the right of the hind D, See Figure 6-45b.

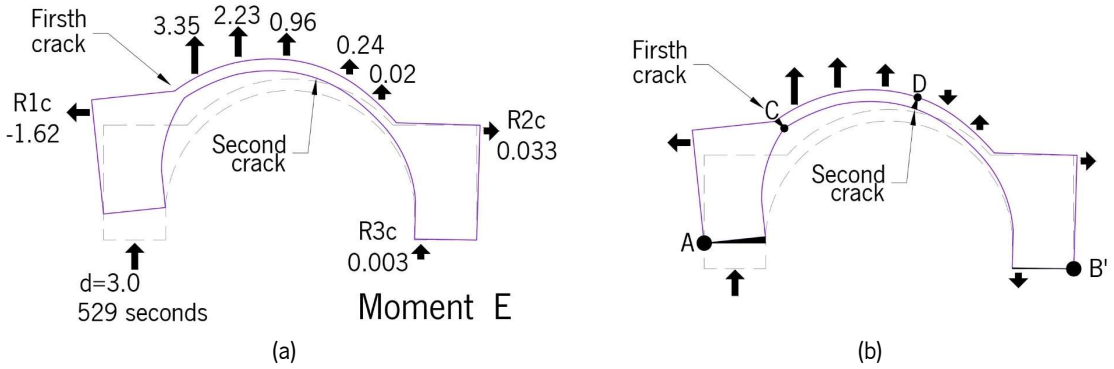


Figure 6-45. Moment E with 3mm of induced displacement. (a) LVDTs records and (b) behaviour description



Figure 6-46. (a) Second crack at the intrados of the vault-wall connexion and (b) crack of belonging to hinge D

Block 1 moves upward and left movement trend, Block 2 presents a relative rotation regarding Block 1 and Block 3, which tends to recover the original positions. These movements are more clear when the induced displacement achieved 3.89mm (645 seconds – Moment F. At this moment, the second crack is clearly visible and located between V3 and V4. R1c records larger displacements which means

that the left wall continues to rotate outwards increasing the thickness of crack 1 (hinge C) located in the wall-vault connection, see Figure 6-48. Furthermore, the hinge at the support of the right wall is closed and the displacements in R2c and V4 continue to decrease, returning to their initial position. Additionally, block 2 (vault section between hinges C and D), moves upward, which is conformed the displacements measures at points V1 to V3.

The configuration of the deformation of the three blocks keeps the same for the induced vertical displacement of 4.86mm at 774 seconds. The cracks at hinges C and D are clearly more visible. The left block exhibits its rotation to the left resulting from the increase of the opening of the crack at hinge C and hinge A, see Figure 6-48. The point R2c continues recover its initial position and point V4 continues to decrease, which should be attributed from the increase in the crack opening of the hinge D. The block between the hinge C and D continue to move upwards. The displacement measured in points V1 to V3 continues to increase, see Figure 6-48.

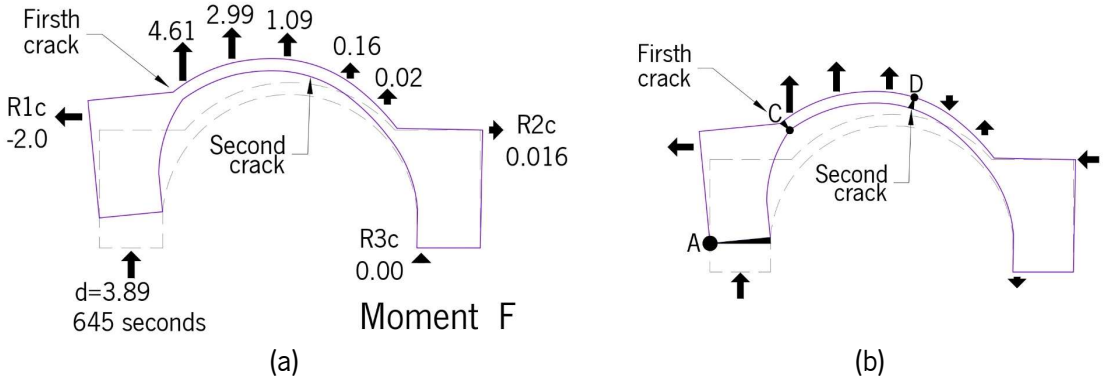


Figure 6-47. (a) Displacements of key points when induced displacement of 3.89mm; (b) Proposal of rigid blocks movement

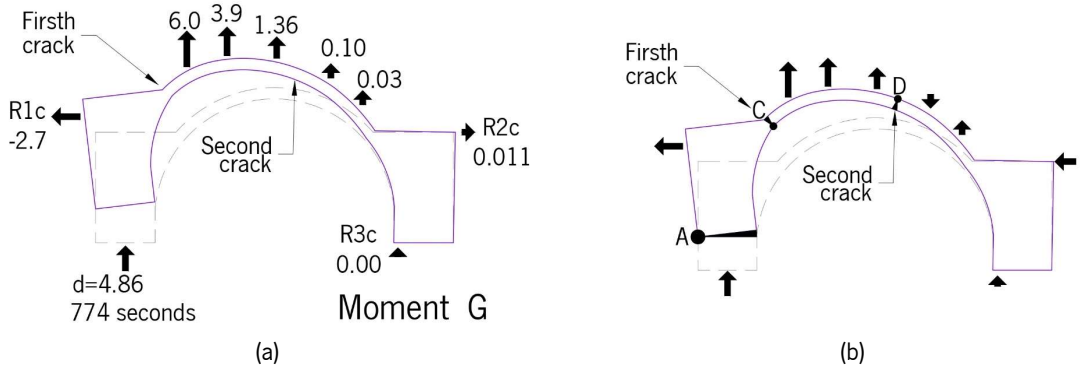


Figure 6-48. (a) Displacements of key points when induced displacement of 4.86mm; (b) Proposal of rigid blocks movement

Finally, the experiment stops when the induced vertical displacement reaches 26 mm at 3508 seconds (Figure 6-49). The displacement at the top of the left wall, R1c, increases Throughout the experimental test reaching 16 mm.

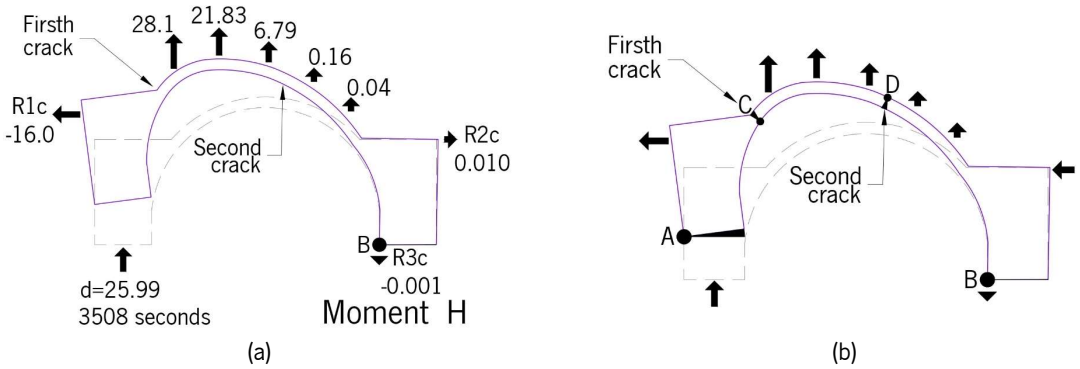


Figure 6-49. (a) Displacements of key points when induced displacement of 25.99mm; (b) Proposal of rigid blocks movement

Since no crack was visibly along the height left wall, it is assumed a hinge at the base of the wall (Hinge A). Unfortunately, the position of the hinge A cannot be clearly identified due to the absence of control transducers in that position.

On the right side, the block between hinge D and right wall present very small displacement: (a) point at the top of the right wall, R2c, record a permanent deformation of 10 microns; (b) point R3c also presents a residual displacement of 1 micron and V4 and V5 present also residual values of 0.16mm and 40 microns. These displacements show that once the crack in D opens, the third block presents very slow displacements, mainly when compared to Block 1 and Block 2. This is confirmed through the illustration of the movements of the experimental models along the experimental tests, see Figure 6-50.

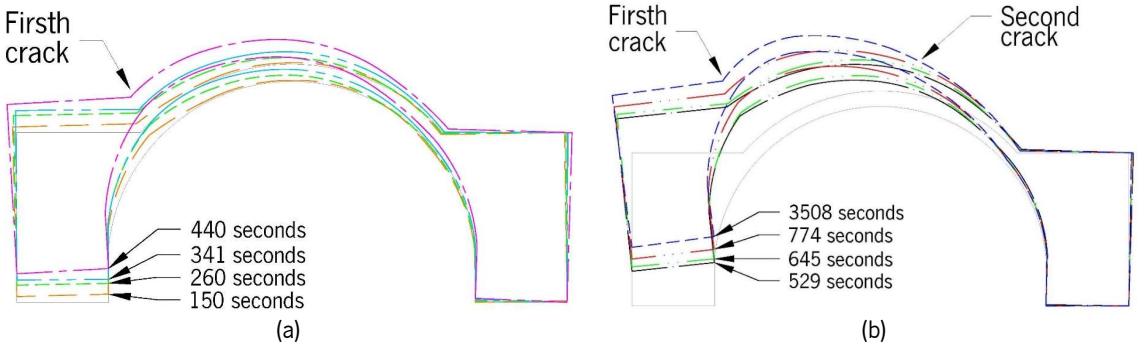
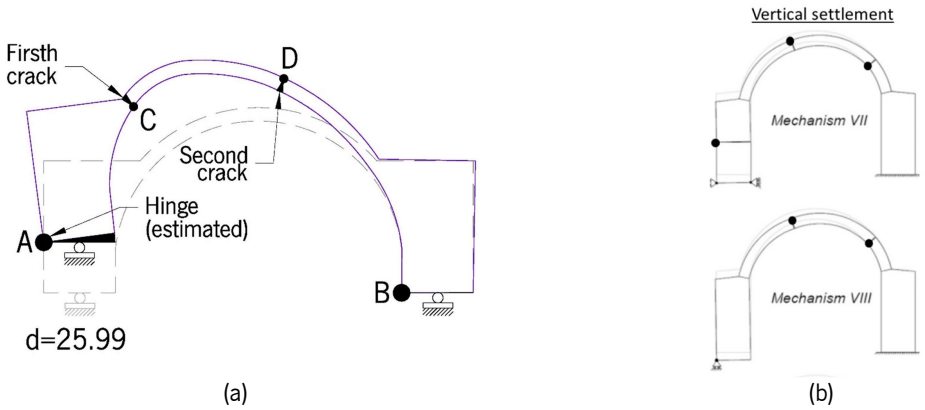


Figure 6-50. Behaviour of the experimental model. (a) From 150 to 529 seconds and (b) from 645 to 3508 seconds

The proposal for the final collapse mechanism is presented Figure 6-51a. It is observed that the mechanism of collapse was clearly identified along the experimental test, mostly through the deformations measured by the different LVDTs, being compatible with the cracks opened.



(a) (b)

Figure 6-51. a) Proposal for the final collapse mechanism at the end of this experiment and (b) Mechanism VII and VIII from (Zampieri et al., 2019b)

It should be mentioned that in the numerical model, the rotation of the left wall was not allowed, and it rises perfectly vertical until the appearance of the three hinges. This boundary condition does not apply to the experimental model, since a rotation in the left walls was clearly identified. On the other hand, the experimental works developed by other authors do not consider the interaction between the vault and the wall, they generally contemplate infinitely rigid supports capable of avoiding any rotation, which causes the hinge to be generated in the weak section, the connection between the vault and the support (Ferrero et al., 2021, 2022; Zampieri et al., 2018a; Zampieri et al., 2018b) in contrast to the theorical analysis developed by Zampieri in (2019b).

6.10 Concluding Remarks

In this work, both 1) masonry wallets and 2) the cross section of typical Yucatan churches with semi-circular cannon vaults submitted to differential vertical settlements was analysed. The experimental tests intended to replicate the behaviour of the vault-wall system without lateral restriction in the plane.

Based on the results obtained, it can be concluded that:

- Higher resistances were observed in wall wallets, in contrast to the vault wallets, despite their morphological characteristics. That means, 1) the wall samples were made up mainly of the inner cyclopean layer of the three layer of masonry studied system, while 2) the vault wallets were made up with an ordered arrangement of stones joined with mortar (according to the construction detail in Annex 1).
- Both walls and vaults masonry showed very rigid behaviour, which was reflected in very high modulus of elasticity, a condition not expected in masonry.

- Different stages were identified throughout the experiment, all displacement were well record, including really small displacement at the scale of microns and it was possible to completely follow the deformation trajectory of the model. This was rather difficult when simultaneously manage two actuators and 21 transducers. It should be mentioned that the set of LVDTs enabled to follow the deformation and movements exhibited by the structure with rather accuracy along the experimental test.

- Stone masonry vaults will have a monolithic behaviour until before the appearance of the first hinge (crack) after which it divides into rigid blocks.

- Vaults supported on walls, as the one represented by the experimental model analysed, are not capable of withstanding large vertical settlements without visibly damage. The first visible crack appeared at extrados of the vault at the vault-wall connection and the second visible crack appeared close to the key stone. Based on the information of displacements measured, it was possible to identify the other hinge located at the left wall, assumed to be at the base.

- It should be mentioned that both the buttresses and the continuity of the walls that support the vault can be important reasons for the third hinge to be located in the vaults according to the prediction of the numerical model and the collapse mechanisms proposed by some authors. Because both the buttresses and the continuity of the walls provide rigidity to the system and prevents the in-plane rotation of the support.

- In a similar experiment, it would advisable to closely monitor the connection of the walls and the support surface, to identify any in-plane rotation regarding the wall. It would be also interesting to place LVDTs in the horizontal direction in the vault, at some position also considered for vertical displacements to completely record the rigid block movements with more accuracy.

Chapter 7
Assessment of the structural behaviour of the retrofitted experimental model

Abstract:
This chapter presents the description of retrofitting technique and experimental testing on the retrofitted experimental model subjected to differential vertical settlements and provides a comparison of results between the reference and the retrofitted models.

7.1 Introduction

In Chapter 7 it was presented and discussed the main results obtained in an experimental test on a slice of stone semi-circular barrel vault supported on stone masonry walls subjected to an imposed vertical settlement of one support in addition to self-weight. The main aim was to assess the mechanical behaviour of the vault-wall system under vertical settlements identifying the main cracking patterns and failure mechanisms.

Aiming at analysing the improvement of the displacement capacity of the structural system, it was decided to retrofit the tested experimental model and test it again under the same loading configuration. This procedure has already been carried out by other authors (Garmendia et al., 2014; Girardello et al., 2013; Ramaglia et al., 2016). The experimental model was strengthened with a composite Glass Fibber Reinforced Mortar (GFRM) system composed of different components: fiberglass mesh, hydraulic lime mortar strengthened with fiberglass and fiberglass rod anchors.

In this chapter it is intended to provide details on the strengthening materials and technique of the experimental model, on the retrofitted experimental model, testing procedures and the main results. A comparison between retrofitted and original experimental models is also presented and discussed.

7.2 Strengthening techniques

In the context of historical masonry structures, three levels of intervention can be identified: (1) treatments and conservation procedures, (2) repair techniques and (3) reinforcement and consolidation techniques. The treatments include minimally invasive superficial and protective interventions, and the repair techniques deal mostly with replacing lost material in the joints, repairing or replacing mortar or filling empty spaces, replacing masonry units or partial reconstruction. The strengthening and consolidation techniques involve generally more invasive interventions with different purposes such as: (1) replacing lost materials inside of masonry such as mortar injection; (2) restraining deformation and increase strength with the addition of materials such as steel, fibreglass or carbon fibre in the form of turnbuckles, transverse reinforcing bars, reinforcing rings or reinforcing anchors at joints: (3) retrofitting of the masonry through techniques such as (i) the Overlay (jacketing), (ii) the seam (Scuci-cuci), (iii) reinforcement with polymeric reinforced fibres (FRP in sheets or bars) and (iv) fibre reinforcement and inorganic matrix (FRM) or glass fibre–reinforced mortar (GFRM).

Several experimental studies pointed out the enhanced structural capacity of arches and vaults after the application of strengthening techniques (e.g. FRP strips bonded at the intrados or extrados surfaces), through the improvement of the tensile strength, preventing crack opening, and forcing the line of thrust to fall inside the thickness of structural elements (Girardello et al., 2013; Rovero et al., 2012). By restraining crack opening, the hinge development can be prevented, but further local collapse mechanisms are activated, due to both the material and bonded interface (Rovero et al., 2012). Regarding FRP strengthening technique used in several cases to improve the tensile strength, three most common failure modes of FRP-strengthened arches have been identified: (1) masonry compressive failure, (2) sliding along the mortar joints (shear failure), and (3) FRP debonding from the masonry (Valluzzi et al., 2001). Giamundo (2015, 2016) assessed the structural performance of a masonry vault and its retrofitting with an Inorganic Matrix Grid, IGM system, under several shaking table tests. The IGM performance was assessed by means of comparison between the damages detected prior and after retrofitting. The experimental results showed that IMG provides both a significant increase of seismic capacity and ductility. It is also common that strengthening of vaulted and arched structures is carried out with fibre and inorganic matrix (FRM) also called or glass fibre–reinforced mortar (GFRM). The system is composed of an inorganic matrix (mortar) reinforced with fibres in the form of a mesh embedded in the inorganic mortar matrix. These strengthening techniques has been used in multiple cases such as in the bell tower of Santa Maria Gloriosa dei Frari in Venice Italy, Natività della Beata Maria Vergine church located in Vigarano Mainarda, Italy, masonry Girls' High School and clay brick masonry Shirley Community Centre from Christchurch, New Zealand, San Esteban Church's located in Valencia Spain, ribbed barrel vault from Novi Ligure, Italy, masonry vault from L'Aquila, Italia, among others (Boem and Gattesco, 2021; Carozzi et al. , 2018; Chulia, 2017; Dizhur et al., 2015; Milani et al., 2017; Modena et al., 2011; Valvona et al, 2017).

7.3 Strengthened vault process

The GFRM technique was selected for the retrofitting of the experimental model tested previously (Chapter 7). The strengthening system is composed of a fibreglass mesh embedded in natural a hydraulic lime mortar and mechanically connected to the stone masonry with fibreglass bars anchors. This technique could be combined with the injection of cracks. In the present case, injection of cracks was not possible due to its closing after the release of the induced vertical displacement. Due to the opening of cracks at the intrados and extrados of the masonry vaults, it was decided to apply the strengthening mesh at both sides of the vault.

7.3.1 Materials, tools and equipment's

Before the application of the strengthening technique, all instrumentations were removed, leaving the experimental model fully available for intervention. The strengthening was designed and applied by a company that develops materials and strengthening solutions for construction industry. Thus, strengthening was proposed by the company technicians using the 'Fassanet Solid System', which is a glass fibre–reinforced mortar (GFRM) system that can be used to strengthen masonry structural elements. It is composed of: (1) a mesh of fibber glass 'Fassanet ARG plus' (Figure 7-1a), (2) natural hydraulic lime mortar reinforced with fibers 'Malta Structturale NHL 77' (Figure 7-1b), (3) L shape connectors 'Fassa Glass Connector L' (Figure 7-2a) and (4) chemical anchorage namely 'Fassa Anchor V' (Figure 7-2b).



(a) (b)

Figure 7-1. Strengthening system; (a) Mesh of fibber glass and (b) hydraulic lime mortar



(a) (b)

Figure 7-2. Strengthening system; (a) Connector elements and (b) chemical anchorage

Table 7-1. Mesh Fassanet ARG plus

Characteristics	Standards	Values according to technical sheets
Density	ISO 1183-1:2004	2,68 g/cm³
Tension strength	Linee Guida Ministeriali CRM	1173 MPa (medium) 1056 MPa (characteristic)
Average value of elastic modulus referred to the compressive section	Linee Guida Ministeriali CRM	68060 MPa
Average value of the ultimate deformation	Linee Guida Ministeriali CRM	1,71%

Fassanet ARG plus (Figure 7-1a) is a mesh of bidirectional fibber glass with impregnation treatment to make it resistant to the alkaline environment. It has 305 g/m^2 and mesh grid spacing of 38 ± 0.2 mm. It is recommended to repair and to strengthen masonry elements as walls, vaults, arches, almost others because give high ductility at masonry. Table 7-1 and Annex 7.1 include the complete technical information.

Malta Structturale NHL 77 (Figure 7-1b) is a fibber reinforced mortar (FRM) with high pozzolanic activity, with natural hydraulic lime (NHL 3.5). classified sands, synthetic fibbers and additives to improve the plasticity and adhesion to the support of masonry, stone, tuff or others. It was supplied in especial bags with of approximately 25 kg. It can be used in combination with suitable reinforcement meshes, both in fiberglass and metal in the fibre reinforced mortar strengthening technique, for strengthening vaults and walls in brick, stone and tuff. Table 7-2 and Annex 7.1 shows all technical information.

Table 7-2. Mortar Malta Structural NHL 77

Characteristics	Standards	Values according to technical sheets
Density	EN 1015-10	2,68 g/cm^3
Flexion strength at 28 days	EN 1015-11	≥ 3 N/mm^2
Compression strength at 28 days	EN 1015-11	≥ 10 N/mm^2
Static elastic modulus	EN 13412 - Method 2	≥ 7.000 N/mm^2

Fassa Glass Connector L (Figure 7-2a) is a pre-formed L-shaped connector made with fiberglass and epoxy resin, roughened with mineral quartz. It is supplied in boxes with 50 pieces, and it is available in different lengths. It is used to connect the layers of mortar reinforced with fiberglass mesh in the GFRM strengthening technique. This connector can be cut with wire cutters to achieve the desired length. The technical information is shown in Table 7-3.

Table 7-3. Fassa Glass Connector L

Characteristics	Standards	Values according to technical sheets
Lengths	-	200, 380, 500, 700 mm
Compressive resistant area (resin + fibber)	-	20 mm^2
Equivalent diameter of the bar	CNR-DT 203/2006	7,8 mm
Ultimate tension resistance of fiber	Linee Guida Ministeriali CRM	1120 MPa (average) 1062 MPa (characteristic)
Tensile stiffness modulus- medium value	Linee Guida Ministeriali CRM	44.713 MPa

Fassa Anchor V (Figure 7-2b) is a chemical anchorage based on vinylester resin without styrene, suitable for any type of masonry to fix the structural connector of fibbers and anchoring of metal bars in holes made on building materials such as concrete, stone, solid/semisolid/ hollow brick and wood. It can be used for vertical and horizontal fixings with variable anchoring depth and can be used on dry,

wet or flooded holes. The resin has high adhesion value and easy penetration into porosities and hollow areas allowing a safe fixing without expansion and, therefore, without tension in the base material during installation. It is supplied on boxes of 12 cartridges of 400 ml each.

The application of the strengthening solution requires the use of different tools and equipment's such as construction scissors, driller machine with drills of 14 mm and 20mm, metallic trowel, rock hammer, caulking gun, metallic rule, mini angle grinder, mortar mixed machine, among others (Figure 7-3).



Figure 7-3. Tools and equipment's

7.3.1 Description of strengthened process

As mentioned previously, the glass fibre–reinforced mortar (GFRM) technique was applied on the masonry vault at both intra and extrados, using a mesh of fibber glass, lime mortar and anchorages connections with L connectors fixed with chemical anchorage.

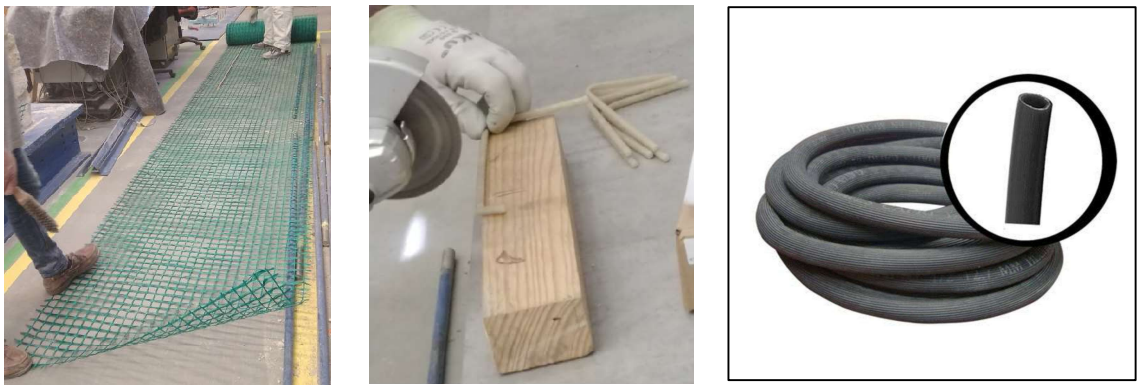
The optimization of the performance of the reinforced system requires the development of good adhesion between the new and existing mortar. For this, a rough and clean surface is necessary and for this reason, it was necessary to remove the existing plaster on both intra and extrados until to achieve a rough surface (Figure 7-4).



(a) (b) (c)

Figure 7-4. Removal of existing plaster (a) at intrados, (b) at extrados and (c) rough and clean surface

All necessary materials were prepared and cut at exactly size before starting the strengthening process as shown in Figure 7-5. The mesh should be only one piece to cover intra and extrados, L-shape connectors should have a length equal to the vault thickness. The mesh was extended until the extension of the lateral walls. Protector hose should be placed on holes to avoid mortar filling during the strengthening process.



(a) (b) (C)

Figure 7-5. Preparation of materials (a) mesh, (b) L-shape connectors and (c) protector hose

The anchorage position was suggested by the company´s technicians (Fassa Bortolo). The general criterion was to distribute the L-shape connectors along the span and length of the vault with a space close or lower than 50 cm, see Figure 7-6. For this strengthening, it was necessary to perform two types of anchorages (1) double L connector assuring the connection of the mesh simultaneously at the intra and extrados and (2) single L connector on superficies with a thickness bigger than the length of the connector.

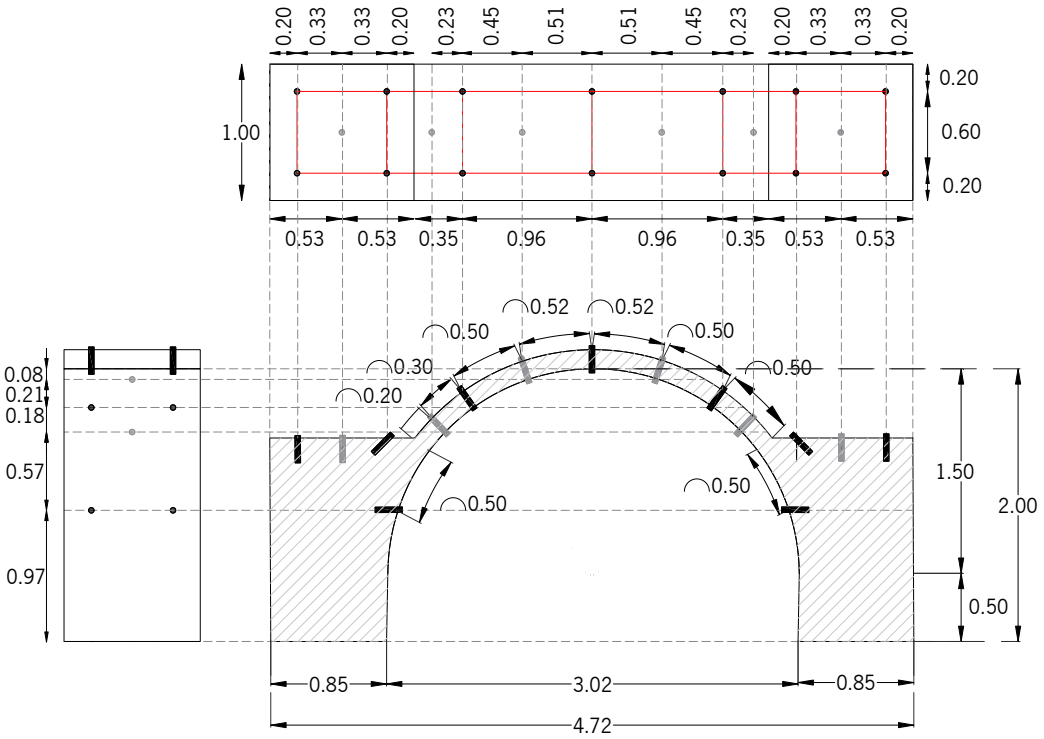


Figure 7-6. Anchorage position. In plant view, elevation view and intrados view

The double L connector are composed of two L-shape connectors crossing the total thickness of the vault, see Figure 7-7a. In the top of the wall's extension, single L connectors were considered with a minimum depth of 20 cm, see Figure 7-7b. The anchorages in the wall located at the top and near the vault-wall connection need to be made diagonally, that is, parallel to the direction of the tension stresses (see point A in Figure 7-7b).

The double L connector involves the use of two L-shape connectors introduced at the same point from intra and extrados of the vault. The injection of the FASSA ANCHOR V chemical fixing must be applied in the entire overlapping length of the two connectors (thickness of the vault equal to 15 cm). It is recommended to check that the holes allow easy insertion of the second connector.

For the Single L connection (Figure 7-7b), it is advisable to insert the FASSA GLASS CONNECTOR L into the hole after filling 75% of its volume with FASSA ANCHOR V chemical fastener. After inserting the connector, the filling of the hole was complete up to the outer face of the masonry. It is recommended not to force the insertion of the connector inside the hole beyond the point of contact of the bend with the reinforcement mesh to avoid deleterious flatness defects of the mesh itself.

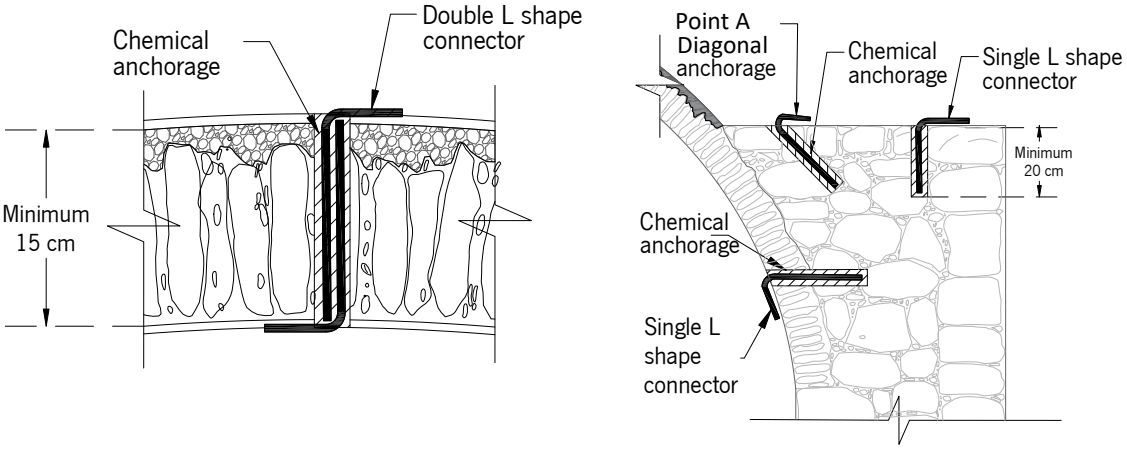


Figure 7-7. Anchorage of the mesh to the structure; (a) double L connector and (b) single L connector

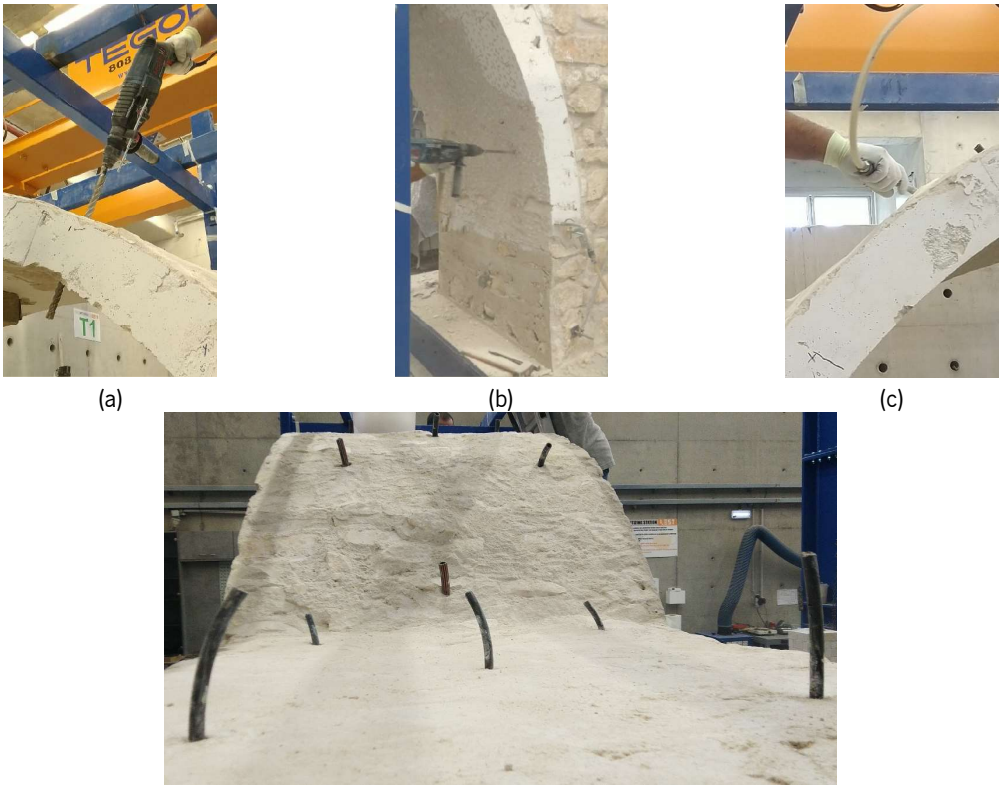


Figure 7-8. Preparation of the anchorages; (a) drill on vault, (b) drill on walls (c) clean with air and (d) protective hose placement

Before the placement of the L-shape connectors and the chemical anchorage, a hole was drilled, cleaned with pressed air and a protector hose was placed inside the hole, see Figure 7-8. Finally, after the drilling process, the structure looked as shown Figure 7-9 and it is ready for the application of the reinforcing mortar and embedding the mesh.



(a) (b) (c)

Figure 7-9. Prepared vault. (a) intrados left side, (b) elevation view and (c) intrados left view

The mortar was mixed in a mortar mixer machine until adequate workability was achieved, see Figure 7-10a. Throughout the entire strengthening process, the quality control of the mortar was carried out through: (1) mortar workability tests in the fresh state, see Figure 7-10b and (2) flexural and compression tests on specimens with 4 x 4 x 16 cm, seeFigure 7-10c.



(a) (b) (c)

Figure 7-10. Quality control of the mortar (a) mortar preparation, (b) mortar workability tests and (c) preparation of test specimens

To avoid loss of water in the mortar before its application it was necessary to wet the existing mortar surface (Figure 7-11a). In this process, some protections were placed to avoid water spread of water through equipment if the laboratory, see Figure 7-11b.



(a) (b)

Figure 7-11. (a) wetting of the structure and (b) protection of the space



(a) (b)



(c) (d) (e)

Figure 7-12. Strengthening process (a) projection of mortar, (b) uniform distribution of mortar layer, (c) embedment of the mesh on fresh mortar, (d) insertion of the L-shape connectors and (e) second layer of mortar

The strengthening of the stone masonry vault involved the following steps: (1) projection of mortar as a uniform layer of mortar with a thickness of 15-20 mm (Figure 7-12a and b), (2) embedment of the mesh on fresh mortar by applying pressure with a metallic trowel assuring that the mortar comes out of the holes of the mesh, see Figure 7-12c, (3) removal of the protector hoses and insertion of the L-shape connectors as described before , see Figure 7-12d, (4) covering the mesh with a second layer of mortar with a thickness of 15-20 mm , see Figure 7-12e. The mesh was placed in the middle of the

total thickness (excluding the levelling of the support). The process was completed with the smoothing of the surface with a plastic trowel in order to compact the mortar.

7.4 Experimental setup and loading protocol

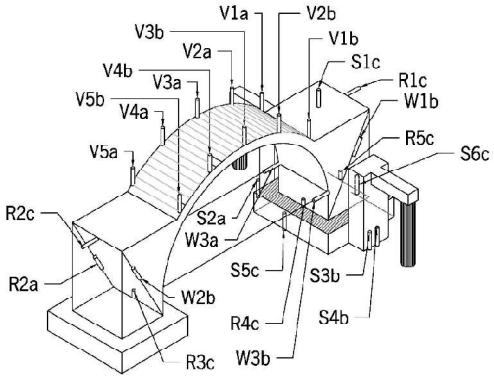
The experimental test of the retrofitted experimental model was carried out under the same conditions of the reference (unreinforced) model. Load damage was induced with the application of induced vertical displacement on one support, simulating a vertical settlement. The test was performed under displacement control through two hydraulic jacks considering a linear increasing displacement history. The test was carried out at a displacement rate of 0.008 mm per second.

From the observations carried out on the unreinforced model, few changes on the instrumentation setup and photographic record design were decided and both are explained in this section.

7.4.1 Instrumentation of the experimental model

The general instrumentation adopted test of the unstrengthen model was preserved, namely the two actuators with a capacity of 300 kN each, 21 Linear Variable Differential Transformer (LVDT) devices to record: (1) the induced vertical displacement, (2) the in-plane rotation of the model, (3) deformation of the walls and (4) the deformation of the vault.

Nevertheless, as mentioned in Chapter 7, some information was missing about: (1) the possible uplift of the wall regarding to the steel platform where the induced vertical displacement is applied; (2) the possible in-plane rotation of the steel base at the left wall. Therefore, more 4 LVDT were added at the instrumentation setup, reaching to 25 the monitored points in the experimental model; (i) LVDTs R4 and R5 measured the wall uplift; (ii) LVDTs S5c and S6c measured the possible rotation on the lifting platform, see Figure 7-13.



Nomenclature:	
Objective of measurement	**Code of control**
Rotation control	R
Settlement control	S
Vault	V
Wall	W

Figure 7-13. Increased LVDT in instrumentation setup

7.4.2 Photographic record design

The photographic record design was conditioned by the number and format of cameras available. Six camaras were available. Based on the capabilities and limitations of each camera, the best configuration for the photographic record was sought. Cameras 1, 2, and 3 were placed to record the damage in the theoretical places of the hinges and were programmed to capture a photo every 2 seconds. Cameras 2 was controlled with the open-source program namely digiCamControl by Duka Istvan, whereas cameras 1 and 3 were controlled with the open-source namely Open Camera V1.48.3. Camera 4 recorded a video of the full views and finally, cameras 5 and 6 were mobile cameras to record additional details along the test (Figure 7-14).

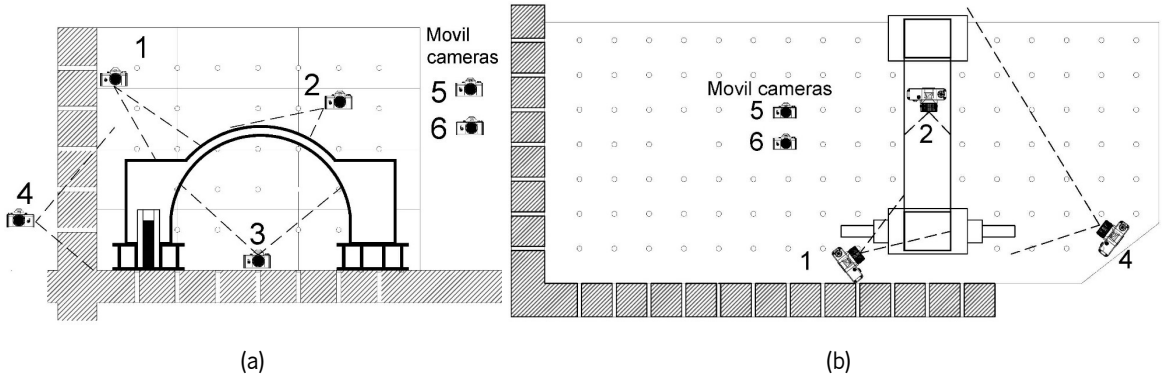


Figure 7-14. Photographic device positions (a) elevation view and (b) plant view

7.5 Analysis of experimental results

The experimental test on the retrofitted structure lasted for 117 minutes (1h 57 min) and the maximum induced vertical displacement was 41.16 mm. The analysis of the displacement records was carried out by considering the up and right displacements as positive in all diagrams, see Figure 7-15.

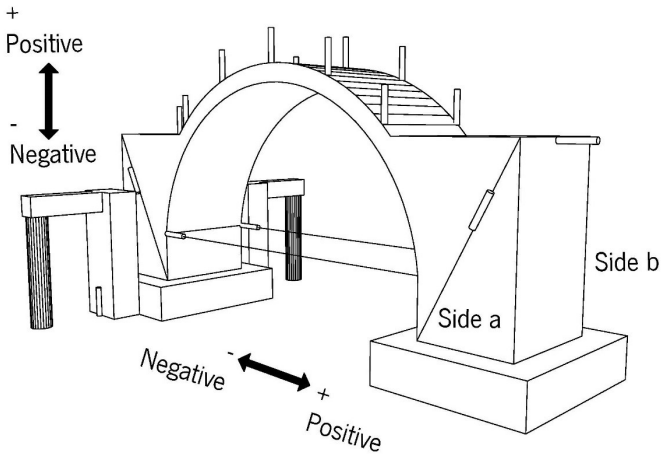
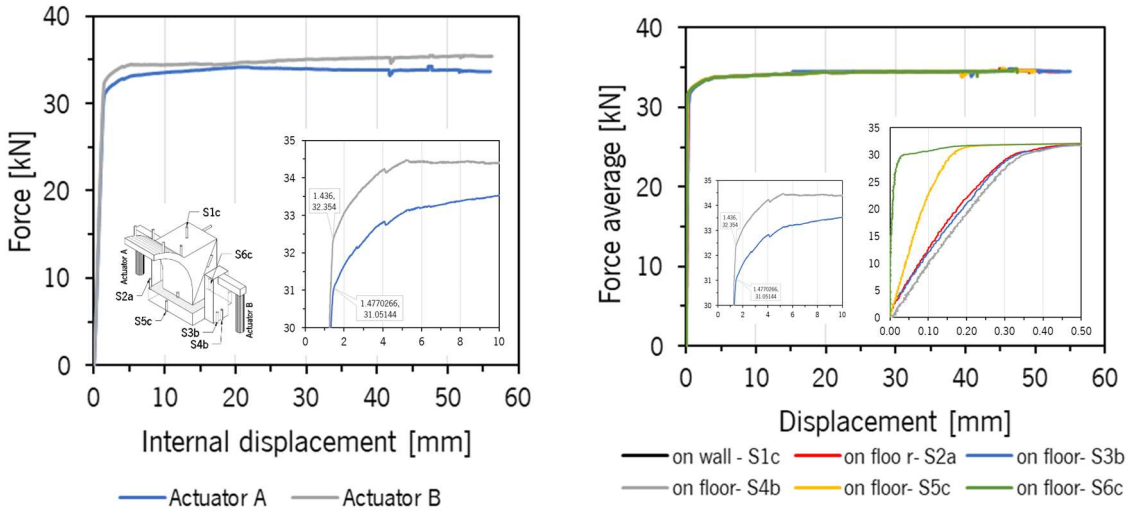


Figure 7-15. Definition of displacement signs

The analysis of the results is divided mainly in two stages: (1) validation of the experimental procedure. For the validation of the experimental test, all control points at the steel base and of the hydraulic jacks were considered; (2) analysis of the displacement patterns exhibited by the model, taking into account the displacement measured in key points located in the masonry walls and vault. In addition, crack pattern analysis and the collapse mechanism were also analysed.

7.5.1 Validation of the experimental test

The validation of the test setup implies the analysis of the: (1) forces measured by the vertical actuators; (2) displacements measured by external control LVDTs at the steel base where the induced vertical displacement is applied. The diagram relating the force measured by the load cells attached to the hydraulic jacks and the displacement of the internal transducers are shown in Figure 7-16a. It is observed that forces measured by the load cells in both actuators are very close, see Figure 7-16a. The maximum difference between the forced measured is about 1.8kN (5%). The effective vertical displacement applied in the left wall of the experimental model started when the actuators achieved in average 31.5kN. The maximum load was about 34.26kN and 35.48kN in actuators B and A respectively. That load is approximately the half of the structure's weight and corresponds to the reaction in the displaced support.



(a) (b)

Figure 7-16. Evolution of the experimental test (a) force regarding to induced displacement records by internal transducers of the actuator and (b) force regarding to settlement control point in the steel base

To avoid in-plane and out-of-plane rotation of the steel base where the vertical displacement was applied, the uniform lifting of the platform was essential, being this condition monitored by the LVDTs placed in the control points at the steel base (LVDTs S). LVDT S1 was placed at the top of the wall to

measure possible uplift, and LVDTs S2a to S6c monitored the in-plane and out-of-plane displacement of the steel base (Figure 7-16b). Figure 7-17a displays the relation between the vertical displacements measured at the steel base and the vertical induced displacement. It is observed that displacement measured at points S2a and S3b-S4b indicate that there are no important out-of-plane plane displacements (maximum 1.5mm, 2.9%), which is accordance to what it would be expected. It is also seen that these displacements in points S5c and S6c are slightly smaller the out-of-plane displacements but are of the order of the other displacement at the base. This means that the displacements of the steel base are very close, not showing significant in-plane and out-of-plane rotation at the beginning of the test. The evolution of these displacement with vertical induced displacement is shown in Figure 7-17.

It is possible to observe that displacements measured at points S5c and SF are practically overlapped until the vertical induced displacement reaches 30mm. After this stage, the vertical displacement at S6c is slightly higher than displacement in S5c (maximum 2.5mm, 6%). Displacement measured in points S2a, S3b and S4b are overlapped from the beginning of the test until approximately 3500s (58 min), see Figure 7-17b. After this stage, little differences were found between side A and B, which means that there is a little out-of-plane rotation, probably because the structure suffers some damage.

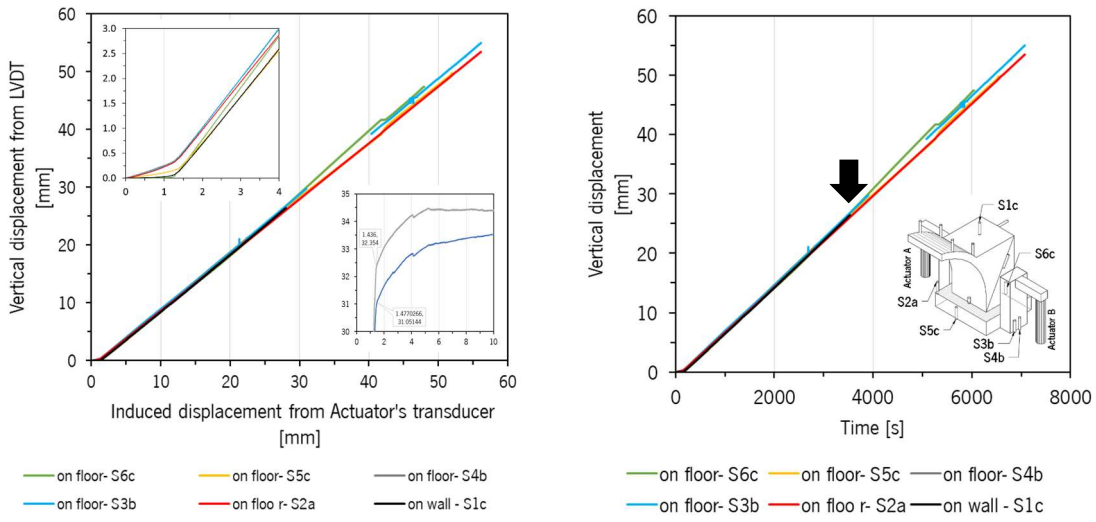


Figure 7-17. Evolution of the steel base´s displacements; (a) displacement comparison between internal transducer of the actuator and settlement control points and (b) Settlement control point behaviour though the experiment

Additional analysis was performed to assess the rotation's angle of the platform on both octagonal directions. For that, the rotation angle was calculated by dividing the difference between the opposite displacement by the distance between them. Table 7-4 shows that any observed rotation on the

platform is negligible since the rotation angles are really close to zero, which reveals the uniform lifting of the platform. The analysis of the rotation values in degrees allowed to observe that: 1) all displacements discussed in this section were really small, 2) the platform moves upwards uniformly, and no significant rotations developed.

Table 7-4. Platform rotation during the test

Moment	Time (s)	In-plane rotation S5c and S6c	Out-of- plane rotation S2a and (S3b-S4b)
A	162.7	0°0'0.36''	0°0'0.03''
B	662.7	0°0'1.02''	0°0'0.30''
C	1725.9	0°0'0.51''	0°0'0.52''
D	2097.4	0°0'1.47''	0°0'0.59''
E	2371.6	0°0'1.98''	0°0'0.64''
F	2685.9	0°0'1.80''	0°0'0.74''
G	3529.8	0°0'0.95''	0°0'1.08''
H	3901.4	0°0'2.45''	0°0'1.26''
I	5265.5	0°0'7.21''	0°0'2.01''
J	6512.5	0°0'5.85''	0°0'2.38''
End of Experiment	7072.77	0°0'7.51''	0°0'2.64''

7.5.2 Analysis of the structural behaviour

The analysis of the structural behaviour of the strengthened experimental models is carried out based on the displacements measured at the different structural elements, namely: (1) at top and base of the walls and (2) in the masonry vault. The evolution of displacements is analysed together with the identification of the crack patterns developing in the structure.

The evolution of displacements of key points in walls and vaults as the induced vertical displacement increased is shown in Figure 7-18a. Throughout the experiment, ten critical moments were identified, which were named from A to J.

The structure started to exhibit significant displacements after 162s of the beginning of the test, being this moment identified as Moment A. At this stage, the vertical induced displacement is 0.25mm and corresponds to the point at which the half weight of the model is recorded in both hydraulic jacks. The structure tends to move in a monolithic way in the negative direction, as it can be seen from the analysis of the horizontal displacements at the top of the left and right walls (R1c and R2c), see Figure 7-18c and Figure 7-19a. The absence of cracks indicates that the tensile strength of the mortar is not yet exceeded, and the reinforcement is monolithic with the vault. At the stage, the displacement at the masonry vault is still practically zero.

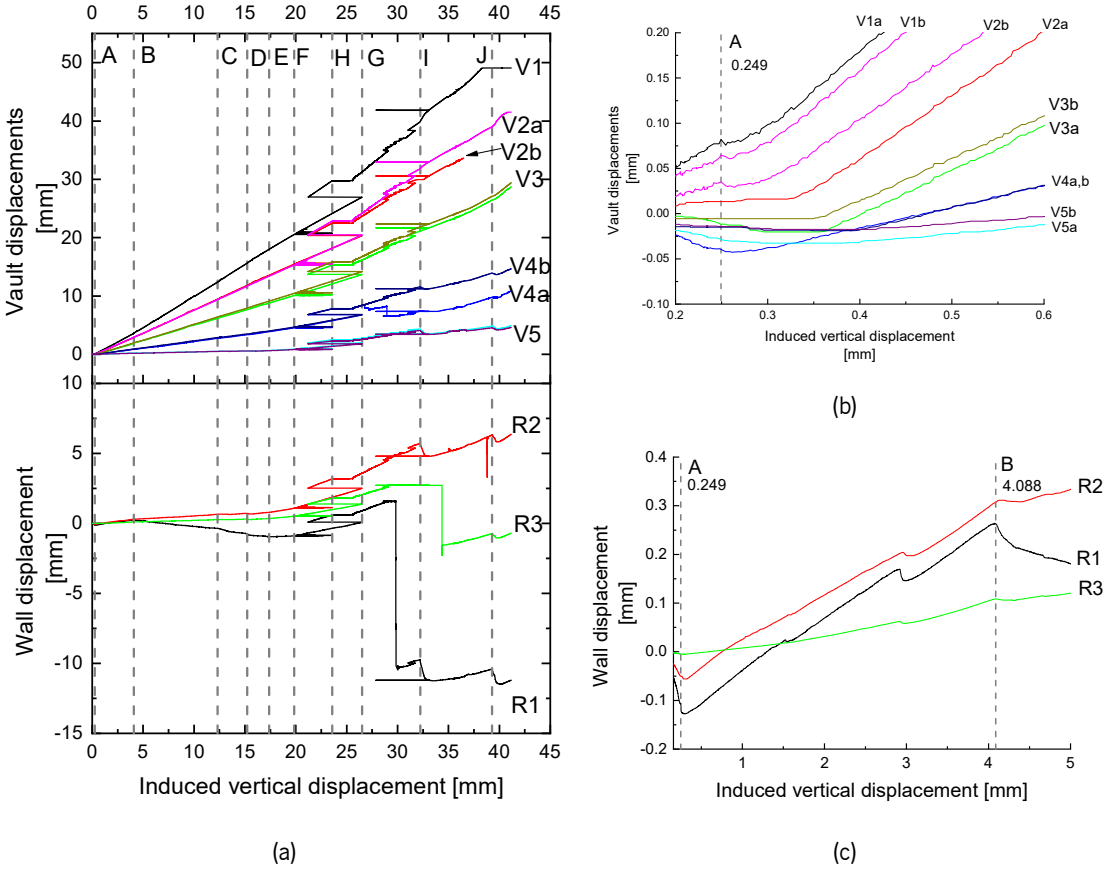


Figure 7-18. (a) Evolution of displacement in the masonry vault and walls for increasing induced vertical displacement. (b) Vault displacement close up view and (c) wall displacement close up view

The structural model appears to keep moving monolithically until the induced vertical displacement reaches the value of 4.09mm (Moment B), see Figure 7-19b. At this stage, the displacement at the top of the walls keep positive and simultaneously the displacement at the base of the right wall (R3c) is also positive (0.11mm) indicating the trend for the uplift of the left bottom corner. This is confirmed by the crack opened at the base of the right wall at the interface between mortar and the steel base, see Figure 7-20a. This means also that an hinge develops at the base of this wall (hinge A), as illustrated in the scheme shown in Figure 7-20b. According to Figure 7-18c and Figure 7-19c, the horizontal displacement at the top of the left wall becomes negative after this moment until reaching the value of -0.35mm, when the induced vertical displacement reaches the value of 12.2mm at 1725s (Moment C), see Figure 7-21a. This is associated to the opening of cracks at the vault-wall connections, which is also confirmed by the photographic record (Figure 7-22a). This means that an hinge B develops in the intrados of the wall-vault connection, see Figure 7-22b. The development of hinge B divides the structure into two large blocks: (1) the left wall supported by the steel platform and (2) the vault and the right wall. The horizontal displacements at the top of the walls (R1c and R2c) show that the blocks move in opposite direction confirming the presence of hinge B. Furthermore, vertical

displacement at the left corner of the right wall (point R3c) increases, confirming that hinge A is still active (Figure 7-19c and Figure 7-18c).

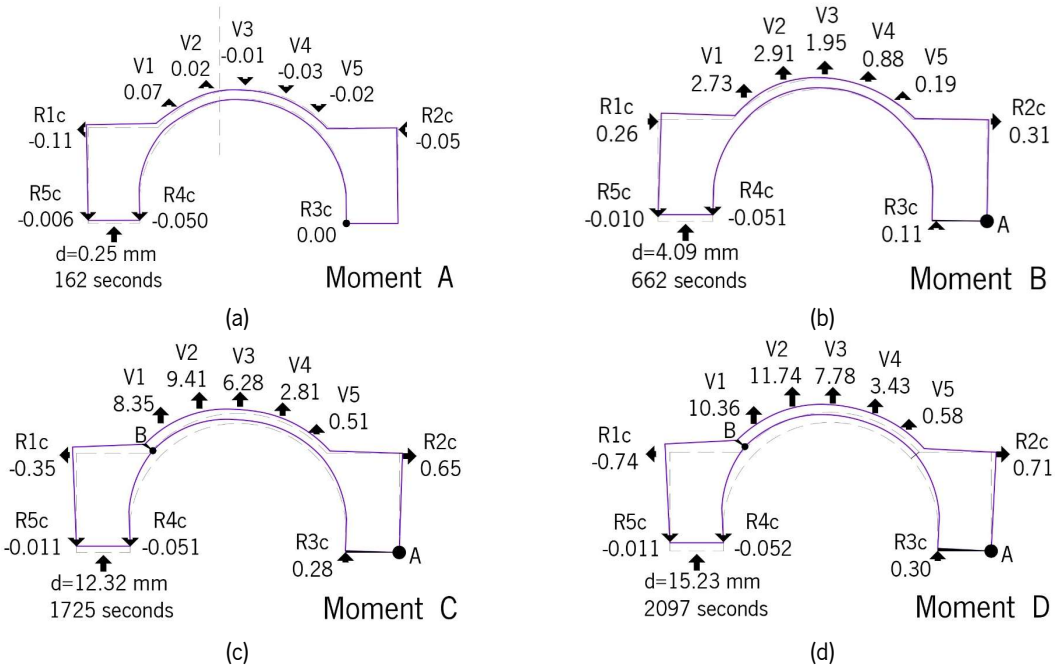
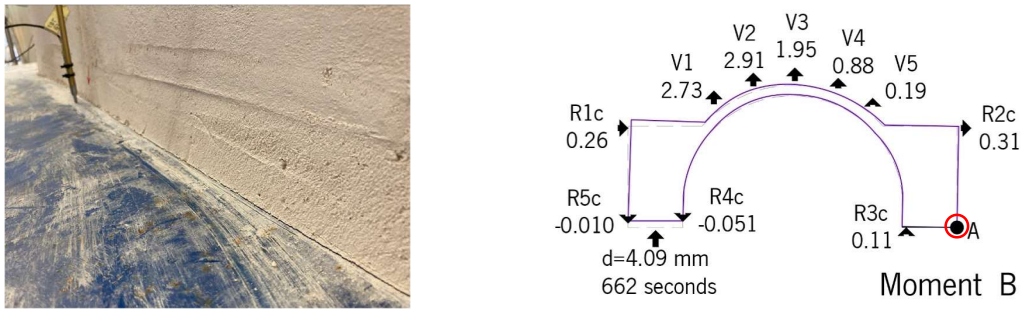


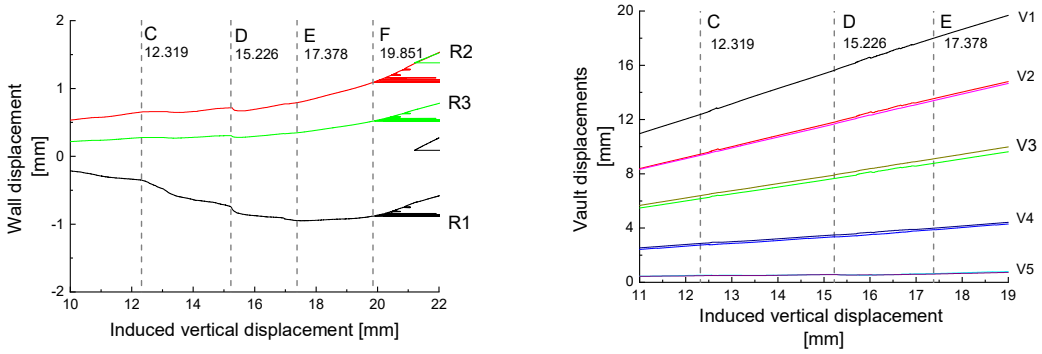
Figure 7-19. Deformation behavior of the model: (a) Moment A at 162s, (b) Moment B at 662s, (c) Moment C at 1725s, and (d) Moment D at 2097s

Between the induced displacement of 12.2mm (Moment C) and of 15.23 at 2097 s (Moment D), it is possible to observe that: (a) there is an increase on the lateral movement at the top of the left wall, which is associated to the relative displacement of the block at the left of the hinge B and the right block at the hinge B (Figure 7-19d). In fact, the control points R1c and R2c indicate that the two identified blocks are moving in opposite directions towards the outside, but the R1c slope increase which means R1c record greater displacements (Figure 7-21a); (b) vertical displacement at R3c continues to increase which means that the fixed support continues rising, (c) the vault continues to register upward displacements where V2 is the control point with the largest increase in displacements (2.34mm), see (Figure 7-19d and Figure 7-21b). This behaviour keeps rather similar until the induced vertical displacement reaches the value of 17.38s at 2371 seconds (Moment E), see Figure 7-23a and Figure 7-21a and b.



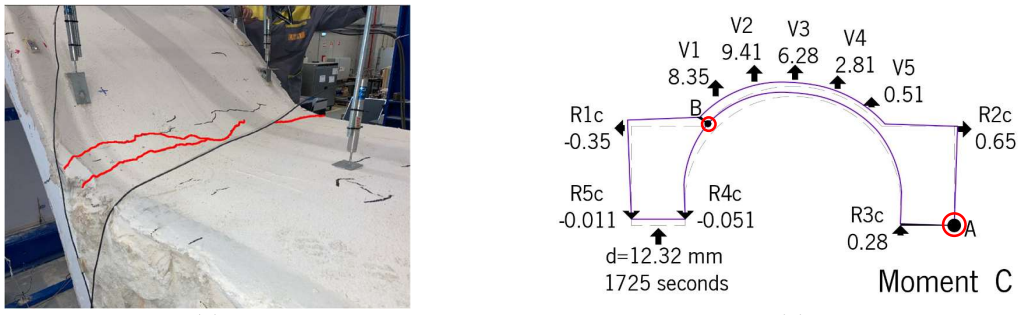
(a) (b)

Figure 7-20. (a) Crack the at the base of the right wall; (b) scheme of the hinge at the base of the right wall



(a) (b)

Figure 7-21. Displacement of the model at Moments from C to E. (a) R points plot and (b) V points plot



(a) (b)

Figure 7-22. Development of hinge at the vault-wall connection; (a) cracking at the vault-wall connection, (b) scheme of hinge B

It is important to note that the increase in the horizontal displacements at the top of the left wall (R1c) continues as the result of the continuous opening of the hinge B, whereas the displacement increases also at point R2c, see Figure 7-23a. After this stage (Moment E), the horizontal displacement measured at the top of left wall (R1c) started to decrease at a very slow rate, being then the maximum of the displacement measured at moment E, see Figure 7-21a. It is after the induced vertical displacement reaches the value of 19.85mm at 2685 seconds (Moment F) that the lateral displacement measured at R1c started to decrease at much higher rate. This is, in turn, followed by the higher increasing rate of displacement measured at R2c and R3c, see Figure 7-24a.

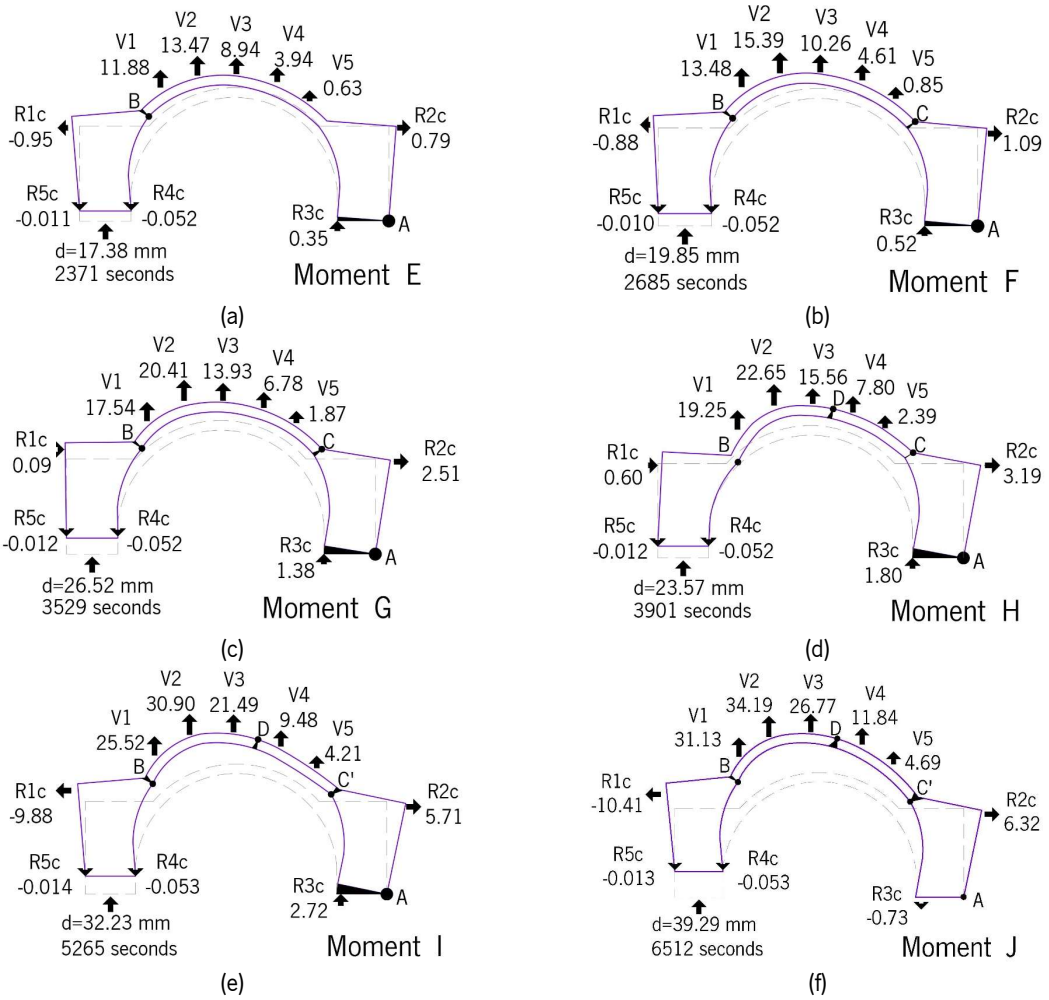
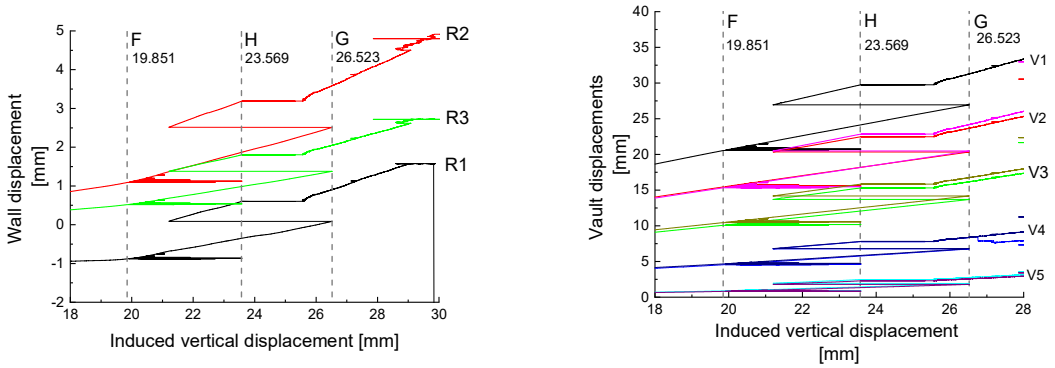


Figure 7-23. Deformation behaviour of the model: (a) Moment E at 2371s, (b) Moment F at 2685s, (c) Moment G at 3529s, (d) Moment H at 3901s, (e) Moment I at 5265s and (f) Moment J at 6512s

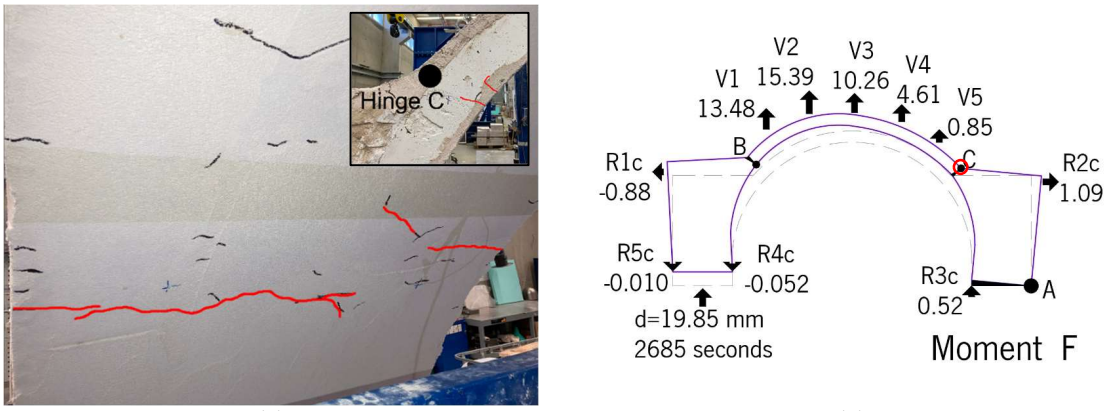
It should be mentioned that just at this stage (moment F), something happened to the structure, since sudden and repetitive movements were recorded in displacements measured both at walls and vault, see Figure 7-24. Moreover, the behaviour of displacement measured at the top of the left walls (R1c) suggests that hinge B is closing (compare Figure 7-23a and f). The analysis of the photographic record reveals that the third hinge appeared on the extrados of the vault-right wall connection, probably due to the concentration and redistribution of forces in the block on the right side. The new hinge was named hinge C, see Figure 7-25b.

The cracks developed at the intrados in the vault-right wall connection are firstly very thin and are marked in Figure 7-25a. The opening of cracks should be the result of the progressive failure of the reinforcing mesh, which was also responsible for the zig-zag displacements measured in all displacement transducers (Figure 7-24).



(a) (b)

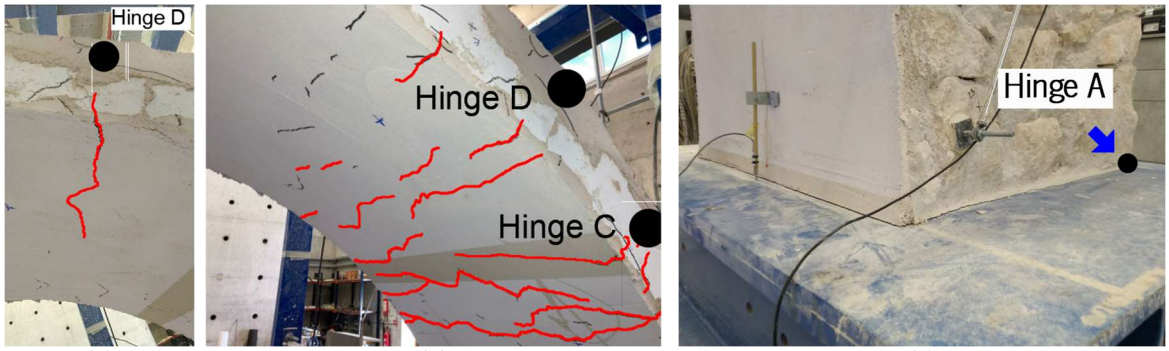
Figure 7-24.Displacement of the model at Moments from F to H. (a) R points plot and (b) V points plot



(a) (b)

Figure 7-25. Moment F with 19.85mm of induced displacement. (a) LVDTs records and (b) behaviour description, (c) hinge C locations and damage

After the displacements stabilize, there is an almost linear increase of the displacement measured at the walls (R1c, R2c and R3c) until the induced vertical displacement reaches the value of 26.52mm at 3529 seconds (Moment G), see Figure 7-24. At this stage, the horizontal displacement at the top left wall (R1c) is practically zero, meaning that it recovered practically the initial position and consequently, hinge B should be closing (Figure 7-23c). After the closure of the hinge, a new configuration of the thrust line develops, leading to the increase of displacement at points R3c and R2c (compare Figure 7-23b and c), resulting from the opening of cracks at hinge A and C. The redistribution of stresses appears to be the cause of the zig-zag displacements observed at moment G, leading to the reduction of the induced vertical displacement from 26.52 for 23.57mm, increasing then up to 23.57 at 3901 seconds (Moment H), see Figure 7-24. This stage is attributed to the opening of new cracks located between points V3 and V4 in the vault, being thus identified a new hinge D, see Figure 7-23d. The presence of a new hinge was supported by the photographic record (Figure 7-26a). Since the new hinge appears at the extrados, it is believed that the presence of hinge D results in the sudden closure of hinge C, which explains the rebound effect observed in the graphs (Figure 7-24).



(a) (b) (c)

Figure 7-26. (a) Damage corresponding to hinge D, (b) relative location of hinges D and C locations and (c) hinge A location

This may be also associated to the incapacity of the control system to sustain the vertical induced displacement during the sudden failure of the reinforcing mesh at intrados of the vault. It is stressed that at this stage (Moment H), the horizontal displacement at the top of the let wall is now positive, confirming again the closure of hinge B. At the same time, it is observed that the hinge A continues to open (Figure 7-23d and Figure 7-26).

The structural configuration of the experimental model changes between the Moment H and Moment I (induced vertical displacement equal to 32.23mm at 5265 seconds), in which a considerable increase of the vertical displacements on the vault, namely displacement V2, are observed, see Figure 7-27. Firstly, it was observed that the next 2mm after Moment H, the model shows a period of inactivity, that is, no deformations were recorded in walls. This is identified as horizontal lines in the graphic that relate the induced vertical displacement with the displacements measured in points R1c, R2c and R3c, see Figure 7-24a. In contrast, the vault shows small zigzag movements on the graphs from 23.57mm until Moment I is reached, see Figure 7-28b. When the induced displacement was about 30mm, the displacement at point R1c exhibits a sudden drop, from 1.5mm to approximately -9.88mm, see Figure 7-23e and Figure 7-28a, being associated to a sudden movement of the left wall from right to left (compare Figure 7-23d and f). This movement appears to be the result of the progress of the crack developed at the right wall-vault connection, where hinge C was located, but according to the photographic record, this appeared at the intrados, and it was assigned to hinge C'. A view of the progress of the extrados cracking at the right wall-vault connection is displayed in Figure 7-29a. It is believed that the opening of hinge C' made hinge B active again, see Figure 7-23e and f.

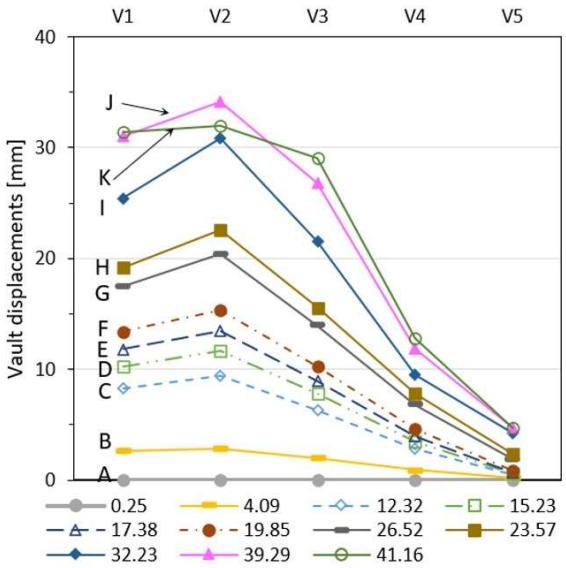
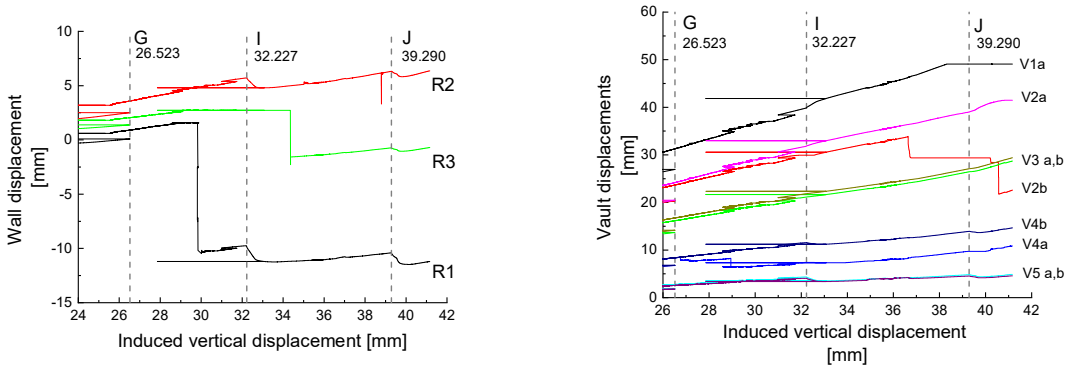
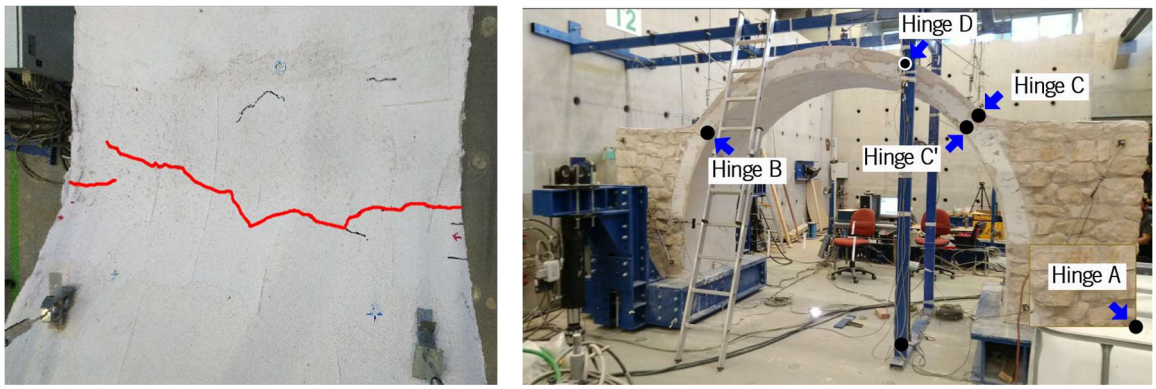


Figure 7-27. Evolution of the vertical vault´s displacements



(a) (b)

Figure 7-28. Displacement of the model at Moments from G to J. (a) R points plot and (b) V points plot



(a) (b)

Figure 7-29. (a) Progress to the extrados of cracking related to hinge C' and (b) general view of the four hinges

It is important to note that at this moment, the model became a mechanism with four hinges. All these changes experienced by the model are reflected in a large number of zigzag and abrupt readings in the wall's and vault's displacements diagrams (Figure 7-28).

The experimental test continued until the induced vertical displacement reached 39.29mm at 6512 seconds (Moment J). At this stage, the left wall continues to register negative displacements that tend to open the vault, but at a slower rate, which suggests that the hinge B is active and continues to open, but slowly, see Figure 7-23f. The vault continues to register positive vertical displacements indicating that it is moving upwards. The control point V2 registers again the maximum displacement equal to 34.19mm. At this moment, the relative displacement of V2 is approximately 7.31mm, see Figure 7-27. The hinge A at the base of the right wall appeared to close, as displacement at the left bottom corner (R3c) abruptly changes from positive to negative values (Figure 7-23f and Figure 7-28a). This should be associated to the spreading of cracking at mid height of the right wall. With all of the above, it can be noted that, in order to reach equilibrium, the model has closed hinge A, while the hinge C' and D remain active. That is, it has reverted to a failure mode of three hinges, B, C' and D.

7.6 Assessment of the retrofitting effectiveness

As presented in the beginning of this chapter, among possible techniques to rehabilitate and strengthening masonry structures, there has been an increasing interest in composite fibre materials, commonly known as fibre-reinforced polymers (FRP), as they easily adapt to the surface to be strengthened, on the external face of the element locally (e.g. strips) or to the whole surface of the structure (e.g. grid reinforcement). The bond to the masonry is normally obtained with the use of epoxy resins or mortar. Composite materials made with grid reinforcement both with polymeric and cementitious matrices are often adopted for the retrofitting of masonry arches and vaults.

In this research, fibreglass grids embedded in mortar (GFRM) and fibreglass FRP bars as anchorage ties were used. The performance of ancient masonry vaults strengthened with GFRM was previously analysed and discussed in this chapter. But in this section a comparative analysis of the structural behaviour before and after strengthening is analysed at the level of displacement patterns and is presented. The analysis involved: (1) the evolution of displacements and (2) formation of hinges and collapse mechanism. According to literature, when the hinges are formed, they subdivide the vault structure in different blocks with rigid body movements (Cancelliere et al., 2010) but when composite material is bonded at the structure, both at the intrados or extrados, the collapse mechanism changes and the thrust line can be external with respect to the arch thickness (Zampieri et al, 2018), which modifies significantly the structural behaviour. As long as the thrust line remains inside the vault thickness, the vault is only compressed, but when cracks appear, the thrust line touch the vault thickness edge, which indicate the formation of an hinge in the opposite edge of the crack. The collapse

of a masonry vault is linked with the development of four or five alternate hinges (Borri et al., 2009). In retrofitted vaults the strengthening modifies the type of collapse mechanism, which can be linked with: 1) the damage observed in masonry vault, 2) the failure of the composite materials or 3) on both damage masonry and composite elements (Zampieri et al., 2018).

Figure 7-30 allows compare the displacement exhibited by the control points considered at the walls, namely in points R1c, R2c and R3c, in the reference (BS) and retrofitted models (AS). It is observed that the evolution of the key displacement placed at the walls is completely different in BS and AS models. The reference model shows deformations at very early stages of the experimental test. It is observed that the major events develop for an induced vertical displacement of 5mm, being the model stabilized after this. The maximum displacement of 16mm is recorded at the top of the left wall, whereas keys points considered in the right walls (R2c and R3c) record the smallest displacements with less than 1 mm (Figure 7-30a).

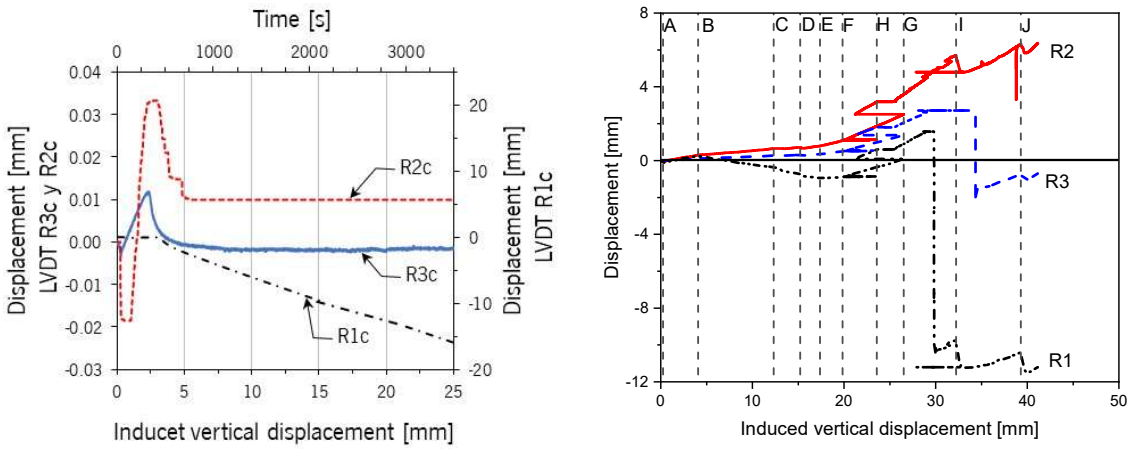
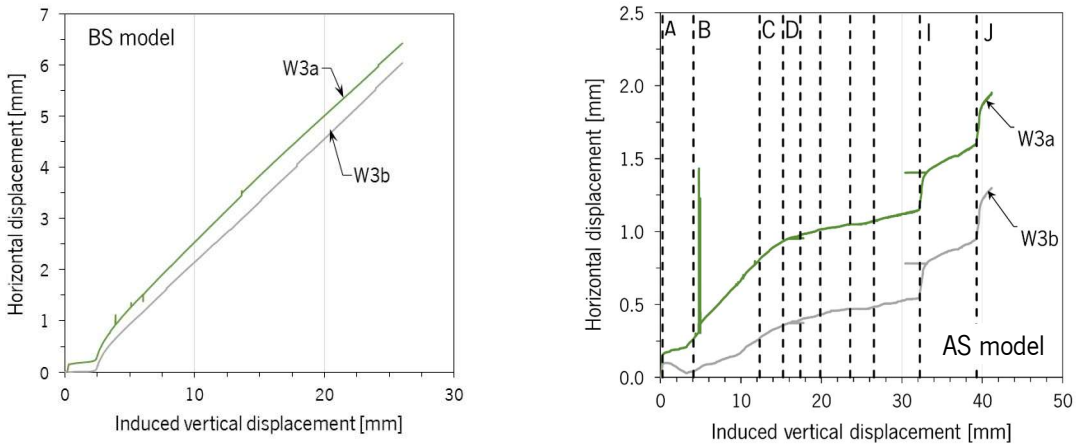


Figure 7-30. Evolution of displacements of key points in walls (a) experimental model and (b) strengthening experimental model

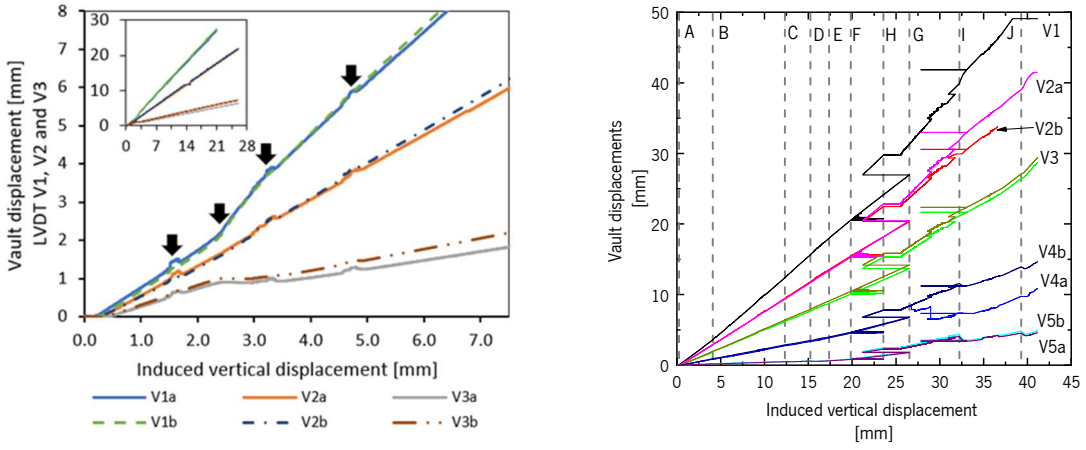
In turn, the displacements measured in these key points in the AS model are very low but exhibit a trend for increasing after the induced displacement of 5mm (Figure 7-30b). This means that the retrofitted model is considerably stiffer compared to the reference model. This feature is also confirmed by the considerable higher separation (given by displacement measures as W3a and W3b) of the masonry walls in the BS model when compared to the AS model, see Figure 7-31. It appears that the addition of the fibber glass meshes stiffened the walls to vault connection, leading to the reduction of the spacing between masonry walls. This results directly also from the much lower rotation of the left wall in case of AS model. The evolution of the spacing between the stone masonry walls is also much more complex in case of AS model. In BS model, the evolution of the spacing between

walls increases linearly, whereas in AS model the evolution is not uniform, being the rate of spacing variable and related to the opening and closing of hinges. Indeed, a sequence of events occurs during the complete duration of the experimental test the retrofitted model (maximum displacement of 45mm) corresponding to the development of cracks and corresponding hinges. In case of the reference model, three hinges develop for very low displacements, being then the displacements measured the result of the movement of different rigid blocks.



(a) (b)

Figure 7-31. Evolution of the spacing between stone masonry walls measured by W3a and W3b displacements: (a) BS model; (b) AS model



(a) (b)

Figure 7-32. Evolution of displacements of key points in vaults (a) BS experimental model and (b) strengthening experimental model (AS model)

Figure 7-32 shows the evolution of displacements on vault key points as the induced vertical displacement increased both for BS and AS models. It is clear that in BS model the vertical displacements are about 30mm but in AS model the displacement are in the order of 50 mm. An increase of approximately 70% in displacement capacity is observed due to strengthening. This behaviour is mostly due to the improvement of the walls to vault connections, which avoid early

development hinges at the walls-vault connection, as it happens in the BS model (hinge C at 2.34mm), see Figure 7-33. In fact, in the AS model, the first hinge developed at the base of the right walls, where there is no retrofitting, see Figure 7-33d. The second hinge at the left wall-vault connection only develop for an induced displacement of 12.32mm Figure 7-33f. This means the retrofitting technique increases the settlement capacity by 9.98mm (426%) before the hinge B develop.

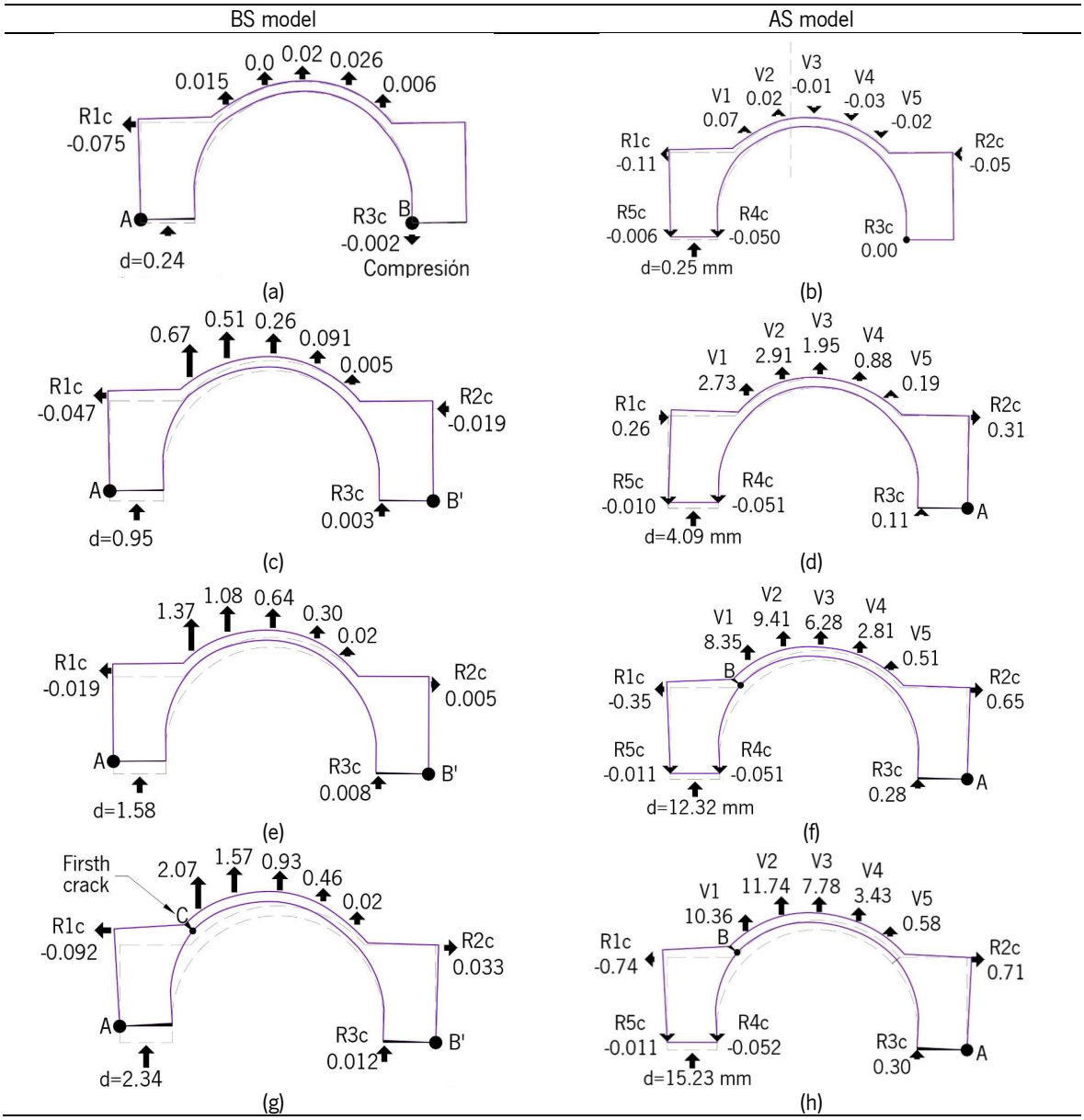


Figure 7-33. Comparative behaviour between the BS model and AS model (a) Moment A of the BS model, (b) Moment A of the AS model, (c) Moment B of the BS model, (d) Moment B of the AS model, (e) Moment C of the BS model, (f) Moment C of the AS model, (g) Moment D of the BS model, (h) Moment D of the AS model

This is in fact appeared to be a re-opening of the hinge C developed in the BS model. As mentioned previously, after the induced displacement was released in the BS model, the cracks closed, and it was not possible to inject them with mortar grout.

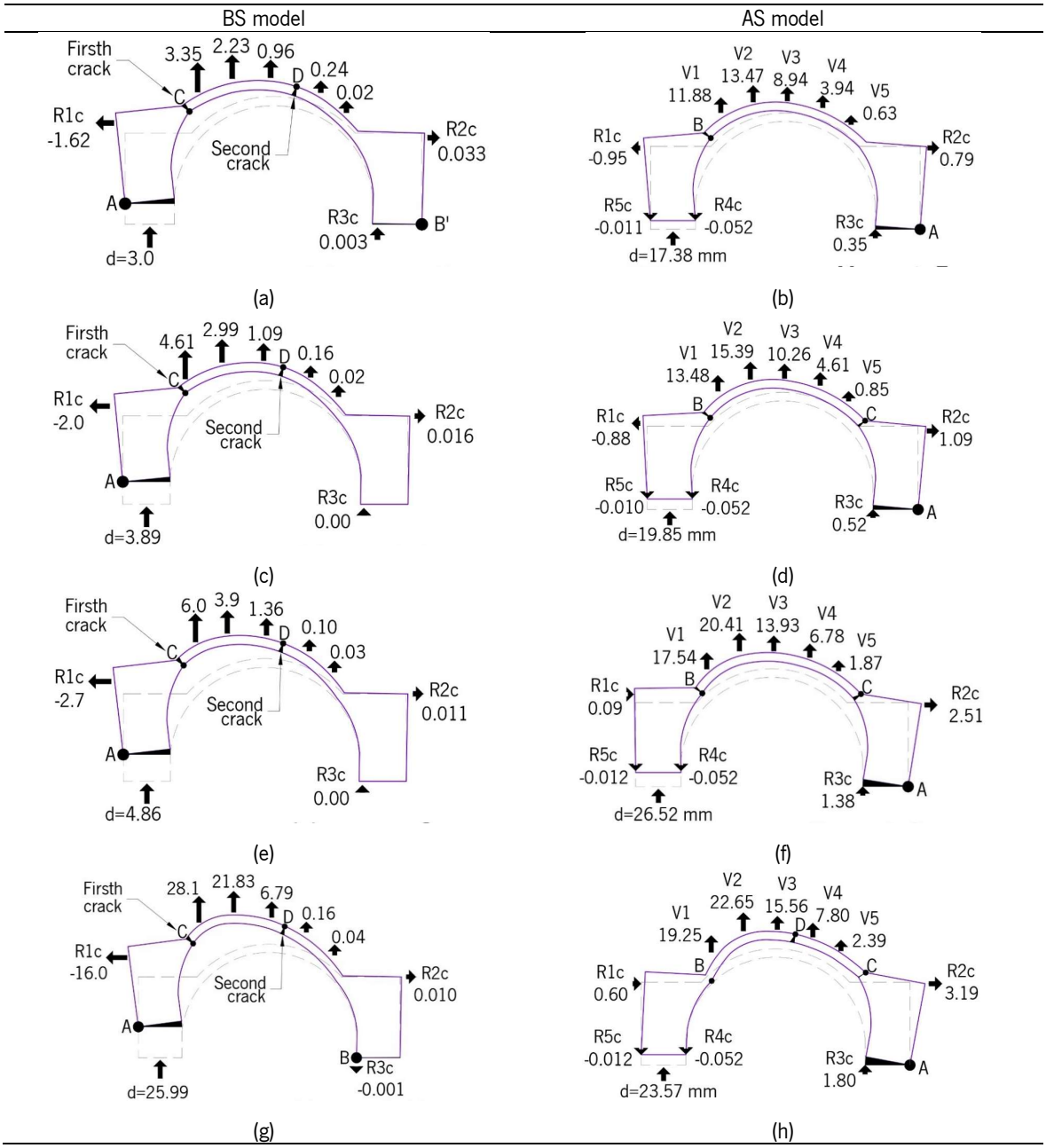


Figure 7-34. Comparative behaviour between the BS model and AS model (a) Moment E of the BS model, (b) Moment E of the AS model, (c) Moment F of the BS model, (d) Moment F of the AS model, (e) Moment G of the BS model, (f) Moment G of the AS model, (g) Moment H of the BS model, (h) Moment H of the AS model

In the experimental test of BS model two cracks were identified in the vault, corresponding to the development of two hinges at intra and extrados, whereas two others were identified on the supports. The behaviour of AS model is rather more complex. The AS model experienced very different displacement patterns and sequence of hinges formed at different locations. The formation of hinges C, D and C' results from the cracking of the reinforced cover (intra and extrados) and progressive failure of the fiberglass mesh. This type of cracking is responsible for important zig-zag patterns observed in the walls and vaults key measurements points. It is also important that the crack opening in the retrofitted model is accompanied by stress redistributions. The formation of hinge C (third hinge)

only occurs for an induced vertical displacement of 19.85mm at 2685s, see Figure 7-34d. The fourth hinge developed when cracks started to open between the key points V3 and V4 in the vault (hinge D). This occurs for an induced displacement of 23.57mm (Figure 7-34h). It should be noticed that hinge D in the AS model is in the same zone where a continuous crack developed in BS model, corresponding also to the formation of an hinge (hinge D), see Figure 7-34a. When hinge D develops in the AS model, hinge B close suddenly and lead to a zig-zag displacement patterns in the main walls and vault key measurements points. It is important to notice that the continuous cracks developed in BS model though the length of the vault and are rather localized. On the contrary, due to the ability of the reinforcing mortar layer to redistribute stresses, smeared cracking develops around a certain region, here identified as hinge zones (C and D), see Figure 7-26b. Figure 7-35a shows the final configuration of developed and active hinges, showing that AS model becomes at the final of the test a mechanism that when 32.23mm (5265s) of induced displacement were achieved the hinge B at vault-wall connection of displaced wall was reactivated while the hinge C close suddenly and a new hinge namely C' was activated in the same position of C but on opposite edge of the thickness vault. At that moment the experimental vault has active 4 hinges which can conduce at collapse, nevertheless in order to achieve the balance the hinge A place at the base of fixed wall is closed achieving 39.29mm (6512mm) in order to avoid the collapse mechanism Figure 7-35b.

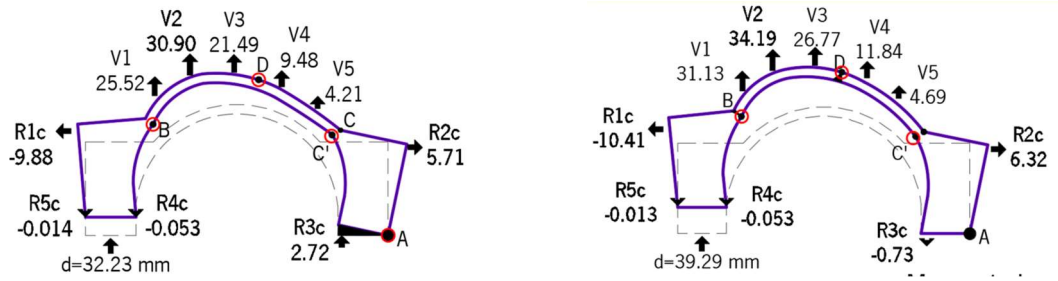


Figure 7-35. Final hinge configuration of the AS model

7.7 Concluding Remarks

In this chapter the previously damaged and retrofitted stone masonry vault model submitted to differential vertical settlements was analysed. The experimental model was retrofitted with glass fibre-reinforced mortar (GFRM) and glass fibre L shape anchorages placed at intra and extrados. Based on the results obtained, it can be concluded that:

- The overall behaviour of the retrofitted structure is very different from the reference model, both at the levels of damage distribution and location of hinges and the displacement needed to induce damage.

- The application of the glass fibre-reinforced mortar (GFRM) reinforcement system provided greater stiffness to the structure, which is reflected in a significant increase of displacement needed to induce damage in the model. The appearance of the first crack changed from 2.34mm in the unreinforced model to 12.32mm in the retrofitted model.
- In the retrofitted experimental model, the first cracks appear at the base of the right wall, whereas in the reference model the first crack appeared at the left wall-vault connection. This means that in spite of the previous cracks (reference model) was not injected, the retrofitting technique was efficient in postpone the opening of this crack.
- Despite of small detachments on sensible areas were observed on cracks belonging to hinge B, C and D, the anchorage works properly, and the retrofitting system was able to stiffen the masonry wall-vaults connection and improving the monolithic behaviour.
- It was also observed that the cracks in the retrofitted model was much more distributed and not so well localized as in the reference model, which indicated the ability of the retrofitted model to redistribute compressive stresses.
- The collapse mechanism in the retrofitted experimental is completely different from the reference model, being possible to clearly identify the collapse mechanism.

Chapter 8.
Conclusions and future research

Abstract:
The present chapter is mainly intended to summarize the conclusions drawn from the research work developed. The chapter firstly provides a general description of the developed work and then outlines the most relevant conclusions, with a particular focus on providing an answer to the four fundamental objectives specified in Chapter 1. Finally, the chapter and the thesis conclude by acknowledging the limitations of the research work carried out and adds some suggestions for continues developing new knowledge within the research line of the protection of heritage buildings with masonry vaults.

8.1. Introduction

This research focused on the study of stone masonry churches built between the sixteenth and eighteenth centuries, located in Yucatan state and recognized as an important built heritage of Mexico. Yucatan churches are massive structures based on loadbearing stone masonry walls and stone masonry vaults with irregular masonry bonds. Generally, the churches are based on superficial foundations with the same construction system used for the walls and, in the best case scenario, by using slightly larger stones (Kalisch, 2005; Rodríguez Pérez et al., 2021; Tamayo, 2004).

Nowadays, although the vaults and walls show visible cracks, deformations, tilts and settlements, the nature and origin of the damage is not clear. Possible reasons for the damages are: 1) ageing of material, 2) differential settlements generated by lateral wall instability, 3) settlement of the foundations due to soil degradation or non-uniform soil stratigraphy, 4) support failure due to poor foundations or 5) stress concentrations. It was observed that most of the reasons was the absence of foundation design. It is believed that these reasons, together with the material ageing and environmental effects, such as surface alterations, disintegration and biological growth, led to partial collapses at some churches, which need urgent rehabilitation works. Therefore, new knowledge about the structural behaviour of Yucatan religious buildings is relevant in the scope of the preservation of these buildings.

The present thesis aimed at overcome a research gap related to the absence of information on (i) the mechanical characterization of masonry materials and stone masonry that are representative of the materials from the Yucatan churches; (ii) structural analysis of masonry typical barrel vaults against differential vertical settlements; (iii) possible improvement of the structural behaviour of masonry vaults against differential vertical settlements after strengthening.

The research plan was divided in different tasks aiming at answering to the research objectives (Chapter 1): (1) Morphological characterization of Yucatan churches (research objective 1); (2) Geometrical Characterization (research objective 2); (3) experimental materials characterization (research objective 3); (4) structural assessment of Yucatan masonry barrel vaults under differential vertical settlements before and after retrofitting taking into consideration the masonry walls-vault interaction (research objective 4).

The present chapter intends to summarize the conclusions drawn from the research work developed and provide ideas about future research works by acknowledging the limitations of the research work

carried out and by providing suggestions to gather new knowledge within the research line of the protection of heritage buildings with masonry vaults.

8.2. Summary of conclusions

8.2.1. Characterization of Yucatán churches (research objective from 1 to 3)

In this research, it was necessary to reproduce typical cross section of Yucatan churches with barrel vaults. This required to have information about: (1) the morphological characteristics of the structural elements (masonry walls and vaults), (2) geometrical characteristics of structural elements and (3) the material mechanical properties of stone materials. The accomplishment all this information answered directly to Objectives 1 to 3 defined at the beginning of the research work. Additionally, the identifications of damages present in the Yucatan churches was also important to support the hypothesis of the main reason for the observed damage.

Therefore, a deep survey to identified and define all morphological features was necessary and relevant in the scope of the preservation of these buildings. For that, exploratory research was carried out throughout three research techniques: (i) Archive research, which include historical and architectonic styles overview; (ii) data collection of morphological and geometrical information available from public and private repositories, such as National Institute of Anthropology and History (INAH, acronym in Spanish), Dimension of Ecclesiastical properties and Sacred Art of the Archdiocese of Yucatan (DIBEAS, acronym in Spanish), Yucatan State Government Restoration Department, School of Architecture of the Autonomous University of Yucatan (FAUADY, acronym in Spanish) and Specialized engineering services of private businesses. According to the available information, a morphological configuration of Yucatan churches was defined and a database with materials and geometrical information of Yucatan churches was achieved; (iii) complementary in-situ works were carried out based on visual inspection on partially collapsed churches and photographic record on Yucatan churches. From the photographic surveys and the visual inspections on partially collapsed churches, a morphological characterization of the main structural elements such as walls, vaults and connections was performed and later confronted with the literature review.

From the data collected and definition of a database of Yucatan churches, it was concluded that Yucatan churches are mostly of single span, have stone barrel vaults and thick stone masonry walls. Morphological studies revealed that the masonry walls are three-leaf walls and were constructed

mostly as rubble masonry with horizontal joints roughly aligned and the round stone units roughly cut. Regarding the connections between transversal walls, it was seen that: (1) in walls built at the same time, the connection is assured by the monolithic behaviour of the composite material composed of round limestone with different dimensions linked by lime mortar; (2) there is no connection between church's walls built at different times, or it exists, the connection is poor by using stones units as connectors each 2 or 3 stones layers. The vaults have a configuration similar to the stone roman vaults, characterized by longitudinal mortar joints aligned and the transversal mortar joints not aligned with a minimum interlocking associated to the irregular size of flat stones.

The damages observed are the result of the lack of both maintenance and use of the churches. These two factors contribute to increase both the percentage of humidity inside and the biological colonization outside. The roots of biological colonization outside open the way to the rainwater, which wash the fine material and cause the deterioration of the masonry in both vaults and walls. While the excess moisture causes loss of cohesion, erosion, blistering, detachment, and disintegration of the mortar. This results in the decay of mortar and triggers the mechanical damage observed since the system with a decayed mortar is not capable of resisting the mechanical stresses demand. Among the mechanical damages observed are cracking, deformation, and tilting. It is suggested, the most dangerous structural cracks develop longitudinally in the vault, while the largest tilting and deformations were located at middle of the vault length. All these decay, cracks, deformations and tilting must be addressed in a timely manner, since they produce mechanisms that can conduce at structure collapse. The knowledge developed in this research provides experimental data that can be used in the future in the development and calibration of analytical models that allowing to explain in more detailed manner the origin of the observed mechanical damage.

8.2.2. Geometrical Characterization (research objective 2).

Following the selection of Yucatan churches with single nave and barrel vaults, which represent about 59% of the Yucatan churches studied, it was decided to define the geometry of the typical cross section of these churches, which was further used to design the experimental to be tests at laboratory. The geometrical characterization was performed aiming at identifying: (1) significant statistic correlations between basic geometric parameters of the structural elements and (2) empirical rules to describe the representative profile of the typical cross-section of the churches.

The statistical geometrical study was performed on a database of 44 churches in Yucatan. Linear correlations were carried out between the geometric parameters (e.g. span, total height, thickness and height for both walls and vaults, etc). Churches from different regions of Mexico were also analysed and included in the data base for a systematic comparison. The empirical rules obtained between the geometric parameters defining the typical cross section of the churches were then compared with empirical relations provided in historical treatises from sixteenth to eighteenth centuries.

This study revealed that the height of the walls (*Hw*) was probably governed by the total height of the churches (*H*), being defined approximately as 75% of *H* (±1.8m), independently on the type of vaults adopted. On the other hand, taking only single span churches with barrel vaults, corresponding to about 60% of the churches in the database, it was possible to derive three statistically significant empirical rules between the height of the vaults (*Hv*) and height of the walls (*Hw*) with the span (*L*): *Hv=0.39L+1.06* (r^2*=0.73*), *Hv=0.28H+1.18* (r^2*=0.64*) and *Hw=0.72H-1.18* (r^2*=0.92*). This appeared to indicate that the height of the vaults is related to both the height of the walls and to the span. As expected, when only semi-circular barrel vaults are considered, the correlation between the height of vaults and the span (*Hv=0.5L)* is very significant (r^2*=0.92*). Significant correlations were also found between *Hw* and *H* (r^2 *= 0.90*) and between *H* and *L* (r^2 *= 0.61*) but no other significant statistical correlations between the key geometric parameters were obtained. Based on these results, it was decided to derive empirical rules by considering only the data that resulted in significant statistical data ($r^2 \geq 0.6$). From this procedure, it was possible to derive expressions as a function of the span (*L*) for the height of the walls (Hw), height of the vaults (Hv), thickness of the walls (*tw*) and for the thickness of the vaults (*tv*). Additionally, from the comparative analysis performed between Yucatan churches and other Mexican churches from Morelia, Oaxaca and Morelos, all them with single span and barrel vaults, significant statistical correlations between the key geometric parameters *Hw*, *Hv*, *tw* and *H* and the span of the churches, *L*, were found. An interesting finding regarding to the backfill height at extrados of the barrel vaults of Yucatan churches is the variation of centre angles from 33° to 46°, which means that the free vault span reduces from 10.6% to 13.9%. The comparisons with other Mexican churches from Oaxaca and Morelia show a strong concentration of backfill height with centre angles between 30° and 65°. However, there are other examples where the backfill covers completely the vaults.

By reviewing empirical rules for key geometric parameters in European historical constructions treatises from sixteen to eighteen century, namely, thickness and height of the walls, thickness of the

vaults and backfill height at extrados of the barrel vaults, it was possible to see that the empirical geometric rules found for Yucatan churches can be compared with some geometric rules proposed by different authors. In addition, the analysis of other Mexican churches, which appear to have been built at an empirical or intuitive basis, reveals that geometrical key parameters are in the range of the several values proposed in the historical construction treatises, which indicates that the Mexican builders had incorporated some existing knowledge, possibly introduced by Spanish explorers.

8.2.3. Material characterization (research objective 3).

The definition of the experimental models also required information about the type of stone most commonly used in Yucatan churches. Therefore, an extensive multi-scale experimental characterization was carried out on stone and mortar samples collected during the field work on partially collapse churches from sixteenth to eighteenth centuries. Several characteristics were identified through different laboratory test techniques: (1) petrographic characterization, (2) analysis of micro-structures through scanning electron microscopy (3) chemical and mineralogical composition analysis; (4) physical and mechanical experimental testing under uniaxial load. Statistical correlations based on the experimental data and using single regression analysis and further correlations were obtained between physical and mechanical properties with indexes given from two simple non-destructive techniques extensively used for in situ materials assessment, namely Schmidt hammer and Ultrasonic pulse velocity.

It was concluded that Yucatan churches are located on a lithological area mostly of Coquinoid limestone and Fossiliferous crystalline limestone. The results from mineralogical analysis revealed that: (1) in mortar samples, the mineral phase of calcite ($CaCO_3$) was the most abundant compound. Additional studies are needed to identify the binder to aggregate ratio and possible additives on the mortar; (2) the stones studied are limestone with some traces of others additional minerals. The SEM, X-ray and petrography revealed that there is no clear dependence of the anisotropy of the stones on the mineralogical and textural varieties.

The limestone samples under analysis were arranged in three groups according to the physical properties, namely open porosity, water absorption by immersion at atmospheric pressure and apparent density. Based on this, it was possible to define group 1 with limestone samples with high porosity ($31.8\% \leq \eta \leq 41.6\%$), group 2 encompassing limestone with porosity ranging from low to medium values ($10.5\% \leq \eta \leq 27.8\%$) and group 3 with limestone of low porosity ($2.5\% \leq \eta \leq 14.9\%$)

Regarding to this grouping: (1) the distribution of the water absorption by capillarity (Cw) was coherent with the grouping carried out mostly on the other physical parameters. This is justified by the strong correlations ($r^2 > 0.9$) among the physical properties; (2) the mechanical properties, namely compressive strength and modulus of elasticity, are also very well distributed among the limestone groups. In terms of compressive strength, it was possible to observe that group 1 can be classified as low strength (10.6 MPa ≤ fc ≤ 13.8 MPa), group 2 can be classified as average strength (19.9 MPa ≤ fc ≤ 48.5 MPa), and group 3 can be classified as high strength (55.7 MPa ≤ fc ≤93.4 MPa).

From the results it is also possible to conclude that: (1) it was noticed that higher water capillary coefficients were obtained mostly for the parallel direction to the bedding planes; (2) if strength anisotropy index is considered, the stones are mostly classified as low anisotropic and most of the stones present higher compressive strength in the parallel direction to the bedding planes; (3) most of the samples tested under uniaxial compression failed in shear, even if both shear and tensile-splitting failure modes could be recorded in stone belonging to the three groups. As expected, high strength stone presented a brittle failure, being not possible to record the post-peak behaviour.

Regarding to the correlations between physical and mechanical properties with the non-destructive techniques, the results revels very good statistical correlations among the physical properties. Non-destructive indexes based on Schmidt hammer (N) and ultrasonic pulse velocity (UPV) on limestone showed reasonably accurate to predict mechanical and physical properties. Influencing factors, as anisotropy and moisture content, were also analyzed. For both dry and saturated conditions, higher values of UPV were recorded along the stratification's layers. The denser samples show higher velocities than samples with low density. The results appear to confirm that UPV and Schmidt hammer tests can be effectively used as non-destructive methods for a preliminary prediction of mechanical and physical properties.

8.2.4. Structural assessment stone masonry vaults under vertical differential settlement (research objective 4).

The research objective 4 included: (i) obtainment of the key mechanical properties of stone masonry under uniaxial compression; (ii) structural analysis of barrel stone masonry vaults submitted to vertical differential settlements. The main aim was to identify the failure modes and collapse mechanisms, as well as to assess the effectiveness of a retrofitting technique based on fibreglass mesh embedded in

natural hydraulic lime mortar and mechanically connected to the stone masonry with fibreglass bars anchors.

The design of the experimental was supported on the previous analysis on the morphological and geometrical features of the structural elements of Yucatan churches.

The masonry specimens tested under uniaxial compression load were supposed to be built according to the masonry bonds representative of stone masonry walls and stone masonry vaults. However, some deviations in the construction were identified, namely the uneven distribution of stone in the length of the small specimens. Despite this, it is considered that important data is provided for the scientific community. The masonry vaults presented a compressive stress average equal to 7.3 MPa (Co.V 26%) and elasticity modulus average was about 3565MPa (Co.V 22%). The masonry wall presented a compressive stress average equal to 2.1Mpa (Co.V 15%) and elasticity modulus average equal to 4349MPa (Co.V 15%).

From the experimental tests on the reference model of the stone masonry vault it was possible to conclude that:

- Different stages were identified throughout the experiment, all displacement were well record, including really small displacement at the scale of microns and it was possible to completely follow the deformation trajectory of the model. This was rather difficult when simultaneously management of two actuators is needed. It should be mentioned that the set of LVDTs enabled to follow the rigid block movements of the structure.
- Vaults supported on walls, as the one represented by the experimental model analyzed, are not capable of withstanding large vertical settlements without visibly damage. The first visible crack appeared at extrados of the vault at the vault-wall connection and the second visible crack appeared close to the key stone for very small vertical induced displacements.
- It should be mentioned that both the buttresses and the continuity of the walls that support the vault can be important reasons for the third hinge to be located in the vaults according to the prediction of the numerical model and the collapse mechanisms proposed by some authors. Because both the buttresses and the continuity of the walls provide rigidity to the system and prevents the in-plane rotation of the support.

The analysis of the results of the experimental tests carried out on the retrofitted previously damaged stone masonry vault model with glass fibre reinforced mortar (GFRM) technique and glass fibre L shape anchorages placed at intra and extrados submitted to differential vertical settlements it was possible to observe that:

- The overall behaviour of the retrofitted structure is very different from the reference model, both at the levels of damage distribution and location of hinges and the displacement needed to induce damage.
- The application of the glass fibre-reinforced mortar (GFRM) reinforcement system provided greater stiffness to the structure, which is reflected in a significant increase of displacement needed to induce damage in the model. The appearance of the first crack changed from 2.34mm in the unreinforced model to 12.32mm in the retrofitted model.
- In the retrofitted experimental model first cracks appear at the base of the right wall, whereas in the reference model the first crack appeared at the left wall-vault connection. This means that in spite of the previous cracks (reference model) was not injected, the retrofitting technique was efficient in postpone the opening of this crack.
- Despite of small detachments on sensible areas were observed on cracks belonging to hinge B, C and D, the anchorage works properly, and the retrofitting system was able to stiffen the masonry wall-vaults connection and improving the monolithic behaviour.
- It was also observed that the cracks in the retrofitted model was much more distributed and not so well localized as in the reference model, which indicated the ability of the retrofitted model to redistribute compressive stresses.
- The collapse mechanism in the retrofitted experimental is completely different from the reference model, being possible to clearly identify the collapse mechanism.

8.2.5. Thesis outcomes

Besides the main conclusions outlined and the answering to the research objectives, it is important to remark that the knowledge created within this work can be applied in structures around the world with similar characteristics. Therefore, it is considered that the results of this thesis contribute not only to feed the knowledge in materials and structural behaviour of barrel vaults from Yucatan churches, but also contributes to provide useful information to calibrate numerical models to use in the development

of possible interventions and strengthening of existing stone masonry buildings with characteristic similar to this research. Moreover, the experience gathered on the mechanical behaviour and collapse mechanism of the masonry vaults-wall system not strengthened and strengthened, under differential settlements can be of great advantage in the decision process related to the strengthening possibilities of ancient masonry structures.

8.3. Future research

Differential settlements are considered to be the origin of several common structural damages on historical masonry constructions, but the accurate understanding of the collapse mechanism and strengthening possibilities needs further research. Throughout the literature review, it was observed that few studies have dealt with the problem of foundations. Since vertical settlements are much more difficult to simulate in laboratory tests than horizontal displacement, few research focused on this topic. Consequently, the effect of the settlement on the structural behaviour of masonry vaults and arches is not yet explored in detail.

The present work contributed to enlarge the experimental data concerning the mechanical behaviour and collapse mechanisms under differential settlement. Nevertheless, the works do not stop there. Further research should be developed in the scope of the preservation of Yucatan churches or buildings with similar characteristics worldwide.

All tools provided in this PhD research are the first approach to the preservation of Yucatan churches. Based on the experimental research carried out in this thesis, it is suggested to;

(1) calibrate numerical model of the structure tested under induced vertical displacement;

(2) carry out a parametric study to analyses the influence of the materials properties on the structural behaviour of masonry vaults to different loading configurations;

(3) assess the influence of the experimental boundary conditions on the structural behaviour of stone masonry vaults;

(4) assess the effectiveness of possible interventions of existing stone masonry vaults.

(5) extend the numerical simulation to real scale Yucatan churches and assess the effectives of retrofitting techniques.

REFERENCES

Acikgoz, S., Soga, K., and Woodhams, J. (2017). Evaluation of the response of a vaulted masonry structure to differential settlements using point cloud data and limit analyses. *Construction and Building Materials, 150,* 916–931.

Aggistalis, G., Alivizatos, A., Stamoulis, D., and Stournaras, G. (1996). Correlating uniaxial compressive strength with schmidt hardness, point load index, young's modulus, and mineralogy of gabbros and basalts (northern Greece). *Bulletin of the International Association of Engineering Geology, 54,* 3–11.

Aldeeky, H., and Al Hattamleh, O. (2018). Prediction of Engineering Properties of Basalt Rock in Jordan Using Ultrasonic Pulse Velocity Test. *Geotechnical and Geological Engineering, 36*(6), 3511–3525. Retrieved from https://doi.org/10.1007/s10706-018-0551-6

Alejo, L. E., Zavala, M., Martinez, G., and Jara, J. M. (2014). Influence of the Geometric Empirical Rules in the Seismic Fragility of Religious Historical Buildings of Morelia City, Mexico. In *SAHC2014 – 9th International Conference on Structural Analysis of Historical Constructions* (pp. 14–17). México.

Al-Omari, A., Beck, K., Brunetaud, X., Török, Á., and Al-Mukhtar, M. (2015). Critical degree of saturation: A control factor of freeze-thaw damage of porous limestones at Castle of Chambord, France. *Engineering Geology, 185,* 71–80.

Alonzo, S. L., and Espinosa, L. (2003). Estudio de las propiedades de la roca caliza de Yucatán. *Ingeniería Revista Académica, 7*(1), 27–36.

Alves, R., Faria, P., and Simão, J. (2017). Experimental characterization of a Madeira Island basalt traditionally applied in a regional decorative mortar. *Journal of Building Engineering, 13*(September), 326–335. Retrieved from http://dx.doi.org/10.1016/j.jobe.2017.09.004

Amadei, B. (1996). Importance of anisotropy when estimating and measuring in situ stresses in rock. *International Journal of Rock Mechanics and Mining Sciences and Geomechanics, 33*(3), 293–325.

Andriamihaja, S., Padmanabhan, E., and Ben -Awuah, J. (2016). Characterization of pore systems in carbonate using 3d X–ray computed tomography. *Petroleum & Coal, 58* (4), p507-516. Retrieved from https://eds.b.ebscohost.com/eds/pdfviewer/pdfviewer?vid=0&sid=f44a4c6d- 359e-42e0-bf98-4568eddc5ba7%40sessionmgr102

Angelillo, M., Lourenço, P. B., and Milani, G. (2014). Masonry behaviour and modelling. *CISM International Centre for Mechanical Sciences, Courses and Lectures, 551,* 1–26.

ASTM C170, S. (1999). Standard Test Method for Compressive Strength of Dimension Stone. ASTM C170, S. (1999). Standard Test Method for Compressive Strength of Dimension Stone. ASTM D 3148, S. (2002). Standard Test Method for Elastic Moduli of Intact Rock Core Specimens in Uniaxial Compression. Standard ASTM International. Retrieved from http://www.dres.ir/fanni/khak/DocLib4/D 314802; RDMXNDG_.pdf

ASTM D 5873, S. (1995). Determination of Rock Hardness by Rebound Hammer Method.

ASTM D4543, S. (2001). *Standard Practices for Preparing Rock Core Specimens and Determining Dimensional and Shape Tolerances 1.* Retrieved from http://www.dres.ir/fanni/khak/DocLib4/D 454301; RDQ1NDM_.pdf

Aufmuth, R. E. (1973). A systematic determination of engineering criteria for rock. *Bull. Assoc. Eng. Geol., 11,* 235–245.

Ayuntamiento_de_Mérida. (2000). Historia de la Arquitectura de Mérida. Retrieved July 13, 2 0 2 0 , from https://web.archive.org/web/20151020234957/http://thematrix.sureste.com/cityview/merida1/artic ulos/arquimer.htm

Azimian, A., and Ajalloeian, R. (2015). Empirical correlation of physical and mechanical properties of marly rocks with P wave velocity. *Arabian Journal of Geosciences, 8*(4), 2069–2079.

Bachmann, M., and Schwarting, A. (2008). Conservation projects in Pergamon. Building Z and the shelter constructed above it. *Conservation and Mgmt of Arch. Sites, 2*(2), 157–173.

Balen, K. V., and Hendrickx, R. (2008). Preservation of workmanship or workmanship for preservation. Structural Analysis of Historic Construction: Preserving Safety and Significance: Proceedings of the Sixth International Conference on Structural Analysis of Historic Construction, 2-4 July 2008, Bath, United Kingdom, 3–12.

Baratta, A., Corbi, I., Corbi, O., and Rinaldis, D. (2008). Experimental survey on seismic response of masonry

models. Struct. Anal. Hist. Constr. Preserv. Saf. Significance Proc. Sixth Int. Conf. Struct. Anal. Hist. Constr. 2-4 July 2008, Bath, United Kingdom, 1, 799–807.

Barbieri, A., Borri, A., Corradi, M., and Di Tommaso, A. (2002). Dynamic Behaviour of Masonry Vaults Repaired with FRP: Experimental Analysis (pp. 7–16).

Basu, A., Celestino, T. B., and Bortolucci, A. A. (2009). Evaluation of rock mechanical behaviors under uniaxial compression with reference to assessed weathering grades. *Rock Mechanics and Rock Engineering, 42* (1), 73–93.

Basu, A., Mishra, D. A., and Roychowdhury, K. (2013). Rock failure modes under uniaxial compression, Brazilian, and point load tests. *Bulletin of Engineering Geology and the Environment, 72*(3–4), 457–475. Retrieved from https://link.springer.com/article/10.1007/s10064-013-0505-4

Bednarik, M., Moshammer, B., Heinrich, M., Holzer, R., Laho, M., Rabeder, J., ... Unterwurzacher, M. (2014). Engineering geological properties of Leitha Limestone from historical quarries in Burgenland and Styria, Austria. *Engineering Geology, 176,* 66–78.

Bélidor, B. F. de. (1725). *Nouveau Cours de mathématique à l' usage de l' artillerie et du génie*. Paris Francia: Académie Royale des Sciences.

Bélidor, B. F. de. (1729). La science des ingénieurs dans la conduite des travaux de fortification et d'architecture civile. Paris Francia: Chez Claude Jombert.

Bélidor, B. F. de. (1755). Dictionnaire portatif de l' ingénieur, où l' on explique les principaux termes des sciences les plus nécessaires à un Ingénieur, sçavoir. Paris Francia: Chez Charles; Antoine Jomd.

Bell, F. G. (1993). Durability of carbonate rock as building stone with comments on its preservation. *Environmental Geology, 21,* 187–200.

Beverly, B. E., Schoenwolf, D. A., and Brierly, G. S. (1979). Correlations of rock index values with engineering properties and the classification of intact rock. *Federal Highway Administration, Waschington DC, Technical Report, 228,* 229.

Binda, L., Fontanal, A., and Mirabella, G. (1994). Mechanical Behaviour and Stress DIstribution in Multiple-Leaf Stone Walls. In *International Brick and Block Masonry Conference.* Galgary, Canada.

Binda, L., Modena, C., Baronio, G., and Abbaneo, S. (1997). Repair and investigation techniques for stone masonry walls. *Construction and Building Materials, 11* (3), 133–142. Retrieved from http://linkinghub.elsevier.com/retrieve/pii/S0950061897000317

Bissell, H. J., and Chilingar, G. V. (1967). Classification of Sedimentary Carbonate Rocks. In Carbonate Rocks Origin, Occurrence and Classification (pp. 87–168).

Blondel, F. (1683). Cours d'Architecture V3.

Boem, I., and Gattesco, N. (2021). Cyclic behavior of masonry barrel vaults strengthened through Composite Reinforced Mortar, considering the role of the connection with the abutments. Engineering Structures, 228(September 2020).

Bolis, V., Preti, M., Marini, A., and Giuriani, E. (2017). Experimental cyclic and dynamic in-plane rocking response of a masonry transverse arch typical of historical churches. Engineering Structures, 147, 285–296. Retrieved from http://dx.doi.org/10.1016/j.engstruct.2017.05.058

Borri, A., and De Maria, A. (2009). Eurocode 8 and Italian Code. A Comparison About Safety Levels and Classification of Interventions on Masonry Existing Buildings. *Eurocode 8 Perspectives from the Italian Standpoint Workshop, 2008*(2003), 237–246.

Borri, A., Casadei, P., Castori, G., and Hammond, J. (2009). Strengthening of Brick Masonry Arches with Externally Bonded Steel Reinforced Composites. *Journal of Composites for Construction, 13*(6), 468–475. Retrieved from https://ascelibrary.org/doi/abs/10.1061/%28ASCE%29CC.1943-5614.0000030

Borri, A., Corradi, M., Castori, G., and De Maria, A. (2015). A method for the analysis and classification of historic masonry. *Bulletin of Earthquake Engineering, 13*(9), 2647–2665. Bravo, S. G. (2013). Origen, geometría y construcción de las bóvedas por cruceros de la catedral de San Ildefonso en Mérida, Yucatán. In S. Huerta & F. L. Ulloa (Eds.), *Actas del Octavo Congreso Nacional de Historia de la Construcción* (pp. 9–12). Madrid: Instituto Juan de Herrera.

Brencich, A., and Morbiducci, R. (2007). Masonry arches: Historical rules and modern mechanics. *International Journal of Architectural Heritage, 1*(2), 165–189.

Bretos, M. A. (1987). *Arquitectura y arte sacro en Yucatán, 1545-1823* (1st ed.). Mérida, Yucatán, México: Producción Editorial Dante.

Bretos, M. A. (1992). *Iglesias de Yucatán* (1. ed.). Mérida: Producción Editorial Dante.

BS EN 14580, S. (2005). Natural stone test methods. Determination of static elastic modulus, *44*(0).

Calderini, C., Abbati, S., Cotič, P., Kržan, M., and Bosiljkov, V. (2015). In-plane shear tests on masonry panels with plaster: correlation of structural damage and damage on artistic assets. *Bulletin of Earthquake Engineering, 13*(1), 237–256.

Calvo-Lopez, J. (1999). *Cerramientos y trazas de montea, de Ginés Martínez de Aranda.* (Departamento de Ideación Gráfica Arquitectónica Escuela Técnica Superior de Arquitectura de Madrid, Ed.). Madrid, España. Retrieved from http://hdl.handle.net/10317/778

Camara de Diputados, H. congreso de la U. (2018). Ley Federal sobre Monumentos y Zonas Arqueológicos, Artísticos e Históricos. México.

Camón Aznar, J. (1941). La intervención de Rodrigo Gil de Hontañón en el manuscrito de Simón García. *Archivo Español de Arte, 45*(14), 6. Retrieved from https://dialnet.unirioja.es/servlet/revista?codigo=151

Cancelliere, I., Imbimbo, M., and Sacco, E. (2010). Experimental tests and numerical modeling of reinforced masonry arches. *Engineering Structures, 32*(3), 776–792.

Candeias, P., Campos Costa, A., and Coelho, E. (2004). SHAKING TABLE TESTS OF 1:3 REDUCED SCALE MODELS OF FOUR-STORY UNREINFORCED MASONRY BUILDINGS. *13th World Conference on Earthquake Engineering.* Retrieved from https://www.iitk.ac.in/nicee/wcee/article/13_2199.pdf

Cardos, M. (2008). Tetiz. Retrieved from https://www.flickr.com/photos/10783001@N06/3140741606/

Carozzi, F. G., Poggi, C., Bertolesi, E., and Milani, G. (2018). Ancient masonry arches and vaults strengthened with TRM , SRG and FRP composites : Experimental evaluation. Composite Structures, 187(October 2017), 466–480.

Carpinteri, A., and Mainardi, F. (2014). *Fractals and Fractional Calculus in Continuum M e c h a n i c s .* (CISM International Centre for Mechanical Sciences. Volume 378, Ed.) (Vol. 1). Springer. Retrieved from https://books.google.pt/books?id=1fHtCAAAQBAJ&pg=PA92&lpg=PA92&dq=in+uniaxial+tests+the+macroscopic+cracks+essentially+starts+parallel+to+the+direction+to+the+axial+loading&source=bl&ots=sS8JggTFMy&sig=ACfU3U1UIuI3rtiARlg3I9D0fnXLO4MrEg&hl=es-419&sa=X&ved

Carrasco, R. (2004, July). Friso y bóveda única, últimos descubrimientos en Calakmul - Proceso. *Proceso.*

Carrillo, D. (1991). Módulo de elasticidad de rocas calizas superficiales del estado de Yucatán. Universidad Autónoma de Yucatán, México.

Cascini, L., Gagliardo, R., and Portioli, F. (2020). LiABlock_3D: A Software Tool for Collapse Mechanism Analysis of Historic Masonry Structures. *International Journal of Architectural Heritage, 14*(1), 75–94.

Castellano, A., Camassa, D., Fraddosio, A., Scacco, J., Piccioni, M. D., and Milani, G. (2021). Dynamic damage identification for a full-scale parabolic tuff barrel vault under differential settlements of the supports. *Construction and Building Materials, 291,* 123271. Retrieved from https://doi.org/10.1016/j.conbuildmat.2021.123271

Cescatti, E., Porto, F., Modena, C., Cescatti, E., Porto, F., and Modena, C. (2018). In-Situ Destructive Testing of Ancient Strengthened Masonry Vaults In-Situ Destructive Testing of Ancient Strengthened Masonry Vaults. *International Journal of Architectural Heritage, 12* (3), 350–361. Retrieved from https://doi.org/10.1080/15583058.2017.1323243

Chang, C., Zoback, M. D., and Khaksar, A. (2006). Empirical relations between rock strength and physical properties in sedimentary rocks. *Journal of Petroleum Science and Engineering, 51*(3–4), 223–237.

Chávez, M., and Meli, R. (2008). Shaking table testing of a typical Mexican colonial temple. Structural Analysis of Historic Construction: Preserving Safety and Significance: Proceedings of the Sixth International Conference on Structural Analysis of Historic Construction, 2-4 July 2008, Bath, United Kingdom, 825–832.

Chávez, M., Sánchez-Ramírez, R., and Meli, R. (2012). Characterization of the historic masonry buildings of Mexico. *Proceeding of Structural Analysis of Historical Constructions (SAHC2012),* 651–658. Retrieved from http://www.hms.civil.uminho.pt/sahc/2012/651.pdf

Ching, F. D. K. (2011). Una historia universal de la arquitectura. Volumen 2, Del siglo XV a nuestros días: un análisis cronológico comparado a través de las culturas (1 traducid). Barcelona España: Gustavo Gili. Retrieved from https://www.wook.pt/livro/historia-universal-de- la-arquitectura-vol-2-francis-d-k-ching/11686785

Chulia, A. A. (2017). Numerical simulation of structural integrity of lime concrete numerical simulation of structural integrity of lime concrete reinforced by GFRP. Case study. In Conference: 25th International Conference on Composites/Nano-Engineering. Rome, Italy. Retrieved from http://hdl.handle.net/10251/58200

Çobanoğlu, İ. (2015). Prediction and identification of capillary water absorption capacity of travertine dimension stone. *Arabian Journal of Geosciences, 8*(11), 10135–10149.

Collis, J., and Hussey, R. (2003). *Business Research: A Practical Guide for Undergraduate and Postgraduate Students.* Houndmills, Basingstoke, Hampshire, England: Palgrave Macmillan.

Conde, B., Díaz-Vilariño, L., Lagüela, S., and Arias, P. (2016). Structural analysis of Monforte de Lemos masonry arch bridge considering the influence of the geometry of the arches and fill material on the collapse load estimation. *Construction and Building Materials, 120,* 230–242.

Corradi, M., Borri, A., Castori, G., and Coventry, K. (2015). Experimental analysis of dynamic effects of FRP reinforced masonry vaults. *Materials, 8*(12), 8059–8071.

D'Altri, A. M., De Miranda, S., Castellazzi, G., Sarhosis, V., Hudson, J., and Theodossopoulos, D. (2020). Historic Barrel Vaults Undergoing Differential Settlements. *International Journal of Architectural Heritage, 14*(8), 1196–1209.

D'Ayala, D., Shi, Y., and Stammers, C. (2008). Dynamic multi-body behaviour of historic masonry buildings models. Structural Analysis of Historic Construction: Preserving Safety and Significance: Proceedings of the Sixth International Conference on Structural Analysis of Historic Construction, 2-4 July 2008, Bath, United Kingdom, 489–496.

Day, M. J., and Goudie, A. S. (1977). Field assessment of rock hardness using the Schmidt test hammer. *BGRG Technical Bulletin, 18,* 19–29.

Day, Michael J. (1980). Rock hardness: Field assessment and geomorphic importance. *Professional Geographer, 32*(1), 72–81.

De Canio, G., and Ranieri, N. (2009). *La sperimentazione dinamica delle strutture.* Italy. Retrieved from http://old.enea.it/produzione_scientifica/pdf_EAI/2009/3/SperimentazioneDinamica.pdf

De Guglielmo, F. De, Ribera, F., and Angelillo, M. (2015). Analysis and consolidation of masonry vaults in the restoration of historical constructions. In *Rehab 2015 - 2nd International Conference on Preservation, Maintenance and Rehabilitation of Historic Buildings and Structures.* Porto - Portugal.

De Sousa Gago, A. M. C. (2004). *Análise Estrutural de Arcos, Abóbodas e Cúpulas.* Universidad tecnica de Lisboa. Retrieved from http://www.civil.ist.utl.pt/~gago/Partilha/tese_PhD_ASGago.pdf

Deere, D. U., and Miller, R. (1966). Engineering classification and index properties for intact rock. *Technical Report, Air Force Weapons Laboratory, 1,* 65–116.

Derand, F. (1643). *L'Architecture des voutes.* Paris: Imprimeur ordinaire du Roy.

Di Benedetto, C., Cappelletti, P., Favaro, M., Graziano, S. F., Langella, A., Calcaterra, D., and Colella, A. (2015). Porosity as key factor in the durability of two historical building stones: Neapolitan Yellow Tuff and Vicenza Stone. *Engineering Geology, 193,* 310–319.

Dinçer, I., Acar, A., Çobanoğlu, I., and Uras, Y. (2004). Correlation between Schmidt hardness, uniaxial compressive strength, and young's modulus for andesites, basalts and tuffs. *Bulletin of Engineering Geology and the Environment, 63*(2), 141–148.

Direção-Geral do Território. (2022). Sistema Nacional de Informação Geográfica. Retrieved from https://snig.dgterritorio.gov.pt/

Dizhur, D., Bailey, S., Griffith, M., and Ingham, J. (2015). Earthquake Performance of Two Vintage URM Buildings Retrofitted Using Surface Bonded GFRP: Case Study. Journal of Composites for Construction, 19(5).

Eccott, D. J. (2003). The true arch: an absent trait in Precolumbian America? *Migration and Diffusion, 4* (Number 13), 41–63. Retrieved from https://www.google.com/imgres?imgurl=x-raw-image%3A%2F%2F%2Fcce370494c86bd90ee63d171c1ce6340d7539c330a247fb957125ae84019c099&imgrefurl=http%3A%2F%2Fwww.migration-diffusion.info%2Fpdfdownload.php%3Fid%3D72%26file%3D1&tbnid=kL2GTElw48y9TM&vet=12ahUKEwii_P2b

Echánove, C. A. T. (1944). Enciclopedia yucatanense (1944 edition). In C. A. T. Echánove (Ed.) (1st ed., p. 1022). México: Edición oficial del gobierno de Yucatán. Retrieved from

https://openlibrary.org/books/OL17165612M/Enciclopedia_yucatanense

El-Khalili, M. (2014). Restoration Interventions at the Roman Nymphaeum in Amman: Identification and Evaluation. *Conservation and Management of Archaeological Sites, 16*(4), 341–358. Retrieved from http://www.tandfonline.com/doi/full/10.1179/1350503315Z.000000000102

Ellwood, B., Burkart, B., Raieshwar, K., Darwin, R. L., Neeley, R. A., Mccall, A. B., ... Hickcox, C.W. (1989). Are the iron carbonate minerals, ankerite and ferroan dolomite, like siderite, Important in Paleomagnetism? *Jornal of Geophysical Research, 94*(B6), 7321–7331.

EN 14579, S. (2005). Métodos de ensaio de pedra natural. Determinação da velocidade de propagação do som, 1–41.

EN 15801, S. (2008). Conservation of cultural property - Test methods - Determination of absorption by capillarity.

EN 1936, S. Natural stone test methods-determination of real density and apparent density, and of total and open porosity. European committee for Standadization (2006).

EN 998-1: (2010). Specification for mortar for masonry - Part 1: Rendering and plastering mortar Définitions. *CEN (Comité Européen de Normalisation),* 1–23.

Estrada-Medina, H., Valdez, S., Zanatta, A., and Casolco, S. R. (2008). Análisis de compresión en rocas calizas de Yucatán. *Memorias Del 14 Congreso Internacional Anual de La SOMIM,* 602–608.

Fatz, O., Reches, Z., and Roegiers, J. C. (2000). Evaluation of mechanical rock properties using a Schmidt Hammer.pdf. *Rock Mechanics and Mining Sciences, 37,* 723–728.

Fener, M., Kahraman, S., Bilgil, A., and Gunaydin, O. (2005). A comparative evaluation of indirect methods to estimate the compressive strength of rocks. *Rock Mechanics and Rock Engineering, 38*(4), 329–343.

Fernandes, F., and Lourenço, P. B. (2007). Evaluation of the Compressive Strength of Ancient Clay Bricks Using Microdrilling. *Journal of Materials in Civil Engineering, 19*(9), 791–800.

Fernández, B., Gómez, M., Varela, R., and Vargas, M. (2009). Determinación de la resistencia a compresión diagonal y el módulo de cortante de la mampostería de bloques huecos de concreto. *Ingeniería, 13*(2), 41–50.

Ferrero, C., Calderini, C., and Roca, P. (2022). Experimental response of a scaled dry-joint masonry arch subject to inclined support displacements. *Engineering Structures, 253*(November 2021).

Ferrero, C., Calderini, C., Portioli, F., and Roca, P. (2021). Large displacement analysis of dry- joint masonry arches subject to inclined support movements. *Engineering Structures, 238*(November 2020), 112244. Retrieved from https://doi.org/10.1016/j.engstruct.2021.112244

Figueiredo, B. (2015). *Descodificação do De Re Aedificatoria de alberti. Gramáticas de forma para a análise e geração de edifícios sagrados.* Universidade do Minho. Retrieved from http://hdl.handle.net/1822/41518

Folk, R. (1980). Petrology of sedimentary rocks. Retrieved from https://repositories.lib.utexas.edu/bitstream/handle/2152/22930/folkpetrology.pdf?sequence=3

Fr Laurencio, de S. N. (1639). Arte y uso de Arquitectura. Primera parte. (Corte de Madrid, Ed.). Madrid: Plácido Barco López. Retrieved from https://ia801407.us.archive.org/3/items/arteyusodearquit01lore/arteyusodearquit01lore_bw.pdf

Frézier, A. F. (1737). La théorie et la practique de la coupe de pierres et des bois pour la constution des voûtes et autres parties des bâtimnts civils et militaires. Tome 1 (Vol. 1). Paris Francia: Chez Charles; Antoine Jomdert.

Frézier, A. F. (1768). La théorie et la practique de la coupe de pierres et des bois pour la constution des voûtes et autres parties des bâtimnts civils et militaires. Tome 2 (Vol. 2). Paris Francia: Chez Charles; Antoine Jomdert.

Frézier, A. F. (1769). La théorie et la practique de la coupe de pierres et des bois pour la constution des voûtes et autres parties des bâtimnts civils et militaires. Tome 3 (Vol. 3). Paris Francia: Chez Charles; Antoine Jomdert.

Gaetani, A. (2016). Seismic Performance of Masonry Cross Vaults: Learning from Historical Developments and Experimental Testing. Universidade do Minho, Portugal.

Gaetani, A., Lourenço, P. B., Monti, G., and Moroni, M. (2017). Shaking table tests and numerical analyses on a scaled dry-joint arch undergoing windowed sine pulses. *Bulletin of Earthquake Engineering, 15*(11), 4939–4961.

Gaetani, A., Lourenço, P., Monti, G., and Milani, G. (2017). A parametric investigation on the seismic capacity of masonry cross vaults. *Engineering Structures, 148,* 686–703. Retrieved from http://dx.doi.org/10.1016/j.engstruct.2017.07.013

Gaetani, A., Monti, G., Lourenço, P., and Marcari, G. (2016). Design and Analysis of Cross Vaults Along History. *International Journal of Architectural Heritage, 10*(7), 841–856.

Gago, A. S., Alfaiate, J., and Lamas, A. (2011). The effect of the infill in arched structures: Analytical and numerical modelling. *Engineering Structures, 33* (5), 1450–1458. Retrieved from http://dx.doi.org/10.1016/j.engstruct.2010.12.037

Garcia Berruguilla, J. (1747). Verdadera practica de las resoluciones de la geometría, sobre las tres dimensiones para un perfecto arquitecto, con una total resolución para medir, y dividir la planimetría para los agrimensores. (I. de L. F. Mojados, Ed.). Madrid: Imprenta de Lorenzo Francisco Mojados.

García, G., and Graniel, E. (2010). EL ESTADO 4 Geología. In Durán R. & Méndez M. (Eds.), *Biodiversidad y Desarrollo Humano en Yucatán.* (1st ed., p. 496). Mérida, Yucatán, México: CICY, PPD-FMAM, CONABIO, SEDUMA. Retrieved from http://www.sds.yucatan.gob.mx/biodiversidad-yucatan/libro-biodiversidad-yucatan.php

García, N., and Meli, R. (2007). Estudio de las bases estructurales de los templos conventuales mexicanos del siglo XVI. *Boletin de Monumentos Históricos, 11*(0188–4638), 4–18. Retrieved from http://www.boletin-cnmh.inah.gob.mx/boletin/boletines/3EV11P4.pdf

García, N., and Meli, R. (2008). On Structural Bases for Building the Mexican Convent Churches from the Sixteenth Century. *International Journal of Architectural Heritage, 3* (1), 24–51. Retrieved from https://www.tandfonline.com/action/journalInformation?journalCode=uarc20

García, S. (1681). Compendio de architectura y simetría de los templos: conforme a la medida del cuerpo humano, con algunas demostraziones de geometría. Salamanca, España. Retrieved from http://bdh-rd.bne.es/viewer.vm?id=0000042291&page=1

Gariup, G., Pitacco, I., and Fabregat, P. R. (2008). A method for studying multi-body dynamics and its applications to masonry structures analysis. *Structural Analysis of Historic Construction,* (c), 533–540.

Garmendia, L., Larrinaga, P., San-Mateos, R., and San-José, J. T. (2015). Strengthening masonry vaults with organic and inorganic composites: An experimental approach. *JMADE, 85,* 102–114. Retrieved from https://ac.els-cdn.com/S0264127515300447/1-s2.0-S0264127515300447-main.pdf?_tid=78f026c4-af82-4ff6-a36e-7b0638cbd92c&acdnat=1529455749_aa65faa46c0089a084505a2a82557450

Garmendia, L., Larrinaga, P., San-Mateos, R., and San-José, J. T. (2015). Strengthening masonry vaults with organic and inorganic composites: An experimental approach. *Materials and Design, 85,* 102–114. Retrieved from http://dx.doi.org/10.1016/j.matdes.2015.06.150

Garmendia, L., Marcos, I., Garbin, E., and Valluzzi, M. R. (2014). Strengthening of masonry arches with Textile-Reinforced Mortar: experimental behaviour and analytical approaches. *Materials and Structures, 47*(12), 2067–2080.

Gea, S. B., Flores, C., and Toledo, M. W. E. (2014). Influencia del Relleno en Bóvedas de Mampostería. In *Universidad Nacional de Salta* (pp. 1–8).

Ghose, A., and Chakraborti, S. (1986). Empirical strength indices of Indian coals—an investigation. In *Proceedings of 27th US sym- posium on rock mechanics* (pp. 59–61). Balkema, Rotherdam.

Giamundo, V., Lignola, G. P., Maddaloni, G., Balsamo, A., Prota, A., and Manfredi, G. (2015). Experimental investigation of the seismic performances of IMG reinforcement on curved masonry elements. *Composites Part B: Engineering, 70,* 53–63. Retrieved from http://dx.doi.org/10.1016/j.compositesb.2014.10.039

Giamundo, V., Lignola, G. P., Maddaloni, G., da Porto, F., Prota, A., and Manfredi, G. (2016). Shaking table tests on a full-scale unreinforced and IMG retrofitted clay brick masonry barrel vault. *Bulletin of Earthquake Engineering, 14*(6), 1663–1693.

Giaretton, M., Dizhur, D., da Porto, F., and Ingham, J. (2015). Constituent material properties of New Zealand unreinforced stone masonry buildings. *Journal of Building Engineering, 4,* 75–85.

Girardello, P., da Porto, F., Modena, C., and Valluzzi, M. R. (2013). Comportamento sperimentale di volte in muratura rinforzate con materiali compositi a matrice inorganica. *Anidis.* Retrieved from http://www.ingenio-web.it/immagini/CKEditor/P8.pdf

Giuriani, E., Marini, A., Porteri, C., and Preti, M. (2009). Seismic vulnerability for churches in association with transverse arch rocking. *International Journal of Architectural Heritage, 3*(3), 212–234.

Gogoy, I. (1984). Codigos e ideologia en la arquitectura monastica del siglo XVI. (J. B. Artigas, Ed.), *Cuadernos de Arquitectura Virreinal, 1,* 48–55. Retrieved from https://biblat.unam.mx/es/buscar/codigos-e-ideologia-en-la-arquitectura-monastica-del-siglo-xvi

Golebiewski, M., Lubowiecka, I., and Kujawa, M. (2017). Dynamic research of masonry vault in a technical scale. *AIP Conference Proceedings, 1822.*

González-Gómez, W. S., Quintana, P., May-Pat, A., Aviles, F., May-Crespo, J., and Alvarado- Gil, J. J. (2015). Thermal effects on the physical properties of limestones from the Yucatan Peninsula. *International Journal of Rock Mechanics and Mining Sciences, 75,* 182–189. Retrieved from http://dx.doi.org/10.1016/j.ijrmms.2014.12.010

Goudie, A. S. (2006). The Schmidt Hammer in geomorphologial research. *Progress in Physical Geography, 30* (6), 703–718.

Guglielmo, F. De, Ribera, F., Angelillo, M., De Guglielmo, F. De, Ribera, F., and Angelillo, M. (2015). Analysis and consolidation of masonry vaults in the restoration of historical constructions. *Rehab 2015 - 2nd International Conference on Preservation, Maintenance and Rehabilitation of Historic Buildings and Structures,* (February 2016).

Gulick, S. P. S., Christeson, G. L., Barton, P. J., Grieve, R. A. F., and Morgan, J. V. (2013). Geophysical characterization of the Chicxulub impact crater. *Reviews of Geophysics, 51* (1), 22. Retrieved from https://agupubs.onlinelibrary.wiley.com/doi/10.1002/rog.20007

Haramy, K. Y., and DeMarco, M. J. (1985). Use of the Schmidt Hammer for Rock and Coal Testing. *Proceedings - Symposium on Rock Mechanics, 1* (June), 549–555.

Hassan Fangary, A. A. (2010). *Graphics analysis of gothic Vaults.* Universitat Politècnica de Catalunya, Spain. https://doi.org/10.1017/CBO9781107415324.004

Hatir, M. E., and Ince, I. (2021). Lithology mapping of stone heritage via state-of-the-art computer vision. *Journal of Building Engineering, 34.*

Hendry, J. P. (1978). Ankerite (in sediments). In *Sedimentology* (pp. 31–35). Berlin, Heidelberg: Springer Berlin Heidelberg. Retrieved from https://doi.org/10.1007/3-540-31079-7_8

Herbario CICY, U. de R. N. (2020). Ficus maxima Mill-álamo. Retrieved October 29, 2022, from https://www.cicy.mx/sitios/flora digital/ficha_virtual.php?especie=1839

Hernandez, J. (2019). Analisis de tecnicas constructivas a base de piezas ceramicas en bovedas de edificaciones virreinales en Guanajuato Mexico. *Arquitectura y Ciudad. Patrimonio En Mexico, 214* (14), 45.

Heyman, J. (1966). The stone skeleton. *International Journal of Solids and Structures, 2* (2), 249, IN1,257,IN5,265. Retrieved from http://search.ebscohost.com/login.aspx?direct=true&db=edselp&AN=0020768366900187&site=eds-live

Hohmann, H. (2005). A Maya Keystone Vault at La Muñeca. *JSTOR Mexicon, 27* (4), 73–77. Retrieved from https://www.jstor.org/stable/23759556?read- now=1&seq=5#page_scan_tab_contents

Hojdys, Ł., and Krajewski, P. (2014). Laboratory Tests on Masonry Vaults Strengthened at the Extrados, (October), 14–17.

Hudyma, N., Avar, B. B., and Karakouzian, M. (2004). Compressive strength and failure modes of lithophysae-rich Topopah Spring Tuff specimens and analog models containing cavities. *Engineering Geology, 73* (1–2), 179–190.

Huerta Fernández, S. (2007). *Informe estructural sobre las bóvedas del Claustro de los Medallones del Convento de Celanova (Ourense).* Madrid, España. Retrieved from http://oa.upm.es/604/

Huerta, S. (1990). *Diseño estructural de arcos bóvedas y cupulas en España ca. 1500 - ca. 1800.* Universidad Politécnica de Madrid, España. Retrieved from http://oa.upm.es/549/

Huerta, S. (2004). *Arcos, bóvedas y cúpulas. Geometría y equilibrio en el cálculo tradicional de estructuras de fábrica* (1st ed.). Madrid: Instituti Juan de Herrera. Retrieved from http://oa.upm.es/1136/1/Huerta_2004_Arcos_bovedas_y_cupulas.pdf

Huerta, S. (2006). Galileo was wrong: The geometrical design of masonry arches. *Nexus Network Journal, 8* (2), 25–52.

Huerta, S., and Hemando, R. (1998). La teoría de bóvedas en el siglo XVIII: La contribución de Philippe de La Hire. In F. Bores, J. Fernández, S. Huerta, & E. Rabasa (Eds.), *Congreso Nacional de Historia de la Construcción* (pp. 22–24). Coruña: I. Juan de Herrera, SEdHC, U. Coruña, CEHOPU.

INAH. (2020). Catálogo Nacional de Monumentos Históricos Inmuebles. Retrieved April 1, 2020, from https://catalogonacionalmhi.inah.gob.mx/autenticacion/login

INAH. (2020a). Catálogo Nacional de Monumentos Históricos Inmuebles. Retrieved April 1, 2020, from https://catalogonacionalmhi.inah.gob.mx/autenticacion/login

INAH. (2020b). Ficha del Catálogo Nacional de Monumentos Históricos Inmuebles número I- 0013101933. Retrieved from http://www.catalogonacionalmhi.inah.gob.mx/consulta_publica/detalle/79017

INIFED. (2014). Seguridad Estructural. Diseño por Sismo. In *Normas y especificaciones para estudios, proyectos, construcción e instalaciones* (2014th ed., Vol. 4, p. 30). Mexico: SEP Secretaría de Educacicón Pública. Retrieved from https://www.gob.mx/cms/uploads/attachment/file/105540/Tomo_I Instalaciones_Electricas_V_2.1.pdf

Kahraman, S., and Yeken, T. (2008). Determination of physical properties of carbonate rocks from P-wave velocity. *Bulletin of Engineering Geology and the Environment, 67*(2), 277–281.

Kalisch, M. A. R. (1997). La tecnología de la construcción de la arquitectura religiosa virreinal de Yucatán. Método de observación y descripción de sistemas constructivos. Universidad Autónoma de Yucatán.

Kalisch, M. A. R. (2005). El proceso constructivo de apoyos y cubiertas y sus transformaciones en la arquitectura religiosa virreinal de Yucatán. Universidad Nacional Autónoma de México, México.

Karakul, H., and Ulusay, R. (2013). Empirical correlations for predicting strength properties of rocks from P-wave velocity under different degrees of saturation. *Rock Mechanics and Rock Engineering, 46*(5), 981–999.

Karakuş, A., and Akatay, M. (2013). Determination of basic physical and mechanical properties of basaltic rocks from P-wave velocity. *Nondestructive Testing and Evaluation.* Taylor & Francis. Retrieved from http://dx.doi.org/10.1080/10589759.2013.823606

Katz, O., Reches, Z., Roegiers, J. C., O, K., Z, R., J-C, R., ... Roegiers, J. C. (2000). Evaluation of mechanical rock properties using a Schmidt Hammer. *International Journal of Rock Mechanics and Mining Sciences, 37*(4), 723–728.

Kidybiński, A. (1981). Bursting liability indices of coal. *International Journal of Rock Mechanics and Mining Sciences & Geomechanics Abstracts, 18* (4), 295–304. Retrieved from http://www.sciencedirect.com/science/article/pii/0148906281911943

Kiliç, A., and Teymen, A. (2008). Determination of mechanical properties of rocks using simple methods. *Bulletin of Engineering Geology and the Environment, 67*(2), 237–244.

Korinets, A., and Alehossein, H. (2002). On the initial non-linearity of compressive stress-strain curves for intact rock. *Rock Mechanics and Rock Engineering, 35*(4), 319–328.

Krajewski, P., and Hojdys, Ł. (2015). Experimental Studies on Buried Barrel Vaults. *International Journal of Architectural Heritage, 9* (7), 834–843. Retrieved from http://dx.doi.org/10.1080/15583058.2013.860499

Krstevska, L., Tashkov, L., Gramatikov, K., Landolfo, R., Mammana, O., Portioli, F., and Mazzolani, F. M. (2008). Shaking table tests on the large-scale model of Mustafa Pasha Mosque without and with FRP. *Structural Analysis of Historic Construction: Preserving Safety and Significance: Proceedings of the Sixth International Conference on Structural Analysis of Historic Construction, 2-4 July 2008, Bath, United Kingdom,* 383–391.

Kubler, G. (2009). *Arquitectura mexicana del siglo XVI.* (2a ed.). México: Fondo de cultura económica.

Kurtulus, C., Caklr, S., and Yoğurtcuoğlu, A. C. (2016). Ultrasound Study of Limestone Rock Physical and Mechanical Properties. *Soil Mechanics and Foundation Engineering, 52*(6), 348–354.

La Hire, P. de. (1695). *Traité de mécanique, ou l'on explique.* Paris Francia: Chez Jean Anissons.

La Hire, P. de. (1712). Sur la construction des voûtes dans les édifices. *Mémoires de Mathématique et de Physique de l'Académie Royale Des Sciences.* Académie royale des sciences.

Lajtai, E. Z. (1998). Microscopic Fracture Processes in a Granite. *Rock Mechanics and Rock Engineering, 31* (4), 237–250. Retrieved from https://link.springer.com/content/pdf/10.1007%2Fs006030050023.pdf

Landa, D. de. (1566). *Relación de las cosas de Yucatán. Versión en línea.* (Sistemas y Computadores S.A, Ed.). España: La Fundación El Libro Total. y (Sic) Editorial. Retrieved from http://www.ellibrototal.com/ltotal/?t=1&d=2807_2959_1_1_2807

Liu, J. bin, Zhang, Z. jian, and Li, B. (2019). Microscopic & macroscopic characterizations of Beijing marble as a building material for UNESCO heritage sites: new insights into physico- mechanical property estimation and weathering resistance. *Construction and Building Materials, 225,* 510–525.

Loçano, F. (1582). *Los Diez Libros de Architectura de Leon Baptista Alberto.* Madrid, España: Alfonso Gómez impresor de su magestad.

López, A. I. (2020). Palacio Cantón Mérida Yucatán. Retrieved from https://aws.admagazine.com/prod/designs/v1/assets/620x413/66860.jpg

Lourenço, P. (1998). Experimental and numerical issues in the modelling of the mechanical behaviour of masonry. *STRUCTURAL ANALYSIS OF HISTORICAL CONSTRUCTIONS II.* Retrieved from http://citeseerx.ist.psu.edu/viewdoc/download?doi=10.1.1.527.4989&rep=rep1&type=pdf Lourenço, P. (2009). *Recent Advances in Masonry Modelling: Micromodelling and Homogenisation* (Vol. 3). Retrieved from http://ebooks.worldscinet.com/ISBN/9781848163089/9781848163089.html

Lourenço, P. (2009). *Recent Advances in Masonry Modelling: Micromodelling and Homogenisation* (Vol. 3). Retrieved from http://ebooks.worldscinet.com/ISBN/9781848163089/9781848163089.html

Lourenço, P. B. (2008). Structural masonry analysis: recent developments and prospects. In *STRUCTURAL MASONRY ANALYSIS: RECENT DEVELOPMENTS AND PROSPECTS* (p. 16). University of Newcastle, Australia. Retrieved from http://hdl.handle.net/1822/17176

Lyew-Ayee, P. (2004). Digital topographic analysis of cockpit karst: a morpho-geological study of the cockpit country region, Jamaica.

Magalhães, A., and Veiga, R. (2009). Caracterización física y mecánica de los morteros antiguos. Aplicación a la evaluación del estado de conservación. *Materiales de Construcción, 59*(295), 61–77. Retrieved from http://materconstrucc.revistas.csic.es/index.php/materconstrucc/article/view/147/187 Maldonado, L., Veleva, L., and Díaz-Ballote, L. (2011). Characterization of limestones for building in the Yucatan Peninsula, Mexico. *Applied Physics A: Materials Science and Processing, 103*(4), 1105–1110.

Marini, A., Belleri, A., Preti, M., Riva, P., and Giuriani, E. (2017). Lightweight extrados restraining elements for the anti-seismic retrofit of single leaf vaults. *Engineering Structures, 141,* 543–554. Retrieved from http://dx.doi.org/10.1016/j.engstruct.2017.03.038

Marini, A., Giardina, G., Riva, P., and Giuriani, E. (2008). Seismic behaviour of barrel vault systems. Structural Analysis of Historic Construction: Preserving Safety and Significance - Proceedings of the 6th International Conference on Structural Analysis of Historic Construction, SAHC08, 1 (07), 413–421. Retrieved from http://www.scopus.com/inward/record.url?eid=2-s2.0- 79952323646&partnerID=tZOtx3y1

Martínez de Aguirre, J. (1995). Espiritualidad Franciscana y Arquitectura Gótica: Del Recelo a la Revitalización. In García Turza (Ed.), *Semana de Estudios Medievales de Nájera* (1st ed., p.21). Nájera: Instituto de Estudios Riojanos. Retrieved from https://dialnet.unirioja.es/servlet/articulo?codigo=554304

Martinez_de_Arana, X. (1600a). Cerramientos i trazas de montea segunda parte. Martinez_de_Arana, X. (1600b). Cerramientos y trazas de montea primera parte.

Martins, L., Vasconcelos, G., Lourenço, P. B., and Palha, C. (2015). Influence of the freeze-thaw cycles on the physical and mechanical properties of granites. *Journal of Materials in Civil Engineering, 28*(5).

Masciotta, M. G., Pellegrini, D., Girardi, M., Padovani, C., Barontini, A., Lourenço, P. B., ... Fabbrocino, G. (2020). Dynamic characterization of progressively damaged segmental masonry arches with one settled support: Experimental and numerical analyses. *Frattura Ed Integrita Strutturale, 14*(51), 423–441.

May-Crespo, J., Martínez-Torres, P., Alvarado-Gil, J. J., Quintana, P., and Vilca-Quispe, L. (2012). Photothermal radiometry characterization of limestone rocks from the peninsula of Yucatán. *International Journal of Thermophysics, 33*(10–11), 1908–1915.

Mendes, N. (2012). Seismic Assessment of Ancient Masonry Buildings: Shaking Table Tests and Numerical Analysis . PhD Thesis. Universidade do Minho.

Mendes, N., and Lourenço, P. (2009). Comparison of Different Seismic Non-Linear Analyses of an Ancient Masonry Building.

Mendez, L. (2017). Tizimin. Retrieved from https://www.flickr.com/photos/eltb/12532194294/in/album-72157640992348565/

Méridaelite. (2020). Catedral de San Idelfonso-Fachada. Retrieved from https://meridaelite.com/blog/images/catedral-san-idelfonso.jpg

Michiels, T., and Adriaenssens, S. (2018). Form-finding algorithm for masonry arches subjected to in-plane earthquake loading. *Computers and Structures, 195,* 85–98. Retrieved from https://doi.org/10.1016/j.compstruc.2017.10.001

Milani, G., Shehu, R., and Valente, M. (2017). Seismic Vulnerability Mitigation of a Masonry Church by Means of CFRP Retrofitting. Procedia Engineering, 195, 40–47. Retrieved from http://dx.doi.org/10.1016/j.proeng.2017.04.521

Modena, C., Valluzzi, M. R., Da Porto, F., and Casarin, F. (2011). Structural aspects of the conservation of historic masonry constructions in seismic areas: Remedial measures and emergency actions. International Journal of Architectural Heritage, 5(4–5), 539–558.

Molins, C. (1998). Numerical simulation of the ultimate response of arch bridges. In *SAHC 1998. 2nd International Seminar on Structural Analysis of Historical Constructions.* Barcelona, Spain.

Monroy-Ríos, E. (2020). Advancements in our Understanding of the Yucatán Platform: Sedimentary Geology and Geochemistry, Speleogenesis, Chicxulub Ring of Cenotes, and Tectonic Stability. Northwestern University, Evanston, IL. Retrieved from https://sites.northwestern.edu/monroyrios/phd-dissertation/

Montaño, H. (2020). Capilla Abierta, Dzibilchaltún. Retrieved from https://www.inah.gob.mx/boletines/17-arqueologia/5375-wahyis-O

Moreno, H. A. T. (2020). Motul. Retrieved from https://web.archive.org/web/20161001114555if_/http://mw2.google.com/mw-panoramio/photos/medium/27408226.jpg

Motlagh, M. M. (2010). A Comparison between Sasanid Vaults and those of the Roman and Byzantine Periods. *Iran, 48*(1), 43–58.

MTMM. (2013). Nuestra Señora de Lourdes, Mérida. Retrieved from http://www.informaciondelonuevo.com/2013/05/conmueve-feligreses-de-lourdes-homilia.html

Nash, K. (1961). K. Terzaghi: Founder of the Science of Soil Mechanics. *Nature, 191* (4785), 210–210. Retrieved from http://www.nature.com/articles/191210a0

Nasseri, M. H. B., Rao, K. S., and Ramamurthy, T. (2003). Anisotropic strength and deformation behavior of Himalayan schists. *International Journal of Rock Mechanics and Mining Sciences, 40*(1), 3–23.

Navarrete, I. B. L. (1998). *Estilos arquitectónicos de Mérida: historia ilustrada, desde su fundación hasta la actualidad: más de 250 fotografías*. (Ayuntamiento de Mérida Yucatán Dirección de Desarrollo Urbano, Ed.) (1st ed.). Mérida, Yucatán, México: Dante. Retrieved from https://books.google.pt/books/about/Estilos_arquitectónicos_de_Mérida.html?id=fmddAAAAMAAJ&redir_esc=y

Navascués Palacio, P. (1974). *El libro de arquitectura de Hernán Ruíz, el Joven. Estudio y edición critica.* (Escuela Técnica Superior de Arquitectura, Ed.). Madrid.

Niglio, O., and Checa-Artasu, M. (2016). *El Neogótico en la Arquitectura Americana.* (M. M. C.- A. O. Niglio, Ed.). Italy: Ermes. Servizi editoriali integrati S.r.l.

Nohlen, K. (1999). The partial re-erection of the Temple of Trajan at Pergamon in Turkey: A German Archaeological Institute project, Conservation and Management of Archaeological Sites, *3,* 91–102. Retrieved from https://www.tandfonline.com/action/journalInformation?journalCode=ycma20

NP EN 13755, S. NP EN 13755:2008 Metodos de ensaio para pedra natural. Determinaçao da absorçao de agua a pressao atmosferica (2008).

NP EN 1925, S. (2000). Determination of water absortion coefficienr by cappillary. European committee of standardization.

NP EN 1926, S. (2000). Resistência à compressão. European committee of standardization. NP EN 1926, S. (2000). Resistência à compressão. European committee of standardization. NP EN 1926, S. (2000). Resistência à compressão. European committee of standardization.

O'rourke, J. E. (1989). Rock index properties for geoengineering in underground development. *International Journal of Rock Mechanics and Mining Sciences & Geomechanics, 26*(3–4), A174- 106 110. Retrieved from https://linkinghub.elsevier.com/retrieve/pii/0148906289925138

Olmos, C. C. (1994). *Arquitectura del siglo XVI: temas escogidos*. Mérida, Yucatán, México: Facultad de Arquitectura, Universidad Nacional Autónoma de México.

Orduña, A., and Lourenço, P. (2005). Three-dimensional limit analysis of rigid blocks assemblages. Part I: Torsion failure on frictional interfaces and limit analysis formulation. *International Journal of Solids and Structures,* (42), 5140–5160. Retrieved from www.elsevier.com/locate/ijsolstr

Ortiz y Sanz, J. (1787). Los diez libros De Architecture de M. Vitruvio Polión. (I. Real, Ed.). Madrid.

Ortiz y Sanz, J. F. (1797). *Los quatro libros de arquitectura de Andrés Paladio, Vicentino.* Madrid: Imprenta Real. Retrieved from http://www.sedhc.es/bibliotecaD/1797_Andrea_Palladio_Los_cuatro_libros_de_arquitectura.pdf

Özkahraman, H. T., and Işık, E. C. (2003). Determination of Thermal Conductivity of Building Stones from P-Wave Velocity. *International Mining Congress and Exhibition Of Turkey-IMCET,* 557–564. Retrieved from http://www.maden.org.tr/resimler/ekler/7ed94744426295f_ek.pdf

Padilla, A. (2018). Tecoh.

Panoramio. (2018). Capilla Nuestra Señora Del Carmen, Mérida. Retrieved from www.panoramio.com

Paolo Girardello, Pappas, A., Porto, F. da, and Valluzzi, M. R. (2013). Experimental testing and numerical modelling of masonry vaults. *Rehabilitation and Restoration of Structures,* (1), 1–10.

Pappalardo, G., Mineo, S., and Monaco, C. (2016). Geotechnical characterization of limestones employed for the reconstruction of a UNESCO world heritage Baroque monument in southeastern Sicily (Italy). *Engineering Geology, 212,* 86–97.

Pappalardo, G., Punturo, R., Mineo, S., Ortolano, G., and Castelli, F. (2015). Engineering geological and petrographic characterization of migmatites belonging to the Calabria-Peloritani Orogen (Southern Italy). *Rock Mechanics and Rock Engineering, 49*(4), 1143–1160.

Pappalardo, Giovanna. (2014). Correlation Between P-Wave Velocity and Physical–Mechanical Properties of Intensely Jointed Dolostones, Peloritani Mounts, NE Sicily. *Rock Mechanics and Rock Engineering, 48*(4), 1711–1721. Retrieved from http://dx.doi.org/10.1007/s00603-014-0607-8

Parland, H., Heinisuo, M., and Koivula, R. (1982). On the Problem of Bending and Compression of Masonry Structures. In LATERCONSULT s.r.l. (Ed.), *6th International Brick Masonry Conference. I.B.Ma.C.* (pp. 430–441). Rome, Italy: ANDIL -Associazione Nazionale degli Industriali dei Laterizi.

Peña, F., and Chávez, M. M. (2016). Seismic Behavior of Mexican Colonial Churches. *International Journal of Architectural Heritage, 10* (2–3), 332–345. Retrieved from http://dx.doi.org/10.1080/15583058.2015.1113341

Perrault, C. (1761). *Compendio de los diez libros de Arquitectura de Vitruvio (Joseph Castaneda, Traduction)* (2nd ed.). Madrid: Imprenta de D. Gabriel Ramirez. Retrieved from http://www.cehopu.cedex.es/img/bibliotecaD/1761_C_Perrault_Los_diez_libros_de_arqu_de_Vitruvio

Petti john, F. J. (1975). *Sedimentary rocks* (3rd ed.).

Plo y Camin, A. (1767). *El arquitecto practico, civil, militar y agrimensor* (1st ed.). Madrid, España: Imprenta de Pantaleón Aznar.

Ponce de León, P. A. C. (2000). *Transformaciones y evolución de la arquitectura religiosa de Yucatán durante los siglos XVII y XVIII.* UNAM_Universidad Nacional Autónoma de México, México. Retrieved from http://132.248.9.195/pd2000/285774/Index.html

Portioli, F., and Cascini, L. (2016). Assessment of masonry structures subjected to foundation settlements using rigid block limit analysis. *Engineering Structures, 113,* 347–361. Retrieved from http://dx.doi.org/10.1016/j.engstruct.2016.02.002

Portioli, F., and Cascini, L. (2017). Large displacement analysis of dry-jointed masonry structures subjected to settlements using rigid block modelling. *Engineering Structures, 148,* 485–496.

PRODISIS. (2017). PRODISIS (PROgrama de DIseño SÍSmico) version 4.1 (2017-08-15). Retrieved July 30, 2020, from https://www2.ineel.mx/prodisis/es/prodisis.php

Ramaglia, G., Lignola, G. P., and Prota, A. (2016). Collapse analysis of slender masonry barrel vaults. *Engineering Structures, 117,* 86–100. Retrieved from http://dx.doi.org/10.1016/j.engstruct.2016.03.016

Ramamurthy, T., Rao, G. V., and Singh, J. (1993). Engineering behavior of phyllites. *Engineering Geology, 33* (3), 209–225.

Ramos, A. (2011). Caracterización estructural de los rellenos en bóvedas históricas de fábrica Trabajo. Universidad Politécnica de Madrid, Madrid.

Ramos, A., and León, J. (2013). Clasificación morfológica de los rellenos en el trasdós de bóvedas de fábrica

Classification of backfill at the extrados of masonry vaults. *Informes de La Construccion, 65*(532), 471–480.

Ramos, A., and León, J. (2017). Diferencias entre el comportamiento de los rellenos en bóvedas históricas de fábrica de puentes y edificios. In Asociación Española de Ingeniería Estructural (ACHE) (Ed.), *VII congreso de ACHE* (pp. 1–10). España: Revista Hormigón y Acero.

Ramos, J. L. F. da S., and Lourenço, P. (2008). Damage identification in masonry structures with vibration measurements, 311–319.

Ramos, R. C. (1989). Arquitectura y feudalismo en México: los comienzos del arte novohispano en el siglo XVI. Universidad Nacional Autónoma de México.

Rivera, D. B. (2003). Comportamiento Estructural de Bóvedas de Mampostería de Cañón Corrido. Universidad Nacional Autónoma de México.

Rivero, E. C., and Gutiérrez, N.-H. R. (2013). Las Manifestaciones Artísticas de la Ciudad Blanca: Centro Histórico de Mérida, Yucatán, México. *ASRI Arte y Sociedad, 4.*

Roca, P., López-Almansa, F., Miquel, J., and Hanganu, A. (2007). Limit analysis of reinforced masonry vaults. *Engineering Structures, 29*(3), 431–439.

Rodríguez Campera, O. (2008). La Arquitectura Petén en Calakmul: Una Comparación Regional. USA.

Rodríguez Pérez, I., Vasconcelos, G., Lourenço, P. B., Quintana, P., García, C., and Dionísio, A. (2021). Physical-mechanical characterization of limestones from Yucatan churches, Mexico. *Journal of Building Engineering, 44,* 102895. Retrieved from https://doi.org/10.1016/j.jobe.2021.102895

Rodríguez, I. (2006). *Diagnóstico estructural de la bóveda de cañón corrido en la iglesia de Mama Yucatán.* Universidad Autónoma de Yucatán. Retrieved from https://scholar.google.es/citations?hl=es&pli=1&user=U7u0x1n8bTsC

Rovero, L., Alecci, V., Mechelli, J., Tonietti, U., and De Stefano, M. (2016). Masonry walls with irregular texture of L'Aquila (Italy) seismic area: validation of a method for the evaluation of masonry quality. *Materials and Structures, 49*(6). Retrieved from http://link.springer.com/10.1617/s11527-015-0650-2

Rovero, L., Focacci, F., and Stipo, G. (2012). Structural Behavior of Arch Models Strengthened Using FRP Strips of Different Lengths. *Journal of Composites for Construction,* (February 2016), 120822052708008.

Ruppert, K., and Denison, J. H. jr. (1943). *Bookmark Archaeological reconnaissance in Campeche, Quintana Roo, and Peten* (1st ed.). Washington, D.C., Carnegie institution of Washington. Publication 543.

Sachpazis, C. I. (1990). CORRELATING SCHMIDT HARDNESS WITH COMPRESSIVE

STRENGTH AND YOUNG'S MODULUS OF CARBONATE ROCKS. *International Association of ENGINEERING GEOLOGY, 42,* 75–83.

Saeidi, O., Rasouli, V., Vaneghi, R. G., Gholami, R., and Torabi, S. R. (2014). A modified failure criterion for transversely isotropic rocks. *Geoscience Frontiers, 5*(2), 215–225.

Sagredo, D. de. (1549). Medidas del romano o Vitruvio nuevamente impressas y añadidas muchas pieças e figuras muy necessarias a los officiales que quieren seguir las formaciones de las bazas, columnas, capiteles y otras pieças de los edificios antiguos. Toledo: Casa de Iván de Ayala.

Sanabria, S. L. (1982). The Mechanization of Design in the 16th Century: The Structural Formulae of Rodrigo Gil de Hontañón. *Journal of the Society of Architectural Historians, 41*(4).

Saptono, S., Kramadibrata, S., and Sulistianto, B. (2013). Using the Schmidt Hammer on rock Mass Characteristic in Sedimentary Rock at Tutupan coal Mine. *Procedia Earth and Planetary Science, 6,* 390–395.

Saroglou, H., and Tsiambaos, G. (2007). Classification of anisotropic rocks. *11th Congress of the International Society for Rock Mechanics,* (March), 191–196.

Satterthwaite, L. (1944). Archaeological Reconnaissance in Campeche, Quintana Roo, and Peten. Karl Ruppert and John H. Denison Jr., (Carnegie Institution of Washington, Publication 543. Washington, 1943.). *American Antiquity, 10* (02), 216–218. Retrieved from https://www.cambridge.org/core/product/identifier/S0002731600030651/type/journal_article

Selçuk, L., and Nar, A. (2016). Prediction of uniaxial compressive strength of intact rocks using ultrasonic pulse velocity and rebound-hammer number. *Quarterly Journal of Engineering Geology and Hydrogeology, 49*(1), 67–75.

Serrano, P. Á. (2012). *Porfirio Díaz y el Porfiriato Cronología (1830-1915) Cronología (1830- 1915).* (L. O.

Martínez, Ed.) (1st ed.). México: Instituto Nacional de Estudios Históricos de las Revoluciones de México (INEHRM). Retrieved from http://www.inehrm.gob.mx/work/models/inehrm/Resource/437/1/images/porfirio_porfiriato.pdf

Sharma, P. K., Khandelwal, M., and Singh, T. N. (2011). A correlation between Schmidt hammer rebound numbers with impact strength index, slake durability index and P-wave velocity. *International Journal of Earth Sciences, 100*(1), 189–195.

Sheorey, P. R., Barat, D., Das, M. N., Mukherjee, K. P., and Singh, B. (1984). Technical note technical note. *Rock Mech. Min. Sci. & Geomech, 21*(1), 39–42.

Sikora, P., Sharpton, L., Marin, E., Geofisica, D., and Carney, L. (1996). A model of the Chicxulub impact basin based on evaluation of geophysical data, well logs, and drill core samples a model of the Chicxulub data, impact well logs, basin based on evaluation of geophysical and drill core samples. *Geological Society of America,* (February), 21.

Silva, A. S., Ricardo, J. M., Salta, M., Adriano, P., Mirão, J., Candeias, A. E., and Macias, S. (2006). Characterization of Roman mortars from the historical town of Mertola (Vol. 1, pp.85–90). Retrieved from https://www.scopus.com/record/display.uri?eid=2-s2.0-60749102900&origin=resultslist&sort=plf-f&src=s&st1=Characterization+of+Roman+mortars+from+the+historical+town+of+Mertola&st2=&sid=860cc83cfa56b132b58930450839913e&sot=b&sdt=b&sl=84&s=TITLE-ABS-KEY%28Ch

Singh, R., Hassani, F., and Elkington, P. (1983). The application of strength and deformation index testing to the stability assess- ment of coal measures excavations. In A&M Univ. (Ed.), *Proc. 24th US Symp. On Rock Mech.* (pp. 599–609). Texas.

Structural Vibration Solutions A/S. (2019). ARTeMIS Modal.

Suárez Quevedo, D. (2008). Sobre las primeras ediciones del De re aedificatoria de Leon Battista Alberti. *Pecia Complutense: Boletín de la Biblioteca Histórica de la Universidad Complutense, 9*(5), 65. Retrieved from https://eprints.ucm.es/8434/

Sulu, V., and G. Navarrete. (2014). Iglesia de Nuestra Señora de Lourdes. Retrieved from https://www.meridadeyucatan.com/iglesia-de-lourdes/

Sun, J., Wu, Z., Cheng, H., Zhang, Z., and Frost, R. L. (2014). Spectrochimica Acta Part A: Molecular and Biomolecular Spectroscopy A Raman spectroscopic comparison of calcite and dolomite. *Spectrochimica Acta Part A: Molecular and Biomolecular Spectroscopy, 117,* 158–162. Retrieved from http://dx.doi.org/10.1016/j.saa.2013.08.014

Szwedzicki, T. (2007). A hypothesis on modes of failure of rock samples tested in uniaxial compression. *Rock Mechanics and Rock Engineering, 40*(1), 97–104.

Talavera Gonzalez, J. A., and Serrano Espinosa, T. E. (2015). La capilla de visita de san Martín Cuetlajuchitlán: un vestigio del avance agustino en el Estado de Guerrero, México. *Tiempo y Escritura,* 7–24. Retrieved from https://eds.a.ebscohost.com/eds/pdfviewer/pdfviewer?vid=0&sid=8db97836-e43c-4d5a-b8af-5d8b267dce59%40sdc-v-sessmgr02

Tamayo, M. O. (2004, June 30). Arquitectura religiosa virreinal de Yucatán. El conocimiento històrico-técnico de las iglesias con estructura espacial conventual. El conocimiento de la arquitectura histórica como condicionante de la restauración. TDX (Tesis Doctorals en Xarxa). Universitat Politècnica de Catalunya. Retrieved from http://www.tdx.cat/handle/10803/6115

Tejeda, J., and Silva, C. (2002). ESTUDIO DE RESISTENCIAS A COMPRESIÓN DIAGONAL (CORTANTE), DE MURETES DE MAMPOSTERÍA FABRICADOS CON MATERIALES DE LA ZONA CONURBADA COLIMA-VILLA DE ÁLVAREZ. In A. C. Sociedad Mexicana de Ingeniería Estructural (Ed.), *XIII Congreso Nacional de Ingeniería Estructural* (pp. 349–356). Puebla, México: Sociedad Mexicana de Ingeniería Estructural, A.C.

Tixkuncheil, O. religiosa. (2020). Capilla “San Miguel Arcángel” Tixkuncheil. Yucatan. Retrieved from https://www.facebook.com/Capilla-San-Miguel-Arcángel-Tixkuncheil-Yuc-104890200867615/photos/285370246152942/

Tomašić, I., Lukić, D., Peček, N., and Kršinić, A. (2011). Dynamics of capillary water absorption in natural stone. Bulletin of Engineering Geology and the Environment, 70 (4), 673–680.

Torabi, S., Ataei, M., and Javanshir, M. (2011). Application of Schmidt rebound number for estimating rock strength under specific geological conditions. *Journal of Mining and Environment, 0*(0), 1–8.

Torok, A. (2003). Surface strength and mineralogy of weathering crusts on limestone buildings in Budapest.

Building and Environment, 38, 1185–1192. Retrieved from www.sciencedirect.comwww.elsevier.com/locate/buildenv

Torres, B., Bertolesi, E., Moragues, J. J., Calderón, P. A., and Adam, J. M. (2019). Experimental investigation of a full-scale timbrel masonry cross vault subjected to vertical settlement. *Construction and Building Materials, 221,* 421–432. Retrieved from https://doi.org/10.1016/j.conbuildmat.2019.06.015

Tubaldi, E., Macorini, L., and Izzuddin, B. A. (2018). Three-dimensional mesoscale modelling of multi-span masonry arch bridges subjected to scour. *Engineering Structures, 165*(June 2017), 486–500. Retrieved from https://doi.org/10.1016/j.engstruct.2018.03.031

Ündül, Ö. (2016). Assessment of mineralogical and petrographic factors affecting petro-physical properties, strength, and cracking processes of volcanic rocks. *Engineering Geology, 210,* 10–22.

UNE-EN 1996. (2011). Eurocódigo 6: Proyecto de estructuras de fábrica.

Urióstegui, A. J. A., Checa-Artasu, M. M., Domínguez, J. de J. C., Ortiz, J. G., Chiang, A. G., García, K. A. G., … Nochebuena, M. C. V. (2014). *Territorialidades y Arquitecturas de lo Sagrado en el México Contemporáneo.* (M. M. Checa-Artasu, J. J. López, & M. C. Valerdi, Eds.) (Primera ed.). Aguascalientes, Aguascalientes, México: Departamento Editorial de la Dirección General de Difusión y Vinculación de la Universidad Autónoma de Aguascalientes.

Uyanık, O., Sabbağ, N., Uyanık, N. A., and Öncü, Z. (2019). Prediction of mechanical and physical properties of some sedimentary rocks from ultrasonic velocities. *Bulletin of Engineering Geology and the Environment, 78*(8), 6003–6016.

Valluzzi, M. R., da Porto, F., and Modena, C. (2001). Behaviour of multi-leaf stone masonry walls strengthened by different intervention techniques. *Historical Constructions,* 1023. Retrieved from http://www.hms.civil.uminho.pt/sahc/2001/page 1023-1032 _89_.pdf

Valluzzi, M. R., Valdemarca, M., and Modena, C. (2001). Behavior of Brick Masonry Vaults Strengthened by FRP Laminates. *Journal of Composites for Construction, 5* (3), 163–169. Retrieved from http://ascelibrary.org/doi/10.1061/%28ASCE%291090- 0268%282001%295%3A3%28163%29

Valvona, F., Toti, J., Gattulli, V., and Potenza, F. (2017). Effective seismic strengthening and monitoring of a masonry vault by using Glass Fiber Reinforced Cementitious Matrix with embedded Fiber Bragg Grating sensors. Composites Part B: Engineering, 113, 355–370.

Vasconcelos, G. (2005). Experimental investigations on the mechanics of stone masonry: Characterization of granites and behavior of ancient masonry shear walls. University of Minho.

Vasconcelos, G., and Lourenço, P. (2009). Experimental characterization of stone masonry in shear and compression. *Construction and Building Materials, 23*(11), 3337–3345.

Vasconcelos, G., Lourenço, P., Alves, C. A. S., and Pamplona, J. (2008). Ultrasonic evaluation of the physical and mechanical properties of granites. *Ultrasonics, 48*(5), 453–466.

Vasconcelos, G., Lourenço, P., Alves, C. S. A., and Pamplona, J. (2007). Prediction of the mechanical properties of granites by ultrasonic pulse velocity and Schmidt hammer hardness. In *10 North America Masonry conference.* St. Lous, Missouri. Retrieved from https://www.researchgate.net/publication/237291120_Prediction_of_the_mechanical_properties_of_granites_by_ultrasonic_pulse_velocity_and_Schmidt_hammer_hardness

Vega, L. B., Rubio, J. I. M., García, J. P., Barrera, A. V., and Fernández, J. (1945a). *Catálogo de construcciones religiosas del estado de Yucatán. Vol. 1* (1st ed.). México: Talleres Gráficos de la Nación.

Veiga, M. do R. (2015). ARGAMASSAS DE CAL: O que falta saber para a sua utilização em conservação e reabilitação? In *V Jornadas FICAL.* Lisboa: Laboratorio NAcional de Engenharia Civil. Retrieved from http://vfical.lnec.pt/apresentacoes/Rosário Veiga.pdf

Villalpaldo, F. de. (1552). Tercero y Quarto Libro de Architetura de Sebastian Serlio. Toledo: Casa de Ivan de Ayala.

Worotnicki, G. (1993). *CSIRO triaxial stress measurement cell.* (Hudson, Ed.), *Comprehensive rock engineering* (Vol. 3). Oxford: Pergamon Press. Retrieved from http://dx.doi.org/10.1016/B978-0-08-042066-0.50020-3

Xu, S., Grasso, P., and Mahtab, A. (1990). Use of Schmidt hammer forestimating mechanical properties of weak rock. In *6th Int. IAEG Congress* (pp. 511–519). Balkema, Rotterdam.

Yagiz, S. (2011). P-wave velocity test for assessment of geotechnical properties of some rock materials. *Bulletin of Materials Science, 34*(4), 947–953.

Yaşar, E., and Erdoğan, Y. (2003). Estimation of rock physicomechanical properties using hardness methods. *Engineering Geology, 71* (3–4), 281–288.

Yasar, E., and Erdogan, Y. (2004). Correlating sound velocity with the density, compressive strength, and young's modulus of carbonate rocks. *International Journal of Rock Mechanics and Mining Sciences, 41* (5), 871–875.

Yilmaz, I., and Sendir, H. (2002). Correlation of Schmidt hardness with unconfined compressive strength and young's modulus in gypsum from Sivas (Turkey). *Engineering Geology, 66* (3–4), 211–219.

Zampieri, P., Amoroso, M., and Pellegrino, C. (2019). The masonry buttressed arch on spreading support. *Structures, 20* (March), 226–236.

Zampieri, P., Cavalagli, N., Gusella, V., and Pellegrino, C. (2018). Collapse displacements of masonry arch with geometrical uncertainties on spreading supports. *Computers and Structures, 208,* 118–129. Retrieved from https://doi.org/10.1016/j.compstruc.2018.07.001

Zampieri, P., Faleschini, F., Zanini, M. A., and Simocello, N. (2018). Collapse mechanisms of masonry arches with settled springing. *Engineering Structures, 156* (November 2017), 363–374. Retrieved from https://doi.org/10.1016/j.engstruct.2017.11.048

Zampieri, P., Faleschini, F., Zanini, M. A., and Simoncello, N. (2018). Collapse mechanisms of masonry arches with settled springing. *Engineering Structures, 156* (November 2017), 363–374.

Zampieri, P., Simoncello, N., and Pellegrino, C. (2017). Structural behaviour of masonry arch with no-horizontal springing settlement. *Frattura Ed Integrità Strutturale, 12* (43), 182–190. Retrieved from https://www.fracturae.com/index.php/fis/article/view/IGF-ESIS.43.14

Zampieri, P., Simoncelo, N., Tetougueni, C. D., and Pellegrino, C. (2018). A review of methods for strengthening of masonry arches with composite materials. *Engineering Structures, 171* (May), 154–169. Retrieved from https://doi.org/10.1016/j.engstruct.2018.05.070

Zhang, Y., Macorini, L., and Izzuddin, B. A. (2018). Numerical investigation of arches in brick- masonry bridges. *Structure and Infrastructure Engineering, 14* (1), 14–32. Retrieved from http://doi.org/10.1080/15732479.2017.1324883

Zhu, W., Baud, P., and Wong, T.-F. (2010). Micromechanics of cataclastic pore collapse in limestone. *Journal of Geophysical Research: Solid Earth, 115* (B04405). Retrieved from http://doi.wiley.com/10.1029/2009JB006610

Annex 2.1
Database of churches from sixteenth to eighteenth centuries

Abstract: In this section is shown the database of Yucatan churches from sixteenth to eighteenth centuries. Three sections are available 1) General information, 2) Physical characteristics and 3) Geometrical characteristics.

GENERAL INFORMATION				PHYSICAL CHARACTERISTICS							GEOMETRICAL CHARACTERISTICS												
					Wall		Vault		Buttress		Principal nave dimensions						Wall		Vault				
ID	Name	Location	Century construction	Kind of plant	Materials	Cross section	Typology	Materials	Have? Yes or No	Dimension a x b	Span	Three nave Span 1	Three nave Span 2	Three nave Span 3	Length	Height	Height	Thickness	Height	Constant Thickness Yes or No	Thicknees in key stone	Tickness in ribs	Tickness in start
1	Cacalchen	Cacalchen	XVI	One nave	Masonry	3 layers	Segmental barrel vaults	Rebuilding with Filler block	Yes	-	9.34	-	-	-	30.58	11.35	9.78	1.24	1.57	-	-	-	-
2	Calotmul	Calotmul	XVII	One nave	Masonry	3 layers	Wooden logs and masonry on arches and pilasters	Wooden logs-masonry	Yes	-	11.37	-	-	-	40.95	13.97	8.78	1.54	5.19	-	-	-	-
3	Cansahcab	Cansahcab	XVII	One nave	Masonry	3 layers	Cannon vault - Reinforced with Arches, on pilasters	Masonry	Yes	-	9.20	-	-	-	26.90	10.50	5.90	2.90	4.6	-	-	-	-
4	Catedral	Mérida	XVI	Three nave	Masonry	3 layers	Sail vaults with coffers on arches, pilasters and columns	Masonry	No	-	30.80	7.82	11.09	7.86	65.24	22.27	-	2.95	-	-	-	-	-
5	Cenotillo	Cenotillo	XVII	One nave	Masonry	3 layers	Wooden logs and masonry on arches and pilasters	Wooden logs-masonry	Yes	-	12.57	-	-	-	27.62	19.40	9.32	1.40	10.08	-	-	-	-
6	Chancenote	Chancenote	XVI	One nave	Masonry	3 layers	Cannon Vault on Walls	Masonry	No	-	11.20	-	-	-	40.07	14.10	8.35	3.10	5.75	Yes	0.50	-	-
7	Chichimilá	Chichimilá	XVI	One nave	Masonry	3 layers	Wooden logs and masonry on arches and pilasters	Wooden logs-masonry	Yes	4.50	10.15	-	-	-	46.85	-	8.80	0.90	-	-	-	-	-
8	Conkal	Conkal	XVII	One nave	Masonry	3 layers	Cannon Vault on walls. Reinforced with Arcos	Masonry	Yes	-	11.72	-	-	-	26.95	18.35	11.75	1.90	6.6	-	-	-	-
9	Dzidzantun	Dzidzantun	XVI	One nave	Masonry	3 layers	Cannon Vault on Walls	Masonry	Yes	-	11.30	-	-	-	68.11	17.95	13.00	2.81	4.95	No	0.43	0.69	1.58
10	Ekmul	Ekmul		One nave	Masonry	3 layers	Without vault nowadays or information	Not available	No	-	8.25	-	-	-	24.35	10.70	6.55	0.76	4.15	-	-	-	-
11	Espita	Espita	XVII	One nave	Masonry	3 layers	Without vault nowadays or information	Not available	Yes	1.70 x 2.02	13.62	-	-	-	48.37	17.60	12.02	2.14	5.58	No	0.24	0.26	0.31
12	Hocabá	Hocabá	XVII	One nave	Masonry	3 layers	Cannon Vault on Walls	Masonry	No	-	10.40	-	-	-	35.50	12.95	7.70	2.70	5.25	-	-	-	-

GENERAL INFORMATION				PHYSICAL CHARACTERISTICS							GEOMETRICAL CHARACTERISTICS												
					Wall		Vault		Buttress		Principal nave dimensions						Wall		Vault				
ID	Name	Location	Century construction	Kind of plant	Materials	Cross section	Typology	Materials	Have? Yes or No	Dimension a x b	Span	Three nave Span 1	Three nave Span 2	Three nave Span 3	Length	Height	Height	Thickness	Height	Constant Thickness Yes or No	Thicknees in key stone	Tickness in ribs	Tickness in start
13	Homún	Homún	XVII	One nave	Masonry	3 layers	Cannon Vault on Walls	Masonry	No	-	9.73	-	-	-	23.00	13.44	8.68	2.55	4.76	-	-	-	-
14	Hunucmá	Hunucmá	XVI	One nave	Masonry	3 layers	Canon vaults with arches and pilasters	Rebuilding with steel bean and masonry	Yes	-	16.20	-	-	-	43.87	-	-	1.00	-	-	-	-	-
15	Ichmul *	Ichmul	XVIII	Latin cross	Masonry	3 layers	Canon vaults with arches and pilasters	Uuncovered	No	-	10.99	-	-	-	37.60	-	8.60	3.20	S/C	S/C	-	-	-
16	Izamal	Izamal	XVI	One nave	Masonry	3 layers	Cannon Vault on Walls	Masonry	No	-	10.70	-	-	-	52.59	16.22	10.79	L:3.10/ R:3.80	5.43	Yes	0.50	-	-
17	La Mejorada	Mérida	XVII	One nave	Masonry	3 layers	Sail vaults on arches and pilasters	Masonry	No	-	8.54	-	-	-	19.15	15.75	8.50	1.00	7.25	-	-	-	-
18	Mama	Mama	XVII	One nave	Masonry	3 layers	Cannon Vault on Walls	Masonry	Yes	1.92 x 2.57	10.81	-	-	-	57.61	14.77	9.47	L:1.10/ R:1.28	5.3	No	0.37	0.45	0.65
19	Maní	Maní	XVI	One nave	Masonry	3 layers	Cannon Vault on Walls	Masonry	No	-	8.45	-	-	-	36.80	11.74	7.52	L:2.45/ R:3.51	4.22	-	-	-	-
20	Maxcanú	Maxcanú	XVIII	One nave	Masonry	3 layers	Cannon vault - Reinforced with Arches, on pilasters	Masonry	Yes	-	9.16	-	-	-	34.40	12.96	8.38	1.80	4.58	Yes	0.50	-	-
21	Mocochá	Mocochá	XVII	Latin cross	Masonry	3 layers	Cannon Vault On walls. Reinforced with Arcos	Masonry	No	-	9.09	-	-	-	32.00	13.10	9.09	1.19	4.01	-	-	-	-
22	Motul	Motul	XVII	One nave	Masonry	3 layers	Cannon Vault on Walls	Masonry	Yes	-	10.70	-	-	-	40.30	19.90	13.50	2.90	6.4	-	-	-	-
23	Muna	Muna	XVII	Three nave	Mampostería	3 paños	Canon vaults with arches and pilasters	Rebuilding with steel bean and masonry	Yes	-	11.18	-	-	-	34.20	12.55	5.90	2.33	6.65	-	-	-	-
24	Oxcutzcab	Oxcutzcab	XVIII	Three nave	Masonry	3 layers	Canon vaults with arches, columns and pilasters	Rebuilding with steel bean and masonry	Yes	1.70 x 2.51	18.31	-	-	-	42.11	13.66	11.55	2.10	2.11	-	-	-	-
25	Sisal	Sisal	XVI	One nave	Masonry	3 layers	Cannon Vault on Walls	Masonry	No	-	10.50	-	-	-	20.90	17.50	10.64	2.60	6.86	-	-	-	-

GENERAL INFORMATION				PHYSICAL CHARACTERISTICS							GEOMETRICAL CHARACTERISTICS												
					Wall		Vault		Buttress		Principal nave dimensions						Wall		Vault				
ID	Name	Location	Century construction	Kind of plant	Materials	Cross section	Typology	Materials	Have? Yes or No	Dimension a x b	Span	Three nave Span 1	Three nave Span 2	Three nave Span 3	Length	Height	Height	Thickness	Height	Constant Thickness Yes or No	Thicknees in key stone	Tickness in ribs	Tickness in start
26	Sotuta	Sotuta	XVII	One nave	Masonry	3 layers	Cannon Vault on Walls	Masonry	Yes	-	11.74	-	-	-	36.60	12.07	7.31	2.40	4.76	-	-	-	-
27	Teabo	Teabo	XVII	Three nave	Masonry	3 layers	Sail vaults on arches and pilasters	Masonry	Yes	1.70 x 3.20	7.62	3.98	7.62	3.45	57.13	12.18	7.52	2.05	4.66	-	-	-	-
28	Tecoh	Tecoh	XVII	One nave	Masonry	3 layers	Cannon Vault On walls. Reinforced with Arcos	Masonry	No	-	10.10	-	-	-	30.80	13.20	7.98	2.99	5.22	-	-	-	-
29	Tekantó	Tekantó	XVII	Three nave	Masonry	3 layers	Canon vaults with arches and pilasters	Wooden logs-masonry	Yes	-	15.90	-	-	-	38.05	10.84	9.17	1.27	1.67	-	-	-	-
30	Tekax	Tekax	XVII	Three nave	Masonry	3 layers	Sail vaults on arches, pilasters and columns	Masonry	Yes	1.55 x 2.23	20.49	-	-	-	51.30	12.86	-	1.44	-	-	-	-	-
31	Tekit	Tekit	XVI	One nave	Masonry	3 layers	Cannon Vault on Walls	Masonry	Yes	2.20 x 3.00	11.93	-	-	-	40.53	13.06	9.10	1.80	3.96	No	0.80	0.91	1.02
32	Telchac	Telchac	XVIII	One nave	Masonry	3 layers	Cannon Vault on Walls	Masonry	No	-	10.32	-	-	-	34.85	15.10	-	0.90	-	-	-	-	-
33	Temax	Temax	XVII	One nave	Masonry	3 layers	Cannon Vault on Walls	Masonry	No	-	10.28	-	-	-	35.55	12.45	7.52	2.90	4.93	Yes	0.47	-	-
34	Tetiz	Tetiz		One nave	Masonry	3 layers	Cannon Vault on Walls	Masonry	No	-	8.15	-	-	-	43.20	12.17	8.08	2.28	4.09	No	0.40	0.45	0.60
35	Teya	Teya	XVIII	One nave	Masonry	3 layers	Cannon Vault on Walls	Masonry	No	-	8.50	-	-	-	30.74	13.18	8.30	-	4.88	-	-	-	-
36	Ticul	Ticul	XVII	One nave	Masonry	3 layers	Cannon Vault On walls. Reinforced with Arcos	Masonry	No	-	9.75	-	-	-	39.75	14.17	9.52	3.00	4.65	-	-	-	-
37	Tixcacalcupul	Tixcacalcupul	XVII	One nave	Masonry	3 layers	Canon vaults with arches and pilasters	Wooden logs-masonry	No	-	12.00	-	-	-	32.91	15.23	8.54	2.20	6.69	Yes	0.35	-	-
38	Tixkokob	Tixkokob	XVIII	One nave	Masonry	3 layers	Cannon vault - Reinforced with Arches on pilasters	Masonry	No	-	12.94	-	-	-	34.67	13.40	7.84	1.65	5.56	-	-	-	-

GENERAL INFORMATION				PHYSICAL CHARACTERISTICS							GEOMETRICAL CHARACTERISTICS												
					Wall		Vault		Buttress		Principal nave dimensions						Wall		Vault				
ID	Name	Location	Century construction	Kind of plant	Materials	Cross section	Typology	Materials	Have? Yes or No	Dimension a x b	Span	Three nave Span 1	Three nave Span 2	Three nave Span 3	Length	Height	Height	Thickness	Height	Constant Thickness Yes or No	Thicknees in key stone	Tickness in ribs	Tickness in start
39	Tixmehuac	Tixmehuac	XVIII	One nave	Masonry	3 layers	Cannon Vault on Walls	Masonry	Yes	1.60 X 2.40	11.74	-	-	-	35.64	12.50	6.90	1.60	5.6	Yes	0.55	0.57	0.55
40	Tizimin	Tizimin	XVIII	One nave	Masonry	3 layers	Cannon Vault On walls. Reinforced with Arcos	Masonry	No	-	12.00	-	-	-	38.80	17.05	10.90	-	6.15	-	-	-	-
41	Uayma	Uayma	XVII	Latin cross	Masonry	3 layers	Cannon Vault on Walls	Masonry	No	-	11.45	-	-	-	35.56	15.48	9.70	3.06	5.78	Yes	0.50	-	-
42	Umán	Umán	XVIII	Latin cross	Masonry	3 layers	Groin vaults on arches and pilasters	Masonry	Yes	-	13.62	-	-	-	44.70	19.35	15.45	2.80	3.9	-	-	-	-
43	Xcan	Xcan	XVIII	One nave	Masonry	3 layers	Cannon Vault on Walls	Rebuilding	Yes	2.40 x 2.00	10.67	-	-	-	43.10	14.07	9.07	2.60	5	Yes	0.62	0.54	0.59
44	Yaxcaba	Santa María, Yaxcaba	XVIII	One nave	Masonry	3 layers	Canon vaults with arches and pilasters	Wooden logs-masonry	No		8.76	-	-	-	32.26	-	-	1.43	-	S/C	-	-	-
											11.64 Aver	5.90 Aver	9.36 Aver	5.66 Aver	38.46 Aver	14.48 Aver	9.17 Aver	2.09 Aver	5.10 Aver	Aver	0.48 Aver	0.55 Prom	0.76 Prom

a = parallel dimension to the longitudinal wall

b = perpendicular dimension to the longitudinal wall

L = Left

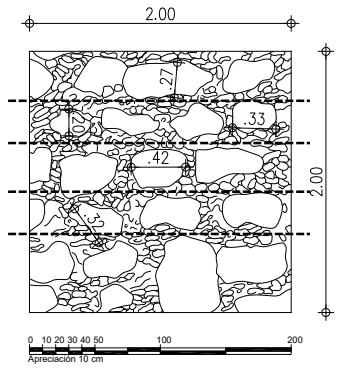
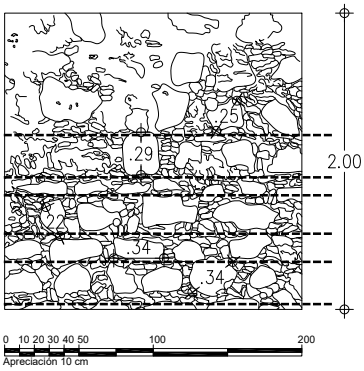
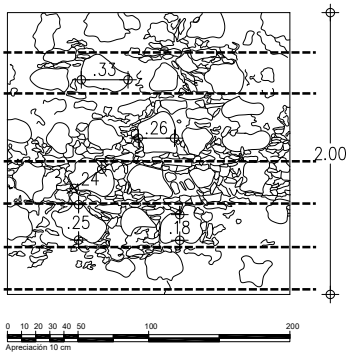
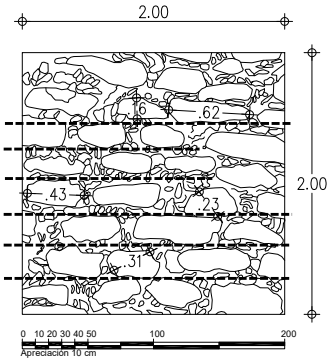
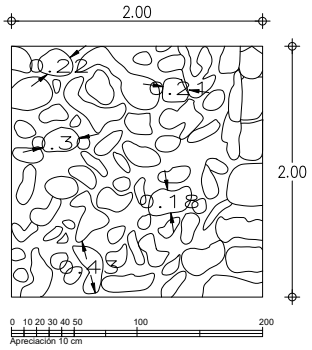
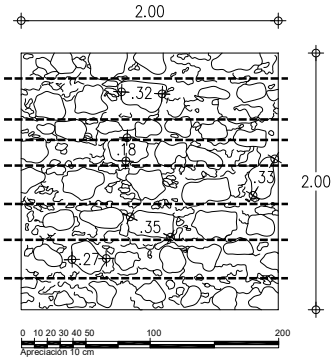
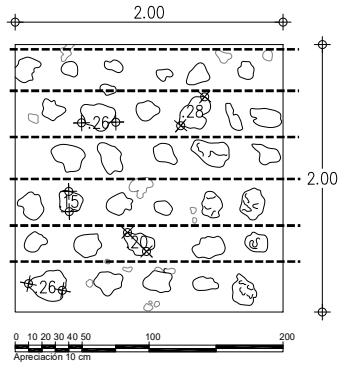
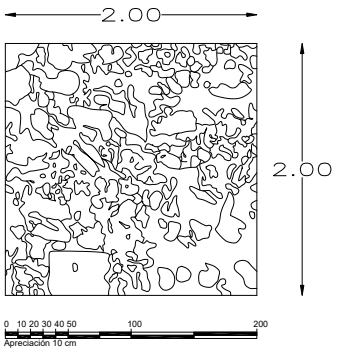
R=Right

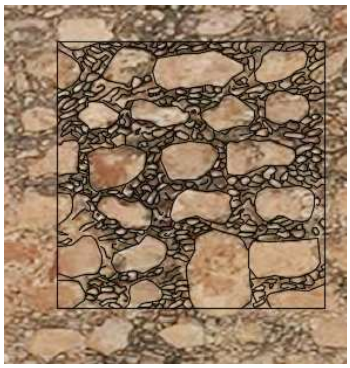
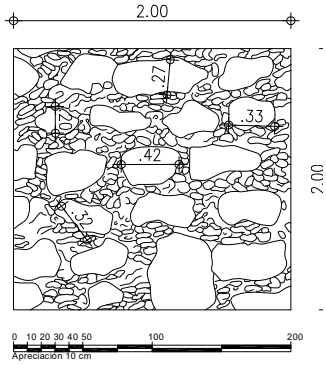
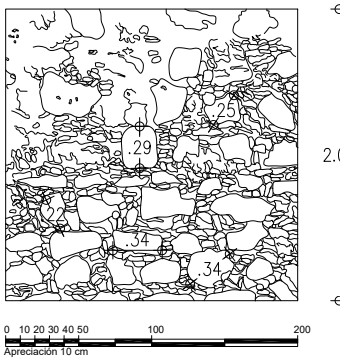
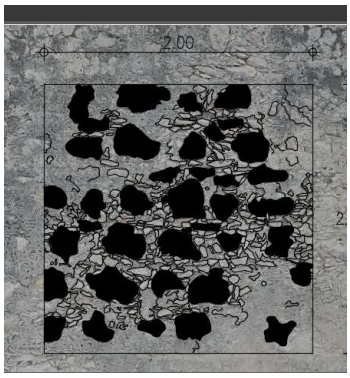
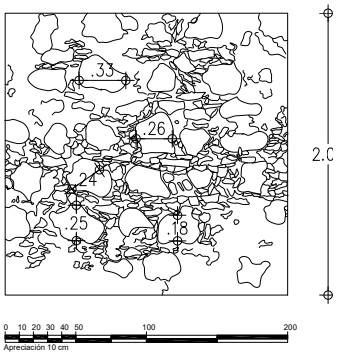
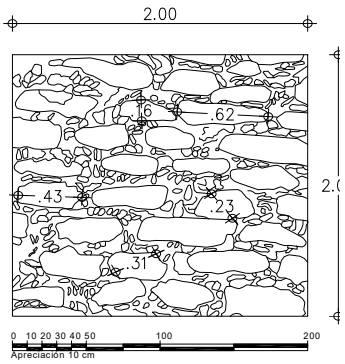
Aver = Average

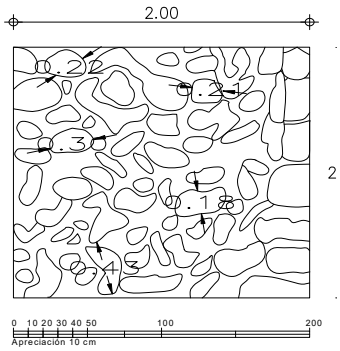
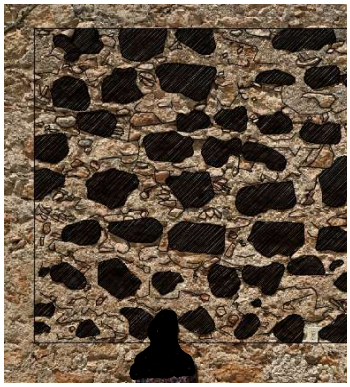
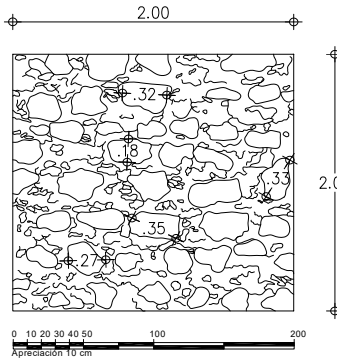
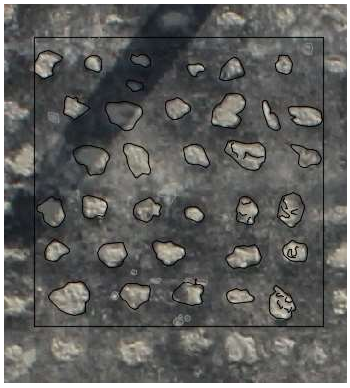
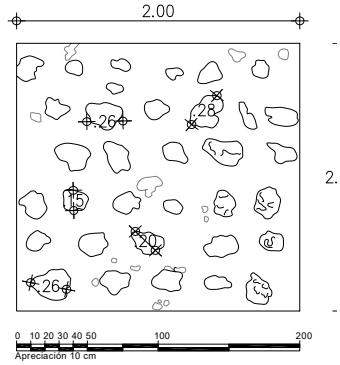
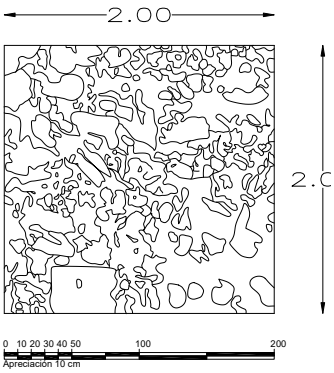
Annex 2.2
Characterization of masonry bond in walls

Abstract: Analysis of masonry bond were carried out by sketches. The photographs from visual inspection in situ and photographic record were scaled and processed on a drawing platform (.CAD). Sections of 2 m x 2m were analyzed and the characteristics of the masonry were drawn. In each picture, five dimensions of the stones were recorded, and its average was calculated (d = average). A general average of stone dimension (da) was calculated.

Masonry bond

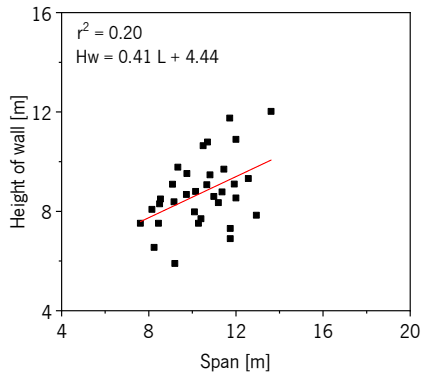
Conkal	Dzidzantun	Hocabá
		
d = 0.31	d = 0.29 m	d = 0.25 m
Izamal	Mococha	Motul
		
d = 0.35 m	d = 0.27 m	d = 0.29 m
Telchac	Ticul	
		Average
d = 0.23m		da = 1.99 m/7= 0.28 m

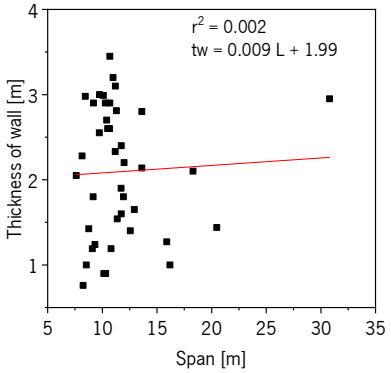
Location	Zoom photography	Draw of masonry section	Dimension of stone
Conkal		 d = 0.31	 d = 30 cm
Dzidzantun		 d = 0.29 m	
Hocabá		 d = 0.25 m	
Izamal		 d = 0.35 m	

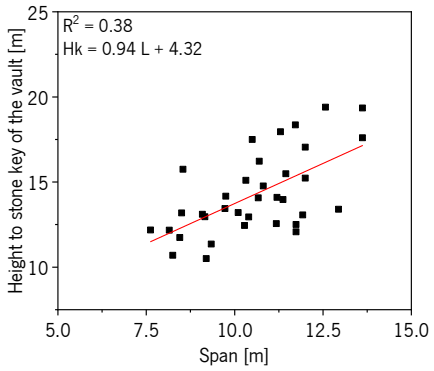
Location	Zoom photography	Draw of masonry section	Dimension of stone
Mococha		 d = 0.27 m	 d = 0.37 m
Motul		 d = 0.29 m	 d = 0.20 m
Telchac		 d = 0.23	 d = 0.35 m
Ticul			

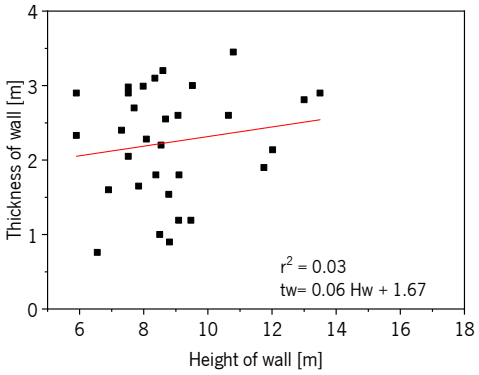
Annex 3.1
Statistical analysis of main geometric parameters

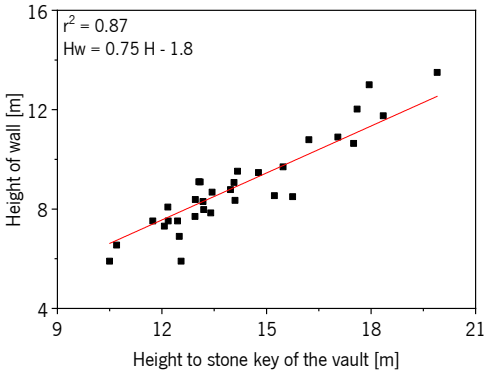
Phase 1. Statistical analysis. Single regression.



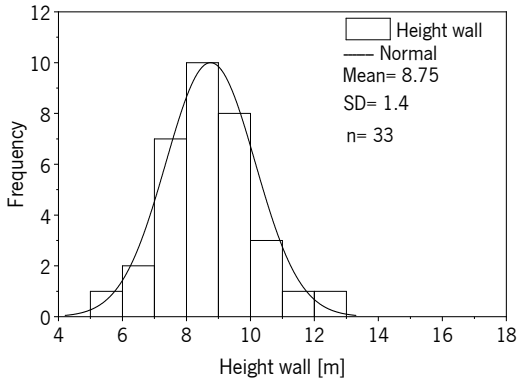


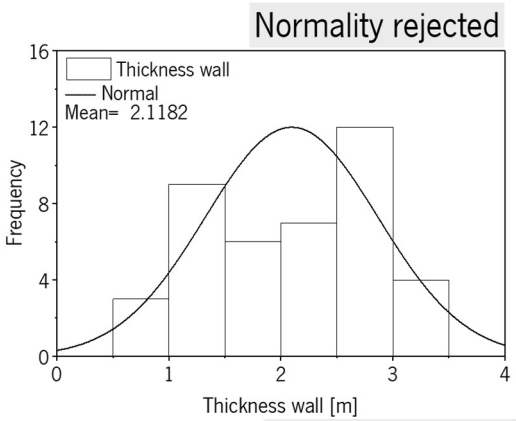


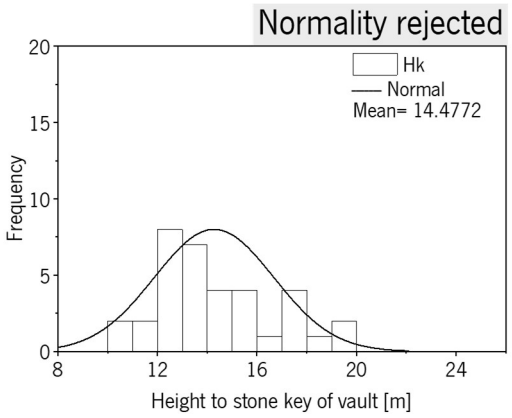


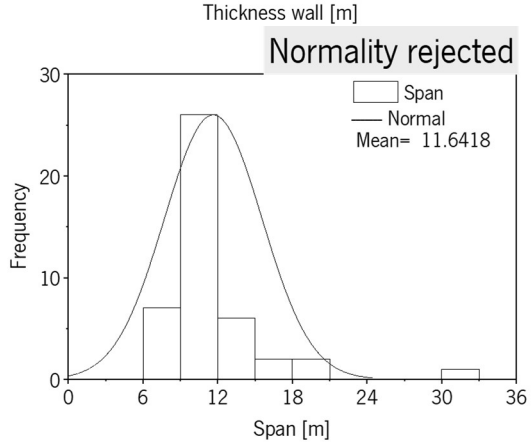


Phase 1. Statistical analysis. Histogram for each variable.

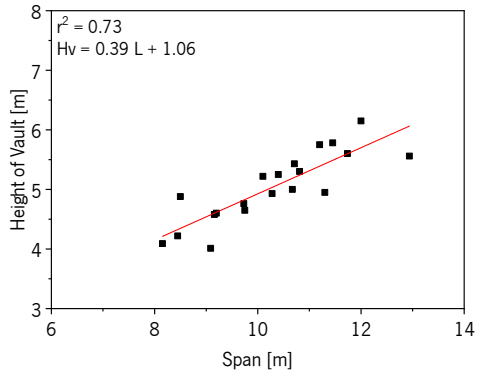


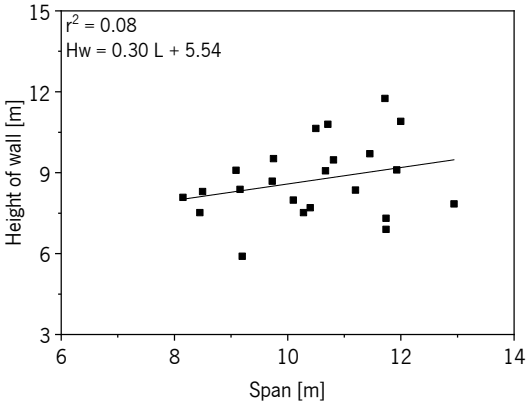


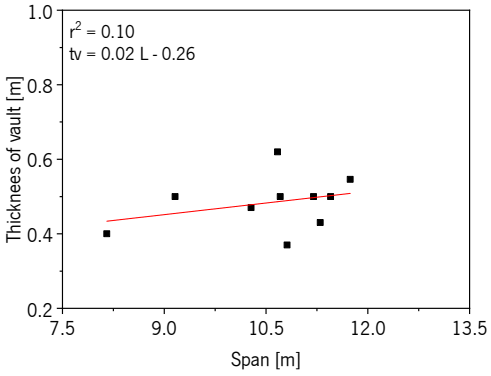


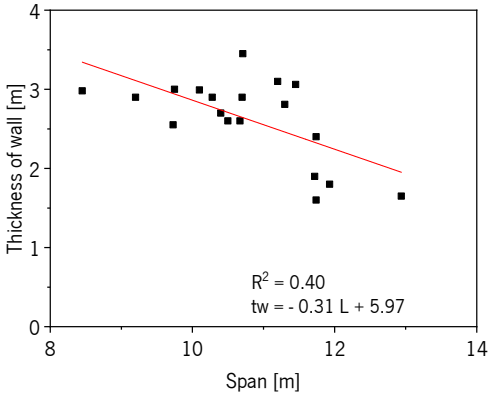


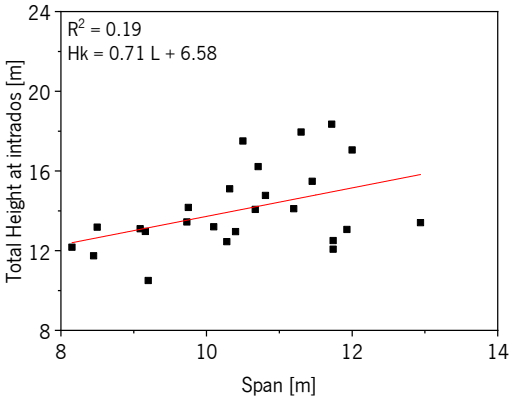
Phase 2. Statistical analysis. Single regression.

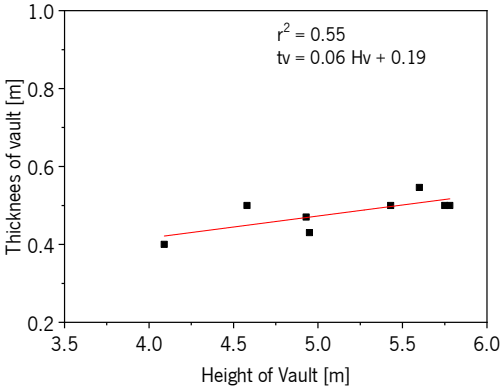


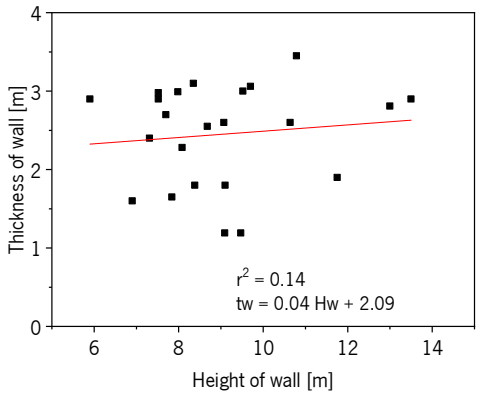


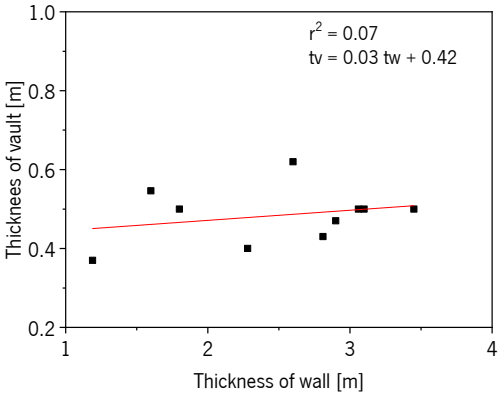


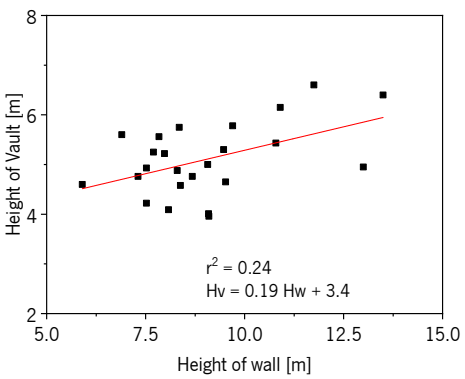


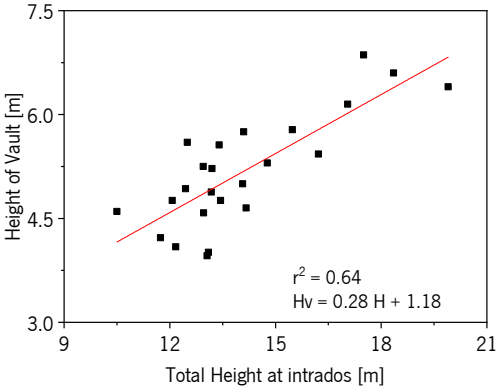


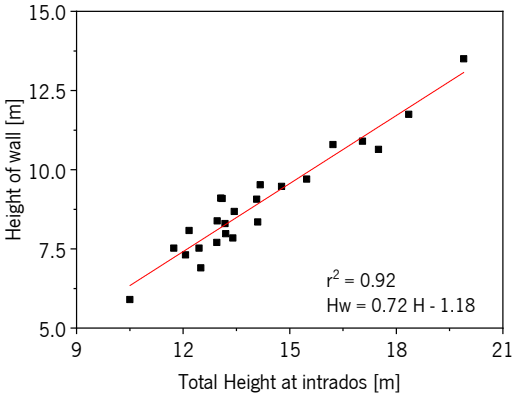




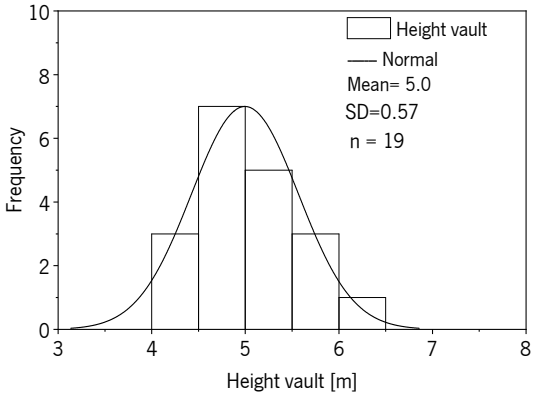


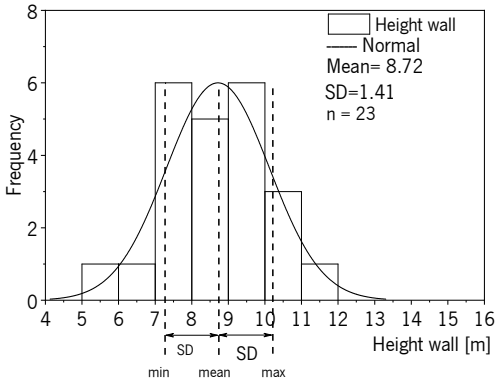

Height of Vault [m]
Height of wall [m]
r² = 0.24
Hv = 0.19 Hw + 3.4

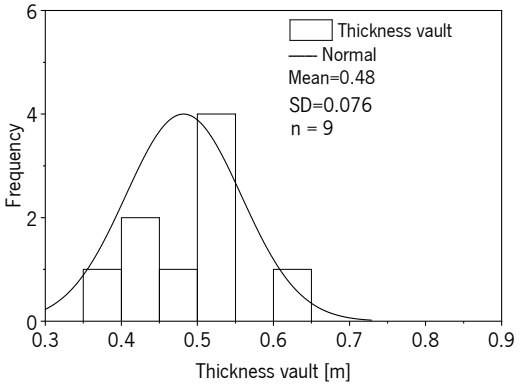

Height of Vault [m]
Total Height at intrados [m]
r² = 0.64
Hv = 0.28 H + 1.18

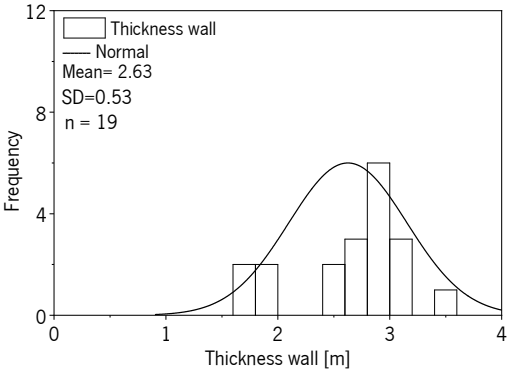

Height of wall [m]
Total Height at intrados [m]
r² = 0.92
Hw = 0.72 H - 1.18

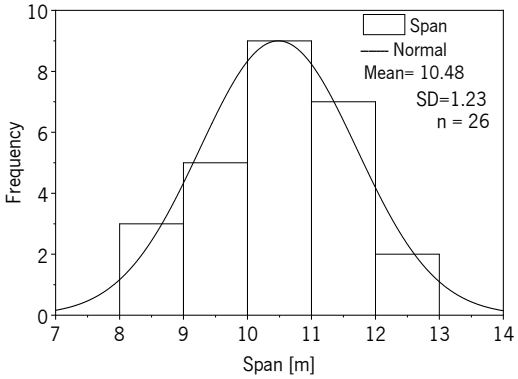
Phase 2. Statistical analysis. Histogram for each variable.

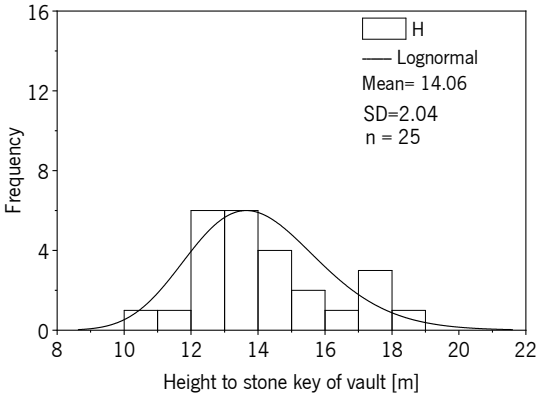




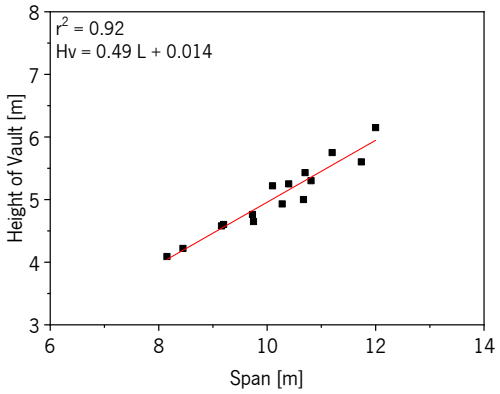


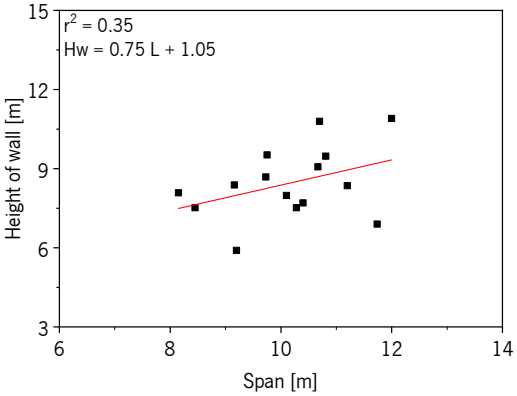


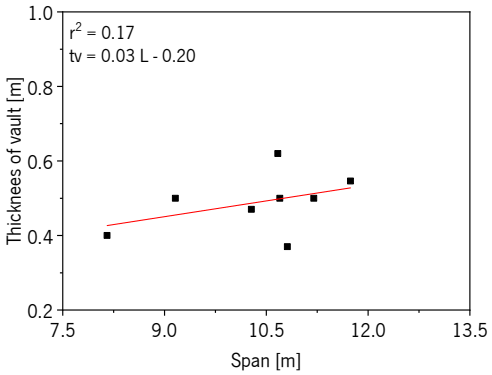


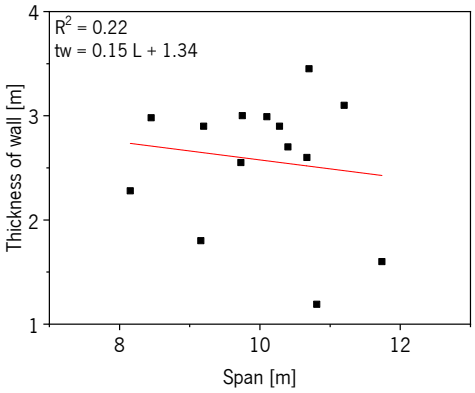


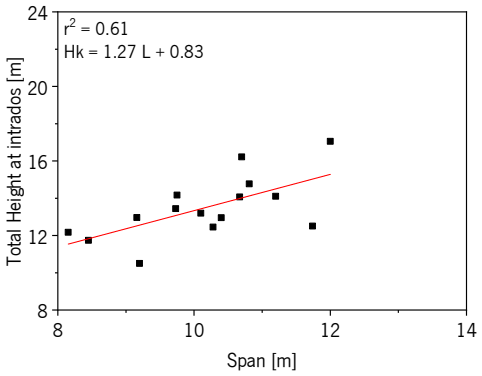
Phase 3. Statistical analysis. Single regression.

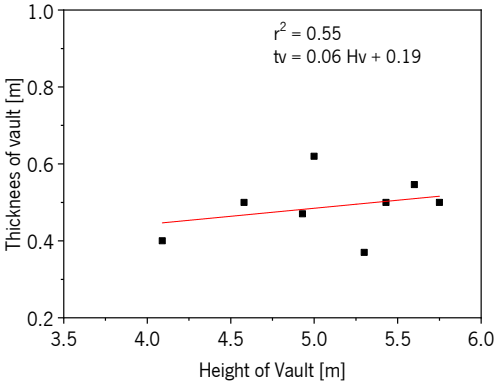


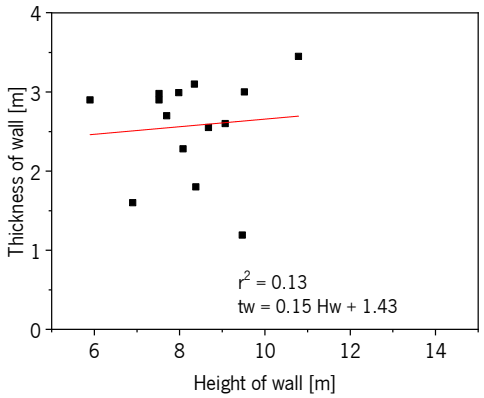


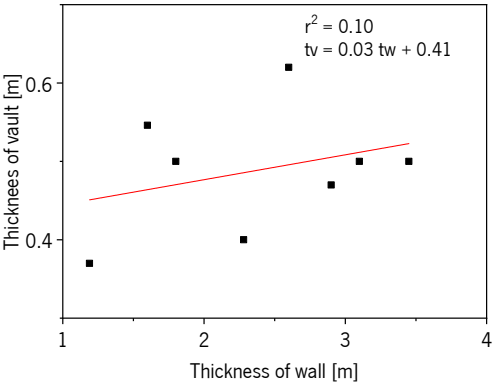


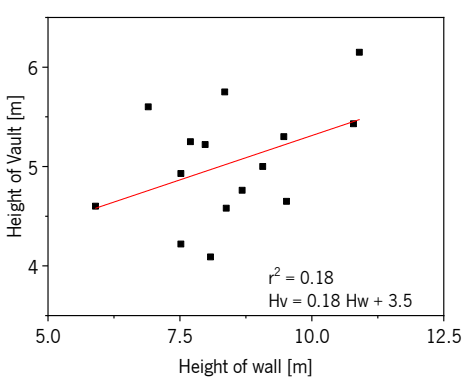


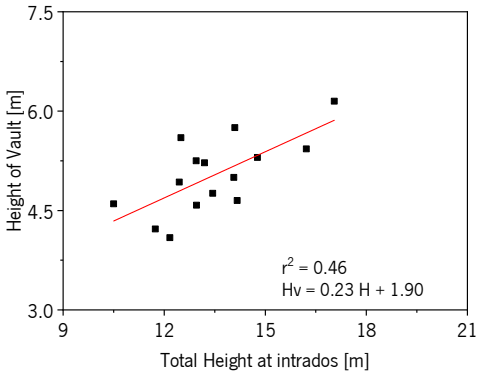


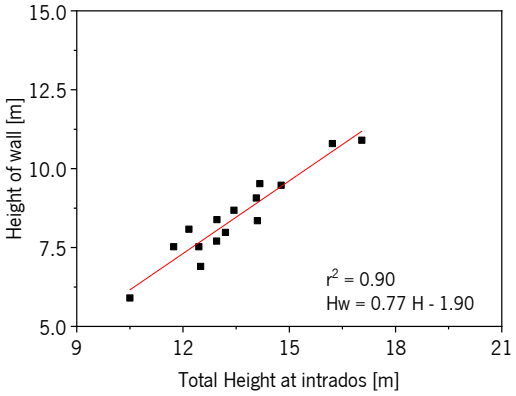




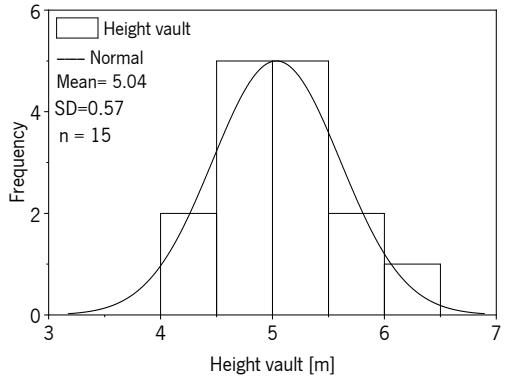


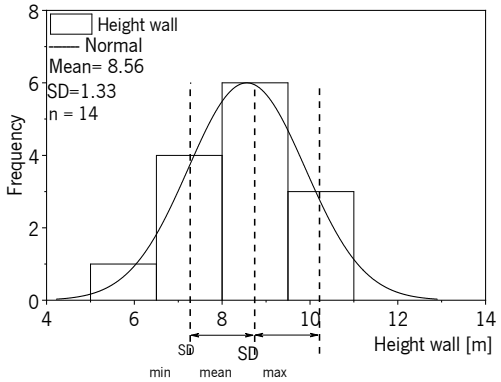

Height of Vault [m]
Height of wall [m]
r² = 0.18
Hv = 0.18 Hw + 3.5

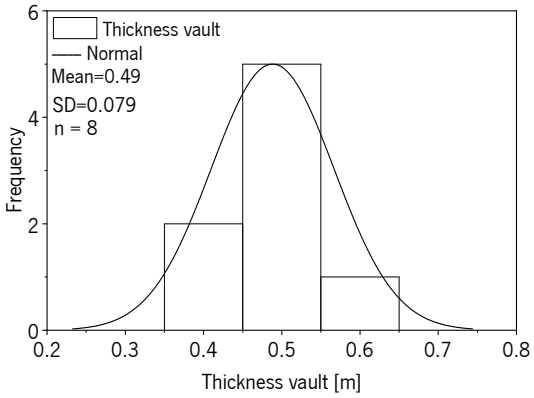

Height of Vault [m]
Total Height at intrados [m]
r² = 0.46
Hv = 0.23 H + 1.90

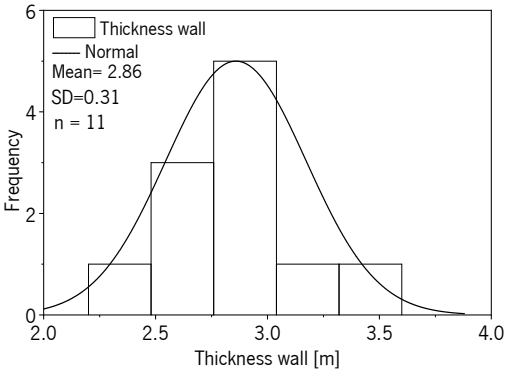

Height of wall [m]
Total Height at intrados [m]
r² = 0.90
Hw = 0.77 H - 1.90

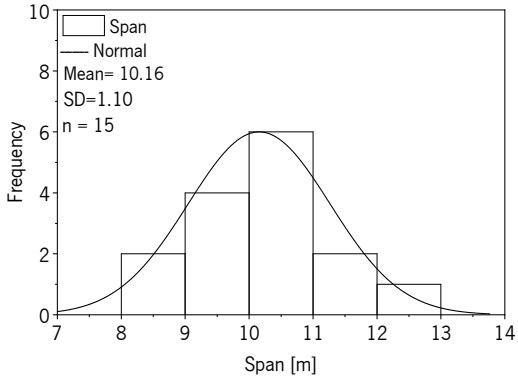
Phase 3. Statistical analysis. Histogram for each variable.

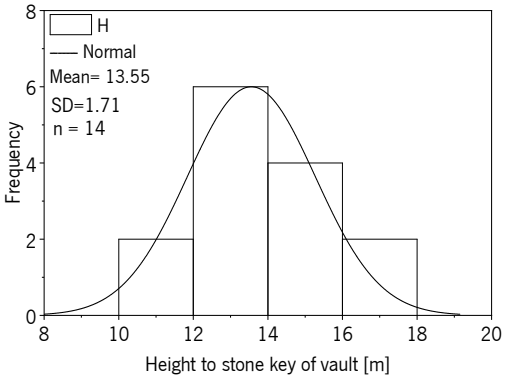






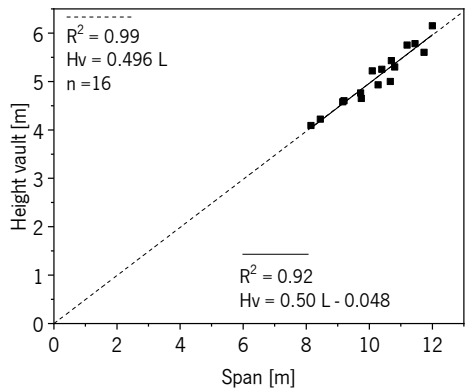


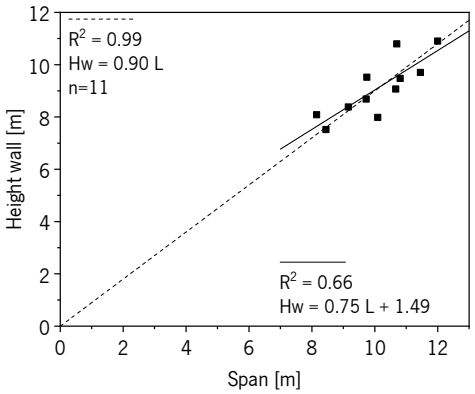


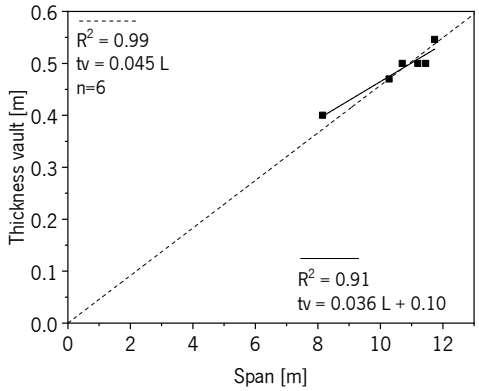


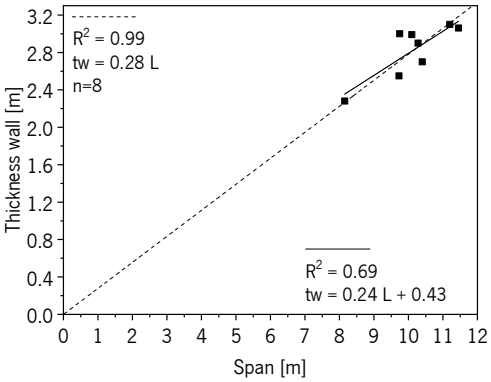
Annex 3.2
Derivation of empirical relations from statistical analysis

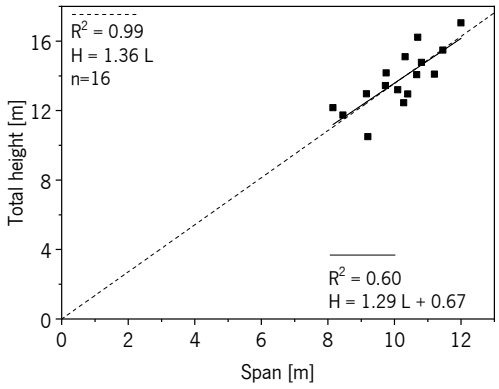
Derivation of empirical relations from statistical analysis. Single regression.



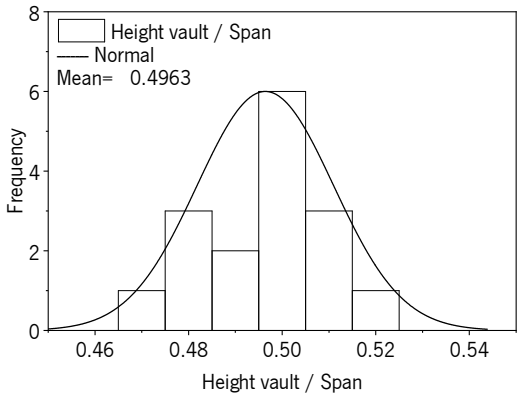


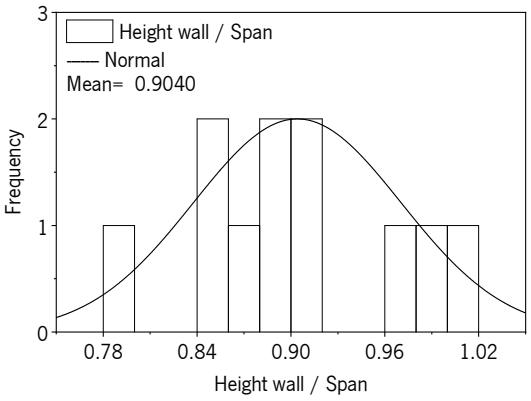


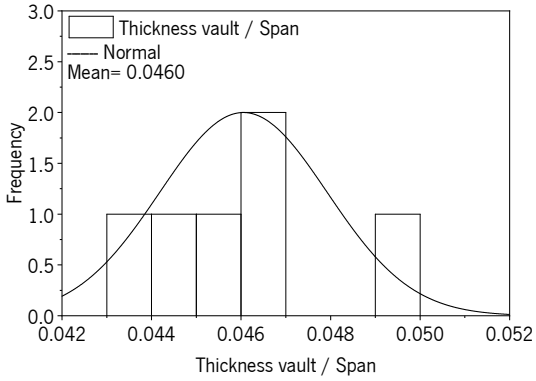


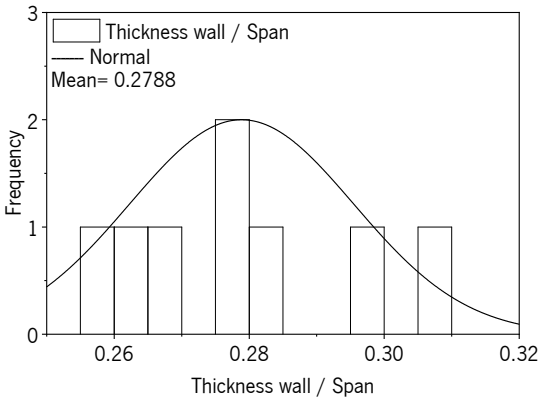


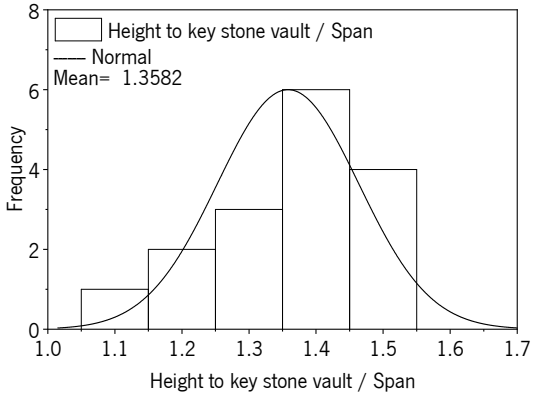
Derivation of empirical relations from statistical analysis. Histogram for each variable between span.





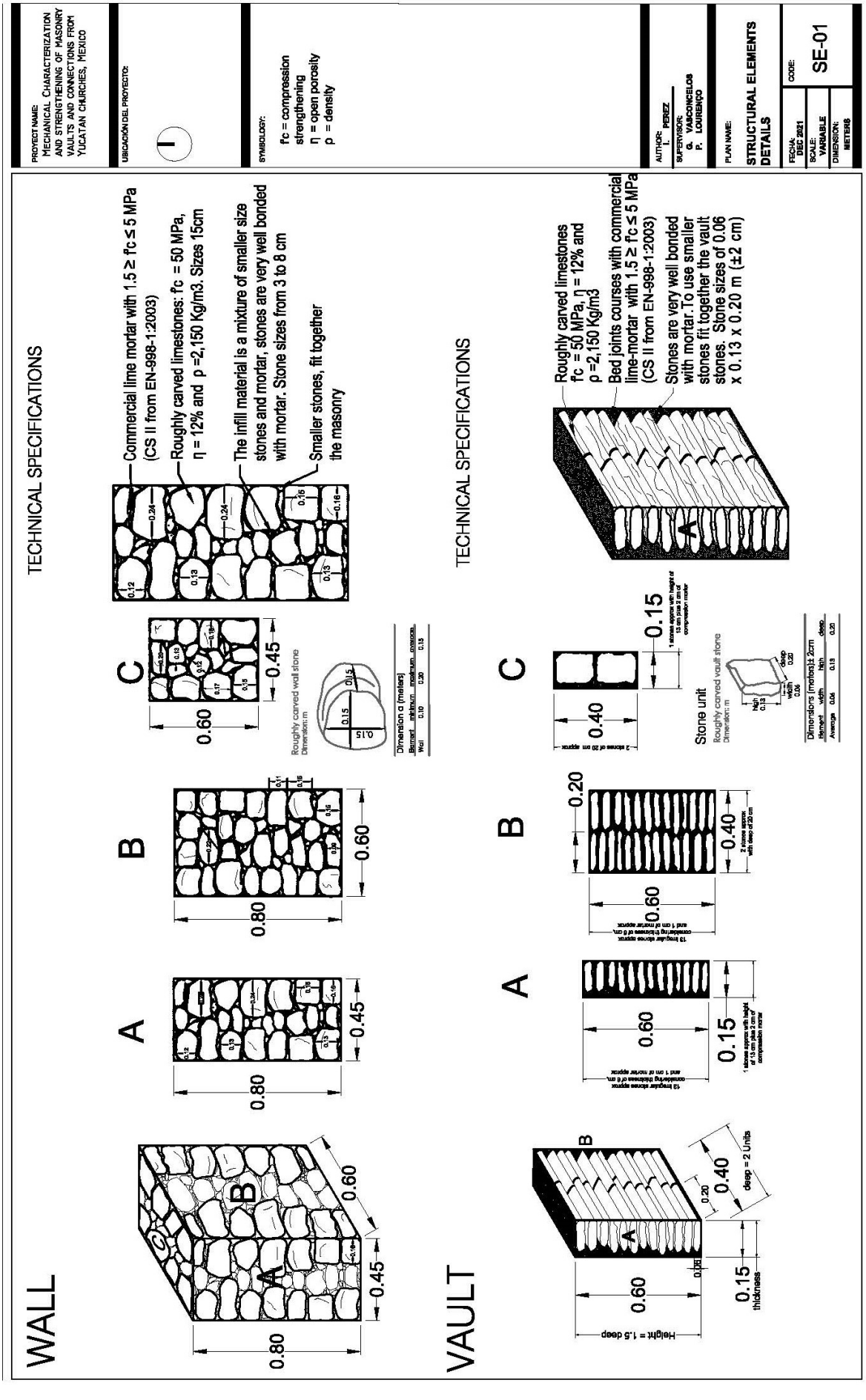


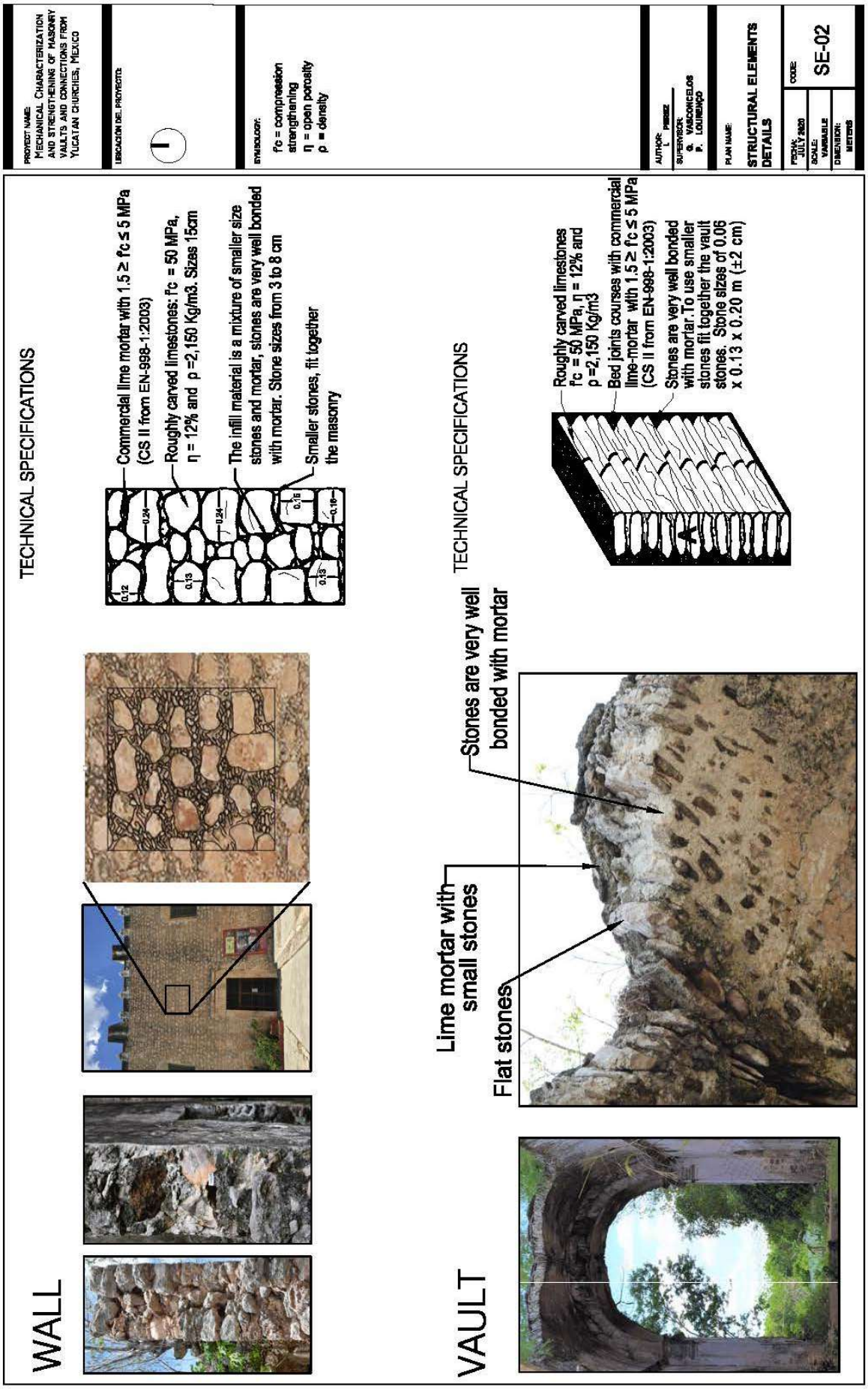




Annex 6.1
Technical specifications for masonry wallets

Abstract: Since this constructive process is not common on Portugal two planes were created to provide all necessary technical information to carried out the panel constructions. These planes include the dimensions of the wallets, technical information, all views, masonry arrangements of both vault and walls and photographies as support.


PROYECT NAME:
MECHANICAL CHARACTERIZATION AND STRENGTHENING OF MASONRY VAULTS AND CONNECTIONS FROM YUCATAN CHURCHES, MEXICO
UBICACIÓN DEL PROYECTO:
1
SYMBOLOGY:
fc = compression strengthening
η = open porosity
ρ = density
AUTHOR:
I. PEREZ
SUPERVISOR:
G. VASCONCELOS
P. LOURENÇO
PLAN NAME:
STRUCTURAL ELEMENTS DETAILS
FECHA:
DEC 2021
SCALE:
VARIABLE
DIMENSION:
METERS
CODE:
SE-01
WALL
TECHNICAL SPECIFICATIONS
A
B
C
0.80
0.60
0.45
Commercial lime mortar with 1.5 ≥ fc ≤ 5 MPa (CS II from EN-998-1:2003)
Roughly carved limestones: fc = 50 MPa, η = 12% and ρ =2,150 Kg/m3. Sizes 15cm
The infill material is a mixture of smaller size stones and mortar, stones are very well bonded with mortar. Stone sizes from 3 to 8 cm
Smaller stones, fit together the masonry
Roughly carved wall stone
Dimension: m
Dimension a (meter)
Element minimum maximum oversize
Wall 0.10 0.20 0.15
VAULT
TECHNICAL SPECIFICATIONS
Roughly carved limestones fc = 50 MPa, η = 12% and ρ =2,150 Kg/m3
Bed joints courses with commercial lime-mortar with 1.5 ≥ fc ≤ 5 MPa (CS II from EN-998-1:2003)
Stones are very well bonded with mortar.To use smaller stones fit together the vault stones. Stone sizes of 0.06 x 0.13 x 0.20 m (±2 cm)
Stone unit
Roughly carved vault stone
Dimension: m
Dimensions (meters)± 2cm
Element width high deep
Average 0.06 0.13 0.20
Height = 1.5 deep
deep = 2 Units
0.15 thickness
0.20
0.40


PROJECT NAME:
MECHANICAL CHARACTERIZATION AND STRENGTHENING OF MASONRY VAULTS AND CONNECTIONS FROM YUCATAN CHURCHES, MEXICO
UBICACIÓN DEL PROYECTO:
1
SYMBOLOGY:
f'c = compression strengthening
η = open porosity
ρ = density
AUTHOR:
SUPERVISOR:
PLAN NAME:
STRUCTURAL ELEMENTS DETAILS
CODE:
SE-02
WALL
TECHNICAL SPECIFICATIONS
Commercial lime mortar with 1.5 ≥ f'c ≤ 5 MPa (CS II from EN-998-1:2003)
Roughly carved limestones: f'c = 50 MPa, η = 12% and ρ =2,150 Kg/m3. Sizes 15cm
The infill material is a mixture of smaller size stones and mortar, stones are very well bonded with mortar. Stone sizes from 3 to 8 cm
Smaller stones, fit together the masonry
VAULT
TECHNICAL SPECIFICATIONS
Roughly carved limestones f'c = 50 MPa, η = 12% and ρ =2,150 Kg/m3
Bed joints courses with commercial lime-mortar with 1.5 ≥ f'c ≤ 5 MPa (CS II from EN-998-1:2003)
Stones are very well bonded with mortar.To use smaller stones fit together the vault stones. Stone sizes of 0.06 x 0.13 x 0.20 m (±2 cm)
Stones are very well bonded with mortar
Lime mortar with small stones
Flat stones

Annex 7.1
Mechanical characteristics of strengthened materials.

Abstract: technical information of all materials used in the strengthened process.

Fassanet ARG plus'

Dati Tecnici

Caratteristiche	*Metodo di prova*	*Prestazioni del prodotto*
Composizione fibra di vetro AR	ISO 11667:1997	in peso ca. 84% in volume ca. 68%
Composizione resina epossidica termoindurente	-	in peso ca. 16% in volume ca. 32%
Tipo di fibra	EN15422	Fibra di vetro alcali resistente
Densità della fibra vetro AR	ISO 1183-1:2004	2,68 g/cm³
Densità della resina epossidica termoindurente	ISO 1183-1:2004	1,1 g/cm³
Temperatura di transizione vetrosa della resina epossidica (ISO 11537-2:2013)	ISO 11537-2:2013	51°C
Grammatura ISO 3374 (rete apprettata)	ISO 3374	305 g/m² (± 10%)
Grammatura ISO 3374 (rete greggia)	ISO 3374	255 g/m² (± 10%)
Ampiezza della maglia (trama e ordito)	-	38 ± 0,2 mm
Sezione nominale delle barre (trama)	CNR DT 203:2006	1,831 mm²
Sezione nominale delle barre (ordito)	CNR DT 203:2006	1,814 mm²
Area nominale delle fibre (trama)	CNR DT 200:2004 e CNR DT 203:2006	0,91 mm²
Area nominale delle fibre (ordito)	CNR DT 200:2004 e CNR DT 203:2006	0,45 mm²
Resistenza ultima a trazione delle fibre (trama)	Linee Guida Ministeriali CRM	1173 Mpa (medio) 1056 Mpa (caratteristico)
Valore medio del modulo elastico riferito alla sezione complessiva del campione (trama)	Linee Guida Ministeriali CRM	68060 MPa
Valore medio della deformazione ultima (trama)	Linee Guida Ministeriali CRM	1,71%
Resistenza ultima a trazione delle fibre (ordito)	Linee Guida Ministeriali CRM	1095 Mpa (medio) 1006 Mpa (caratteristico)
Valore medio del modulo elastico riferito alla sezione complessiva del campione (ordito)	Linee Guida Ministeriali CRM	78460 MPa
Valore medio della deformazione ultima (ordito)	Linee Guida Ministeriali CRM	1,43%

Malta Structturale NHL 77

Dati Tecnici

Caratteristiche	*Prestazioni del prodotto*
Aspetto	polvere chiara
Peso specifico della polvere	1.350 g/l
Granulometria	< 3 mm
Spessore minimo e massimo	10-50 mm
Acqua d'impasto	20-22%
Resa	ca. 15,6 kg/m² per cm di spessore
Tempo di lavorazione	45 minuti a 20°C
Massa volumica malta fresca (EN 1015-6)	ca. 1.900 kg/m³
Densità malta indurita (EN 1015-10)	ca. 1.750 kg/m³
Resistenza a flessione a 28 giorni (EN 1015-11)	≥ 3 N/mm²
Resistenza a compressione a 28 giorni (EN 1015-11)	≥ 10 N/mm²
Adesione al supporto per trazione diretta (EN 1015-12)	≥ 0,5 N/mm²
Coefficiente di assorbimento d'acqua per capillarità (EN 1015-18)	≤ 0,5 kg/m²·min^{0,5}
Modulo elastico statico (EN 13412 - Metodo 2)	≥ 7.000 N/mm²
Permeabilità al vapore acqueo (EN 1015-19)	μ ≤ 13
Contenuto di cloruri (EN 1015-17)	< 0,005%
Coefficiente di conducibilità termica (EN 1745)	λ = 0,77 W/m²K (valore tabulato)
Conforme alla Norma EN 998-1	GP-CSIV-W0
Conforme alla Norma EN 998-2	M10

Fassa Glass Connector L

Dati Tecnici

Caratteristiche	*Metodo di prova*	*Prestazioni del prodotto*
Composizione fibra di vetro AR (EN 15422)	ISO 11667:1997	in peso ca. 81% in volume ca. 65%
Composizione resina epossidica termoindurente	-	in peso ca. 19% in volume ca. 35%
Lunghezza	-	200, 380, 500, 700 mm
Forma	-	ad L
Area resistente complessiva (resina + fibra)	-	20 mm^2
Area equivalente della sezione	CNR-DT 203/2006	48 mm^2
Diametro equivalente della barra	CNR-DT 203/2006	7,8 mm
Temperatura di transizione vetrosa della resina	ISO 11357-2:2013	106°C
Carico di rottura medio	Linee Guida Ministeriali CRM	22400 N
Resistenza ultima a trazione delle fibre	Linee Guida Ministeriali CRM	1120 MPa (medio) 1062 MPa (caratteristico)
Modulo di rigidezza a trazione medio	Linee Guida Ministeriali CRM	44.713 MPa
Allungamento a rottura	Linee Guida Ministeriali CRM	2,5%